INVESTIGATION OF COXSACKIEVIRUS A21 AS A POTENTIAL TREATMENT FOR PANCREATIC CANCER

Lincoln Smith

B. Biotechnology (Hons)

A thesis submitted in fulfilment of the requirements for the degree of

Doctor of Philosophy in Immunology and Microbiology

School of Biomedical Sciences and Pharmacy,

The University of Newcastle

2018

This research was supported by an Australian Government Research Training Program (RTP) Scholarship

Declaration

I hereby certify that the work embodied in the thesis is my own work, conducted under normal supervision. The thesis contains no material which has been accepted, or is being examined, for the award of any other degree or diploma in any university or other tertiary institution and, to the best of my knowledge and belief, contains no material previously published or written by another person, except where due reference has been made in the text. I give consent to the final version of my thesis being made available worldwide when deposited in the University's Digital Repository, subject to the provisions of the Copyright Act 1968 and any approved embargo.

Signed: _____

Acknowledgements

It has been a great honour and privilege to conduct this research. The potential impact that CVA21 has as a treatment for pancreatic cancer is phenomenal. I am extremely blessed to have been able to contribute to advancing the field of pancreatic cancer research. My greatest hope is that this research will inspire clinical investigation and lead to improved treatment options and quality of life for pancreatic cancer patients worldwide.

There are many people that I would like to express my gratitude and appreciation for their support throughout my PhD. The journey has been monumental and accomplished with the reinforcement of everyone who has influenced me along the way. Dr Gough Au, you are a champion. Your perpetual tutelage and the wisdom and knowledge you have imparted to me as my supervisor and friend have helped develop me into a better scientist and human being. I have enjoyed working with you immensely and I hope the opportunity to conduct research with you in the future arises.

Immeasurable appreciation to Associate Professor Darren Shafren who allowed me to conduct and provided funding for this research. I thank you for your mentorship and the opportunity to work with Viralytics. The experience has shaped me into a better investigator and provided invaluable experience as a young researcher with commercial enterprise and drug development. Thank you also for the incredible opportunities and monetary sponsorship to travel and present at conferences in Boston and Vancouver.

Huge appreciation to my Viralytics colleagues, Dr Roberta Karpathy, Dr Susanne Johansson, Dr Yvonne Wong, Dr Camilla Salum De Oliviera, Dr Min Yuan Quah, Robert Herd, Browyn Davies, Rebecca Ingham, Amanda Kelly, Jack Hockley, Sophie Wells, Olivia Lisle, Penny Yates, Avril Williams, Isabella Mackay, Celeste Harrison and Brydie Page. It has been a pleasure to work alongside all of you. You have all been a great support mentally and emotionally helping me through this. Specifically, thank you to Dr Gough Au, Dr Yvonne Wong, Dr Min Yuan Quah, Sophie Wells and Jack Hockley for your assistance with the animal models. It has been great fun!

Thank you to all of my friends, in particular Kate Harvey, Heather Robertson and Benjamin Smith, who have been incredible emotional and mental supports for me over these last four years. Enormous thanks to my brothers, Clint, Quinn, and Tyson Smith for always being a mate, and supporting and accepting me and my endeavours.

Finally, but most importantly, thank you to my parents, Sherryl and Thomas Smith. Without your unconditional Love, support, encouragement, guidance, wisdom, discernment, and knowledge that you have imparted in me throughout my upbringing and this PhD I would not have been able to achieve any of this. You did an excellent job raising us boys and I will always appreciate and value the morals and principles that you taught us. I am honoured to be your son. I know that both of you are incredibly proud of me; nevertheless, part of the motivation to achieve a PhD was to honour you. Achieving a PhD is just as much a success for me, as it is for you.

Table of Contents

List of Figures

List of Tables

Abbreviations

5-FU	5 fluorouracil
ACC	Acinar cell carcinoma
ADEX	Aberrantly differentiated endocrine exocrine
ALT	Alanine aminotransferase
AOD	Assay on demand
APC	Adenomatosis polyposis coli tumour suppressor
AST	Aspartate aminotransferase
ATCC	American type culture collection
B.L.D.	Below level of detection
BMDC	Bone marrow derived cell
BPE	Bovine pituitary extract
BRCA1	Breast cancer 1
BRCA2	Breast cancer 2
C.R.	Complete response
CA19-9	Serum carbohydrate antigen 19-9
CAA	Cancer associated adipocyte
CD38	ADP-ribosyl cyclase 1
CD46	Trophoblast-lymphocyte cross-reactive antigen
CDKN1C/p57KIP2	Cyclin-dependent kinase inhibitor p57
CFDA	China Food and Drug Administration
CI	Combination index
C_{max}	Maximum plasma concentration
CPE	Cytopathic effect
CPV	Canine parvovirus
CT	Computed tomography
CTLA-4	Cytotoxic t-lymphocyte associated protein 4
CVA21	Coxsackievirus A21
CXCR4	C-X-C chemokine receptor type 4
DAB	3,3-diaminobenzidine
DAF	Decay accelerating factor
DEAE	Diethylaminoethyl
DMEM	Dulbecco’s modified eagle medium

DMSO	Dimethyl sulfoxide
DPTI	Days post tumour inoculation
EC_{50}	50% effective concentration
EC_{75}	75% effective concentration
EC_{95}	95% effective concentration
ECM	Extracellular matrix
ECOG	Eastern Co-operative Oncology Group
EGFR	Epidermal growth factor receptor
ET-1	Endothelin-1
ETM	Epithelial to mesenchymal
EUS	Endoscopic ultrasound
Fa	Fraction affected
FCS	Foetal calf serum
FDG	18[F]-fluorodeoxyglucose
flux	Photons/second
FMRI	Fragile X mental retardation protein
FNA	Fine needle aspiration
FNI	Fine needle injection
FOLFIRINOX	Oxaliplatin, irinotecan, 5-FU, and leucovorin
FOXA2	Forkhead box a2
FOXA3	Forkhead box a3
FPV	Feline parvoirus
GATA6	GATA binding protein 6
GM-CSF	Granulocyte-macrophage colony-stimulating factor
GNAS	Guanine nucleotide binding protein (g protein), alpha stimulating
GPI	Glycosylphosphatidylinositol
HEPES	Hydroxyethyl)piperazine-1-ethanesulfonic acid
HES1	HES family BHLH transcription factor 1
HEV	Human enterovirus
HIV	Human immunodeficiency virus
HNF1A	Hnf1 homeobox a
HNF1B	Hepatocyte nuclear factor 1-beta
HNF1B	Hnf1 homeobox b
HNF4A	Hepatocyte nuclear factor 4 alpha

HNF4G	Hepatocyte nuclear factor 4 gamma
HPDE	Human pancreatic ductal epithelial
HSV	Herpes simplex virus
huICAM-1	Human ICAM-1
I.P.	Intraperitoneally
I.T.	Intratumourally
I.V.	Intravenously
ICAM-1	Intercellular adhesion molecule 1
ICP	Infected cell protein
ICTV	International Committee on Taxonomy of Viruses
IFNγ	Interferon gamma
IGF-1	Insulin-like growth factor
IL-1	Interleukin 1
IL-12	Interleukin 12
IPMN	Intraductal papillary mucinous neoplasms
irAE	Immune related adverse event
IRES	Internal ribosome entry site
K-RAS	Kirsten rat sarcoma 2 viral oncogene homolog
KDM6A	Lysine demethylase 6A
KSFM	Keratinocyte serum free media
LAG-3	Lymphocyte activation gene-3
LFA-1	Lymphocyte function associated antigen 1
MAC-1	Macrophage antigen 1
MAFA	MAF BZIP transcription factor a
MCN	Mucinous cystic neoplasms
MDSC	Myeloid-derived suppressor cell
MIST1	Muscle, intestine and stomach expression 1
MKP-2/DUSP	Dual specificity phosphatase 4
MLH1	DNA mismatch repair protein MLH1
MMP	Matrix metalloproteinase
MNX1	Motor neuron and pancreas homeobox 1
MOI	Multiplicity of infection
MRCP	Magnetic resonance cholangiopancreatography
MRI	Magnetic resonance imaging
MSH2	DNA mismatch repair protein MSH2

MTT	3-(4,5-dimethylthiazol-2-yl)-2,5-diphenyltetrazoliumbromide
MUC1	Mucin 1
MUC2	Mucin 2
MUC4	Mucin 4
MUC5A	Mucin 5AC
N.T.C.	No treatment controls
nAb	Neutralising antibody
nab-paclitaxel	Albumin bound paclitaxel
nCLE	Needle-based confocal laser endomicroscopy
NDV	Newcastle disease virus
NEUROD1	Neuronal differentiation 1
NF-κB	Nuclear factor kappa-light-chain-enhancer of activated B cells
NK	Natural killer
NKX2-2	Nk2 homeobox 2
NOTCH	Translocation-associated notch protein tan
NR5A2	Nuclear receptor subfamily 5 group a member 2
OD	Optical density
OPG	Osteoprotegerin
ORF	Open reading frame
OV	Oncolytic virus
P.R.	Partial response
p16/CDKN2A	Cyclin-dependent kinase inhibitor 2A
PALB2	Partner and localizer of BRCA2
PanIN	Pancreatic intraepithelial neoplasms
PBS	Phosphate buffered saline
PC	Pancreatic cancer
PCC	Pancreatic cancer cell
PD-1	Programmed cell death 1
PD-L1	Programmed death ligand 1
PD-L2	Programmed death ligand 2
PDAC	Pancreatic ductal adenocarcinoma
PDGF	Platelet-derived growth factor
PDX1	Pancreatic and duodenal homeobox 1
PET	Positron emission tomography
PET	Pycoerythrin

Pi3Ks-PKB/AKT	Phosphoinositide-3-kinase–protein kinase B/Akt
PR3	Proteinase 3
PRSS1	Protease, serine 1
PSC	Pancreatic stellate cell
RBPJL	Recombination signal binding protein for immunoglobulin kappa j region like
RNA	Ribonucleic acid
RNF43	Ring finger protein 43
ROBO/SLIT	Roundabout guidance receptor
ROS	Reactive oxygen species
RPMI	RPMI 1640 medium
RT	Room temperature
S.C.	Subcutaneously
S.D.	Stable disease
S100A4	S100 calcium binding protein A4
SEM	Standard error of the mean
SLAM	Signalling lymphocyte-activation molecule
SMAD4/DPC4	Deletion target in pancreatic carcinoma 4
SPF	Specific pathogen free
SPINK1	Serine protease inhibitor Kazal-type 1
SPN	Solid pseudopapillary neoplasm
SRC1	Short consensus repeat unit 1
STK11	Serine/threonine kinase 11
SWI-SNF	Switch/Sucrose Non-Fermentable
TAM	Tumour associated macrophage
TAN	Tumour associated neutrophil
$TCID_{50}$	50% tissue culture infectious dose
TFF1	Trefoil factor 1
TGFβ	Transforming growth factor beta
TGFBR2	Transforming growth factor beta receptor 2
TIL	Tumour infiltrating lymphocyte
TMA	Tumour microarray
TMA	Tumour microarray
TME	Tumour microenvironment
TNFα	Tumour necrosis factor alpha

TNM	Tumour/node/metastasis
Tp53	Tumor protein p53
Tp63ΔN	Tumour protein P63 delta N
Treg	Regulatory T cell
US	Ultrasound
USFDA	United States Food and Drug Administration
UTR	Untranslated region
VEGF	Vascular endothelial growth factor
VPg	Viral protein genome-linked
WNT	Wingless-type MMTV integration site family member
WT	Wild-type

Units of Measurement

Å	Angstrom
°C	Degrees Celsius
Da	Dalton
Flux	Photons/second
g	Gravitational force
g	Grams
L	Litre
M	Molar
m	Metre
MOI	Multiplicity of infection
$TCID_{50}$	50% Tissue culture infectious dose

Prefixes

k	kilo	10^{3}
m	milli	10^{-3}
µ	micro	10^{-6}
n	nano	10^{-9}
p	pico	10^{-12}
f	femto	10^{-15}

Chapter 1

Synopsis

Coxsackievirus A21 (CVA21) is a human specific, non-enveloped, 28 nm icosahedral, group C enterovirus with a single strand positive sense RNA genome. CVA21 causes common cold symptoms upon infection in humans. CVA21 utilises intercellular adhesion molecule 1 (ICAM-1) and decay accelerating factor (DAF) for cell surface binding and cell entry of target cells. Cancer cells commonly overexpress ICAM-1 making them susceptible to CVA21 infection. Upon invasion of a host cell, viral progeny is produced through hijacking cellular machinery. Host cell lysis occurs, and virus is able to infect nearby and distant cells through systemic spread. Furthermore, cancer cell oncolysis may lead to recognition of specific tumour cell epitopes by the host's immune system and generation of an anti-tumour immune response. CVA21 is a potentially efficacious anti-cancer agent for multiple cancer types in preclinical studies and is undergoing investigation in clinical trials as treatments for a range of cancer types with promising early stage results. Investigation of CVA21 as a potential treatment for pancreatic cancer in clinical trials will hopefully be initiated in the near future.

Pancreatic cancer (PC) is the most lethal of all cancer types. PC has the worst survival rates of any cancer type and incidence continues to increase annually. Even though the genomic aberration profiles and molecular pathogenesis of PC are well documented there are still no early detection mechanisms for PC. Pancreatic cancer is characterised by PC cells supported by a dense desmoplastic reaction, composed primarily of pancreatic stellate cells (PSCs), that is highly tumour promoting, with rapid progression. Currently, there are no treatments that can adequately control the disease. Furthermore, present treatment options provide unsatisfactory toxicity and quality of life to suffering patients. Efficacious treatment options are rapidly needed. The oncolytic virus, CVA21, has great potential as a treatment for PC. The capacity to directly lyse tumour cells as well as prompt an adaptive anti-tumour immune response while proving to exert minimal levels of host adverse events makes CVA21 an ideal anti-cancer agent.

Investigation of CVA21 as a potential treatment for PC in the preclinical setting was the major aim of this study. The key hypothesis for this project was that CVA21 would be an effective anti-cancer agent against pancreatic cancer due to high expression of viral entry receptors, ICAM-1 and/or DAF on PC and PSCs. Furthermore, CVA21 would have enhanced anti-tumour activity in combination with chemotherapeutic or

immunotherapeutic agents. Such questions were addressed through specific *in vitro* tissue culture and immunohistochemical analyses, and *in vivo* mouse models.

Initially the study determined the expression levels of CVA21 cell entry receptors, ICAM-1 and DAF, on the surface of PC and PSCs and compared these levels to normal pancreatic cells. Evaluation of expression levels were deduced through quantitative real-time PCR and flow cytometric analyses of a panel of PC, PSCs, and normal pancreatic ductal epithelial cells. Furthermore, ICAM-1 cell surface expression on *ex vivo* patient PC tissues was monitored via immunohistochemical analyses. The second aim of the project was to screen the sensitivity of human PC cells and PSCs to CVA21 in comparison to normal pancreatic cells through viral infectivity and viral growth kinetic assays.

Overall, findings presented demonstrate CVA21 to be a potentially efficacious and suitable treatment for PC. ICAM-1 and DAF, gene, and cell receptor expression showed that PC and PSCs, in general, overexpressed ICAM-1 and/or DAF compared to normal pancreatic ductal epithelial cells. A convincing cell lysis effect of CVA21 on PC and PSCs was observed. Thus, the hypothesis that CVA21 will be a potential effective anti-cancer agent against PC due to overexpression of ICAM-1 and/or DAF was confirmed. Moreover, minimal oncolytic activity of CVA21 on normal pancreatic ductal epithelial cells was observed and is promising when considering translation to a clinical setting. Furthermore, CVA21 was observed to target both PC and PSCs alone, and when co-cultured, implicating CVA21 as a strong candidate for oncolysis of PC cells and the major stromal desmoplastic reaction observed in native PC. Finally, observation of a stepwise increase in ICAM-1 cell surface expression over the progression of PC from immunohistochemically stained patient samples attested CVA21 as a specific and potential candidate for the treatment of PC.

The third aim of the study was to determine the synergistic or antagonistic relationship between CVA21 and conventional chemotherapy on human PC and PSCs, compared to normal pancreatic cells. The sensitivity of the panel of pancreatic cell lines to gemcitabine was investigated through *in vitro* dose-response assays. Checkerboard assays employing the respective experimentally determined concentrations of CVA21 and gemcitabine required to reduce cell viability by 50% were titrated in combination against each cell line to observe the relationship. Computational analyses based off

the Chou-Talalay method of drug calculation using the experimentally recorded values enabled the synergistic or antagonistic relationship between the two agents to be empirically calculated. The fourth aim of the study was to establish an orthotopic mouse model of human PC and investigate CVA21 as a treatment, alone, and in combination with conventional chemotherapy. *In vivo* investigations utilising an athymic nude mouse model of orthotopic PC generated from human Panc-1-luc cells was successfully conducted and the efficacy of CVA21 as a treatment for PC evaluated.

Taken together, the results further enforced the hypothesis that CVA21 is a potential anti-cancer candidate against PC. Furthermore, the findings clearly illustrated the significant high-grade toxicity of gemcitabine as a treatment for PC. Dose-response assays of gemcitabine on a panel of PC, pancreatic stellate, and normal pancreas cells indicated normal pancreatic ductal epithelial cells to be incredibly susceptible, PSCs to be almost entirely refractive, and varying degrees of sensitivity on PC cells. Combination checkerboard assays of CVA21 and gemcitabine on a panel of cell lines revealed a synergistic relationship between the two agents when calculated from accurate experimental data. Thus, the hypothesis that CVA21 in combination with a chemotherapeutic agent would have a synergistic effect was validated in some instances. However, in many examples the calculated concentrations of gemcitabine were not clinically achievable. Moreover, there was a lack of sensitisation of stellate cells to gemcitabine, and increased toxicity towards normal pancreas cells. Therefore, caution should be displayed if using CVA21 and gemcitabine combination treatment in the clinical setting.

The athymic nude mouse model of orthotopic PC generated from Panc-1-luc cells demonstrated CVA21 to be an efficacious and well tolerated treatment for PC when administered intratumourally. Neutralising antibodies for CVA21 were profiled over the course of the study and found to increase after consecutive treatments with CVA21. Furthermore, there was a statistically significant increase in survival time of mice treated with CVA21 compared to saline, or gemcitabine treated mice (P = 0.0021). Gemcitabine proved ineffective at controlling PC either as a single agent, or when combined with CVA21. Moreover, the profound toxic effects of gemcitabine reduced the welfare of mice such that the majority had to be euthanised due to weight loss. Additionally, there was a diminishing effect of gemcitabine towards the anti-viral

immune response generated towards CVA21 when considering the neutralising antibody profiles of CVA21 treated, and CVA21 plus gemcitabine treated mice.

The final aim of this project was to establish an immune competent mouse model of orthotopic, human ICAM-1 expressing, PC and investigate CVA21 as a treatment, alone, and in combination with immunotherapeutic agents. Generation of the model proved difficult and due to time constraints a reliable and well characterised model was not finalised. As such, investigations of CVA21 in combination with immune checkpoint inhibitors were not undertaken.

Findings from three pilot mouse models, indicated C57BL/6 mice were the optimal strain for generation of an orthotopic PC model that showed hallmark metastatic characteristics of native PC; for example, metastases to liver, spleen, and lung. Secondly, both the surgical procedures to generate orthotopic PC and administration of CVA21 were well tolerated by mice. Finally, immune cell recovery was observed late in pilot model #2 while tumours were maintained and progressed in C57BL/6 mice. In this model, mice were administered 200 µg/antibody/mouse three days prior to tumour inoculation to suppress NK1.1, CD4, and CD8 cells. In contrast, in pilot model #3, when mice were administered 50 µg/antibody/mouse three days prior to tumour inoculation, immune cell recovery occurred earlier in the model and subsequent spontaneous remission of tumours in mice was observed.

In conclusion, the presented data indicate CVA21 as a potential anti-cancer treatment for pancreatic cancer that is generally well tolerated in several mouse models. Further investigations are required to overcome immune-competent animal model limitations and optimise experimental protocols.

Chapter 2

Introduction

2.1 Coxsackievirus A21

Coxsackievirus A21 (CVA21) is a human specific, non-enveloped, 28 nm icosahedral, group C enterovirus with a single strand positive sense RNA genome. CVA21 utilises intercellular adhesion molecule 1 (ICAM-1) and decay accelerating factor (DAF) to invade host cells. Subsequently, exponential viral progeny is produced through hijacking host cellular machinery. Host cell lysis occurs and virus infects nearby and distant cells through systemic spread (Newcombe *et al.*, 2004a; Newcombe *et al.*, 2004b; Shafren, 1998; Shafren *et al.*, 1997; Shafren *et al.*, 1998; Xiao *et al.*, 2001; Xiao *et al.*, 2005). CVA21 causes common cold symptoms upon infection in humans (Parsons *et al.*, 1960; Xiang *et al.*, 2012; Zou *et al.*, 2017). CVA21 is a potential efficacious anti-cancer agent for multiple cancer types in preclinical studies (Au *et al.*, 2011; Au *et al.*, 2007; Au *et al.*, 2005; Berry *et al.*, 2008; Shafren *et al.*, 2004; Skelding *et al.*, 2009). CVA21 is undergoing investigation in clinical trials as treatments for a range of cancer types with promising results (Andtbacka *et al.*, 2015a; Bradley *et al.*, 2014; Hamid *et al.*, 2017). Investigation of CVA21 as a treatment for pancreatic cancer in clinical trials will hopefully commence in the near future. Refer to Figure 1 to view the structure of CVA21.

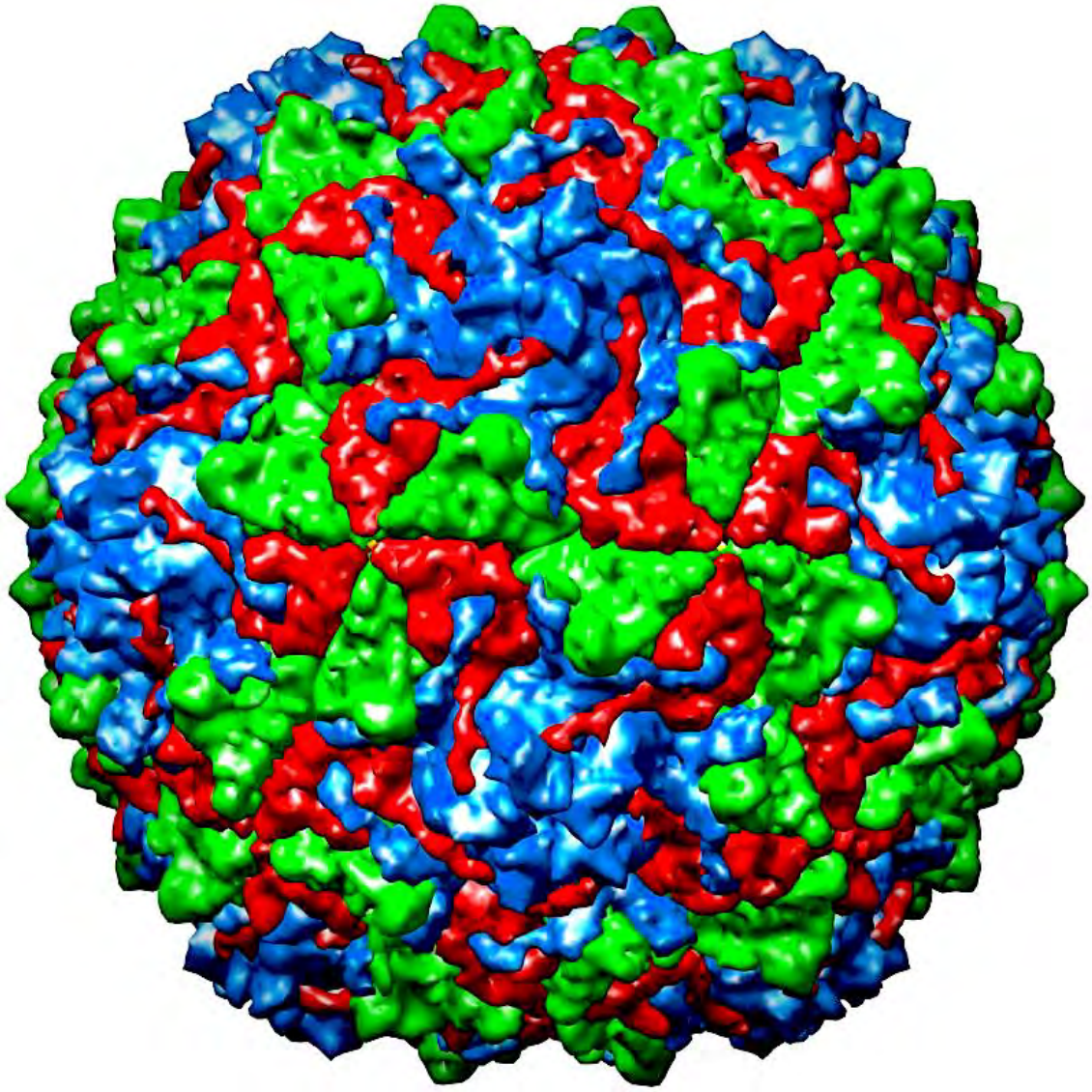

Figure 1: The crystal structure of Coxsackievirus A21 at a resolution of 3.2 *Å*. Image source: **Xiao, C., Bator-Kelly, C. M., Rieder, E., Chipman, P. R., Craig, A., Kuhn, R. J., Wimmer, E. and Rossmann, M. G.** (2005). The crystal structure of coxsackievirus A21 and its interaction with ICAM-1. *Structure* **13**, 1019–1033.

2.1.1 Discovery of Coxsackievirus A21

In 1952 an unknown virus was isolated from a stool sample of a 17-year-old male in California. The unidentified strain was designated Kuykendall. The patient had a dual infection with poliovirus which was thought to be the cause of his paralytic poliomyelitis (Fields *et al.*, 1996). Later, in California from 1954 to 1956 strains of an unknown virus were isolated from throat swabs of four hospitalised patients with acute respiratory disease. The unknown strain was referred to as Coe (Lennete *et al.*, 1958). By 1959 the Coe strain had been isolated from air force personnel in Britain experiencing fever, pharyngitis and cough (Jordan, 1960; Pereira and Pereira, 1959). Later the two strains, Kuykendall and Coe, were serologically identified as identical strains belonging to group A Coxsackie viruses. The strain was assigned Coxsackievirus A21 (Schmidt *et al.*, 1961; Sickles *et al.*, 1959).

2.1.2 Pathogenicity of Coxsackievirus A21

Investigations into the pathogenesis of CVA21 in human volunteers were conducted in the 1960's and determined illness resulted 2-4 days after infection and was characterised by mild upper respiratory illness: coryza, sore throat, malaise, headache and sometimes nausea. Such studies also identified that CVA21 was transmissible in humans, maintained infectivity after passaging in human tissue culture, and was neutralised by antisera (Parsons *et al.*, 1960; Spickard *et al.*, 1963). In 2008 a study by Xiang, *et al.*, determined from 6942 patients with acute respiratory tract infections admitted to the Peking Union Medical College Hospital, China, 34 patients had potential CVA21 infections. Reported symptoms included pharyngeal congestion, headache, myalgia, chills, and sore throat (Xiang *et al.*, 2012). Natural transmission of CVA21 was recently reported in 2016 by the respiratory infections surveillance system of Guangdong Province, China. Twenty-three students and one teacher presented with common-cold like symptoms including fever, sore throat, cough, rhinorrhoea, sneezing, and headache (Zou *et al.*, 2017). A unique case of an enterovirus possibly causing symptoms other than respiratory illness was reported when a four-year-old girl with left thigh swelling was found to have fragments of CVA21 genome detected by reverse transcription-polymerase chain reaction in a muscle tissue biopsy sample. The patient recovered after treatment with corticosteroids. It was noted that the patient's clinical history suggested she had a predilection to enterovirus infection

(Dekel *et al.*, 2002). In comparison to other viruses that cause human diseases, CVA21 is considered low pathogenic and defined as causing common cold symptoms. Moreover, although a common cold virus, CVA21 is not usually the cause of upper respiratory infections (Pereira and Pereira, 1959; Xiang *et al.*, 2012; Zou *et al.*, 2017).

2.1.3 Taxonomy of Coxsackievirus A21

Coxsackievirus A21 (CVA21) belongs to the order of *Picornavirales* and family designated *Picornaviridae*. The most recent Master Species List (2016 v1.3) from the International Committee on Taxonomy of Viruses (ICTV), divides the *Picornaviridae* family into 35 genera. Coxsackievirus comes under the genus of *Enterovirus*, which can be further subdivided by species into *Human Enterovirus (HEV) A, HEV B, HEV C, and HEV D.* CVA21*,* along with Coxsackievirus A 1, 11, 13, 15, 17-22, and 24, and *Poliovirus 1, 2, and 3,* are strains of *HEV C* (Adams *et al.*, 2017; Brown *et al.*, 2009; Brown *et al.*, 2003; King *et al.*, 2011). Refer to Figure 2 for a phylogenetic tree of picornaviruses and CVA21 evolution.

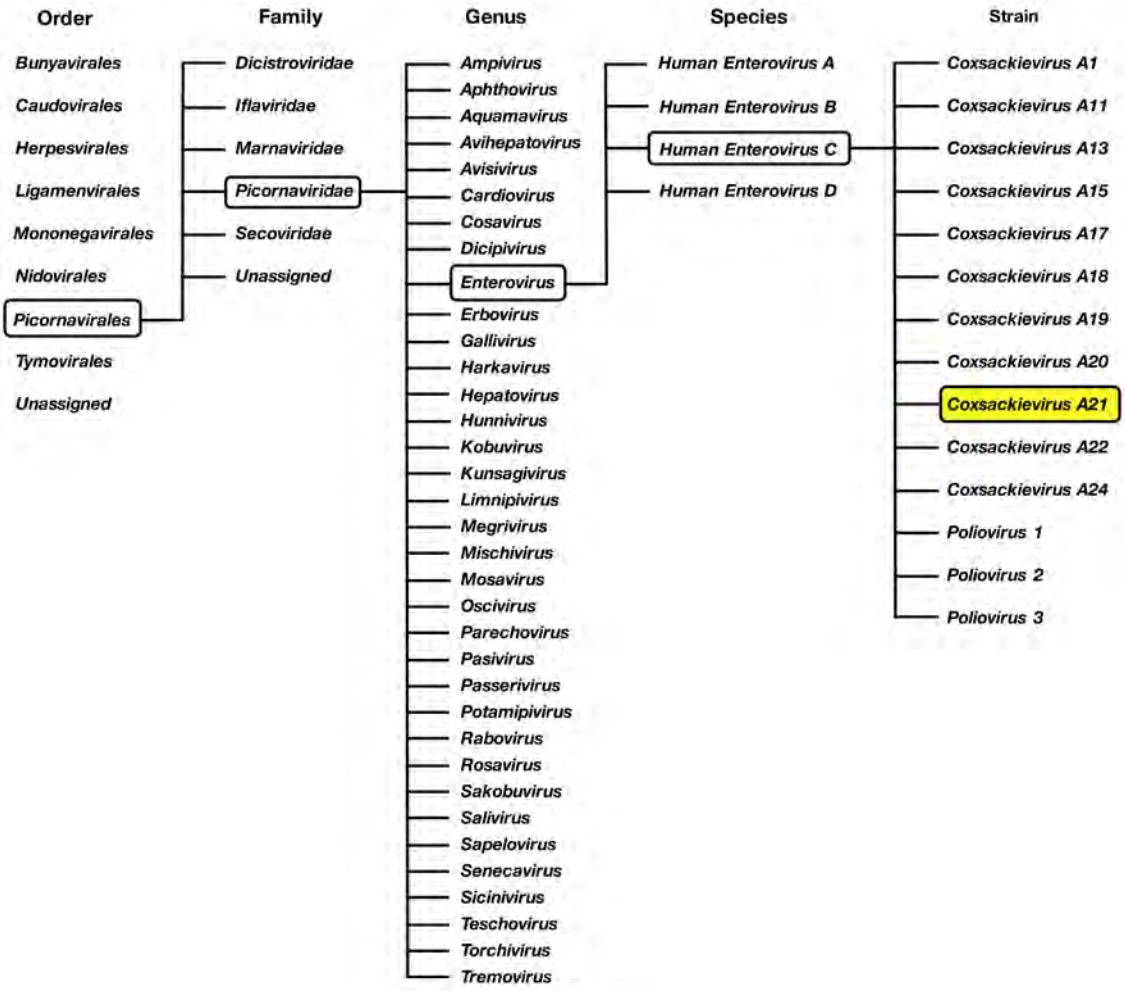

Figure 2: Taxonomy of Coxsackievirus A21. Image compiled from information within the ICTV Master Species List 2016 v1.3 (*talk.ictvonline.org.*).

2.1.4 Overview of Picornavirus Lifecycle

An overview of the obligate intracellular pathogenic lifecycle of a picornavirus (CVA21) is schematically presented in Figure 3. The initial stage of host cell infection by a picornavirus occurs when binding of a virion to host cell surface receptors occurs. Each virus has adapted to utilise specific cell surface receptors to initiate invasion of host cells. Progressive binding of cell receptors leads to invagination of the virus particle by the host cell membrane. Subsequent remodelling of both the virus capsid and host cell membrane and release of genomic RNA into the cytoplasm of host cells occurs. Hijacking of host cell machinery results in translation of viral genomic RNA, replication of viral genomes, and assembly of progeny virions. Concurrently, host cell processes are shut down by viral proteins to favour exponential viral replication and inhibit anti-viral mechanisms. Finally, the host cell is lysed releasing exponential numbers of progeny virus to infect surrounding cells and continue the cycle of viral infection (Boon *et al.*, 2010; Harak and Lohmann, 2015; Jiang *et al.*, 2014; Paul and Wimmer, 2015; Sweeney *et al.*, 2013; Whitton *et al.*, 2005; Zeichhardt *et al.*, 1985).

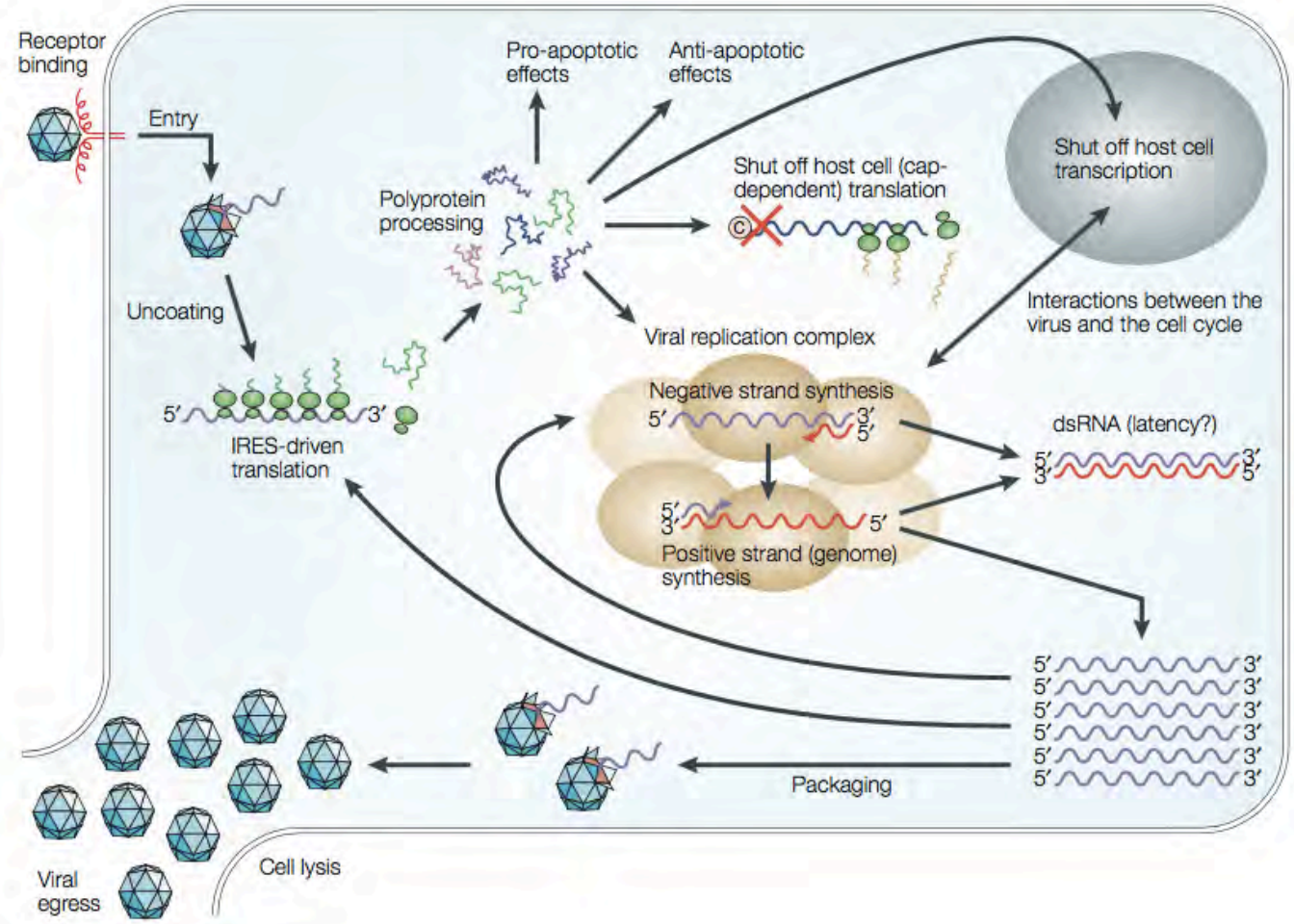

Figure 3: Schematic representation of the picornavirus lifecycle. Copyright © 2005 Nature Publishing Group. Images source: **Whitton, J. L., Cornell, C. T. and Feuer, R.** (2005). Host and virus determinants of picornavirus pathogenesis and tropism. *Nat. Rev. Microbiol.* **3**, 765–776.

2.1.5 Picornaviridae Genome Structure and Processing

Picornaviridae have a single strand of positive-sense ribonucleic acid (RNA) as their genome. Picornavirus genomes are approximately 7400 ribonucleotide bases in length. The Kuykendall strain of CVA21 has a genome of 7405 ribonucleotides (GenBank). Covalently attached to the 5' terminus of picornaviridae genomes is a 20-24 polyuridylic amino acid sequence called viral protein genome-linked (VPg). VPg acts as a primer to recruit host cell translation machinery to the viral genome (Ambros and Baltimore, 1978; Ferrer-Orta *et al.*, 2006; Hyypiä *et al.*, 1997; Nomoto *et al.*, 1977; Steil *et al.*, 2010). The 5' terminus encodes an untranslated region (UTR) that forms *cis*-acting RNA elements. Formation of secondary structures called cloverleaf and internal ribosome entry site (IRES) are involved in docking of host cell ribosomes and initiation of translation. Following the 5' UTR there is a single large open reading frame (ORF) containing eleven genes (Bergamini *et al.*, 2000; Fernandez-Miragall *et al.*, 2009; Jang, 2006; Jang *et al.*, 2017; Martinez-Salas and Fernandez-Miragall, 2004; Svitkin *et al.*, 2001; Sweeney *et al.*, 2013; Yu *et al.*, 2011). At the 3' terminus is a 20-150 adenosine residue poly(A) tail important for initiation of negative-strand RNA synthesis (Ahlquist and Kaesberg, 1979; Paul and Wimmer, 2015; Paulo *et al.*, 2011; Svitkin *et al.*, 2001). Refer to Figure 4 for a schematic depiction of a picornavirus genome structure and cellular processing events discussed hereafter.

Once the viral genome is inside a host cell, the open reading frame is translated into a single polyprotein that elegantly undergoes a pathway of chronologically precise self-cleavage. Proteases, $2A^{pro}$ and $3CD^{pro}/3C^{pro}$, encoded within the viral genome itself, cleave the translated polyprotein to form fragments P1, P2, and P3. P1 is sliced into the structural components of the virus capsid, VP0, VP1, and VP3. Likewise, P2 is divided into $2A^{pro}$ and 2BC. 2BC is then carved into 2B and $2C^{ATP}$ase. $2C^{ATP}$ase is involved in many of the important processes in the life cycle of a virus including uncoating (Li and Baltimore, 1990), host cell membrane binding and remodelling (Aldabe and Carrasco, 1995; Cho *et al.*, 1994; Teterina *et al.*, 1997), RNA transcription (Barton and Flanegan, 1997; Li and Baltimore, 1988; Paul *et al.*, 1994; Teterina *et al.*, 1992), and capsid formation (Liu *et al.*, 2010; Vance *et al.*, 1997; Wang *et al.*, 2012a). Fragment P3 is also divided into 3AB and $3CD^{pro}$. 3AB is further cleaved into proteins 3A and 3B (VPg). Finally, $3CD^{pro}$ divides itself into $3C^{pro}$ and $3D^{pol}$. $3D^{pol}$ is an RNA dependent RNA polymerase that is central to the transcription of the negative-strand

viral RNA genome, and subsequent elongation of positive-strand RNA viral genomes for integration into viral progeny (Barton and Flanegan, 1997; Ferrer-Orta *et al.*, 2006; Jiang *et al.*, 2014; Paul and Wimmer, 2015; Rohayem *et al.*, 2006; Steil *et al.*, 2010).

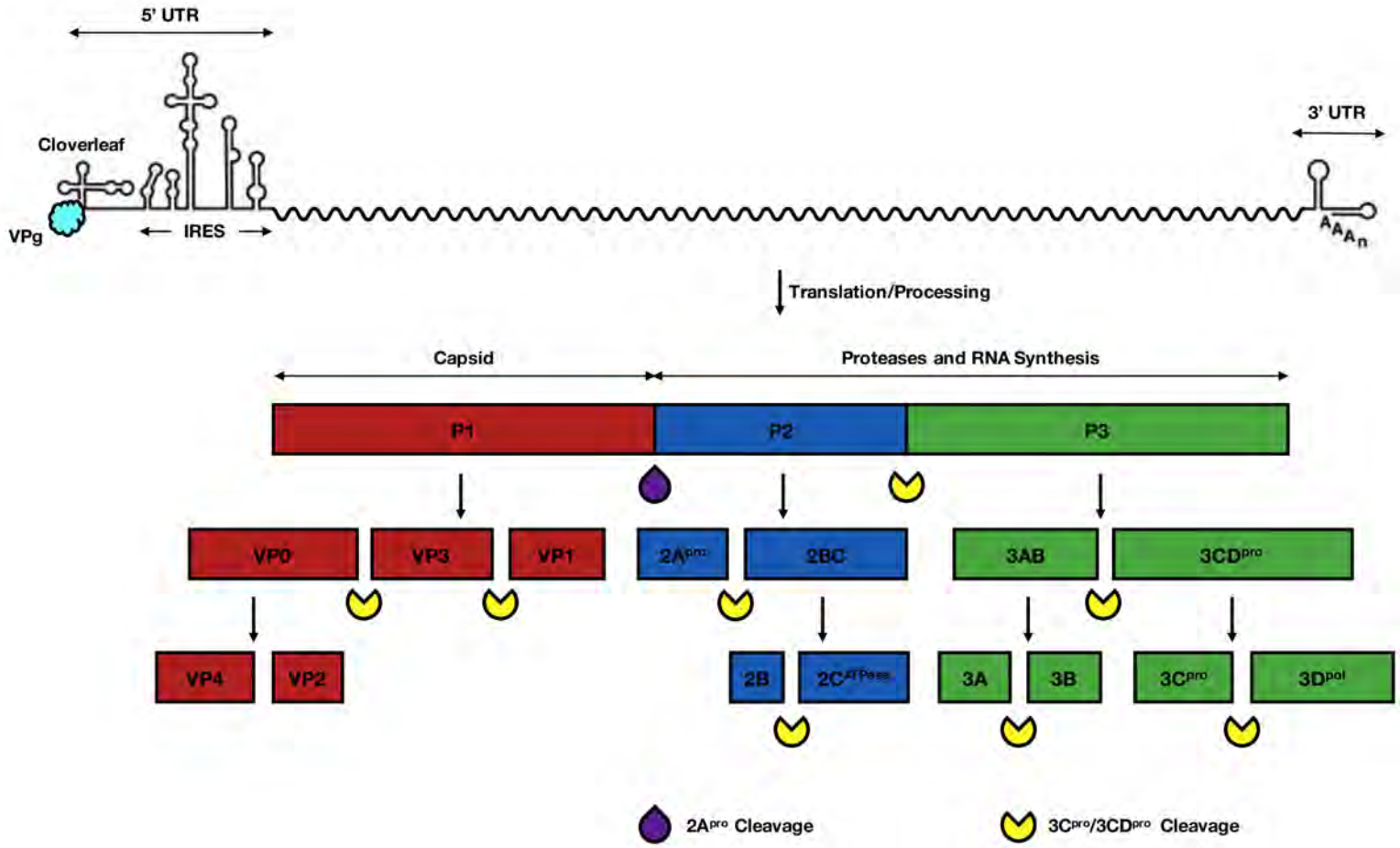

Figure 4: Picornaviridae genome structure and processing. The positive-sense RNA genome of Picornaviridae contains a 5' UTR bound to VPg, followed by a single large ORF, and ends with a 3' UTR poly(A) tail. The immature polyprotein translated from the ORF undergoes a cleavage pathway by proteases $2A^{pro}$ and $3C^{pro}/3CD^{pro}$ to form mature proteins VP0, VP3, VP1, $2A^{pro}$, 2B, $2C^{ATPase}$, 3A, 3B (VPg), $3C^{pro}$, and $3D^{pol}$. VP0 is further cleaved into VP4 and VP2 through an autocatalytic mechanism dependent on RNA encapsidation. Adapted from ***Paul, A. V. and Wimmer, E.*** *(2015). Initiation of protein-primed picornavirus RNA synthesis. Virus Res.* ***206****, 12–26.*

2.1.6 Picornavirus Morphogenesis and Structure

Once transcribed, the structural proteins VP0, VP3, and VP1 immediately associate to form protomers (Ansardi *et al.*, 1992; Lee and Chow, 1992; Martín-Belmonte *et al.*, 2000). Five protomers assemble to form a pentamer, and subsequently, twelve pentamers form a procapsid. There is still debate at which point viral genomic RNA is incorporated during the assembly of the provirion. It is thought that pentamers assemble to form a procapsid around viral RNA forming a provirion, or, the procapsid forms and then viral RNA is shuttled in to form a provirion (Jiang *et al.*, 2014; Nugent and Kirkegaard, 1995; Putnak and Phillips, 1981a; Putnak and Phillips, 1981b; Rombaut *et al.*, 1990; Verlinden *et al.*, 2000). The final process in picornavirus morphogenesis, is an autocatalytic reaction dependent on RNA encapsidation, causing VP0 to cleave into VP2 and VP4. The resulting conformational rearrangement stabilises the formation of an icosahedral virion (Basavappa *et al.*, 1994; Goodwin *et al.*, 2009; Hogle *et al.*, 1985; Jiang *et al.*, 2014; Schneemann, 2006).

The final icosahedral structure of a picornavirus is approximately 28 nm in diameter and consists of 60 protomers, each containing VP1, VP2, VP3, and VP4. VP1, VP2, and VP3 are exposed to the surface of the virus, while VP4 is tucked under on the internal surface. The 60 protomers exhibit 180 β-barrel tertiary structures conforming to two-fold linear, three-fold triangular and five-fold pentagonal symmetry. Distinct protrusions on the virus capsid are formed as a result of these interactions. Star shaped plateaus called mesa are present at the five-fold axes of symmetry, while cavities, termed canyons encircle the mesa. Picornavirus cell surface receptors commonly, but not exclusively, bind in these canyons leading to host cell invasion (Hewat *et al.*, 2000; Newcombe *et al.*, 2003; Rossmann and Johnson, 1989; Xiao *et al.*, 2001; Xiao *et al.*, 2005). Refer to Figure 5 for a diagram of a picornavirus structure.

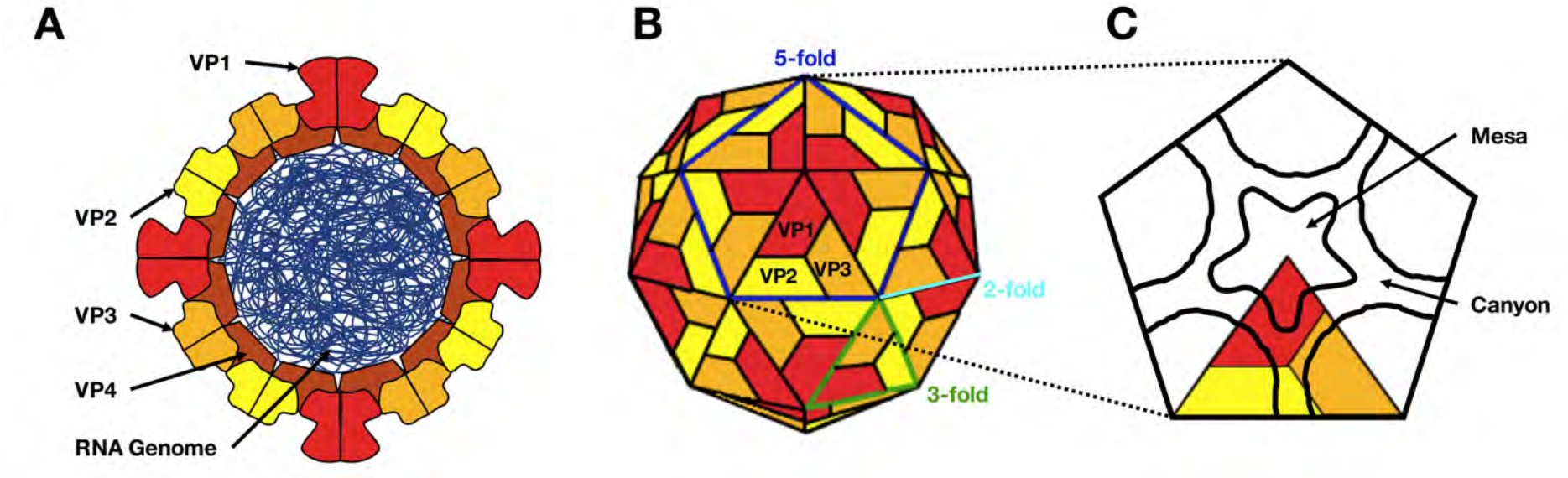

Figure 5: Picornavirus Structure. A: Cross-section at 2-fold symmetry of a picornavirus depicting protomers of VP1, VP2, VP3, and VP4 that make up the viral capsid and encase the RNA genome. B: Picornavirus displaying classic icosahedral shape with 5-fold symmetry (blue), 3-fold symmetry (green), and 2-fold symmetry (cyan). C: Overlay of the raised plateau: mesa, and the continuous cleft: canyon, in relation to protomers. Adapted from: **Jiang, P., Liu, Y., Ma, H. C., Paul, A. V. and Wimmer, E.** (2014). Picornavirus Morphogenesis. Microbiology and Molecular Biology Reviews **78**, 418–437.

2.1.7 Coxsackievirus A21 Cell Surface Receptors

CVA21 utilises intercellular adhesion molecule 1 (ICAM-1/CD54) and decay-accelerating factor (DAF/CD55) to invade host cells. ICAM-1 is essential for cell invasion, whereas, DAF facilitates invasion by sequestering virus particles to the cell surface (Banks *et al.*, 1993; Hayes and Seigel, 2009; Newcombe *et al.*, 2004b; Newcombe *et al.*, 2004a; Shafren *et al.*, 1997). CVA21 anchors to cell surface DAF at short consensus repeat unit 1 (SRC1). The binding is postulated to span canyon regions on the viral capsid at two-fold symmetry axes (Bhella *et al.*, 2004; Shafren, 1998; Shafren *et al.*, 1997). The N-terminal domain of ICAM-1 binds to CVA21 with high affinity in the canyon region of the capsid inducing conformational changes in capsid structure leading to host cell invasion (Rossmann *et al.*, 2002; Xiao *et al.*, 2001; Xiao *et al.*, 2005). Refer to Figure 6 for a depiction of the crystal structure of CVA21 and binding to ICAM-1.

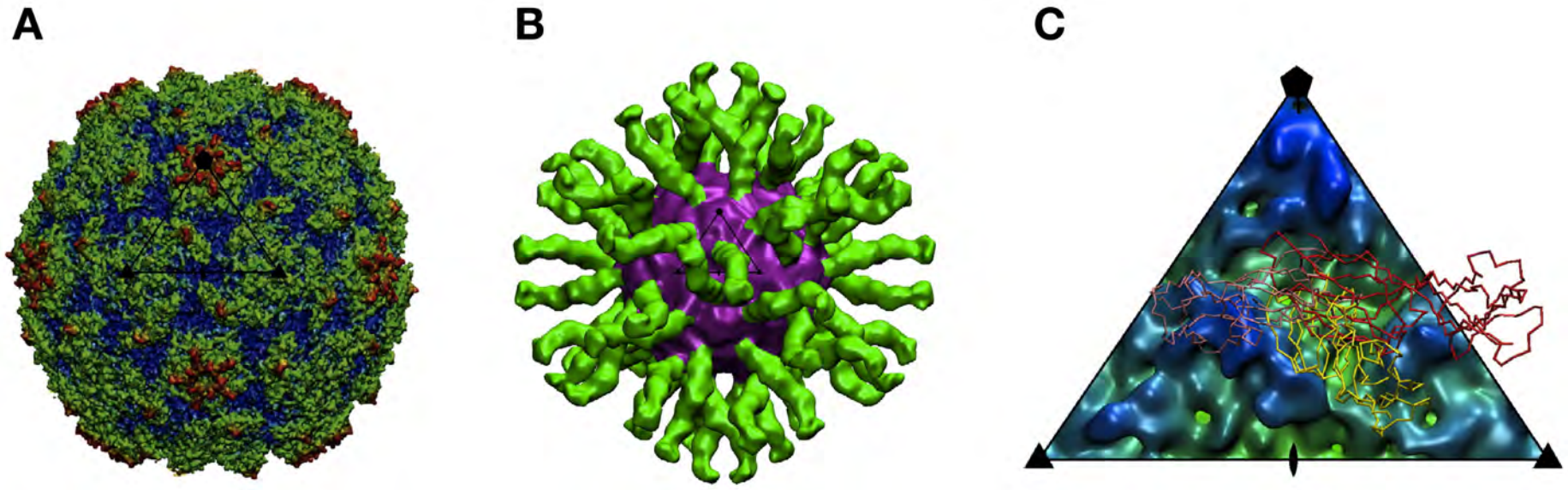

Figure 6: Coxsackievirus A21 binding to intercellular adhesion molecule 1. A: Crystal structure of CVA21 at a resolution of 3.2 Å showing the depressed canyon around each five-fold axis (mesa). B: Stereo view of CVA21 complexed with ICAM-1 calculated to a resolution of 26 Å. C: Binding of N-terminal domain of ICAM-1 with CVA21 capsid at a resolution of 8Å. Five-fold axes depicted by pentagons, three-fold axes depicted by triangles, two-fold axes represented by ellipses. Adapted from **Xiao, C., Bator-Kelly, C. M., Rieder, E., Chipman, P. R., Craig, A., Kuhn, R. J., Wimmer, E. and Rossmann, M. G**. (2005). The crystal structure of Coxsackievirus A21 and its interaction with ICAM-1. Structure **13**, 1019–1033.

2.1.7.1 Intercellular Adhesion Molecule 1 (ICAM-1)

ICAM-1 is a transmembrane glycoprotein of the immunoglobin family of adhesion molecules and is continuously expressed at basal levels on several cell types including fibroblasts, leukocytes, epithelial and endothelial cells. The structure of ICAM-1 consists of five extracellular immunoglobin G-like domains, a transmembrane region, and a small cytoplasmic domain. ICAM-1 binds to lymphocyte function associated antigen 1 (LFA-1) (Binnerts *et al.*, 1994; Newton *et al.*, 2015; Teijeira *et al.*, 2017; Van Seventer *et al.*, 1990; Wawryk *et al.*, 1989) and macrophage antigen 1 (MAC-1). ICAM-1 is involved in numerous immunological and inflammatory processes such as trafficking of inflammatory cells to sites of inflammation, microbiological infections, cell-cell signalling, signal transduction pathways (Diamond and Springer, 1993; Diamond *et al.*, 1990; Diamond *et al.*, 1991; Hubbard and Rothlein, 2000; Marlin and Springer, 1987; Meisel *et al.*, 1998; Smith *et al.*, 1989; Staunton *et al.*, 1988) and directly involved in tumour progression and metastases (Hayes and Seigel, 2009; Howard *et al.*, 2014; Liang *et al.*, 2008; Lin *et al.*, 2006; Roland *et al.*, 2007; Rosette *et al.*, 2005; Tempia-Caliera *et al.*, 2002; Wang *et al.*, 2005). Indeed, studies have consistently shown that ICAM-1 is overexpressed in pancreatic cancer (Banks *et al.*, 1993; Brand *et al.*, 2011; Hayes and Seigel, 2009; Jenkinson *et al.*, 2015; Mohamed *et al.*, 2016; Tempia-Caliera *et al.*, 2002). Expression of ICAM-1 on cells is predominantly transcriptionally regulated by nuclear factor kappa-light-chain-enhancer of activated B cells (NF-κB) binding to the promoter region of the ICAM-1 gene. NF-κB can be activated by multiple cytokines such as tumour necrosis factor α (TNFα), interleukin 1 (IL-1), and interferon gamma (IFN-γ) (Hayes and Seigel, 2009; Hubbard and Rothlein, 2000; Papi and Johnston, 1999; van de Stolpe and van der Saag, 1996).

2.1.7.2 Decay Accelerating Factor

DAF is a 70 kDa membrane bound glycoprotein consisting of four short consensus repeating units with a glycosylphosphatidylinositol (GPI) anchor attached to the C-terminal domain that docks the protein to the external side of a cell membrane. DAF is broadly expressed on haematopoietic and non-haematopoietic cells. DAF regulates the complement mediated cell lysis cascade by binding to intermediate constituents of protein complexes (C3 and C5 convertases) that would otherwise lead to host cell

destruction (Brodbeck *et al.*, 1996; Lublin and Atkinson, 1989; Medof *et al.*, 1984; Newcombe *et al.*, 2003). DAF is upregulated in many neoplasms suggesting circumvention of the complement mediated pathway by cancer cells (Liu *et al.*, 2005). To date, the transcriptional regulation of DAF has not been reported in the literature.

2.2 Pancreatic Cancer

Pancreatic cancer (PC) is the deadliest of all cancer types (Lennon *et al.*, 2014). Reliable early detection and screening mechanisms are non-existent. Treatments that control disease progression while providing adequate quality of life to patients are not currently available. Besides extremely rare cases of PC treatment success, diagnosis is almost always followed by mortality after a short period of time.

2.2.1 The Healthy Pancreas

The pancreas is a glandular organ, approximately 12-15 cm in length located within the abdominal cavity behind the stomach. The pancreas is divided into three regions, the head, neck, and tail. The pancreas has two main ducts that lead into the duodenum, the main pancreatic duct, and the accessory pancreatic duct. The organ has both exocrine and endocrine functions. Approximately 90% of the organ is made up of acini cells that fulfil the exocrine functions of the organ. Acini cells produce digestive enzymes that drain into the main pancreatic duct and eventually the small intestine to assist further digestion of carbohydrates, lipids and proteins. The endocrine functions of the organ are executed by islets of Langerhans that produce several important hormones, including insulin, glucagon, somatostatin and pancreatic polypeptide. (Tortora and Derrickson, 2008). Refer to Figure 7 for a depiction of a normal pancreas *in situ*.

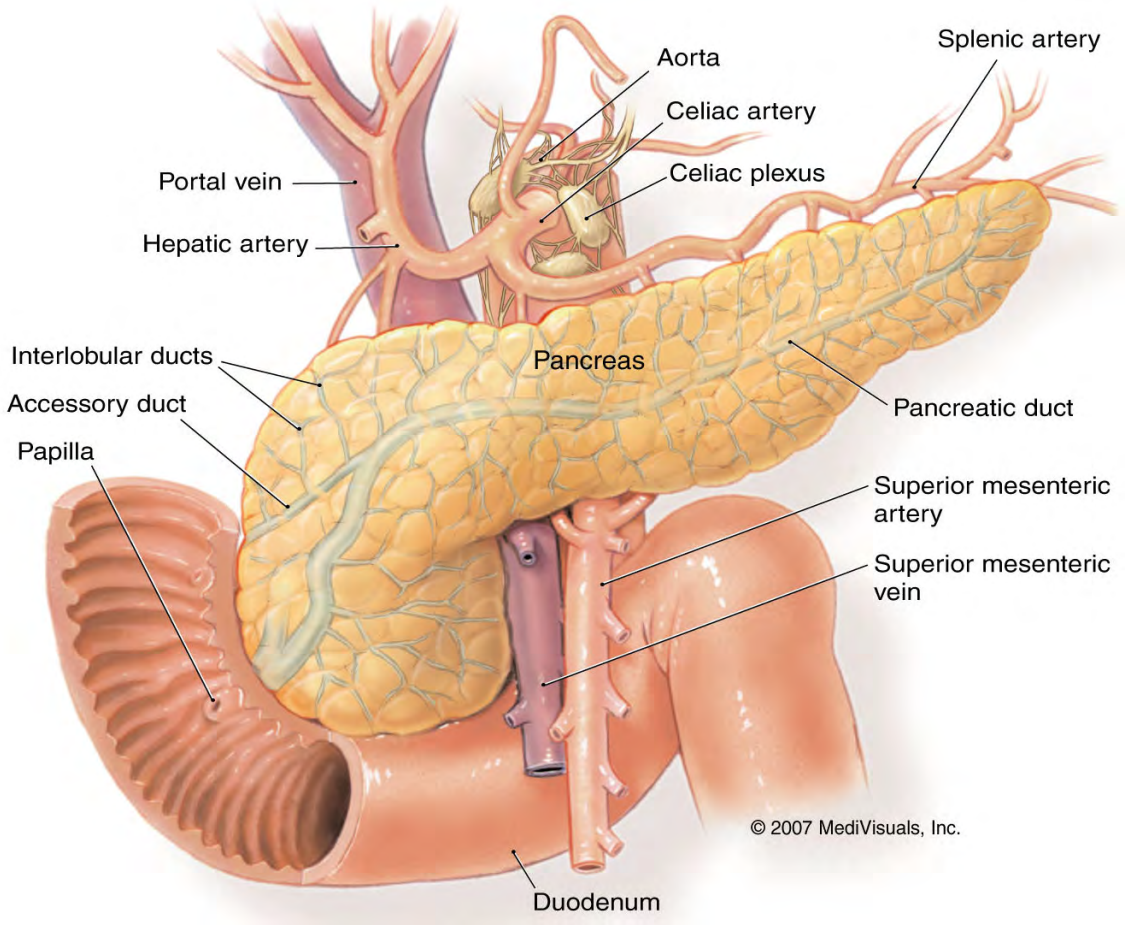

Figure 7: The Pancreas *in situ*. Image source: MedVisuals, Inc. © 2007.

2.2.2 Pancreatic Cancer Symptoms

During early stages of PC development, disease is often asymptomatic, or patients present with broad, non-specific symptoms that could be indicative of numerous illnesses. Consequently, diagnosis of PC is considerably difficult in early stages. Patients have presented with intermittent, non-specific symptoms, such as abdominal pain, appetite changes and tiredness as early as three years before correct diagnosis (Holly *et al.*, 2004; Mills *et al.*, 2017). Consequently, by the time of accurate diagnosis or presentation of clinical symptoms, up to 90% of patients have advanced disease with metastases to distant sites and are ineligible for surgical resection (Muniraj *et al.*, 2013).

Common debilitating symptoms of PC include severe abdominal and back pain, nausea, lethargy, loss of appetite and weight loss that can lead to anorexia, diarrhoea,

constipation, vomiting, exhaustion, fatigue, anaemia, itching, loss of sleep, depression and anxiety. Patients frequently have jaundice due to obstruction of the common bile duct and can develop diabetes mellitus and pancreatitis alongside PC (Boulay and Parepally, 2014; Evans *et al.*, 2014; Gobbi *et al.*, 2013; Gullo *et al.*, 2001; Hippisley-Cox and Coupland, 2012; Holly *et al.*, 2004; Inoue *et al.*, 2003; Jun and Hong, 2016; Keane *et al.*, 2014; Luchini *et al.*, 2016; Mills *et al.*, 2017; Ridd, 2015; Walter *et al.*, 2016).

2.2.3 Pancreatic Cancer Epidemiology

In 2012 there were an estimated 338,000 people with PC and 331,000 deaths worldwide making PC the seventh most common cause of cancer deaths. PC is most common in North America, Europe, Australia and New Zealand, and least frequent in Africa. The average five-year relative survival rate globally is approximately 6% (ranges from 2% to 9%) (Ferlay *et al.*, 2015; Ilic and Ilic, 2016).

In Australia, PC is the fifth leading cause of cancer deaths. PC has a one-year relative survival rate of 27.7% and the lowest five-year relative survival rate of any cancer type at 7.7%. Since 1984 the five-year relative survival rate has increased marginally by 4.3%. In 2017 there are expected to be 3,217 new cases and 2,915 deaths, a total of 6.1% of all cancer deaths. The lifetime risk of developing PC is 1.4%. Rates of incidence and mortality are gradually increasing (AIHW, 2017).

The statistics for PC in the U.S. reflect those of Australia. PC is the fourth leading cause of cancer deaths and has the lowest 5-year relative survival rate at 8.2%. The survival rate has increased by 5% since 1975. In 2017, there were an estimated 53,670 new cases of PC, and 43,090 deaths, a total of 7% of cancer deaths. The lifetime risk of developing PC is 1.3%. (Howlader *et al.*, 2017; Siegel and Jemal, 2017; Siegel *et al.*, 2017). By 2030, PC in the U.S. is predicted to surpass breast, prostate, and colorectal cancers to become the second leading cause of cancer deaths; second only to lung cancer (Rahib *et al.*, 2014).

2.2.4 Pancreatic Cancer Risk Factors

2.2.4.1 Genetic Factors

The risk of PC increases steeply after 55 years of age. Approximately 80% of PC patients are diagnosed between the ages of 60 and 80 years. Average age at diagnosis is 71 years. It is very rare for an individual to have PC under the age of 25 and uncommon under the age of 45 (Ahlgren, 1996; Aoki and Ogawa, 1978; Ghadirian *et al.*, 2003; Gold, 1995; Muniraj *et al.*, 2013; National Cancer Institute, 2017; Pandol *et al.*, 2012; Siegel and Jemal, 2017; Siegel *et al.*, 2017). PC is slightly more common in males potentially because of higher cigarette smoking rates. In the U.S. from 2012-2014 the age-adjusted incidence rate was 14.2 in 100,000 males and 11.1 in 100,000 females (Ilic and Ilic, 2016; Iodice *et al.*, 2008; Kunk *et al.*, 2016; Muniraj *et al.*, 2013; National Cancer Institute, 2017). Individuals with O blood types have been found to have a significantly lower risk of PC compared to non-O blood types (Amundadottir *et al.*, 2009; Wolpin *et al.*, 2009; Wolpin *et al.*, 2010). Hereditary syndromes from autosomal dominant gene mutations such as hereditary pancreatitis (*PRSS1*, *SPINK1*) Peutz–Jeghers syndrome (*STK11*), fragile X syndrome (*FMRI*), familial atypical multiple mole melanoma (*p16/CDKN2A*), familial breast or ovarian cancer (BRCA1, BRCA2, PALB2), Lynch syndrome (*MSH2*, *MLH1*) familial adenomatous polyposis (*APC*) have marked increased risk of PC development. Likewise, a family history of PC correlates with an increased risk of developing the disease (Chang *et al.*, 2014; Colvin and Scarlett, 2014; Gall *et al.*, 2015; Ghadirian *et al.*, 2003; Ghiorzo, 2014; Moutinho-Ribeiro *et al.*, 2017; Muniraj *et al.*, 2013; Sarnecka *et al.*, 2016; Scarlett *et al.*, 2011b).

2.2.4.2 Environmental Factors

Cigarette smoking is well documented as the major environmental factor in the development of PC. Cigarette smoking increases the risk of PC by 75% and accounts for 20-25% of all PC cases. Studies have determined the risk increases by 1% for each year of smoking and by 16% for every decade of smoking. Passive smoking can double the risk of PC. Furthermore, the risks remain elevated up to a decade after cessation (Barone *et al.*, 2016; Barreto, 2016; Blackford *et al.*, 2009; Bosetti *et al.*,

2012; Iodice *et al.*, 2008; Lee *et al.*, 2015; Lugea *et al.*, 2017; Lynch *et al.*, 2009; Vrieling *et al.*, 2010; Weiss and Benarde, 1983; Zhang *et al.*, 2005; Zhang *et al.*, 2017b). Non-genetic pancreatitis and type 2 diabetes mellitus are both diseases correlated with increased risk of development. In fact, diabetes mellitus is inversely related to disease duration (Barone *et al.*, 2016; Gall *et al.*, 2015; Ghadirian *et al.*, 2003; Muniraj *et al.*, 2013; Sarnecka *et al.*, 2016). Obesity, a diet of processed, salty, fried foods and alcohol consumption increases risk, while a diet containing fresh fruits and vegetables has been associated with a lower risk (Baghurst *et al.*, 1991; Bagnardi *et al.*, 2014; Durbec *et al.*, 1983; Ghadirian *et al.*, 2003; Ghadirian *et al.*, 1995; Lee *et al.*, 2015; Lugea *et al.*, 2017; Zhang *et al.*, 2005; Zhang *et al.*, 2017b). Studies have even implied vitamin D production from sun exposure is associated with a lower incidence and mortality rate of PC (Altieri *et al.*, 2017; Bao *et al.*, 2010; Mohr *et al.*, 2010).

2.2.5 Pancreatic Cancer Aetiology

PC develops typically from one of three well-characterised precursor lesions within the pancreas: pancreatic intraepithelial neoplasms (PanINs), intraductal papillary mucinous neoplasms (IPMNs), or mucinous cystic neoplasms (MCNs). Precursor lesions can be present for up to a decade or more before progressing into PC. Progression of precursor lesions is driven by mutations in hallmark PC oncogenes, most notably K-RAS, Tp53, CDKN2A/p16 and SMAD4/DPC4 (Distler *et al.*, 2014; Frič *et al.*, 2017; Hruban *et al.*, 2007a; Lennon *et al.*, 2014; Matthaei *et al.*, 2011; Noë and Brosens, 2016; Patra *et al.*, 2017; Scarlett *et al.*, 2011b; Yonezawa *et al.*, 2008).

2.2.5.1 PanINs

PanINs are the most common of the three precursor lesions and arise from ductal epithelial cells. PanINs can be divided into three grades of dysplasia from minor atypical nuclei (PanIN-1) through to chronic dysplasia or cancer *in situ* (PanIN-3). PanIN-1 is further subdivided into types PanIN-1A and PanIN-1B. Along with telomere shortening, mutation of oncogenes occurs throughout the progression of PanINs and into PC development. Frequent mutations occur in genes including K-RAS, Tp53, SMAD4/DPC4, HER-2/neu, p16/CDKN2A, and BRCA2 (Bryant *et al.*, 2014; Cicenas *et*

al., 2017; Noë and Brosens, 2016; Scarlett *et al.*, 2011b). Refer to Figure 8 for a depiction of PanIN progression from normal ductal epithelial into cancer *in situ*.

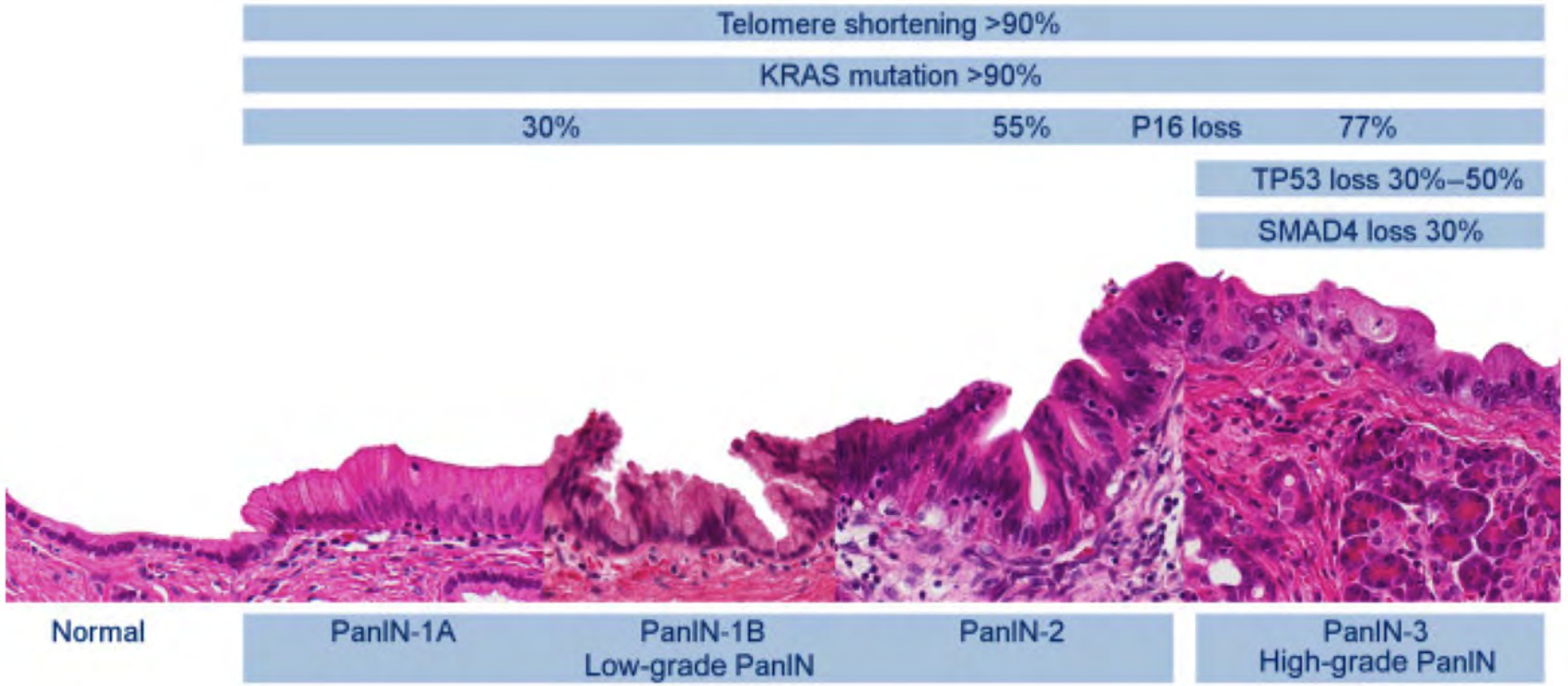

Figure 8: PanIN progression model with genetic aberrations. Adapted from **Noë, M. and Brosens, L. A. A.** (2016). Pathology of Pancreatic Cancer Precursor Lesions. Surgical Pathology **9**, 561–580.

2.2.5.2 IPMNs

IPMNs are mucin producing epithelial neoplasms that typically form in the pancreatic duct or branching ducts. Cells exhibit papillary architecture and produce copious amounts of mucin that often dilates the pancreatic duct (Hruban *et al.*, 2007b). IPMNs are divided into grades of dysplasia: low, intermediate, high, and IPMN with an associated invasive carcinoma (Bosman *et al.*, 2010; Longnecker *et al.*, 2000). Similar to PanINs, IPMNs exhibit mutations in K-RAS, SMAD4/DPC4, Tp53, and CDKN2A/p16 genes. IPMNs also have mutations in GNAS, RNF43, SKT11, Pi3Ks-PKB/AKT, and overexpress MUC4, MUC5AC, claudin 4, CXCR4, S100A4, and mesothelin. CDKN1C/p57KIP2 and MKP-2/DUSP are downregulated in IPMNs (Aronsson *et al.*, 2017; Furukawa *et al.*, 2011; Patra *et al.*, 2017; Scarlett *et al.*, 2011b; Thosani *et al.*, 2010; Wu *et al.*, 2011).

2.2.5.3 MCNs

MCNs are the most infrequent precursor lesion and develop almost exclusively in females. MCNs exhibit mucin producing, columnar epithelial neoplasms supported by a distinct ovarian like stroma. MCNs have cytological similarities to IPMNs, however, MCNs do not develop in the ductal network of the pancreas. MCNs are subdivided into low, moderate, or high grade dysplasia (Bosman *et al.*, 2010; Noë and Brosens, 2016). The molecular pathology of MCNs is not well researched. Mutations in K-RAS, Tp53, CDKN2A/p16 and SMAD4/DPC4 genes are documented throughout the progression of MCNs. Wild-type GNAS and RNF43 are present in MCNs allowing distinction on a molecular level from IPMNs (Fujikura *et al.*, 2017; Patra *et al.*, 2017; Scarlett *et al.*, 2011b).

2.2.6 Pancreatic Cancer Genomic Subtypes

Mutational studies of PC genomes identified 32 persistently aberrant genes that collectively represent 10 molecular pathways: K-RAS, TGF-β, WNT, NOTCH, ROBO/SLIT signalling, G1/S transition, SWI-SNF, chromatin modification, DNA repair and RNA processing. Based on expression profiles PC can be divided into four

subtypes: squamous, pancreatic progenitor, immunogenic, and aberrantly differentiated endocrine exocrine (ADEX). Understanding a patients molecular evolution of PC can identify appropriate treatment regimens on an individual patient level (Bailey *et al.*, 2016; Biankin *et al.*, 2012; Cowley *et al.*, 2013; Jones *et al.*, 2008; Waddell *et al.*, 2015; Wang *et al.*, 2012b). Refer to Figure 9 for a depiction of the profiling of genomic subtypes of pancreatic cancer.

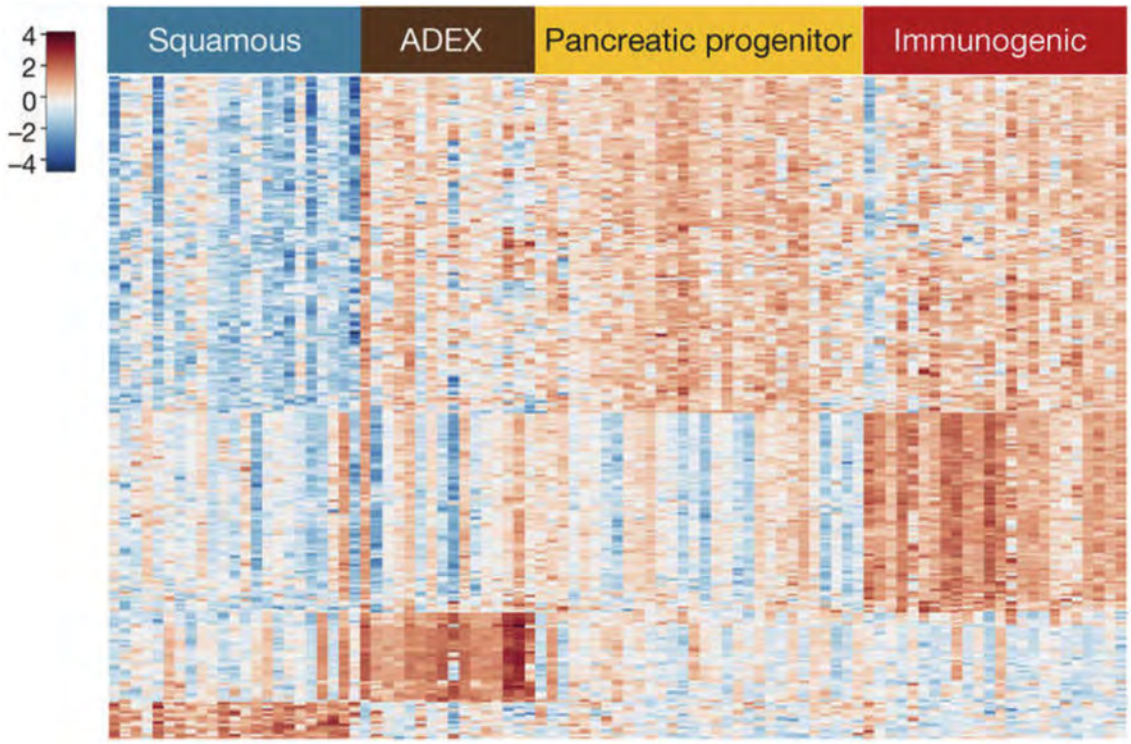

Figure 9: Genomic Subtypes of Pancreatic Cancer. RNA sequencing analyses by Bailey *et al.* revealed four distinct molecular subtypes of PC: Squamous, aberrantly differentiated endocrine exocrine (ADEX), pancreatic progenitor, and immunogenic. Adapted from **Bailey, P., Chang, D. K., Nones, K., Johns, A. L., Patch, A.-M., Gingras, M.-C., Miller, D. K., Christ, A. N., Bruxner, T. J. C., Quinn, M. C., *et al.*** (2016). Genomic analyses identify molecular subtypes of pancreatic cancer. Nature **531**, 47–52.

2.2.6.1 Squamous

K-RAS, Tp53, KDM6A and Tp63ΔN gene mutations, hypermethylation silencing of genes that regulate pancreatic endodermal cell-fate determination (for example HNF1B PDX1, GATA6, MNX1), and upregulation of EGF and α6β1, α6β4 integrin signalling are common genomic irregularities of squamous type PC. Genomic abnormalities lead to increased inflammation, TGF-β signalling, hypoxia response,

MYC pathway activation, metabolic reprogramming, upregulated expression of TP63ΔN and its target genes, and autophagy (Bailey *et al.*, 2016).

2.2.6.2 Pancreatic Progenitor

Characteristic mutations of pancreatic progenitor type PC include K-RAS, Tp53, CDKN2A and SMAD4/DPC4. Dysregulation of signalling pathways including transcription factors PDX1, HNF4G, HNF4A, HNF1B, HNF1A, MNX1, HES1, FOXA2 and FOXA3 predominantly define pancreatic progenitor type PC. Pancreas endodermal cell lineage signalling is disrupted because of this atypical expression. Additionally, regulation of O-linked glycosylation of mucins, steroid hormone biosynthesis, fatty acid oxidation, and drug metabolism are affected through co-expression of MUC5AC and MUC1, but not MUC2 or MUC6, and inhibition of TGFBR2. (Bailey *et al.*, 2016; Hale *et al.*, 2005).

2.2.6.3 ADEX

K-RAS, CKDN2A and Tp53 are commonly mutated in ADEX type PC. ADEX are a discrete subtype of pancreatic progenitor type PC because of upregulation of transcriptional factors in signalling pathways involved in later stage pancreatic development and differentiation. Networks include acinar cell differentiation and regeneration through increased NR5A2, RBPJL and MIST1 (Figura *et al.*, 2014; Hale *et al.*, 2014). Upregulation of genes including NKX2-2, MAFA and NEUROD1 increase endocrine cell differentiation. There are also distinct methylation of gene profiles exhibited in ADEX type PC (Bailey *et al.*, 2016).

2.2.6.4 Immunogenic

Immunogenic type PC is similar to pancreatic progenitor type PC such as harbouring mutations in K-RAS, Tp53, CDKN2A and SMAD4/DPC4. However, immunogenic type PC is a distinct subtype because of significant immune infiltration. CD4 and CD8 T cell signalling, B cell signalling, antigen presentation and toll-like receptor signalling pathways are coupled with an immunogenic subtype (Rooney *et al.*, 2015).

Upregulation of PD-1 and CTLA-4 also suggests immunogenic type PC may be more receptive to treatment with immune modulators (Bailey *et al.*, 2016).

2.2.7 Pancreatic Cancer Phenotypes

PC encompasses both malignancies of the endocrine and exocrine pancreas. Around 85-95% of PCs originate from epithelium of pancreatic ducts, termed pancreatic ductal adenocarcinoma (PDAC) (Adamska *et al.*, 2017; Luchini *et al.*, 2016; Muniraj *et al.*, 2013). Tumours originating from acini or Langerhans cells are termed nonductal pancreatic malignancies. Nonductal pancreatic neoplasms comprise up to 5% of pancreatic tumours including pancreatoblastomas, solid pseudopapillary neoplasms (SPN's), acinar cell carcinomas (ACC's), and neuroendocrine tumours. (Jun and Hong, 2016). Refer to Figure 10 for representative images of gross pathology and microscopic features of PC phenotypes.

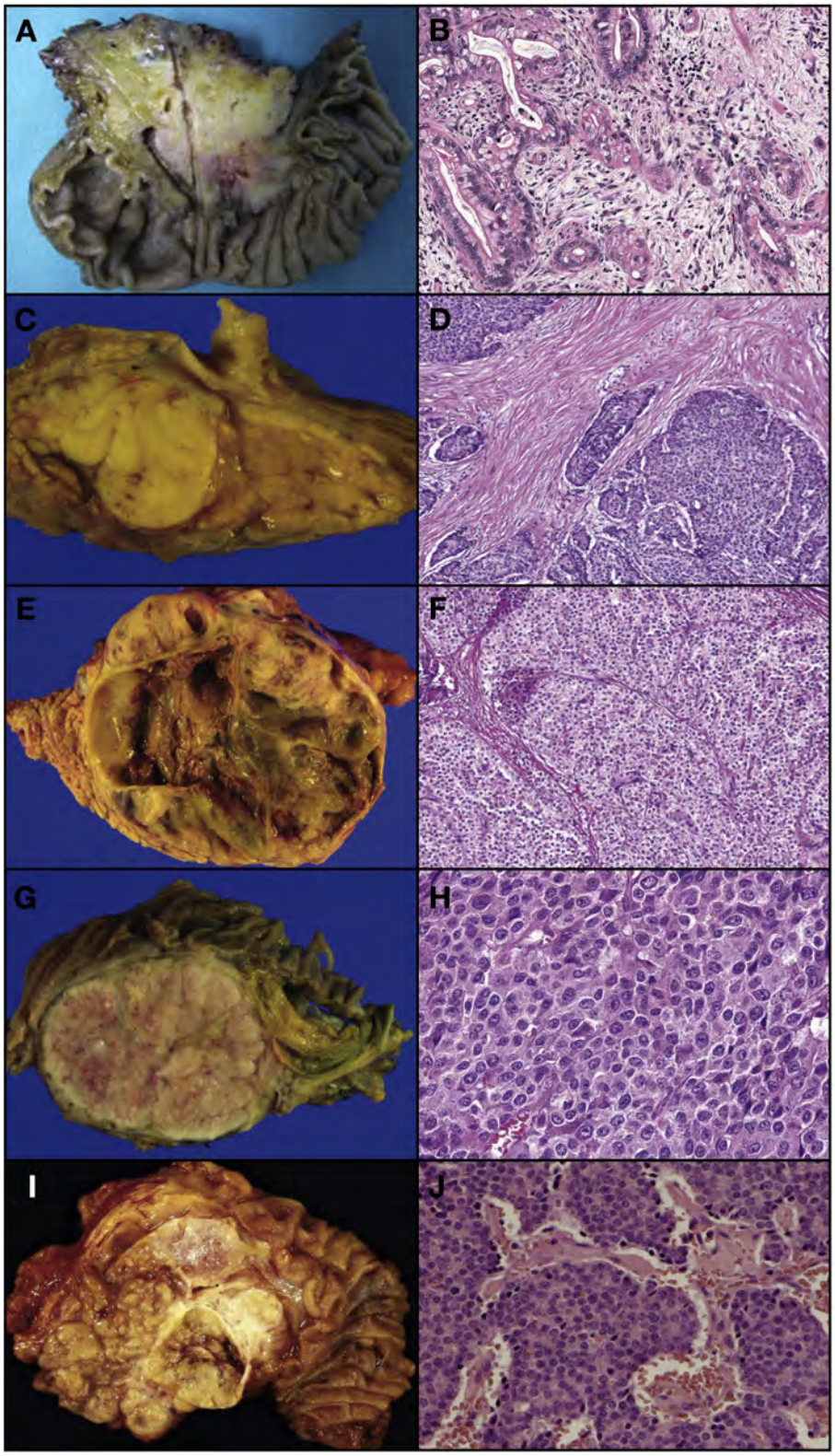

Figure 10: Representative gross pathology (left) and microscopic features (right) of PC phenotypes. (A, B): PDAC, (C, D): Pancreatoblastoma, (E,F): SPN, (G, H): ACC, (I, J): Neuroendocrine Tumour. Magnification: 40-400x. Adapted from: **Luchini, C., Capelli, P. and Scarpa, A.** (2016). Pancreatic Ductal Adenocarcinoma and Its Variants. Surgical Pathology **9**, 547–560 and **Jun, S.-Y. and Hong, S.-M.** (2016). Nonductal Pancreatic Cancers. Surgical Pathology **9**, 581–593 and **Rosenbaum, J. N. and Lloyd, R. V.** (2014). Pancreatic Neuroendocrine Neoplasms. Surgical Pathology **7**, 559–575.

2.2.7.1 PDAC

Sixty to seventy percent of PDAC's are present within the head of the pancreas, while the remaining 30% are equally dispersed between the body and tail. PDAC is usually an isolated neoplasm but occasionally may present with multifocal lesions. Gross pathology of PDAC's are usually white, hard, poorly defined, sclerotic masses that interfere with the normal lobular architecture of the pancreas. Microscopically, PDAC's have differentiated glandular and duct like structures with a dense desmoplastic stromal reaction making up to 80% of the tumour microenvironment. PDAC's commonly obstruct the bile duct causing stenosis and jaundice. Head PDAC's are usually between 1.5-5 cm in diameter, while body and tail PDAC's are commonly larger. The majority of PDAC's at diagnosis have already metastasised, regularly to regional lymph nodes and nearby tissues such as the duodenum and papilla of Vater. Variants of PDAC include adenosquamous carcinoma, colloid carcinoma, undifferentiated or anaplastic carcinoma, signet-ring carcinoma, medullary carcinoma, undifferentiated carcinoma with osteoclastlike giant cells, and finally hepatoid carcinoma (Adamska *et al.*, 2017; Apte *et al.*, 2013; Bosman *et al.*, 2010; Erkan *et al.*, 2012b; Hruban *et al.*, 2007b; Luchini *et al.*, 2016; Sousa *et al.*, 2016; Sun *et al.*, 2016).

2.2.7.2 Nonductal Pancreatic Neoplasms

Pancreatoblastomas are a very interesting case of nonductal PC. Although very infrequent, pancreatoblastomas are more common in children (average age four years) than adults. Pancreatoblastomas are bulky, circumscribed, soft and fleshy neoplasms averaging 11 cm in diameter that are present usually in either the head or tail of the pancreas. Most tumours have lobular architecture and exhibit necrosis, calcification and haemorrhage. Microscopically, squamoid nests of differentiated cells with abundant eosinophilic cytoplasm are surrounded by stromal cells with prominent nuclei (Bien *et al.*, 2011; Bosman *et al.*, 2010; Dhebri *et al.*, 2004; Hosoda and Wood, 2016; Jun and Hong, 2016; Levey and Banner, 1996; Nishimata *et al.*, 2005; Omiyale, 2015; Salman *et al.*, 2013).

SPN's are also very rare, comprising up to 3% of nonductal pancreatic tumours and occur primarily in young females (a ratio of 1:9 males to females). SPN's are

demarcated or partially encapsulated neoplasms averaging 8-10 cm in diameter and occur more frequently in the body and tail of the pancreas. Microscopically, SPN's consist of layers of monomorphic polygonal differentiated cells intermingled with capillary sized blood vessels. Architecture is poorly cohesive and does not exhibit glandular structures (Abraham *et al.*, 2002; Bosman *et al.*, 2010; Jun and Hong, 2016; Law *et al.*, 2014; Lieber *et al.*, 1987; Yang *et al.*, 2016; Yao *et al.*, 2010).

ACC's are isolated bulky soft masses which have well defined boundaries. Most ACC's develop in the head of the pancreas but may be present in any region and average 8-11 cm in diameter. Cystic changes, haemorrhage, necrosis and infiltration into surrounding tissues are present in roughly half of ACC's. Microscopically, ACC's are composed of epithelial like differentiated acinar cells with little stromal reaction. The differentiated acinar cells commonly still express functional digestive enzymes. ACC's exhibit structural patterns of acinar, cribriform, glandular, solid and trabecular (Basturk *et al.*, 2007; Bosman *et al.*, 2010; Cingolani *et al.*, 2000; Fabre *et al.*, 2001; Jun and Hong, 2016; La Rosa *et al.*, 2012; La Rosa *et al.*, 2015; Toll *et al.*, 2011).

Neuroendocrine tumours are an important subpopulation of nonductal pancreatic neoplasms which are the least common PC type, accounting for 1-2% of nonductal pancreatic neoplasms. Neuroendocrine tumours can induce clinical syndromes due to the production of functional hormones. Syndromes include insulinoma, glucagonoma, gastrinoma, somatostatinoma and serotoninoma. Due to the presentation of clinical symptoms early on in the development of neuroendocrine tumours, diagnosis is usually determined earlier than other PC types. Tumours average between 1-5 cm but may grow as large as 20 cm if not diagnosed correctly at the time of clinical presentation. Tumours are usually discrete masses with significant stromal reaction. Calcification, haemorrhage and cystic changes are commonly observed. Microscopically, neuroendocrine tumours exhibit four architectural types: solid, gyriform, glandular or nondescript (undifferentiated or poorly differentiated lesions) (Bosman *et al.*, 2010; Callender *et al.*, 2008; Goh *et al.*, 2006; Klimstra *et al.*, 2010; Kulke *et al.*, 2011; Lewis *et al.*, 2010; Ligneau *et al.*, 2001; Metz and Jensen, 2008; Pereira and Wiskirchen, 2003; Rosenbaum and Lloyd, 2014; Tan and Tan, 2011; Zee *et al.*, 2005).

2.2.8 Pancreatic Cancer Tumour Microenvironment

The pancreatic tumour microenvironment (TME) is composed of uncontrolled proliferative and self-renewing neoplastic cells, non-neoplastic cancer associated fibroblasts (CAFS), inflammatory and immune cells, and extracellular matrix proteins (ECM) such as collagen, fibronectin, hyaluronan and laminin. CAFs become activated through an epithelial to mesenchymal (ETM) transition and manufacture a dense desmoplastic hypoxic stromal reaction contributing up to 80% of the TME (Apte *et al.*, 2015a). The stromal reaction is a multifaceted, well ordered, biological system that intricately cooperates with cancer cells to stimulate tumour progression, metastasis, immune evasion, and therapeutic resistance. PC desmoplasia has become a major focus among PC researchers and many targeted therapies are being developed (Apte *et al.*, 2015a; Apte *et al.*, 2013; Apte *et al.*, 2012; Bolm *et al.*, 2017; Franco *et al.*, 2010; Gebauer *et al.*, 2017; Kalluri and Zeisberg, 2006; Masamune and Shimosegawa, 2013; Masamune and Shimosegawa, 2015; Nielsen *et al.*, 2016a; Orimo and Weinberg, 2014; Rasanen and Vaheri, 2010; Ren *et al.*, 2018; Zhan *et al.*, 2017). Refer to Figure 11 for a depiction of the interactions between the desmoplastic reaction and PC cells.

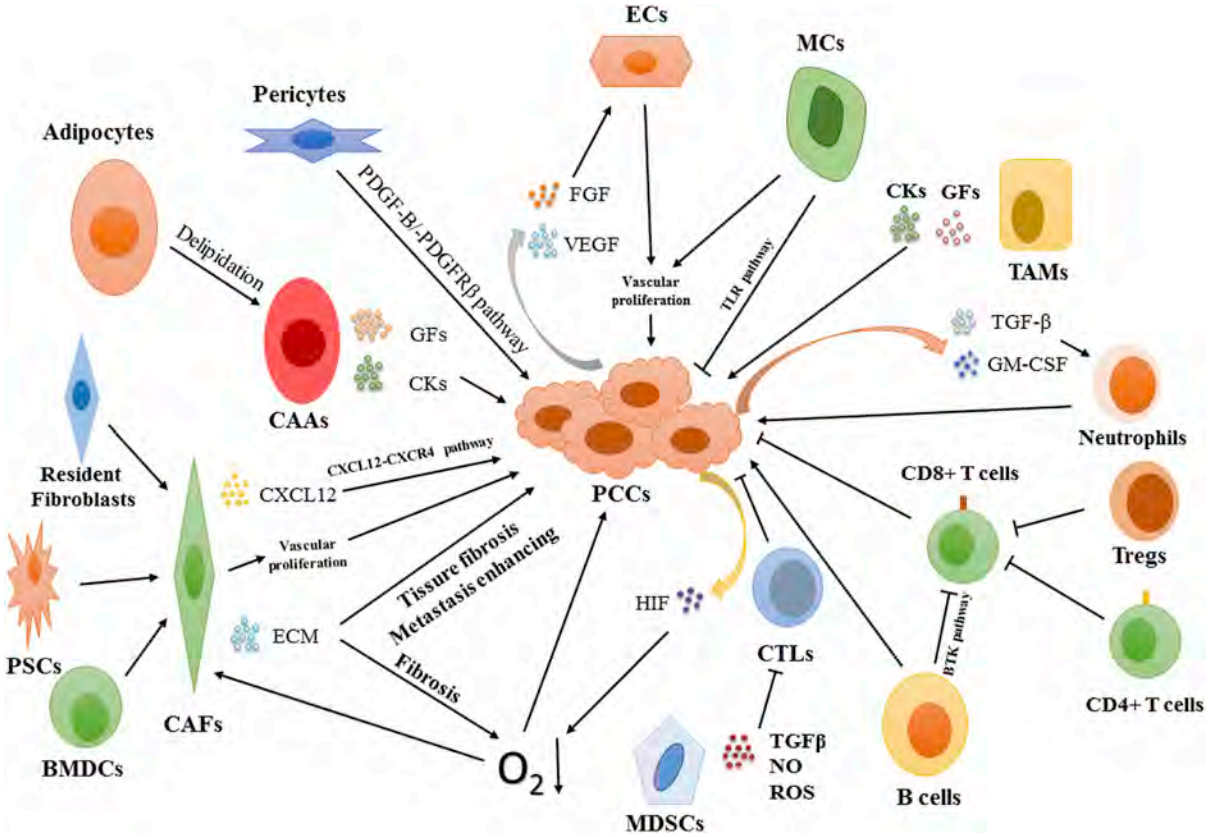

Figure 11: Crosstalk between pancreatic cancer cells (PCCs) and stromal cells. CAFs (Resident fibroblasts, PSCs and bone marrow derived cells [BMDCs]) promote ECM remodelling and tumour progression, metastasis, and chemoresistance through multiple signalling pathways. Immune cells within the TME promote immune suppression and evasion. Cancer associated adipocytes (CAA's) promote inflammation and suppress T cell function. Pericytes promote tumour angiogenesis and metastasis mediated by growth factors and cytokines. MDSC: Myeloid-Derived Suppressor Cell, CTL: Cytotoxic T Lymphocyte, TAM: Tumor-Associated Macrophage, MC: Mast Cell, EC: Endothelial Cell, TAM: Tumor-Associated Macrophage, MDSC: Myeloid-Derived Suppressor Cell, GF: Growth Factor, CKs: Cytokines, CXCL12: Cxc Chemokine Ligand-12, VEGF: Vascular Endothelial Growth Factor, HME: Human Macrophage Metalloelastase, PNT: Peroxynitrite, BTK: Bruton Tyrosine Kinase. Image source: **Zhan, H.-X., Zhou, B., Cheng, Y.-G., Xu, J.-W., Wang, L., Zhang, G.-Y. and Hu, S.-Y.** (2017). Crosstalk between stromal cells and cancer cells in pancreatic cancer: New insights into stromal biology. Cancer Lett. **392**, 83–93.

2.2.8.1 Pancreatic Stellate Cells

Pancreatic stellate cells (PSCs) are the principal CAF and contributor to PC desmoplasia (Apte *et al.*, 2015a; Apte *et al.*, 2012; Apte *et al.*, 2013; Apte *et al.*, 2015b; Erkan *et al.*, 2012a; Pandol *et al.*, 2012; Wilson *et al.*, 2014; Xue *et al.*, 2018; Zhan *et al.*, 2017). In a healthy pancreas, quiescent PSCs make up to 7% of cell population and maintain the physiological ECM around acinar cells. Quiescent PSCs have a central body with long cytoplasmic projections and abundant vitamin A containing lipid droplets (Apte *et al.*, 1998; Bachem *et al.*, 1998; Ikerjiri, 1990; Watari *et al.*, 1982). PSCs become activated early in precursor lesions of PC by cytokines and growth factors including TNFα, IL-1, IL6, IL10, platelet-derived growth factor (PDGF), transforming growth factor β (TGFβ), pigment-epithelium derived factor (PEDF), insulin-like growth factor (IGF-1), trefoil factor 1 (TFF1), and endothelin-1 (ET-1). (Apte *et al.*, 1999; Haqq *et al.*, 2014; Mews *et al.*, 2002; Pandol *et al.*, 2012; Xue *et al.*, 2018). Recall that TNFα and IL-1 are regulators of ICAM-1 expression (Hayes and Seigel, 2009; Hubbard and Rothlein, 2000; Papi and Johnston, 1999; van de Stolpe and van der Saag, 1996). Thus ICAM-1 is postulated to be directly involved in the desmoplastic reaction, progression, and metastasis of PC (Haqq *et al.*, 2014; Liou *et al.*, 2015; Masamune *et al.*, 2002; Tempia-Caliera *et al.*, 2002; van Grevenstein *et al.*, 2006).

Upon activation, PSCs undergo a transformation to exhibit a myofibroblast-like phenotype and star shaped morphology. Activated PSCs have increased proliferation, migration and production of the extracellular matrix proteins comprising the dense stromal reaction of PC. The dense stroma in PC physically inhibits chemotherapeutics from infiltrating tumours. Thus, PSCs can be attributed to conferring chemoresistance. PSCs remain in a perpetually activated and proliferative state due to release of the aforementioned cytokines and growth factors through autocrine signalling. Furthermore, activated PSCs support, promote proliferation, and inhibit apoptosis of cancer cells. Cancer cells in turn support and promote proliferation of PSCs through secreted cytokines and chemokines. Tumour promoting cross-talk is a central component of PC progression and metastasis (Apte *et al.*, 2015b; Apte *et al.*, 1999; Apte *et al.*, 2015a; Apte *et al.*, 2012; Apte *et al.*, 2013; Bynigeri *et al.*, 2017; Ene-Obong *et al.*, 2013; Ferdek and Jakubowska, 2017; Hamada *et al.*, 2014; Hamada *et*

al., 2012; Jaster, 2004; Li *et al.*, 2014; Masamune and Shimosegawa, 2009; Masamune and Shimosegawa, 2013; Masamune and Shimosegawa, 2015; Masamune *et al.*, 2009; McCarroll *et al.*, 2014; Shi *et al.*, 2014; Tien *et al.*, 2009; Vonlaufen *et al.*, 2008; Wilson *et al.*, 2014; Xu *et al.*, 2010).

2.2.8.2 Resident Fibroblasts

Quiescent fibroblasts in the pancreas can be activated by reactive oxygen species (ROS), and cytokines released from cancer cells, particularly vascular endothelial growth factor (VEGF). Activated fibroblasts are myofibroblast-like star shaped cells similar to activated PSCs. Activated fibroblasts express cytoplasmic α smooth muscle actin, and secrete large amounts of ECM proteins including collagen, fibronectin and tenascin C. Thus, like activated PSCs, activated fibroblasts contribute to the dense stromal reaction in PC (Hwang *et al.*, 2008; Kalluri and Zeisberg, 2006; Orimo and Weinberg, 2014; Rasanen and Vaheri, 2010; Zhan *et al.*, 2017).

2.2.8.3 Myeloid-Derived Suppressor Cells

Myeloid-derived suppressor cells (MDSCs) have an increased prevalence in the stromal reaction of PC. MDSCs produce TGFβ, ROS, nitric oxide, and deplete arginine through enzymatic degradation, preventing the activation of T cells. Thus, through immune suppression, MDSCs promote PC progression (Clark *et al.*, 2007; Gabrilovich and Nagaraj, 2009; Goedegebuure *et al.*, 2011; Song *et al.*, 2016; Stromnes *et al.*, 2014; Welte *et al.*, 2016).

2.2.8.4 Mast Cells

Mast cell infiltration in PC stroma is significantly elevated compared to the remainder of the pancreas. Mast cells are responsible for tumour angiogenesis and promote cancer cell and PSC proliferation through cytokine signalling. High concentrations of mast cells in PC are correlated with higher grade tumours and lower survival (Chang *et al.*, 2011; Crivellato *et al.*, 2008; Esposito, 2004; Ma *et al.*, 2013; Strouch *et al.*, 2010; Theoharides, 2008).

2.2.8.5 Bone Marrow Derived Cells

Bone marrow derived cells (BMDCs) are recruited to the desmoplastic stroma in PC and differentiate into a number of cell types including PSCs, activated fibroblasts, MDSCs, and mast cells. Thus, BMDCs are not tumour promoting themselves, but rather constitute the desmoplastic reaction by supplying CAFS, inflammatory and immune suppressive cells to the TME (Nielsen *et al.*, 2016a; Scarlett, 2013; Scarlett *et al.*, 2011a; Zhan *et al.*, 2017).

2.2.8.6 Macrophages

Tumour associated macrophages (TAMs) are recruited from circulating monocytes and are the principal immune cell type in PC TME. TAMs are divided into two types, pro-inflammatory (M1) or anti-inflammatory (M2). M1 TAMs can counteract tumour progression by instigating an anti-tumour immune response through activation of cytotoxic T cells. Contrastingly, M2 TAMs produce cytokines and growth factors (VEGF) that enhance tumour cell proliferation. M2 TAMs also produce ECM degrading enzymes which lead to the remodelling of the stromal environment and migration and metastases of cancer cells and PSCs (Broz *et al.*, 2014; Cui *et al.*, 2016; Dineen *et al.*, 2008; Engblom *et al.*, 2016; Nielsen *et al.*, 2016b; Noy and Pollard, 2014; Shi *et al.*, 2014).

2.2.8.7 Lymphocytes

Tumour infiltrating lymphocytes (TILs) including CD4 and CD8 T cells, B cells, natural killer (NK) cells and regulatory T cells (Tregs) are all present within the desmoplastic reaction of PC (Liyanage *et al.*, 2006; Nielsen *et al.*, 2016a; Nummer *et al.*, 2007). Cytotoxic T cells are rare and are relatively unable to clear cancer cells due to the sequestering of T cells to the stroma of PC by CAFs (Borazanci *et al.*, 2017; Ene-Obong *et al.*, 2013). Furthermore, granulocyte-macrophage colony-stimulating factor (GM-CSF) excreted by cancer cells block the recognition and destruction of cancer cells by CD8 T cells (Bayne *et al.*, 2012). Also, CD4 cells promote dysplasia by

blocking CD8 T cell anti-tumour mechanisms (Clark *et al.*, 2007; De Monte *et al.*, 2011; Neesse *et al.*, 2015). Similarly, Tregs are significantly increased in pancreatic tumours and confer immunosuppression likely by inhibiting CD8 T cell activity (Hiraoka *et al.*, 2006; Linehan and Goedegebuure, 2005; Liyanage *et al.*, 2006; Tang *et al.*, 2014). Finally, NK cells are often dysfunctional in PC due to inhibiting signals from cancer cells (Chang *et al.*, 2016; Peng *et al.*, 2016; Peng *et al.*, 2014). Thus, the TME of PC is immunosuppressive allowing for unchecked PC progression (Zhan *et al.*, 2017).

2.2.8.8 Neutrophils

Tumour associated neutrophils (TANs) assist tumourigenesis through excretion of proteases such as elastase, proteinase 3 (PR3), matrix metalloproteinase (MMP) 8 and 9, and cathepsin G. The secreted proteases encourage quiescent PSCs/fibroblasts to undergo ETM transition to become activated. The proteases also disrupt the ECM leading to invasion and metastases of PC and PSC cells (Bausch *et al.*, 2011; Felix and Gaida, 2016; Gaida *et al.*, 2012; Grosse-Steffen *et al.*, 2012; Wang *et al.*, 2014)

2.2.8.9 Adipocytes

Obesity is a risk factor for PC development because adipocytes infiltrate the PC TME and undergo a delipidation process to become fibroblast-like tumour promoting cells. The delipidated adipocytes, termed cancer associated adipocytes (CAAs), cross-talk with cancer cells through paracrine signalling loops to promote angiogenesis and cancer cell differentiation while prohibiting apoptosis (Deng *et al.*, 2016; Fain *et al.*, 2004; Halberg *et al.*, 2008; Hori *et al.*, 2014; Renehan *et al.*, 2015).

2.2.8.10 Pericytes

In normal tissues, pericytes synthesise vascular basement membranes around endothelial cells to anchor the cells in place and assist withstanding hydrostatic pressure from blood flow. Pericytes are also involved in tumour angiogenesis and metastasis (Armulik *et al.*, 2011; Hanahan and Weinberg, 2011; Hosaka *et al.*, 2016; Raza *et al.*, 2010). The PDGF-BB-PDGFRβ signalling pathway is one of the

mechanisms responsible for pericyte recruitment by endothelial cells. Overexpression of PDGF-BB by tumour cells is thought to create a high PDGF-BB gradient encouraging pericytes to detach from endothelial cells and migrate towards cancer cells. Subsequently, destabilisation and intravasation of tumour cells occurs. Secondly, persistent binding of pericytes to cancer cells due to the high PDGF-BB expression is thought to cause pericytes to transition into CAFs (Hosaka *et al.*, 2016; Zhan *et al.*, 2017).

2.2.8.11 Endothelial Cells

Endothelial cells make up the inner lining of blood vessels. Endothelial cell differentiation and angiogenesis can be indirectly induced by CAFs. Remodelling of the desmoplastic reaction in PC through proteases and release of chemokines to increase the expression of adhesion molecules, including ICAM-1, on endothelial cells leads to increased tumour vascularity (Pothula *et al.*, 2014; Schmidt *et al.*, 2012; Xu *et al.*, 2010).

2.2.9 Pancreatic Cancer Diagnosis

There are still no accurate early detection mechanisms for PC due to the lack of symptoms or presence of non-specific symptoms in early stages of disease, rapid dissemination and progression of disease, absence of sensitive and selective biomarkers, and finally unreliable imaging techniques. There is a dire need for new early detection methods to identify and combat PC in early stages (Zhang *et al.*, 2017a).

2.2.9.1 Biomarkers

Collection of pancreatic juice, blood, urine, saliva or faeces can serve as sources of screening biomarkers for the detection of PC precursor lesions and early onset of PC. Serum carbohydrate antigen 19-9 (CA19-9) is the most extensively evaluated and sensitive biomarker for screening of PC. CA19-9 is the only biomarker currently approved by the United States Food and Drug Administration (USFDA) for screening

PC (Loosen *et al.*, 2017). CA19-9 has on average 80% sensitivity and 80% specificity for PC. However, CA19-9 is not overexpressed in early stages of PC and is commonly overexpressed in many other non-malignant and malignant diseases. Furthermore, patients lacking the Lewis blood group antigen do not overexpress CA19-9 and produce false negatives upon screening. Therefore, CA19-9 is an unreliable biomarker (Ballehaninna and Chamberlain, 2012; Goonetilleke and Siriwardena, 2007; Marrelli *et al.*, 2009; Poruk *et al.*, 2013; Viterbo *et al.*, 2016).

Numerous investigations to identify biomarkers with higher sensitivity and specificity for precursor lesions and early stage PC biomarkers have been and continue to be conducted (Swords *et al.*, 2016; Zhang *et al.*, 2017a). Strategies have included screening for molecules alongside CA19-9 as a panel. One study found that screening for ICAM-1, CA19-9 and osteoprotegerin (OPG) proved superior to screening for CA19-9 alone (88.1% sensitivity at 90% specificity from the panel vs. 57.2% sensitivity at 90% specificity from screening for CA19-9 alone) (Brand *et al.*, 2011). ICAM-1 alone was found to have higher sensitivity and specificity for PC compared to CA19-9 (82% sensitivity at 82.26% specificity from screening for ICAM-1 vs. 64-80% sensitivity at 56.4-61.2% specificity from screening for CA19-9). However, both were concluded to be unsuitable for differentiating between early and late stage disease (Mohamed *et al.*, 2016). Other strategies for detecting PC have included screening for exosomes, circulating tumour cells, microRNAs, cytokines, pancreatic and liver enzymes and gene methylation (Jin *et al.*, 2017; Loosen *et al.*, 2017; Swords *et al.*, 2016; Zhang *et al.*, 2013; Zhang *et al.*, 2017a).

2.2.9.2 Imaging Techniques

As there are no dependable biomarkers for PC precursor lesions and early stages of PC development, diagnosis is usually confirmed through one of many imaging techniques such as ultrasonography, magnetic resonance imaging (MRI), and computed tomography (CT) imaging. Accuracy in detection via each technique is primarily dependent on the expertise of the conducting radiologist (Al-Hawary *et al.*, 2015; Dimastromatteo *et al.*, 2017).

Endoscopic ultrasound fine needle aspiration (EUS-FNA) is a routine method for diagnosis and staging pancreatic cancer. An echoendoscope is inserted through the

gastrointestinal tract to obtain detailed images of the pancreas and collect pancreatic juice and tissue samples via a retractable needle. Pancreatic juice can be screened for biomarkers for precursor lesions and PC. Similarly, the presence and staging of precursor lesions/PC is determined by a pathologist through histochemical analysis of tissue biopsies. EUS-FNA is minimally invasive and provides 85-95% sensitivity and 90-95% specificity for the detection of pancreatic lesions (Bartel and Raimondo, 2017; Bournet *et al.*, 2014; Chen *et al.*, 2012; Han and Chang, 2017; Toshiyama *et al.*, 2017). A recent adaption of EUS has been needle-based confocal laser endomicroscopy (nCLE). The technique visualises pancreatic lesions to a resolution of 3.5 μm providing real-time, *in vivo*, histological diagnostic features. Unfortunately, the cost and expertise required for nCLE has limited the techniques application in clinical settings (Kadayifci *et al.*, 2017; Konda *et al.*, 2013; Krishna *et al.*, 2017; Nakai *et al.*, 2015; Napoléon *et al.*, 2015).

A variation of conventional MRI for increased accuracy in detection of pancreatic lesions is magnetic resonance cholangiopancreatography (MRCP). The minimally invasive technique utilises the intrinsic contrast related qualities of fluids within the pancreatic and biliary ducts to visualise the pancreaticobiliary ductal network without injection of contrast materials. MRCP provides high resolution images superior to standard cholangiopancreatography without risk of complications such as sepsis and bleeding (Adamek *et al.*, 2000; Barish *et al.*, 1999; Coakley and Schwartz, 1999; Dimastromatteo *et al.*, 2017).

18[F]-fluorodeoxyglucose positron emission tomography/computed tomography (FDG-PET/CT) is an improvement on traditional CT for detecting pancreatic malignancy. PET utilising the uptake of 18[F]-fluoreoxyglucose is concurrently performed with CT and resulting images superimposed to align the metabolic and structural characteristics of tissues. The method provides greater diagnostic accuracy and staging of pancreatic tumours and distant metastases. Furthermore, FDG-PET/CT is a very good predictor of patient prognosis (Asagi *et al.*, 2013; Heinrich *et al.*, 2006; Kauhanen *et al.*, 2009; Okamoto *et al.*, 2011; Pinho and Subramaniam, 2017; Topkan *et al.*, 2011).

2.2.10 Pancreatic Cancer Staging

Staging of pancreatic cancer comes under the tumour/node/metastasis (TNM) guidelines implemented by the American Joint Committee on Cancer (AJCC). Additionally, the magnitude of differentiation of cells as a grade from 1 to 4 is factored into the staging of PC (Amin *et al.*, 2016; Chun *et al.*, 2017). Refer to Table 1 for staging criteria of PC.

Table 1: Staging of Pancreatic Cancer according to AJCC criteria.

Grade	Description
1	Well differentiated: Cells appear normal and are not growing rapidly.
2	Moderately-differentiated: Cells appear slightly different than normal.
3	Poorly differentiated: Cells appear abnormal and tend to grow and spread more aggressively.
4	Undifferentiated: (for certain tumours) features are not significantly distinguishing to make it look any different from undifferentiated cancers which occur in other organs.
TNM	
T	**Primary Tumour**
Tx	Primary tumour cannot be assessed
T0	No evidence of primary tumour
Tis	Carcinoma in situ; intraepithelial or invasion of lamina propria
T1	Tumour invades submucosa
T2	Tumour invades muscularis propria
T3	Tumour invades through muscularis propria into subserosa or into non-peritonealised pericolic or perirectal tissues.
T4	Tumour directly invades other organs or structures and/or perforate visceral peritoneum
N	**Regional Lymph Nodes**
Nx	Regional lymph nodes cannot be assessed
N0	No regional lymph node metastasis
N1	Metastasis in 1 to 3 regional lymph nodes
N2	Metastasis in 4 or more regional lymph nodes
M	**Distant Metastasis**
Mx	Distant metastasis cannot be assessed
M0	No distant metastasis
M1	Distant metastasis

2.2.11 Pancreatic Cancer Treatment

Prognosis for PC patients is very bleak regardless of stage at time of detection. In this section, the current approved standards of care for PC patients and outcomes are discussed. Besides surgery available for a lucky few, there are no treatments available for PC patients that control disease progression and/or provide better quality of life for patients before succumbing to the disease. Patients with advanced disease that decline treatment are advised they have approximately three to nine months to live. Chemotherapy may fail to provide a survival advantage in some patients. An overview of treatment strategies for PC patients is presented below in Figure 12.

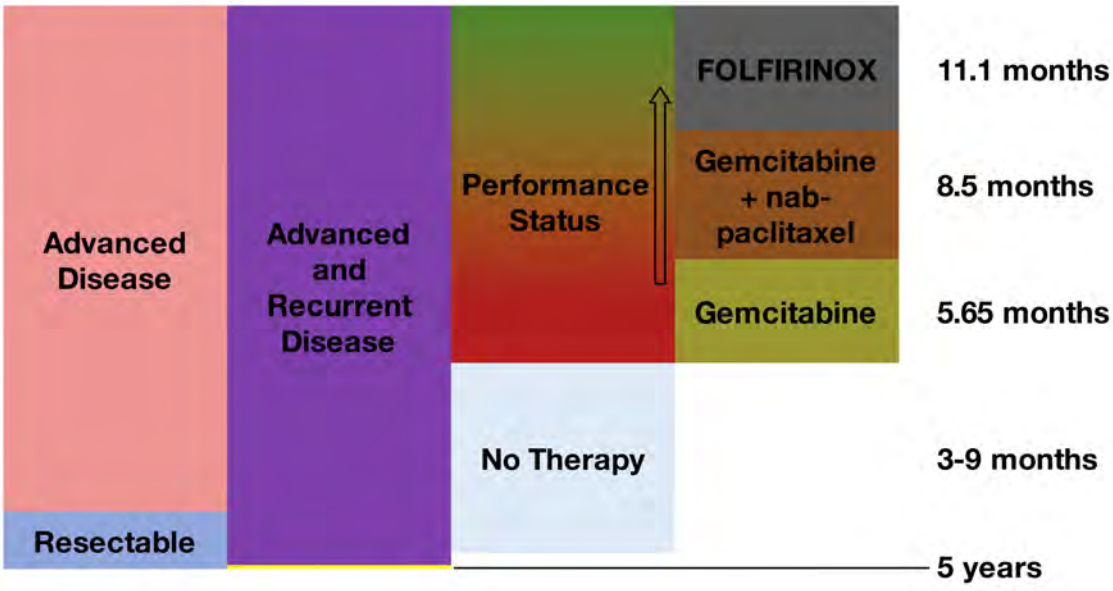

Figure 12: Treatment strategies for PC patients. When diagnosed with PC, patients who are eligible for surgical resection can have a pancreaticduodenectomy in an attempt to cure the disease. Patients that are ineligible for resection or have disease relapse can undergo one of several chemotherapeutic treatment modalities depending on patient performance status. Adapted from **Graham, J. S., Jamieson, N. B., Rulach, R., Grimmond, S. M., Chang, D. K. and Biankin, A. V**. (2015). Pancreatic cancer genomics: where can the science take us? Clin. Genet. **88**, 213–219.

2.2.11.1 Surgery

Surgery is the only intervention that provides a 'cure' for extremely few PC patients. Surgical resection is only available to patients with localised disease to the head of the pancreas. Thus, up to 90% of patients are ineligible for surgical resection as disease is in the body or tail of the pancreas, and/or more likely, has metastasised by the time of diagnosis. A pancreaticoduodenectomy, or similar procedure, is performed to

remove the head of the pancreas containing the tumour and reattach the remainder of the pancreas to the duodenum. Adjuvant chemotherapy is administered to remove any remnant islets of tumour cells. However, 71% of resected patients will have disease relapse and the 5-year relative survival rate is a grim 20% (Barugola *et al.*, 2007; Conroy *et al.*, 2016; Graham *et al.*, 2015; Hirata *et al.*, 1997; Hishinuma *et al.*, 2006; Riall *et al.*, 2006; Schmidt *et al.*, 2004; Schnelldorfer *et al.*, 2008; Van den Broeck *et al.*, 2009; Wagner *et al.*, 2004; Winter *et al.*, 2006). In the US in 2017, there were an estimated 53,670 new cases of PC (Siegel and Jemal, 2017). Based on the above statistics only 5,367 (10%) would be eligible for surgical resection, and only 311 (20% of the 29% of patients who do not have disease relapse = 0.58% of all patients) would survive for five years or more.

2.2.11.2 Gemcitabine

Gemcitabine is a cytidine analogue that interferes with DNA replication in dividing cells leading to cell death (Hertel *et al.*, 1990; Huang *et al.*, 1991). Gemcitabine has been the standard of care for patients with PC since its approval by the USFDA in 1996 (USFDA, 1996). Prior to this, 5-fluorouracil (5-FU) was the standard treatment for over 30 years. The study that lead to gemcitabine's approval was a phase II clinical trial involving 126 patients (n = 63) with unresectable PC comparing 5-FU to gemcitabine (no placebo). The study achieved a greater clinical benefit in patients treated with gemcitabine; 23.8% (15/63 patients) in gemcitabine treated patients vs. 4.8% (3/63 patients) in 5-FU treated patients (P = 0.0022). Clinical benefit was defined as improvement in one or more parameters for a minimum of 4 weeks: pain (assessed by pain intensity and administration of morphine), functional impairment (assessed by Karnofsky performance status) and weight (assessed by body weight). Objective tumour response was a secondary measurement of efficacy. Three of the 63 gemcitabine treated patients (5.4%) achieved a partial response in tumour reduction (≥50% reduction in tumour volume for minimum four weeks). A marginal median survival increase (5 weeks) was observed in gemcitabine treated patients: 5.65 months, compared to 4.41 months in 5-FU treated patients (P = 0.0025). Two patients from each cohort died from treatment related adverse events. All patients succumbed to disease within 19 months. Higher incidence of grade 3 and 4 neutropenia was observed in gemcitabine treated patients (25.9% vs 4.9% P = <0.001). Likewise, higher incidence of grade 3 and 4 leukopenia (9.7% vs. 1.6%) and thrombocytopenia

(9.7% vs. 1.6%) observed for gemcitabine treated patients (no grade 4 observed in either group). Grade 3 elevated liver enzyme related adverse events were higher in gemcitabine patients: alkaline phosphatase (16.4% vs. 9.5%), aspartate transaminase (9.8% vs. 1.6%), and alanine transaminase (8.2% vs. 0%). The investigators of the study concluded that gemcitabine alleviated some disease related symptoms and confers a modest survival advantage in patients with advanced, symptomatic PC (Burris *et al.*, 1997; Casper *et al.*, 1994).

Gemcitabine is astonishingly toxic. It is both astounding and bewildering that it was ever approved for administration to humans. The majority of patients receiving gemcitabine will experience haematological effects as anaemia, neutropenia, leukopenia and thrombocytopenia. Myelosuppression is the dose limiting toxicity. Petechiae, haemorrhage, hyper bilirubinaemia and bone marrow suppression are also very common. Patients will also experience nausea, vomiting, diarrhoea, weight loss, stomatitis and ulceration of the mouth, constipation, ischemia and pruritus. Elevated liver enzymes including alanine aminotransferase (ALT), aspartate aminotransferase (AST) and alkaline phosphatase are indicative of assault to the hepatic system. Kidney damage is detected by the presence of proteinuria, haematuria and increased blood urea nitrogen and creatinine. Renal failure may even occur. Dyspnoea, fever, itching and infection are also common (Abratt *et al.*, 1994; Burris *et al.*, 1997; Conroy *et al.*, 2011; Guchelaar *et al.*, 1996; Marruchella and Tondini, 1999; Mavroudis *et al.*, 2003)

2.2.11.3 Gemcitabine Plus Nab-paclitaxel

Gemcitabine in combination with albumin bound paclitaxel (nab-paclitaxel) has been approved for the treatment of PC after a phase III clinical trial involving 861 patients with metastatic PC proved more efficacious than gemcitabine alone. Gemcitabine plus nab-paclitaxel had a response rate of 23% compared to 7% in gemcitabine treated patients (P = <0.001). Likewise, the combination provided a median overall survival of 8.5 months compared to 6.7 months in the gemcitabine cohort (P = <0.001). The combination proved to be more toxic than gemcitabine alone. Incidences of grade 3 or higher neutropenia, leukopenia, fatigue, and peripheral neuropathy were higher in gemcitabine plus nab-paclitaxel treated patients (Hoff *et al.*, 2013). A second study has confirmed the combination of gemcitabine and nab-paclitaxel provided increased response rate and overall survival. From 41 patients with metastatic PC and an

Eastern Co-operative Oncology Group (ECOG) performance status of 0-2, there was an overall response rate of 36.6%, and median survival of 10 months. The study reported grade 3 adverse events of neutropenia, thrombocytopenia, anaemia, diarrhoea, nausea and vomiting, and fatigue (De Vita *et al.*, 2016). Due to the increased toxicity associated with the combination regimen, only patients with good performance status (ECOG of 0-2, approximately 45% of patients) are eligible for treatment with gemcitabine plus nab-paclitaxel (Hoff *et al.*, 2013; Lau and Cheung, 2017; Peixoto *et al.*, 2015).

2.2.11.4 FOLFIRINOX

FOLFIRINOX, a cocktail of chemotherapeutics (folinic acid [leucovorin], 5-FU, irinotecan, and oxaliplatin) has also recently been approved by the USFDA for the treatment of PC. FOLFIRINOX proved to be a better frontline treatment in a randomised phase III clinical trial of 342 patients with metastatic PC. FOLFIRINOX treated patients had an objective response rate of 31.6% compared to 9.4% for gemcitabine treated patients (P = <0.001). Furthermore, the study concluded a median survival of 11.1 months for FOLFIRINOX treated patients compared to 6.8 months in gemcitabine treated patients (P = <0.001). However, two patients died from the treatment of FOLFIRINOX and there was significantly higher grade three or four neutropenia (P = < 0.001), febrile neutropenia (P = 0.03), thrombocytopenia (P = 0.04), diarrhoea (P = <0.001) and sensory neuropathy (P = <0.001) in FOLFIRINOX treated patients (Conroy *et al.*, 2011). Only patients with very good performance status (ECOG < 2, approximately 25% of patients) are suitable for treatment with FOLFIRINOX due to the increased toxicity (Ho *et al.*, 2015; Lambert *et al.*, 2017; Lau and Cheung, 2017; Liu *et al.*, 2017; Mian *et al.*, 2014; Peixoto *et al.*, 2015; Zhang *et al.*, 2017c).

2.3 Oncolytic Virotherapy

An oncolytic virus (OV) can be defined as a virus with specific and selective tropism for cancer cells that invade, replicate within, and lyse tumour cells while leaving surrounding healthy cells relatively unaffected. Subsequently, viral progeny infects surrounding and distant cancer cells to continue the oncolytic infection cycle. Furthermore, an OV through cancer cell oncolysis may lead to recognition of cancer cell epitopes by the host's immune system and generation of an adaptive anti-tumour immune response (Goldufsky *et al.*, 2013; Hamid *et al.*, 2017; Kaufman *et al.*, 2015; Russell *et al.*, 2012; Wennier *et al.*, 2011; Workenhe and Mossman, 2014). Refer to Figure 13 for the mode of action of CVA21 as a model oncolytic virus.

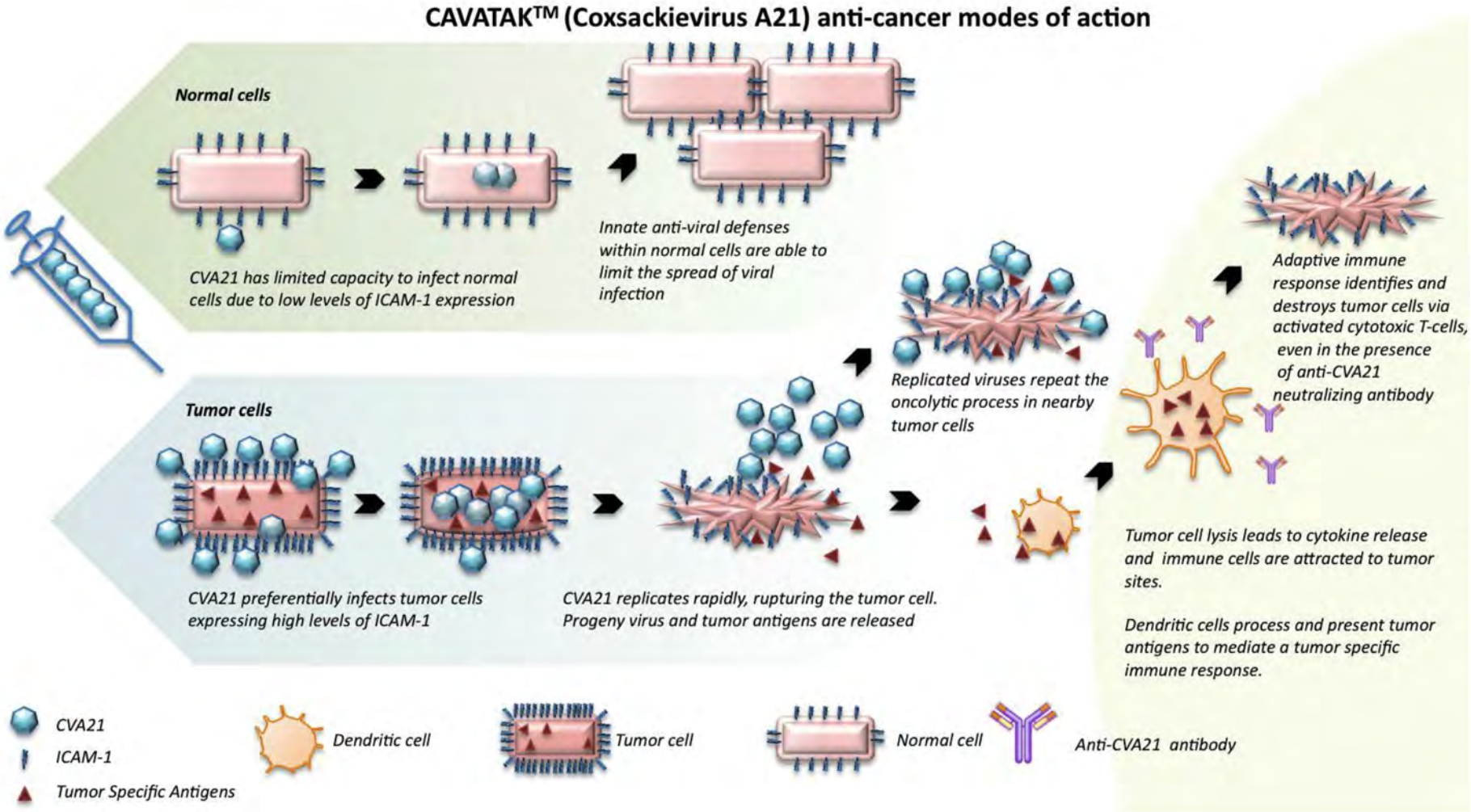

Figure 13: Mode of action of CVA21. Image source: Viralytics Ltd.

2.3.1 History of Oncolytic Viruses

The idea of using a virus to treat cancer, most likely arose out of the simple observation that cancer patients who contracted an infectious disease went into periods of clinical remission (Kelly and Russell, 2007). As far back as 1896 there was a reported case of a patient with leukaemia that went into remission after a presumed influenza infection (Dock, 1904). Numerous clinical cases were reported throughout the 20th century describing the regression of different malignant diseases in relation to viral infections (Bierman *et al.*, 1953; Blank, 1949; Bluming and Ziegler, 1971; DePace, 1912; Erf, 1950; Gross, 1971; Higgins and Pack, 1951; Hoster *et al.*, 1949; Koprowska, 1953; Moore, 1954; Pack, 1950; Pasquinucci, 1971; Salmon and Baix, 1922; Southam and Moore, 1951; Southam and Moore, 1952; Southam and Moore, 1954; Taqi *et al.*, 1981; Zygiert, 1971).

Owing to the observation of viruses causing regression of cancers, Southam and Moore pioneered early oncolytic virotherapy in the 1950s (Moore, 1954; Southam and Moore, 1951; Southam and Moore, 1952; Southam and Moore, 1954). Indeed, they made great progress in the field in both preclinical and clinical trials. However, they ultimately tarnished the field of oncolytic virotherapy, just as it was gaining momentum. The investigators subcutaneously inoculated healthy individuals with HeLa cells to test oncolytic viruses. Tumours caused the death of two patients (Kelly and Russell, 2007; Lerner, 2004; Moore *et al.*, 1957; Southam, 1958). It was not until the advent of DNA recombination technologies in the 1990s that oncolytic virotherapy once again took off (Kelly and Russell, 2007).

An example of an early OV modified to increase its tropism for cancer cells was research conducted by Martuza and colleagues. The thymidine kinase gene was deleted from herpes simplex virus type 1 resulting in a mutant that only replicated in dividing cells. Malignant gliomas in mice were completely eradicated when treatment with the engineered virus was administered. Unfortunately, the issue of encephalitis hindered translation into human trials (Martuza *et al.*, 1991).

Pathogenicity of an OV is a key concern translating into humans. One strategy to overcome pathogenicity has been to genetically modify viruses to recognise different cellular receptors for host cell invasion. Modifications reduce virulence and usually

confer increased tropism for cancer cells. For example, measles virus has been extensively modified to the point where it no longer utilises CD46 and SLAM, but rather epidermal growth factor receptor (EGFR) and CD38, to infiltrate host cells. The knockout-knockin modifications triggered the virus to be selective for cancer cells, particularly glioma cells, due to overexpression of EGFR and CD38. Consequently, the pathogenicity of the modified measles virus is reduced (Allen *et al.*, 2006; Hadac *et al.*, 2004; Hasegawa *et al.*, 2006; Nakamura *et al.*, 2005; Nakamura *et al.*, 2004; Paraskevakou *et al.*, 2007). Several clinical trials have been initiated to investigate variations of measles virus in a number of cancer types (clinicaltrials.gov identifiers: NCT00390299, NCT02192775, NCT01503177, NCT00408590, NCT01846091).

Numerous OVs have since been generated from human, and non-human specific viruses in an attempt to meet the need for improved treatments for different cancer types. Many have advanced into clinical evaluation and to date two have been approved for treatment of selected cancer types (discussed later).

2.3.2 Oncolytic Virus Concerns

There is significant and justified apprehension in using genetically modified, and non-human specific viruses for the treatment of different cancer types in humans. Spontaneous genetic reversion of modified OVs when administered to humans cannot undeniably be ruled out. Likewise, cross-species mutation cannot be absolutely prohibited. Thus, the associated deleterious pathogenicity of parent strain viruses may reappear, or even new mechanisms of virulence may develop in humans or other species.

Newcastle Disease Virus (NDV), an avian virus, has been frequently tested in humans (Sinkovics and Horvath, 2000). Clinical trial data of NDV in metastatic melanoma patients report complete remission in one patient two years post administration (Murray *et al.*, 1977), and another reports over 60% survival in patients who received NDV as adjuvant therapy after resection of stage II melanoma (Cassel and Murray, 1992). Although NDV has shown efficacy in treating cancers, there is an unquantifiable risk of the virus adapting and potentially spreading to humans. Spontaneous cross-species mutation has not been observed with NDV. However, an instance of spontaneous cross-species mutations was observed with feline parvovirus (FPV). FPV

was used in early oncolytic virotherapy investigations for the treatment of infantile leukaemia (Bierman *et al.*, 1953). Around 1977, FPV evolved independently of human intervention to be transmissible to canines. The new virus strain, canine parvovirus (CPV) was the cause of a pandemic that was believed to have affected 80% of dogs worldwide and caused the death of millions from 1978 to 1979. Still to this day, CPV is endemic and puppies require vaccination to avoid serious disease (Horiuchi *et al.*, 1994; Parrish, 1991; Parrish and Kawaoka, 2005; Parrish *et al.*, 1988; Shackelton *et al.*, 2005; Thomas *et al.*, 1984).

CVA21 is a naturally occurring human specific virus associated with low pathogenic effects in the form of upper respiratory tract infections (Xiang *et al.*, 2012; Zhou *et al.*, 2017). The incidence of spontaneous mutation resulting in cross-species specificity or increased pathogenicity is unlikely, given the extensive history and characterisation of the virus. Thus, CVA21 is an ideal OV.

2.3.3 Clinical Investigation of Coxsackievirus A21

Viralytics Ltd. clinical formulation of CVA21, CAVATAK™, has been investigated in multiple phase I and II clinical trials. Table 2 summarises the clinical trials registered with clinicaltrials.gov investigating CAVATAK™ as treatments for different malignancies. CAVATAK™ has proven to be a potentially efficacious anti-cancer agent for multiple cancer types while proving to be well tolerated. The dose limiting toxicity for CAVATAK™ has currently not been observed. Final results from the CALM phase II clinical trial (clinicaltrials.gov identifier: NCT01227551) where 57 patients with unresectable late stage (IIIC-IVM1c) melanoma were treated with CAVATAK™ showed an overall response rate of 28.1% and a 1-year survival rate of 75.4%. Reduction of both injected and distant tumour sites were observed in patients. No grade 3 or 4 treatment-related adverse events were observed (Andtbacka *et al.*, 2015a).

Table 2: Clinical trials investigating CAVATAK™ registered with clinicaltrials.gov

Study Title	**Identifier**	**Phase**	**Initiated**	**Status**
A Safety Study of Two Intratumoural Doses of CAVATAK™ in Melanoma Patients	NCT00438009	I	2007	Completed
CAVATAK™ Administered Intravenously (IV) for Solid Tumour Cancers	NCT00636558	I	2008	Completed
A Study of the Intratumoural Administration of CAVATAK™ to Head and Neck Cancer Patients	NCT00832559	I	2009	Terminated
A Study of Intratumoral CAVATAK™ in Patients with Stage IIIc and Stage IV Malignant Melanoma (CALM)	NCT01227551	II	2010	Completed
Efficacy and Safety of Intratumoral CAVATAK™ in Patients with Stage IIIc or IV Malignant Melanoma to Extend Dosing to 48 Weeks	NCT01636882	II	2012	Completed
Safety and Clinical Activity of CAVATAK™ Alone or With Low Dose Mitomycin C in Non-Muscle Invasive Bladder Cancer (CANON)	NCT02316171	I	2014	Completed
Melanoma Intratumoral CAVATAK™ + Ipilimumab (MITCI)	NCT02307149	I	2014	Recruiting
Systemic Treatment of Resistant Metastatic Disease Employing CAVATAK™ and Pembrolizumab in Non-Small Cell Lung Cancer and Bladder Cancer (STORM/ KEYNOTE-200)	NCT02043665	I	2014	Recruiting
CAVATAK™ and Pembrolizumab in Advanced Melanoma (CAPRA)	NCT02565992	I	2015	Recruiting
Pembrolizumab + CAVATAK™ in Advanced Non-Small Cell Lung Cancer	NCT02824965	I	2016	Recruiting

CAVATAK™ is also being investigated in combination with immune checkpoint inhibitors in several trials. Preliminary data from approximately 25 patients on the "Melanoma Intratumoral CAVATAK™ + Ipilimumab (MITCI)" study (clinicaltrials.gov identifier: NCT02307149) indicates CAVATAK™ in combination with ipilimumab is well tolerated and displays anti-tumour activity in injected, and distant tumour sites including liver and lung metastases (Curti *et al.*, 2017). The data is particularly exciting as several patients enrolled on the MITCI trial have previously failed treatments with immunotherapies, including ipilimumab and anti-PD-1 blockade, suggesting CAVATAK™ activates tumours to become susceptible to immunotherapies. A term colloquially referred to as turning immunologically 'cold' tumours 'hot'. Figure 14 depicts the dramatic tumour reduction after treatment with CAVATAK™ and ipilimumab in two patients. Both patients were refractory to prior immunotherapies.

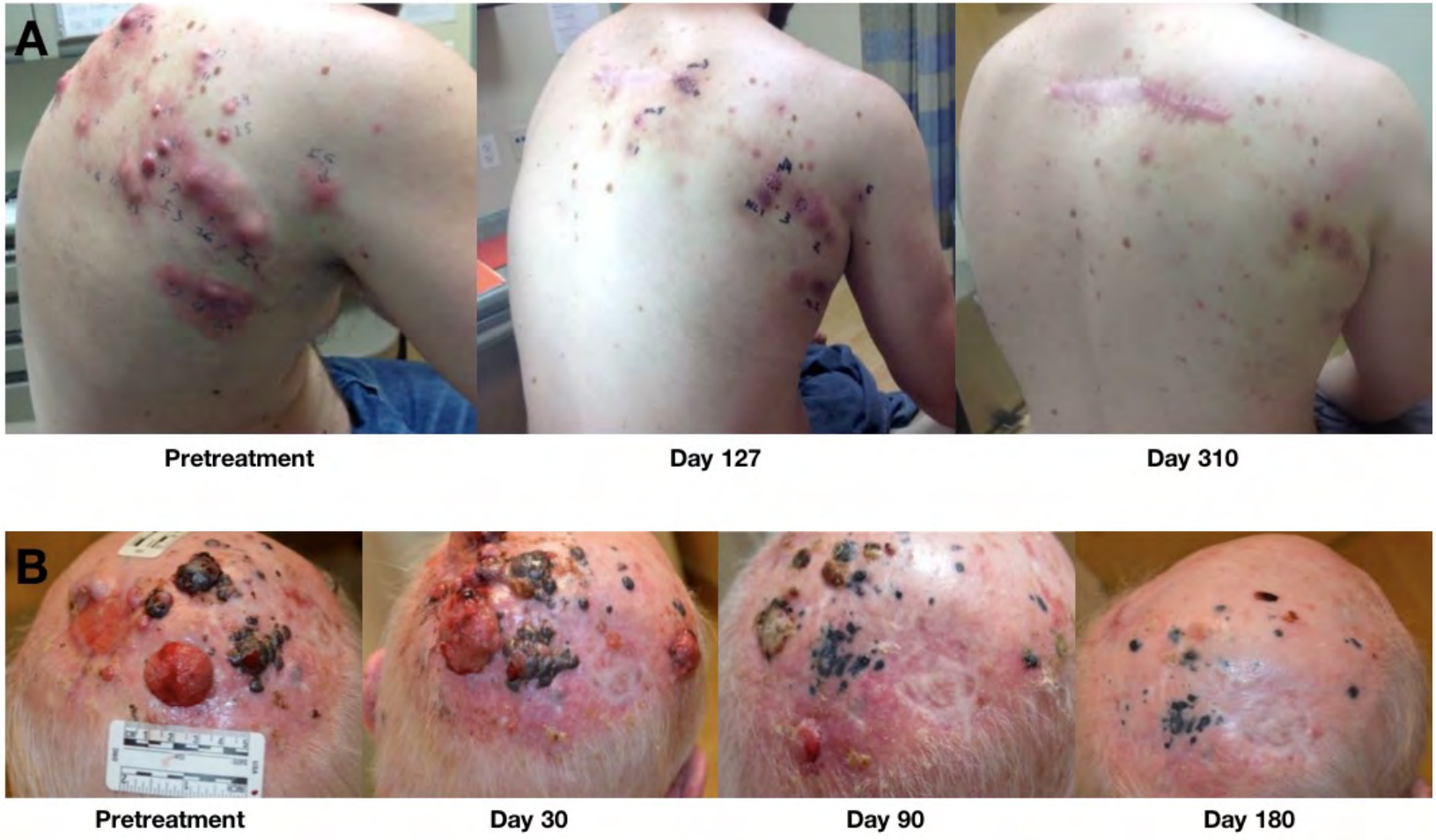

Figure 14: Tumour reduction in CAVATAK™ + ipilimumab treated patients. Patient A (Stage IVM1c melanoma) failed prior treatments with immune checkpoint inhibitors (ipilimumab and nivolumab) and had surgery to reduce tumour burden. Patient B (Stage IIIC melanoma) failed prior treatments with immunotherapies (BCG and nivolumab). After treatment with CAVATAK™ in combination with ipilmumab patient A had a partial response and patient B had a complete response. Image source: Viralytics Ltd.

2.3.4 Oncolytic Virotherapy for the Treatment of Pancreatic Cancer

Several OVs have made it to clinical investigation for the treatment of PC. A discussion of historical and current trials investigating OVs as potential treatments for PC is presented hereafter. To date there are no OVs approved for the treatment of PC by any regulatory body.

2.3.4.1 ONYX-015

The first clinical trial to investigate an oncolytic virus as a treatment for PC was initiated in the year 2000. The phase I trial investigated ONYX-015 as a treatment in combination with gemcitabine. ONYX-015 is a genetically modified serotype 2/5 adenovirus that has a deletion of E1B-55kD. E1B-55kD inhibits Tp53 function which is commonly lost in many cancer types, particularly PC. Thus, the virus selectively replicates in cancer cells while leaving healthy cells unaffected. The study distributed virus via endoscopic ultrasound guided (EUS) fine needle injection (FNI) and was found to be a well-tolerated and practical means of administration. However, the treatments did not ultimately have a significant effect (partial response in two out of 21 patients and provided a median survival time of 7.5 months) (Bischoff *et al.*, 1996; Harada and Berk, 1999; Hecht *et al.*, 2003; Rogulski *et al.*, 2000).

2.3.4.2 HF10

HF10 is a naturally occurring HSV-1 mutant that has tropism for replication in cancer cells compared to healthy cells. The virus has shown efficacy for the treatment of many cancer types in preclinical and clinical trials (Eissa *et al.*, 2017; Fujimoto *et al.*, 2006; Hotta *et al.*, 2017; Kohno *et al.*, 2005; Luo *et al.*, 2012; Nakao *et al.*, 2011; Takakuwa *et al.*, 2003; Tan *et al.*, 2015; Watanabe *et al.*, 2008; Yamamura *et al.*, 2014; Zhang *et al.*, 2006). Takara Bio Inc. conducted a small pilot clinical trial in 2005 on six patients with unresectable PC to determine the efficacy of HF10 over increasing doses. The investigators reported patients experienced no adverse events. Three

patients were reported to have stable disease (one patient for a duration of 80 days), partial response in one patient, and disease progression in two patients. All patients ultimately succumbed to disease (Nakao *et al.*, 2011). Takara Bio Inc. have initiated a phase I clinical trial to test the safety, tolerability, and clinical outcome of HF10 in combination with gemcitabine plus nab-paclitaxel as a treatment for Japanese patients with stage III or IV unresectable PC (clinicaltrials.gov identifier: NCT03252808). Virus will be administered via EUS-FNI, while chemotherapy given conventionally through I.V.

2.3.4.3 T-Vec

T-Vec (Imlygic/Talimogene Laherparepvec), the first oncolytic virus to be approved by the USFDA in 2015 for treatment of melanoma (Vidhya, 2016), is a modified herpes simplex virus (HSV) type 1 that has a knockout of infected cell protein (ICP) 34.5 and knockout-knockin of ICP 47 with granulocyte-macrophage colony-stimulating factor (GM-CSF). The deletion of ICP 34.5 confers suppression of viral pathogenicity, selective replication within tumours, and supports selective oncolysis of cancer cells while leaving healthy cells unaffected (Friedman *et al.*, 2015; Kohlhapp and Kaufman, 2016; Liu *et al.*, 2003; Mohr and Gluzman, 1996; Mohr *et al.*, 2001; Poppers *et al.*, 2000; Taneja *et al.*, 2001). Replacement of ICP 47 with GM-CSF improves antigen presentation and T-cell maturation potentially resulting in a systemic immune response by the infected host. (Andtbacka *et al.*, 2015b; Corrigan *et al.*, 2017; Hill *et al.*, 1995; Kaufman *et al.*, 2014; Liu *et al.*, 2003; Toda *et al.*, 2000; Tomazin *et al.*, 1998).

BioVex Ltd. conducted a phase I trial between 2006 and 2008 to investigate T-Vec as a treatment for unresectable PC in 17 patients (ClinicalTrials.gov Identifier: NCT00402025). Virus was administered by EUS-FNI. Three doses were intended to be administered to four cohorts (C1: 1 dose of 10^4 PFU/ml followed by 2 of 10^5 PFU/ml, C2: 1 dose of 10^5 PFU/ml followed by 2 of 10^6 PFU/ml, C3: 1 dose of 10^6 PFU/ml followed by 2 of 10^7 PFU/ml, and C4: 1 dose of 10^6 PFU/ml followed by 2 of 10^8 PFU/ml). Only seven of the 17 patients received all three treatments. Treatments for C4 were not initiated. Two of the four patients (50%) in C3 had reduction in tumour diameter (-36% and -33%), and three patients in total from C1 and C3 had reduction of greater than one non-injected lesion. Common adverse events included ascites,

dehydration, anaemia, abdominal pain, constipation, nausea and vomiting. The investigators concluded that treatment with T-Vec via EUS-FNI was feasible and tolerable, and that future studies should investigate T-Vec in patients with less advanced disease (Chang *et al.*, 2012). Amgen Inc. who purchased BioVex Ltd. has recently announced a phase I clinical trial investigating T-Vec as a treatment in patients with locally advanced or metastatic pancreas cancer refractory to at least one chemotherapy regimen (clinicaltrials.gov identifier: NCT03086642). Virus is intended to be administered endoscopically to two cohorts (C1: 3 doses of 10^7 PFU/ml, and C2: 3 doses of 10^8 PFU/ml). The study is estimated to complete primary data collection in 2021.

2.3.4.4 Reolysin®

Reolysin, the lead oncolytic virus under investigation by Oncolytics Biotech is a wild-type, serotype 3 Dearing strain reovirus, that preferentially infects cells with an activated RAS pathway (Carew *et al.*, 2013; Gollamudi *et al.*, 2009; Hamid *et al.*, 2017; Mahalingam *et al.*, 2015). Mutation of K-RAS is a hallmark of PC development and progression and is exhibited in up to 90% of tumours (Almoguera *et al.*, 1988; Coffey *et al.*, 1998; Etoh *et al.*, 2003; Grünewald *et al.*, 1989). Consequently, Reolysin has been investigated in clinical trials for the treatment of advanced pancreatic adenocarcinoma in combination with gemcitabine (clinicaltrials.gov identifier: NCT00998322), or Reolysin in combination with chemotherapy (gemcitabine, Irinotecan, Leucovorin, and 5-FU) and pembrolizumab (clinicaltrials.gov identifier: NCT02620423). Results of these trials are yet to be reported in the literature. A third study investigated Reolysin in combination with carboplatin plus paclitaxel to carboplatin plus paclitaxel as first line treatments for recurrent or metastatic PC (clinicaltrials.gov identifier: NCT01280058). From 73 evaluable patients, the study found administration of Reolysin to be safe, but did not increase progression free survival when administered in combination with carboplatin plus paclitaxel vs. the chemotherapy alone (4.9 months vs 5.2 months, respectively). The study also concluded the K-RAS status of a patients tumour did not impact outcome (Noonan *et al.*, 2016).

2.3.4.5 VCN-01

VCN-01 is a genetically modified adenovirus harbouring replacement of the E1A gene with eight E2F binding sites. The deletion-insertion confers selective replication of VCN-01 to cancer cells. Additionally, the virus has an integrin binding amino acid motif (RGDK) knocked into the heparan sulfate glycosaminoglycans domain of VCN-01 which improves anti-tumour immune responses. Finally, VCN-01 also expresses hyaluronidase to degrade hyaluronan (Bayo-Puxan *et al.*, 2009; Guedan *et al.*, 2010; Martínez-Vélez *et al.*, 2016; Rodriguez-Garcia *et al.*, 2015; Rojas *et al.*, 2012; Vera *et al.*, 2016). Hyaluronan makes up part of the stromal reaction in cancers including PC (Apte *et al.*, 2013; Arsene *et al.*, 2014; Cheng *et al.*, 2016; Provenzano and Hingorani, 2013; Provenzano *et al.*, 2012; Sato *et al.*, 2016).

VCN Biosciences, S.L. are investigating VCN-01 in combination with gemcitabine plus nab-paclitaxel as a treatment for PC patients in phase I studies. Virus is administered either I.T. (clinicaltrials.gov identifier: NCT02045589) or I.V. (clinicaltrials.gov identifier: NCT02045602). Chemotherapy is administered I.V. No results have been reported and no dates have been given for estimated primary data collection.

2.3.4.6 LOAd703

Lokon Pharma AB have very recently commenced investigating their lead investigational oncolytic virus, LOAd703, in two phase I/II clinical trials as a treatment for PC in combination with conventional chemotherapy (gemcitabine +/- nab-paclitaxel) (clinicaltrials.gov identifiers: NCT02705196 and NCT03225989). Increasing concentrations of virus are intended to be administered through percutaneous ultrasound guided injection to determine maximum tolerated dose, safety, and clinical outcome. LOAd703 is a genetically modified serotype 5/35 adenovirus that expresses TMZ-CD40L and 4-1BBL. TMZ-CD40L and 4-1BBL lead to apoptosis of cancer cells, activation of cytotoxic and memory T-cells, reduction of immunosuppression, and promotes anti-tumour signalling in stromal cells (Diaconu *et al.*, 2012; Eriksson *et al.*, 2017a; Eriksson *et al.*, 2017b; Li *et al.*, 2015a; Liljenfeldt *et al.*, 2013; Loskog and Eliopoulos, 2009; Loskog *et al.*, 2004; Lynch, 2008).

2.3.4.7 ParvOryx

Oryx GmbH & Co. KG are undergoing investigations of ParvOryx in a phase I/II trial on patients with unresectable PC with at least one liver metastasis (clinicaltrials.gov identifier: NCT02653313). Virus at increasing doses is administered I.V. to patients daily for a total of four injections. Results are anticipated in the near future. ParvOryx is a rat specific naturally occurring Parvovirus H-1 that has tropism for many human cancer types. The virus is reported to have no effect on normal cells and is not pathogenic in humans (Cho *et al.*, 2015; Geletneky *et al.*, 2012; Heinrich *et al.*, 2013; Kaowinn *et al.*, 2015; Sieben *et al.*, 2013).

2.3.5 Immunotherapy for Pancreatic Cancer

Stimulating a patient's immune system to elicit an anti-tumour immune response to clear tumours is the latest approach in cancer research. Along with OVs, immune checkpoint inhibitors have proven to be efficacious immunotherapies in several cancer types. Immune checkpoint inhibitors are monoclonal antibodies that can block the interaction of T cells to inhibitory costimulatory signals on tumour cells. Cells are recognised as self when T cells bind concurrently with an antigen and an inhibitory costimulatory signal on a cells surface (Sharpe, 2009). Thus, immune checkpoint inhibitors block the innate ability of tumour cells to be recognised as self, leading to destruction by T cells. Alternatively, immune checkpoint inhibitors can interfere with T cell regulation by binding to antigen presenting cells allowing activation and proliferation of tumour specific cytotoxic T cells. Essentially, immune checkpoint inhibitors unmask cancer cells to the immune system and/or potentiate an adaptive anti-tumour immune response. Refer to Figure 15 for a schematic representation of the mechanism of action of one immune checkpoint inhibitor, anti-PD-1. Several immune checkpoint inhibitors have been approved by the USFDA for the treatment of cancer types including melanoma, non-small cell lung cancer, renal cell carcinoma, and bladder cancer (Borghaei *et al.*, 2015; Brahmer *et al.*, 2012; Guo *et al.*, 2017; Motzer *et al.*, 2015; Powles *et al.*, 2014; Topalian *et al.*, 2014; Xu *et al.*, 2017).

Unfortunately, PC does not respond to immune checkpoint inhibitors due to 1) the immunosuppressive nature of the tumour microenvironment, 2) sequestration of T cells into the stromal desmoplastic reaction of PC and away from PC cells (1 and 2

previously discussed), and 3) the mutational load of PC (Brahmer *et al.*, 2012; Guo *et al.*, 2017; Johansson *et al.*, 2016; Kotteas *et al.*, 2016; Laheru and Jaffee, 2005; Seo and Pillarisetty, 2016; Skelton *et al.*, 2017; Thind *et al.*, 2017; Torphy *et al.*, 2018). High mutational load, that is, the frequency of mutations leading to the expression of non-self-antigens, or neoantigens on cells, is associated with better response to immune checkpoint therapies. Melanoma, lung, and bladder cancers respond well to immune checkpoint inhibitors because of the high level of mutations and cell surface expression of neoantigens (Gubin and Schreiber, 2015; Rizvi *et al.*, 2015). Comparatively, PC has a low mutational load and subsequently does not express high levels of neoantigens that can be recognised by T cells. Refer to Figure 16 for the relative levels of somatic mutations observed in different cancer types from studies conducted by Alexandrov and colleagues (Alexandrov *et al.*, 2013; Guo *et al.*, 2017; Lawrence *et al.*, 2013). For PC to become sensitised to immune checkpoint inhibitors, an agent that remodelled the TME to allow T cell infiltration, initiate inflammation and upregulation of immune checkpoint molecules, and increased expression of neoantigens on PC cells would be required (Borazanci *et al.*, 2017; Guo *et al.*, 2017; Jiang *et al.*, 2017; Kota *et al.*, 2017). Perhaps CVA21 could achieve this and be a synergistic combination treatment modality for PC with immune checkpoint inhibitors.

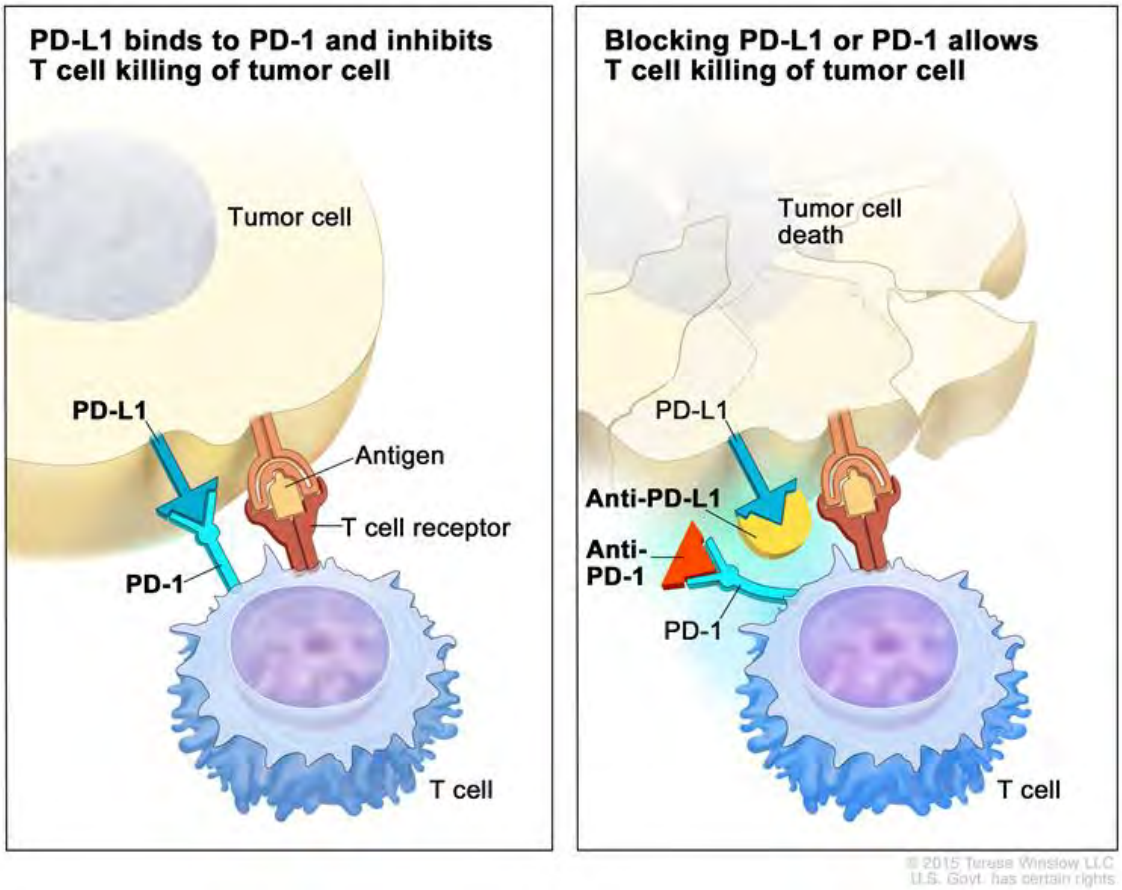

Figure 15: Schematic of immune checkpoint inhibitors (anti-PD1/anti-PD-L1) mechanism of action. © 2015 Terese Winslow LLC U.S. Govt. has certain rights. Image source: National Institute of Health National Cancer Institute.

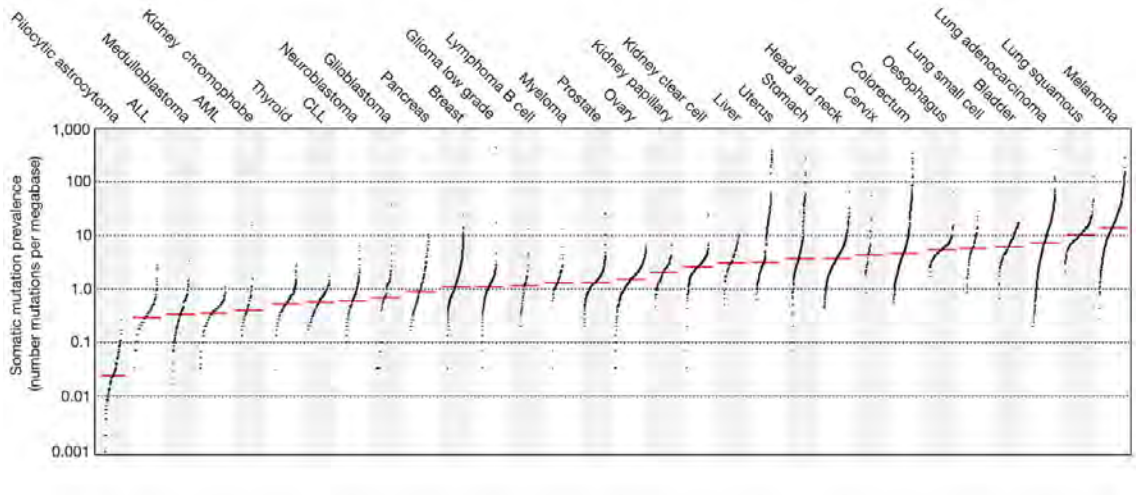

Figure 16: Mutational Landscape of Cancer Types. Image source: **Alexandrov, L. B., Nik-Zainal, S., Wedge, D. C., Aparicio, S. A. J. R., Behjati, S., Biankin, A. V., Bignell, G. R., Bolli, N., Borg, A., Børresen-Dale, A.-L., *et al.*** (2013). Signatures of mutational processes in human cancer. Nature **500**, 415–421.

2.4 Study Hypotheses and Aims

All currently approved treatments for PC fail to control disease and provide satisfactory quality of life to patients. In almost all cases death is a short-term reality. The potential for CVA21 as a treatment for PC is very attractive. Overexpression of the viral cell entry receptor, ICAM-1 in PC warrants investigation of CVA21 as a treatment for PC. Similarly, proven low pathogenicity, tolerability, disease control, and clearance of primary and distant tumours in patients with late stage malignancies assessed in recent clinical trials suggests that CVA21 would likewise be a well-tolerated and efficacious treatment for controlling and even reducing tumour burden in PC patients. Additionally, the profound toxicity associated with current chemotherapeutics immediately favours CVA21 due to a low pathogenic profile suggesting patients may have improved quality of life while undergoing treatment. Furthermore, combination of CVA21 with chemotherapeutics may prove synergistic and thus require lower concentrations of either agent and concordantly less toxicity and better quality of life for patients. Likewise, CVA21 may stimulate PC to become immunologically 'hot' permitting immune checkpoint inhibitors to have an effect.

2.4.1 Hypotheses

The major hypothesis of the present investigation was Coxsackievirus A21 could be an effective anti-cancer agent against PC due to high expression of viral entry receptors, ICAM-1 and/or DAF on PC and pancreatic stellate cells. Furthermore, CVA21 could have a synergistic effect in combination with standard of care chemotherapeutic or immunotherapeutic agents against PC.

2.4.2 Aims

- **Aim 1:** To assess the expression levels of CVA21 entry receptors, ICAM-1 and DAF, on the surface of human PC and pancreatic stellate cells and compare to normal pancreatic cells.

- **Aim 2:** To screen the sensitivity of human PC and pancreatic stellate cells to the oncolytic activity of CVA21 in comparison to normal pancreatic cells.

- **Aim 3:** To determine the synergistic or antagonistic relationship between CVA21 and conventional chemotherapy in combination on human PC and pancreatic stellate cells in comparison to normal pancreatic cells.

- **Aim 4:** To establish an orthotopic mouse model of human PC and investigate the potential of CVA21 as a treatment, alone, and in combination with conventional chemotherapy.

- **Aim 5:** To establish an immune competent mouse model of orthotopic, human ICAM-1 expressing PC and investigate CVA21 as a potential treatment, alone, and in combination with immunotherapeutic agents.

Chapter 3

Materials and Methods

3.1 *In Vitro* Experiments

3.1.1 Cell Lines

Ten human pancreatic cancer cell lines, AsPC-1, BxPC-3, Capan-2, Hs700T, Hs766T, MIA PaCa-2, Panc-1, PL45, SU.86.86, and SW 1990, two human pancreatic stellate cell lines, TAS29 and TAS31, one normal human pancreatic ductal epithelial (control cell line), HPDE, one mouse pancreatic cancer cell line, UN-KPC-961, one mouse pancreatic stellate cell line, ImPSCc2, and the human melanoma cell line (reference cell line), SK-Mel-28, were used in this study. AsPC-1, Panc-1, and SK-Mel-28 cell lines were obtained from the American Type Culture Collection (ATCC). BxPC-3, Capan-2, HPDE, Hs700T, Hs766T, MIA PaCa-2, PL45, SU.86.86 and SW 1990 were generously donated by Associate Professor Christopher Scarlett (University of Newcastle, Australia). TAS29 and TAS31 cell lines were gifted from Professor Steven J. Hughes (University of Florida, USA). ImPSCc2 cells were donated by Professor Raul Urrutia (Mayo Foundation for Medical Education and Research, USA). UN-KPC-961 cells were purchased from Professor Surinder K. Batra (University of Nebraska Medical Center, USA). Specifications of cell lines are presented in Table 3.

Table 3: Cell Lines investigated throughout study.

Cell Line	Species	Age	Sex	Organ	Pathology	Reference
AsPC-1	Human	62	F	Pancreas	Adenocarcinoma	(Chen *et al.*, 1982)
BxPC-3	Human	61	F	Pancreas	Adenocarcinoma	(Tan *et al.*, 1986)
Capan-2	Human	56	M	Pancreas	Adenocarcinoma	(Kyriazis *et al.*, 1986)
HPDE	Human	63	F	Pancreatic Duct	Normal	(Furukawa *et al.*, 1996)
Hs700T	Human	61	M	Pancreas; Pelvis Met	Adenocarcinoma	(Owens *et al.*, 1976)
Hs766T	Human	46	M	Pancreas; Lymph Node Met	Carcinoma	(Owens *et al.*, 1976)
MIA PaCa-2	Human	65	M	Pancreas	Carcinoma	(Yunis *et al.*, 1977)
Panc-1	Human	56	M	Pancreas	Carcinoma	(Lieber *et al.*, 1975)
PL45	Human	-	M	Pancreas	Ductal Adenocarcinoma	(Caldas *et al.*, 1994)
SK-Mel-28	Human	51	M	Skin	Melanoma	(Carey *et al.*, 1976)
SU.86.86	Human	57	F	Pancreas; Liver Met	Ductal Carcinoma	(Drucker *et al.*, 1988)
SW 1990	Human	56	M	Pancreas; Spleen Met	Adenocarcinoma	(Kyriazis *et al.*, 1983)
TAS29	Human	-	-	Pancreas	Tumour Associated Stellate	(Han *et al.*, 2015)
TAS31	Human	-	-	Pancreas	Tumour Associated Stellate	(Han *et al.*, 2015)
ImPSCc2	Mouse (C57BL/6)	-	-	Pancreas	Stellate	(Mathison *et al.*, 2010)
UN-KPC-961	Mouse (KPC)	-	-	Pancreas	Adenocarcinoma	(Torres *et al.*, 2013)

3.1.2 Tissue Culture

Cells were grown in either CELLSTAR® TC-Treated 25 cm^2, 75 cm^2, or 175 cm^2 cell culture flasks (Greiner Bio-One GmbH). AsPC-1, BxPC-3, SU.86.86 and SW 1990 cells were maintained in RPMI 1640 Medium (Hyclone, GE Healthcare Life Sciences). Capan-2, Hs700T, Hs766T, MIA PaCa-2, Panc-1, PL45, TAS29, TAS31, ImPSCc2 and UN-KPC-961 were maintained in Dulbecco's Modified Eagle Medium (DMEM) (Hyclone, GE Healthcare Life Sciences). DMEM and RPMI were supplemented with sterile, 2-10% foetal calf serum (FCS) (SAFC, Sigma Aldrich), 10 mM 4-(2-Hydroxyethyl)piperazine-1-ethanesulfonic acid (HEPES) (Hyclone, GE Healthcare Life Sciences), 2 mM L-glutamine (Gibco, Life Technologies) sodium pyruvate (Gibco, Life Technologies) and 100 IU/ml penicillin-streptomycin (Gibco, Life Technologies). HPDE cells were maintained in Keratinocyte Serum Free Media (KSFM) supplemented with human recombinant Epidermal Growth Factor 1-53 (EGF 1-53) and Bovine Pituitary Extract (BPE) (Gibco, Life Technologies). Cells were sustained in a HERAcell® (Heraeus) 150 incubator at 37°C, 5% CO_2, with humidity. Cells were subcultured every three to four days by decanting media, washing cells with phosphate buffered saline (PBS) (Gibco, Life Technologies), and detaching cells with 0.5% Trypsin-EDTA (10x) (Gibco, Life Technologies) before resuspension in either media or PBS supplemented with FCS to deactivate trypsin. Between 5-20% of detached cells were seeded into new tissue culture flasks and maintained as above. Remaining cells were used for assaying. Cell lines were routinely tested for the absence of contaminating mycoplasma using MycoSensor™ QPCR Assay Kits (Agilent Technologies, Australia).

3.1.3 Seeding Cells Into Tissue Culture Plates For Assaying

Cell counts were conducted on 10 µl of detached cells mixed with 10 µl trypan blue (BIO-RAD) using a TC-10 cell counter (BIO-RAD). Cells were resuspended to a concentration of 1 x 10^5 cells/ml in media and seeded at 100 µl per well of a 96-well Nunclon™ Delta plate (Nunc, Thermo Fisher Scientific), 1 ml of a 24-well Nunclon™ Delta plate (Nunc, Thermo Fisher Scientific), or 3 ml of a 6-well plate Nunclon™ Delta plate (Nunc, Thermo Fisher Scientific), and incubated overnight at 37°C, 5% CO_2, with humidity. For co-culture assays, human pancreatic stellate cells (TAS29 or TAS31) were mixed at a ratio of 4:1 stellate cells to pancreatic cancer cells (AsPC-1, BxPC-3, Capan-2, Hs700T, Hs766T, MIA PaCa-2, Panc-1, PL45, SU.86.86 or SW 1990) and

resuspended to a final concentration of 1 x 10^5 cells/ml in 10% FCS media and seeded at 100 µl per well of a 96-well Nunclon™ Delta plate (Nunc, Thermo Fisher Scientific), Alternatively, for neutralisation assays, SK-Mel-28 cells were resuspended to 5 x 10^4 cells/ml in 10% FCS DMEM and seeded at 50 µl per well of a 384-well Nunclon™ Delta plate (Nunc, Thermo Fisher Scientific).

3.1.4 Quantitative PCR to Determine Transcript ICAM-1 and DAF Levels

RNA from 1 x 10^6 cells in RLT lysis buffer (QIAGEN) were extracted using a RNeasy mini kit - Large samples: Animal tissue and Cells protocol on a QIACube (QIAGEN). Concentration and purity of collected samples were measured using a NanoDrop Spectrophotometer ND-1000 (Thermo Fisher Scientific). RNA samples were reverse transcribed into cDNA by mixing 800 ng of RNA with 4 µl of 5x RT buffer (Bioscript, Bioline) + 1 µl of Ribosafe RNase inhibitor (Invitrogen, Life Technologies) + 1 µl of Bioscript reverse transcriptase (200 µg/µl) (Bioscript, Bioline) + 4 µl of DEPC treated water (Invitrogen) and amplification on a PCR thermal cycler (TaKaRa). Reverse transcription amplification protocol was 10 mins at 25°C followed by 42°C for 60 minutes. The reaction was terminated by heating to 85°C for 5 minutes. cDNA samples were stored at -20°C until used in PCR reactions.

TaqMan® Assay on demand™ (AOD) primers with a FAM™ dye label (Applied Biosystems) specific for ICAM-1, DAF, and the housekeeping genes, ACTB, and GAPDH were used in PCR reactions. PCR reactions were prepared by adding 1 µl of cDNA samples to 9 µl 1x master mix [5 µl Sensimix II (Bioline), 0.5 µl primer, 0.02 µl ROX (Bioline), 3.48 µl DEPC treated water (Invitrogen)] for each target gene. Samples were mixed on an Eppendorf MixMate (Eppendorf) at 1650 rpm for 30 seconds, and pulse centrifuged to ensure solutions were deposited at the base of each well. Samples were cycled on a StepOnePlus™ Real-Time PCR System (Applied Biosystems) at 95°C for 10 minutes, followed by 40 cycles of 95°C for 15 seconds to 60°C for 1 minute. Data were analysed by normalising each sample to GAPDH and ACTB using StepOne Software v2.3 (Applied Biosystems), QBase plus (Biogazelle), and graphs generated using Prism v7.0 (GraphPad).

3.1.5 Flow Cytometry to Determine ICAM-1 and DAF Cell Surface Expression

Cells were detached from tissue culture flasks using 1 x versene (Sigma Aldrich) and resuspended in PBS. After centrifugation at 450 *x g* for 5 minutes, resuspension in PBS, and a cell count using a TC-10 tissue counter (BIO-RAD), 2-5 x 10^5 cells in triplicate were pipetted into 5 ml Polystyrene Round-Bottom Tubes (BD Biosciences) for each cell line. Cells were labelled with Mouse monoclonal [1H4] to ICAM-1, prediluted (Phycoerythrin) (Abcam #ab18222), or Mouse monoclonal Anti-CD55 antibody [143-30] (Phycoerythrin) (Abcam #ab25540). One tube for each cell line was left unstained as controls. Cells were incubated in darkness at 4°C for 20 minutes. PBS was added to each sample to wash off unbound antibody and cells centrifuged at 450 *x g* for 5 minutes to pellet cells. Supernatant was discarded to leave approximately 500 µl volume in each tube. Optimal voltage and threshold settings for fluorescence activated cell scanning (FACS) on a BD FACSCanto™ II (BD Biosciences) were determined and kept constant across each flow cytometry run. Cells were measured for FSC-H, FSC-A, SSC-H, SSC-A, PE-H and PE-A. 1 x 10^4 cells were measured for each treatment (unstained, ICAM-1, or DAF). BD Quantibrite™ PE Beads (BD Biosciences) were measured alongside under the same instrument settings and the number of antibodies bound per cell interpolated according to the manufacturer's protocol (BD Biosciences). Data were analysed using Weasel V3.0.2 software. Graphs were generated using Prism v7.0 (GraphPad).

3.1.6 Virus

The Kuykendall strain of Coxsackievirus A21 (CVA21) was obtained from Dr M. Kennett (Entero-Respiratory Laboratory Fairfield Hospital, Australia). CVA21 used for *in vitro* studies was propagated in the melanoma cell line, SK-Mel-28, for 24 hours before being freeze-thawed three times, centrifuged at 2500 *x g* for 5 minutes and 0.22 µm filtered. Aliquots were stored at -80°C (Shafren *et al.*, 1997). Viralytics Ltd's (Newcastle, Australia) proprietary bio-selected formulation of CVA21, CAVATAK™, was used for *in vivo* studies and produced under good manufacturing practice conditions.

3.1.7 Viral Infectivity Assay ($TCID_{50}$ Assay and Co-culture $TCID_{50}$ Assay)

To determine the concentration of CVA21 in a given sample expressed as 50% tissue culture infectious dose ($TCID_{50}$), SK-Mel-28 cells (reference cell line) were infected in triplicate with 100 µl of 10-fold serial dilutions in 2% FCS media. Negative controls: media only treated wells were included for each replicate. After incubation of cells in a humidified environment at 37°C with 5% CO_2 for 72 hours, cytopathic effect (CPE) was recorded via observation of cells under an Olympus CKX41 light microscope (Olympus). The Karber method of calculating $TCID_{50}$ from CPE was used as follows:

$$\frac{Log_{10}TCID_{50}}{ml} = 10^{1+L+d(s-0.5)}$$

L is the log of the lowest dilution
d is the log difference between dilutions (1 for a 10-fold dilution)
s is the sum of the ratios of CPE positive wells

$TCID_{50}$/ml values were graphed using Prism v7.0 (GraphPad).

Alternatively, to determine the sensitivity of a cell line to CVA21, 96-well plates seeded with cells the previous day (refer to section 3.1.3) were infected in quadruplicate with 100 µl of 10-fold serial dilutions of CVA21 in 2% FCS media, and incubated overnight at 37°C, 5% CO_2, with humidity for 72 hours. The starting concentration of CVA21 (10^{-1} dilution) was constant across the study at 4.51 x 10^7 $TCID_{50}$/ml. Negative controls: media only treated wells were included for each replicate. Cell viability at 72 hours was measured by MTT assays (refer to section 3.1.13).

3.1.8 Viral Replication Kinetics Assay (Growth Curve Assay)

Cells were infected with a multiplicity of infection (MOI) of 10 CVA21 and incubated for 1 hour at 37°C, 5% CO_2, with humidity. Supernatant was discarded, and cells washed with PBS 3 times to remove unbound CVA21. Cells were replenished with media and incubated at 37°C, 5% CO_2, with humidity for 0, 2, 4, 6, 8, 24, 48, and 72 hours. At each set time point cells were frozen to -80°C to inhibit further viral replication. Cells then underwent three freeze-thaw cycles to lyse cells. Total supernatant and cellular material was collected and centrifuged at 450 *x g* for 5 minutes. The concentration of CVA21 at each time point for each cell line was determined by titration against the reporter cell line, SK-Mel-28 cells (refer to section 3.1.7). Graphs were generated using Prism v7.0 (GraphPad) by plotting concentration ($TCID_{50}$) of CVA21 against time for each cell line.

3.1.9 Immunohistochemical Detection of ICAM-1

Two pancreatic cancer tumour microarrays (TMA), Pa1002a and HPan-A150CS-02, were purchased from US Biomax, Inc. Human glioblastoma tissue sections 2343 and 2005 (Canadian Virtual Tumour Bank), previously confirmed to express high ICAM-1 were stained alongside as positive and negative controls for each assay. Excess paraffin wax was removed by incubating slides at 70°C for 1 hour followed by incubation at RT in xylenes (VWR Chemicals) for 5 minutes and 100% ethanol (Ajax Finechem, Thermo Fisher Scientific) for 5 minutes. Sections were rehydrated by incubating in 70% ethanol for 3 minutes, 40% ethanol for 3 minutes, 10% ethanol for 3 minutes and ddH_2O for 3 minutes. Antigen retrieval was conducted by steaming sections in citric acid/EDTA buffer pH 8 [1 mM EDTA disodium salt dehydrate (Ajax Finechem) 1 mM Trisodium Citrate (Merck), 2 mM Tris Base (Merck)] for 30 minutes in a George Foreman GF3TSM Steamer (Spectrum Brands). Sections were washed three times in PBS for five minutes each. Endogenous peroxidase was blocked for by incubating cells in 0.3% hydrogen peroxide (Ajax Finechem) in methanol (VWR Chemicals) for 30 minutes at RT. Sections were washed three times in PBS for five minutes each. Blocking for non-specific binding of antibodies was conducted by incubating sections in normal sera of the species the secondary antibody was raised in, diluted in 1% bovine serum albumin (Sigma Aldrich) in PBS for 60 minutes at RT in a moist sealed container. Sections were incubated overnight at 4°C in a moist sealed

container with 1:500 Mouse Anti-ICAM-1 (G-5) Antibody) (Santa Cruz Biotechnology #sc-8439) in PBS, or mouse IgG (negative control) (Biocare Medical). Sections were washed three times in PBS for five minutes each. Vectastain ABC staining kits (Vector Laboratories) were used for secondary antibody staining. Briefly, secondary biotinylated antibodies diluted in PBS were incubated on sections at RT for 30 minutes in a moist sealed container. Sections were washed three times in PBS for five minutes each before Vectastain ABC reagents diluted in PBS were added to sections and incubated at RT for 30 minutes in a moist sealed container. Sections were washed three times in PBS for five minutes each. 3,3-Diaminobenzidine (DAB) staining kits (Sigma Aldrich) were used for detection of antigen staining. Sections were incubated in 0.22 µm filtered DAB substrate for 5 minutes before being rinsed in water. To counterstain nuclei, sections were incubated in 0.22 µm filtered Carazzi's haematoxylin (Fronine) for 1 minute, washed in water, and then differentiated in Scott's Tap Water Solution (Sigma Aldrich) for 2 minutes before being rinsed in distilled water. Sections were dehydrated by submerging slides in 100% ethanol (Ajax Finechem, Thermo Fisher Scientific) for 5 minutes prior to transfer into xylenes (VWR Chemicals) for 5 minutes. Stained sections were mounted with resin-based Entellan® New Mounting Media (ProSciTech) and cover slips applied before drying sections overnight at RT. Photomicrographs of stained sections were imaged on an Aperio AT2 scanner (Leica Biosystems) at 200x magnification. Quantitative IHC analyses were performed using Halo™ Image Analysis Platform (IndicaLabs). H scores were calculated from DAB staining pixel intensity values using the formula:

$$\mathrm{H} = 3 \times a + 2 \times b + 1 \times c$$

a is the percentage of pixels with strong staining
b is the percentage of pixels with moderate staining
c is the percentage of pixels with weak staining.

Images were generated using Microsoft PowerPoint (Microsoft) and Prism v7.0 (GraphPad). Graphs were generated, and statistical analyses performed using Prism v7.0 (GraphPad) (Refer to section 3.2.11.).

3.1.10 Chemotherapy

Gemcitabine hydrochloride (2'-deoxy-2',2'-difluorocytidine monohydrochloride (β-isomer)) 10 mg/ml was obtained from the Department of Clinical Toxicology and Pharmacology (Calvary Mater Newcastle, Australia).

3.1.11 Chemosensitivity Assay (EC_{50} Assay)

96-well plates seeded with cells the previous day (refer to section 3.1.3) were inoculated in quadruplicate with 100 µl of 10-fold serial dilutions of gemcitabine in 2% FCS media, and incubated at 37°C, 5% CO_2, with humidity for 72 hours. Four times the reported maximum serum concentration (C_{max}) of gemcitabine, 120 µg/ml (Mavroudis *et al.*, 2003), was used as the starting concentration (10^{-1} dilution) for assays. Negative controls: media only treated wells were included for each replicate. Cell viability at 72 hours was measured by MTT assays (refer to section 3.1.13).

3.1.12 Synergy Assay (Checkerboard Assay)

Initially the concentrations of CVA21 ($TCID_{50}$) or gemcitabine (EC_{50}) to induce a 50% reduction in cell viability for each cell line were determined (refer to section 3.1.7 and section 3.1.11). 2-fold serial dilutions starting at 4 x $TCID_{50}$/EC_{50} of each agent in 2% FCS media, alone, and in combination were titrated in quadruplicate against cells in 96-well plates prepared the previous day (refer to section 3.1.3). If the $TCID_{50}$ value could not be determined for a cell line, then 4 x 10^8 $TCID_{50}$ CVA21 was used as the starting dilution. If the EC_{50} value could not be determined for a cell line then 4x the reported maximum serum concentration (C_{max}) of gemcitabine, 120 µg/ml (Mavroudis *et al.*, 2003) was used as the starting dilution. The ratio of CVA21 to gemcitabine was constant across each 2-fold dilution. Negative controls: media only treated wells were included for each replicate. Cells were incubated at 37°C, 5% CO_2, with humidity for 72 hours before cell viability being assessed by MTT assay (refer to section 3.1.13). From the average normalised optical density of each dilution, the combination index (CI) and fraction affected (Fa) values were calculated using CompuSyn software (BioSoft) and graphs generated using Prism v7.0 (GraphPad).

3.1.13 Cell Viability Assay (MTT Assay)

3-(4,5-dimethylthiazol-2-yl)-2,5-diphenyltetrazoliumbromide (Methyl Thiazolyl Tetrazolium/MTT) (Sigma Aldrich) cell viability assays were performed to assess the viability of cells after treatment with CVA21 and gemcitabine, either alone or in combination. 20 µl of MTT was added to each well of 96-well plates with treated cells and incubated at 37°C, 5% CO_2, with humidity for 3 hours (24 hours for Capan-2 cells). Internal negative controls: media only, and positive controls: 100% lysis of cells, were included for each replicate. 100% lysis of cells was achieved by treating cells with 5 µl 10x lysis buffer (Promega). Following crystallisation of MTT, supernatant was aspirated using a syringe manifold (Drummond Scientific Company). 50 µl of dimethyl sulfoxide (DMSO) (Ajax Finechem, Thermo Fisher Scientific) was added to each well to dissolve crystals and the optical density (OD) of each well measured on a Microplate Reader 680XR (BIO-RAD) at λ = 540 while subtracting the λ = 655 nm background or on an iMark Microplate Reader (BIO-RAD) at λ = 490 while subtracting the λ = 655 nm. To determine percentage cell viability, the OD of each treated well was normalised against the internal negative, and positive controls OD for each replicate using Prism v7.0 (GraphPad).

3.1.14 Transfection of Cells With Human ICAM-1 cDNA

The mouse cell lines ImPSCc2 and UN-KPC-961 were transfected with the human gene for ICAM-1 using a pEF-BOS expression vector (Mizushima and Nagata, 1990). Cells were treated with a mixture containing pEF-BOS encoding human ICAM-1 cDNA, p3000™ Reagent (Invitrogen, Thermo Fisher Scientific) and Lipofectamine™ 3000 Reagent (Invitrogen, Thermo Fisher Scientific). Human ICAM-1 transfected cell lines, termed ImPSCc2-ICAM-1 and UN-KPC-961-ICAM-1, were enriched to select stably transfected human ICAM-1 expressing subpopulations by FACS and consecutive subculturing of isolated single cells. Briefly, cells were prepared according to section 3.1.5 using the Mouse Monoclonal [1H4] to ICAM-1, Prediluted (Phycoerythrin) antibody and sorted on a BD FACSAria II (BD Biosciences). Cells expressing phycoerythrin (ICAM-1 positive cells) were collected in 10% FCS DMEM and diluted across a 96-well Nunclon™ Delta plate (Nunc, Thermo Fisher Scientific) to isolate single cells in wells. Single cell clones were expanded (refer to section 3.1.2) and tested for ICAM-1 expression according to section 3.1.5 and susceptibility to

CVA21 according to section 3.1.7 over consecutive cell passages until stably transfected, CVA21 susceptible cell lines were achieved.

3.1.15 Transduction of Cells With Firefly Luciferase Via a Lentiviral Vector

The human pancreatic cancer cell line, Panc-1, and the mouse pancreatic cancer cell line, UN-KPC-961-ICAM-1 were transduced to express the firefly luciferase gene. Cells were treated with media containing 10 mg/ml Diethylaminoethyl-Dextran (DEAE-Dextran) and a lentivirus vector encoding the firefly luciferase gene under a ubiquitin promoter. The lentivirus vector and transduction reagents were provided by Professor Jerry Shay (University of Texas Southwestern Medical Center, USA). After 72 hours incubation in the lentiviral medium, cells were subcultured and analysed for luciferase expression. 20 µl of 50 mg/ml XenoLight™ D-luciferin Potassium Salt (Perkin Elmer) in PBS was added to 2-fold serial dilutions of transduced cells in a black flat-bottom 96-well tissue culture plate (Corning) and luciferase expression measured using an IVIS™ Imaging System 100 (Xenogen) at high resolution (low binning) for 30 seconds exposure at 5 cm field of view (stage A). The transduced cell lines were referred to as Panc-1-luc and UN-KPC-961-ICAM-1-luc.

3.2 *In Vivo* Mouse Models

3.2.1 Ethics Statement and Housing Conditions

Animal procedures were approved by the University of Newcastle Animal Care and Ethics Committee (ACEC) in accordance with the 'Guide for the Care and Use of Laboratory Animals, 8th Edition' (National Research Council, 2010) under protocols A-2015-501, A-2015-527, and A-2015-530. Specific pathogen free (SPF) mice were housed in groups of four in HEPA-filtered Tecniplast individually ventilated cages (Tecniplast) connected to a Tecniplast Smart Flow air handling system (Tecniplast) in the Animal Services Unit at the Hunter Medical Research Institute, Australia. Air was cycled 70 times per hour and humidity and temperature regulated at 23 °C. Food and water were provided *ad libitum*. Mice were exposed to light/dark on a 12/12 hour cycle. Mice were allowed to acclimatise in their cages for seven days before

procedures commenced. All procedures were conducted using sterile technique in a class II biosafety cabinet (Contamination Control Laboratories) to maintain SPF status. Weights of mice were recorded three times a week on a Mettler Toledo MS3002S Precision Balance (Mettler Toledo). Mice were humanely euthanised via CO_2 asphyxiation using a carbon dioxide regulator (Tescom, Emerson) at a rate of 20% volume of container per minute when signs of pain and distress, a weight loss of 10% or more from the maximum recorded weight, or prior endpoints were observed. For example, a mouse was euthanised when a tumour volume of 1 x 10^9 flux (photons/second) or greater was measured via bioluminescence imaging. For each mouse model, four mice deemed no treatment controls (N.T.C.) were excluded from all procedures (such as tumour inoculation and bioluminescence imaging of tumours) with the exception of weighing three times a week and blood collection.

3.2.2 Immune System Depletion

Two or three days prior to tumour inoculation, immune competent (C57BL/6, BALB/c) mice that would be inoculated with tumour cells were given a single dose of anti-NK1.1 (*InVivo*MAb anti-mouse NK1.1 Clone: PK136 #:BE0036 BioXcell), anti-CD4 (*InVivo*Plus anti-mouse CD4 Clone GK1.5 #:BP0003-1 BioXcell), and anti-CD8α (*InVivo*MAb anti-mouse CD8α Clone 2.43 #:BE006 BioXcell) antibodies via the lateral tail vein, or intraperitoneally (I.P.) in a volume of 100 µl. Further injections of the anti-NK1.1, CD4, and CD8α antibodies via the lateral tail vein, or I.P. in a volume of 100 µl could be administered thereafter every 5 days (days 3, 8 and 13 post tumour inoculation).

3.2.3 Tumour Inoculation

3.2.3.1 Orthotopic Pancreatic Tumour Implantation

Before surgery mice (C57BL/6, BALB/c) were shaved to remove fur using rodent clippers. For pain relief, mice were given a single injection of Carprofen (5 mg/kg) (Norbrook) analgesic and Buprenorphine (0.05-0.1 mg/kg) (Reckitt Benckiser) opioid subcutaneously (S.C.). Surgical tools and supplies (surgical scissors (Fine Science Tools), forceps (L.R. Instruments), Castroviejo needle holders (Onyx, Able Scientific),

tissue clip applicator (MikRon), 9 mm tissue clips (MikRon/Cellpoint Scientific), gauze (Independent Dental Supplies) cotton tips (BSN Medical), and paper towel (Kleenex)) were steam autoclaved prior to each surgery session. All procedures were performed using sterile technique. Surgery sessions were conducted in an aseptic environment on a heating pad (Pet-Mat). Mice were anaesthetised via intraperitoneal injection (I.P) of ketamine HCl (100 mg/kg) (Ceva) and xylazine (10 mg/kg) (Troy Laboratories). Top up doses of ketamine HCl and xylazine were given accordingly throughout the surgical procedures to maintain surgical depth of anaesthesia. Alternatively, mice were anaesthetised via gaseous inhalation with isoflurane (Pharmachem) at 5 L/min using a XGI-8 Gas Anaesthesia System (Xenogen) to induce anaesthesia and maintain surgical anaesthesia at a rate of 1-3 L/min. Mice were checked continually to ensure they remained in a surgical level of anaesthesia (lack of standard foot pinch response). Prior to surgical incision, PolyVisc™ eye cream (Alcon) was placed over the eyes of mice to prevent desiccation, and the abdominal/subcostal area of the mice disinfected with a povidine-iodine solution (Betadine) or chlorhexidine solution (Schulke). After verification of surgical plane anaesthesia, sterile surgical scissors were used to make a small 1-2 cm subcostal incision through the skin layer and peritoneum. The pancreas was identified and lifted up by a sterile cotton wool tip or forceps. Cells in a 1:1 mixture with Matrigel® Basement Membrane Matrix (Corning) were injected slowly into the pancreas using a 0.3 ml BD Ultra-Fine II Insulin Syringe (BD Biosciences). Maximum volume of cell solution was 30 µl. A sterile cotton wool tip was pressed onto the injection site for approximately 30 seconds to prevent leakage of cells. The pancreas was carefully returned to its location within the abdominal cavity and the peritoneum closed with Biosyn™ Monofilament 4-0 absorbable sutures (Covidien), and the skin layer closed with 9 mm tissue clips (Cellpoint Scientific). Mice recovered in their cages placed on a heating pad (Pet-Mat) and monitored every 2 hours for 6 hours after surgery. Mice that exhibited symptoms of pain over the following few days were given Buprenorphine (0.05-0.1 mg/kg) opioid S.C. for pain relief. Tissue clips were removed 7-10 days after surgery using a tissue clip remover (Able Scientific).

3.2.3.2 Subcutaneous Pancreatic Tumour Implantation

Prior to injection, mice were lightly anaesthetised using isoflurane and the sites of injections and surrounding area were disinfected with a 70% ethanol swab (Livingstone International). 100 µl of cells in PBS were injected S.C. into the left hind flank of each mouse, and 100 µl of cells in PBS were injected S.C. into the right hind flank of each mouse. If a mouse appeared in pain and discomfort due to injections, then carprofen (5 mg/kg) analgesic was administered S.C.

3.2.4 Tumour Measurements

3.2.4.1 Bioluminescence Imaging of Orthotopic Pancreatic Tumours

Hind flank areas of mice were sterilised with a 70% ethanol swab and 50 µl of 50 mg/ml XenoLight™ D-luciferin Potassium Salt (Perkin Elmer) in PBS administered S.C. approximately 5 minutes before bioluminescence imaging. Mice were anaesthetised by gaseous inhalation with isoflurane at 5 L/min to induce anaesthesia and maintenance of anaesthesia during imaging at a rate of 1-2.5 L/min. Tumours were measured via bioluminescent imaging using an IVIS™ Imaging System 100 (Xenogen) at high resolution (low binning) for 30 seconds exposure at 20 cm field of view (stage C). Peak flux (photons/second) measurements were recorded for auto-contoured regions of interest in each mouse using Living Image® software (Xenogen). Bioluminescent images were depicted as regions of interest overlaid on photographs. Flux values were graphed using Prism v7.0 (GraphPad). Mice were humanely euthanised by CO_2 asphyxiation if a flux value of 1×10^9 photons/second or greater was recorded.

3.2.4.2 Measurement of Subcutaneous Tumours

Subcutaneous tumours on the left and right hind flanks of mice were measured weekly with electronic Vernier callipers (Toolex) using the following formula for volume of a spheroid:

$$V = \frac{\pi}{6} \times a \times b^2$$

a is the longest perpendicular diameter
b is the shortest perpendicular diameter

Mice were humanely euthanised by CO_2 asphyxiation if a tumour volume of 2500 mm^3 or greater was recorded.

3.2.5 Treatments

3.2.5.1 Intratumoural Treatments of Orthotopic Pancreatic Tumours With CAVATAK™

To administer treatments directly into orthotopic pancreatic tumours, surgery was performed according to section 3.2.3.1 to expose tumours. CAVATAK™ (Viralytics) (1 x 10^8 $TCID_{50}$ in 100 µl) or 100 µl PBS was injected into externalised tumours according to treatment groups. Wounds were closed, and post-surgical monitoring of mice was conducted according to section 3.2.3.1. Treatments were repeated twenty days later for a total of two intratumoural treatments.

3.2.5.2 Intratumoural Treatments of Subcutaneous Pancreatic Tumours With CAVATAK™

Mice bearing left and right hind flank subcutaneous tumours were injected into the left flank tumour only. Prior to injection, the hind flank region of mice was disinfected with a 70% ethanol swab. CAVATAK™ (7.5 x 10^6 $TCID_{50}$ in 100 µl) (Viralytics) or 100 µl PBS

was injected into palpated subcutaneous tumours according to treatment groups. Treatments were repeated every three days for a total of four CAVATAK™ treatments.

3.2.5.3 Intraperitoneal Injections With Chemotherapy

Treatments with gemcitabine commenced three days after the second intratumoural treatment of orthotopic tumours with CAVATAK™ (Viralytics), or, concurrently with intratumoural treatments of subcutaneous tumours with CAVATAK™ (Viralytics). Prior to injection, the abdominal region of mice was disinfected with a 70% ethanol swab. 200 µl 10 mg/ml (approximately 120 mg/kg for a 17 g mouse) gemcitabine or 200 µl PBS was administered I.P. to mice according to treatment groups. Treatments were repeated every three to four days for a total of four chemotherapy treatments.

3.2.6 Sera Collection

Sera from mice were collected weekly beginning seven days after tumour inoculation, or, after commencement of first treatment. Mice were restrained, and venepuncture of the saphenous vein conducted using a 26 gauge needle (Terumo). Approximately 100 µl of blood was collected using a Hematocrit Capillary Tube (Bacto). Samples were allowed to clot at room temperature (RT) for 45 minutes before being centrifuged at 3000 $\times$ *g* for 10 minutes at RT. The top sera fraction was collected by pipetting and stored at -80°C for downstream testing.

3.2.7 Detection of CVA21 viremia

10-fold serial dilutions of sera starting at a 1:100 (10^{-2}) dilution in 2% FCS DMEM were titrated against SK-Mel-28 cells according to section 3.1.7. If CPE was not observed in all wells at the starting dilution of 10^{-2}, preventing for $TCID_{50}$ to be calculated via the Karber method, then an arbitrary below level of detection value of 316 $TCID_{50}$/ml CVA21 was recorded. CVA21 viremia as $TCID_{50}$/ml was plotted against time for each sera sample collected weekly using Prism v7.0 (GraphPad).

3.2.8 Detection of Circulating Neutralising Anti-CVA21 Antibodies

2-fold serial dilutions of sera samples in 2% FCS DMEM from 1:32 to 1:2048 were prepared. CVA21 was diluted in 2% FCS DMEM to a concentration of 4 x 10^5 $TCID_{50}$/ml (neat CVA21). 100 µl of sera dilutions were mixed with 100 µl CVA21 at 4 x 10^5 $TCID_{50}$/ml and incubated for 1 hour at 37°C, 5% CO_2, with humidity. In triplicate, 50 µl of each sera/CVA21 dilution was titrated against SK-Mel-28 cells in 384-well plates prepared the previous day (refer to section 3.1.3). Dilutions of 1:32 to 1:2048 +IgG control (positive control) (Sandoglobulin® NF liquid Normal Immunoglobulin [Human]) (CSL) in 2% FCS DMEM, and 10-fold dilutions of neat CVA21 (negative control) in 2% FCS DMEM were plated alongside sera samples. Cells were incubated at 37°C, 5% CO_2, with humidity for 72 hours before being scored for CPE under an Olympus CKX41 light microscope (Olympus). Neutralisation titres were calculated using the Karber method (refer to section 3.1.7), where neutralisation of CVA21, and hence lack of CPE in wells was considered positive. If no neutralisation of CVA21 (CPE) was present at a 1:32 dilution then an arbitrary below level of detection value of 1:32 was recorded. Neutralising titres were graphed against time for each sera sample collected weekly using Prism v7.0 (GraphPad).

3.2.9 Detection of CD4, CD8 and NK Cells in Circulating Blood

Approximately 100 µl of blood was collected from mice according to section 3.2.6 in 1.5 microfuge tubes (Eppendorf) and the volume raised to 1.5 ml with red blood cell lysis solution (150 mM Ammonium Chloride (Sigma Aldrich), 10 mM Sodium Bicarbonate (Sigma Aldrich), 100 µM EDTA disodium (Ajax Finechem)). After approximately 45 minutes incubation at RT samples were centrifuged for 5 minutes at 450 *x g*. Supernatant was discarded and pellets resuspended in PBS. Half of each sample was labelled with Anti-NK1.1 antibody [PK136] (FITC) (Abcam #ab25026), Anti-CD3 epsilon antibody [145-2C11] (PerCP) (Abcam #ab190299), CD4 Antibody (GK1.5) Alexa Fluor® 405 (Santa Cruz Biotechnology #sc13573), Alexa Fluor® 594 anti-mouse CD8α Clone 53-6.7 (BioLegend #100758)/Anti-CD8α antibody [53-6.7] (Phycoerythrin -Texas Red®) (Abcam #ab25294). The remaining sample was left unstained as controls. Samples were incubated in darkness at 4°C for 60 minutes.

PBS was added to each sample to wash off unbound antibody and cells in FACs tubes centrifuged at 450 *x g* for 5 minutes to pellet cells. Supernatant was discarded to leave approximately 500 µl volume in each tube. Alternatively, cells in 96-well plates were centrifuged using a SelctSpin™ Plate Centrifuge (Select BioProducts) for 1 minute. Supernatant was aspirated off and cells resuspended in 100 µl PBS. Optimal settings for FACS on a BD FACSCanto™ II (BD Biosciences) were determined and kept constant across each flow cytometry run. Cells were measured for FSC-A, SSC-A, FITC-A, Pacific Blue-A, PerCP-A, and PE A. 1 x 10^4 cells were measured for each treatment (unstained, or NK, CD3, CD4 and CD8 stained). Data were analysed using Weasel V3.0.2 software. Graphs were generated using Prism v7.0 (GraphPad).

3.2.10 Necropsies and Tissue Collection

After humanely euthanizing mice via CO_2 asphyxiation, cardiac punctures using a 19G needle (Terumo) attached to a 1 mL syringe (Terumo) were conducted to collect terminal blood samples. Sera were extracted from blood samples according to section 3.2.6. Necropsies were conducted to visualise tumours and metastases throughout the peritoneum, chest cavity, and skull. Tissues were fixed in 10% neutral buffered formalin (Sigma Aldrich) and stored at 4°C.

3.2.11 Statistical Analyses

Data were analysed using Prism v7.0 (GraphPad). Data were expressed as mean +/- standard error of the mean (SEM) from three or more independent biological repeats of experiments. Ordinary one-way ANOVA analyses with Tukey's multiple comparisons test or unpaired *t*-tests with Welch's corrections were performed to compare groups. *P* values below 0.05 were considered statistically significant, where * $P = < 0.05$, ** $P = < 0.01$, *** $P = < 0.001$, and **** $P = < 0.0001$.

Chapter 4

Coxsackievirus A21 as a Potential Treatment for Pancreatic Cancer: *In Vitro* Investigations

To examine the susceptibility of human pancreatic cancer to CVA21 oncolysis, preliminary *in vitro* analyses were performed on monolayers of a panel of pancreatic cancer and pancreatic stellate cell lines. Initially, the expression of the CVA21 cell surface receptors, ICAM-1 and DAF, were quantified on a gene transcript and protein level via quantitative real-time reverse transcript PCR, and flow cytometry. Following this, the susceptibility of each cell line to CVA21 oncolysis was defined by viral infectivity assays, and the capacity for each cell line to support CVA21 replication measured through viral growth kinetic assays. Pancreatic cancer cells were co-cultured with pancreatic stellate cells to better recapitulate the tumour microenvironment displayed in native pancreatic cancer, and the susceptibility of these co-cultured cells to CVA21 oncolysis determined through viral infectivity assays. Finally, to determine the susceptibility of human pancreatic cancer to CVA21 oncolysis, *ex vivo* tissue sections of human pancreatic cancer were analysed for the main CVA21 cell entry receptor, ICAM-1, by means of immunohistochemistry.

4.1 ICAM-1 and DAF Gene Expression From a Panel of Human Pancreatic Cancer and Pancreatic Stellate Cell Lines

Initially the cell surface entry receptors, ICAM-1 and DAF, were quantified on a gene transcript level from a panel of pancreatic cancer and pancreatic stellate cell lines. Total RNA was extracted from each cell line, reverse transcribed into cDNA and subsequently amplified by real-time PCR. Refer to methods section 2.14 for a detailed description of the protocol. Figure 17 depicts the gene expression levels of ICAM-1 and DAF normalised against the housekeeping genes ACTB and GAPDH, presented relative to normal human pancreatic ductal epithelial cells (HPDE) for each cell line. HPDE cells were selected as a reference cell line as they are derived from normal human pancreatic cells. Variation in gene expression levels from HPDE cells was considered either upregulation or downregulation. ICAM-1 and DAF gene expression from the melanoma cell line, SK-Mel-28, was included as a comparison to a cancer type which is highly susceptible to CVA21 oncolysis (Au *et al.*, 2005). A summary of ICAM-1 and DAF relative expression levels for each cell line is presented in Table 4 below.

From the results depicted in Figure 17, ICAM-1 expression (red bars) was upregulated in four of the ten pancreatic cancer cell lines (BxPC-3, Capan-2, Panc-1 and PL45), and one of the two pancreatic stellate cell lines (TAS29) compared to HPDE ICAM-1 transcript levels. Of the pancreatic cancer cell lines, Panc-1 cells expressed the highest ICAM-1 gene expression at 5.69-fold higher ICAM-1 transcript compared to normal HPDE cells. The pancreatic stellate cell line, TAS29, expressed 46.9-fold higher ICAM-1 gene transcript than normal HPDE cells. Thus, TAS29 cells expressed higher than the melanoma cell line, SK-Mel-28, at 18.8-fold ICAM-1 gene expression compared to HPDE cells. In contrast, MIA PaCa-2 ICAM-1 gene expression was downregulated the highest in comparison to HPDE cells at a 0.0004-fold relative expression. Likewise, MIA PaCa-2 cells had the lowest relative DAF expression at 0.0353-fold HPDE DAF gene expression.

Similarly, Figure 17 shows that DAF gene expression levels (blue bars) were upregulated in four of the ten pancreatic cancer cell lines (AsPC-1, BxPC-3, Hs700T,

and Hs766T). BxPC-3 cells being the only pancreatic cancer cell line to have both ICAM-1 and DAF gene upregulation compared to HPDE cells. The stellate cell lines, TAS29 and TAS31 displayed upregulation of 162-fold, and 5.11-fold DAF, respectively, compared to HPDE cells. Melanoma, SK-Mel-28 cells expressed relatively the same level of DAF gene transcript as HPDE cells (1.15-fold upregulation).

From these data, ICAM-1 and DAF gene expression varies greatly in pancreatic cancer and pancreatic stellate cells relative to normal ductal pancreatic cells. Additionally, there appears to be upregulation of DAF gene expression in stellate cells compared to HPDE cells. ICAM-1 and DAF cell surface expression was next determined by flow cytometry.

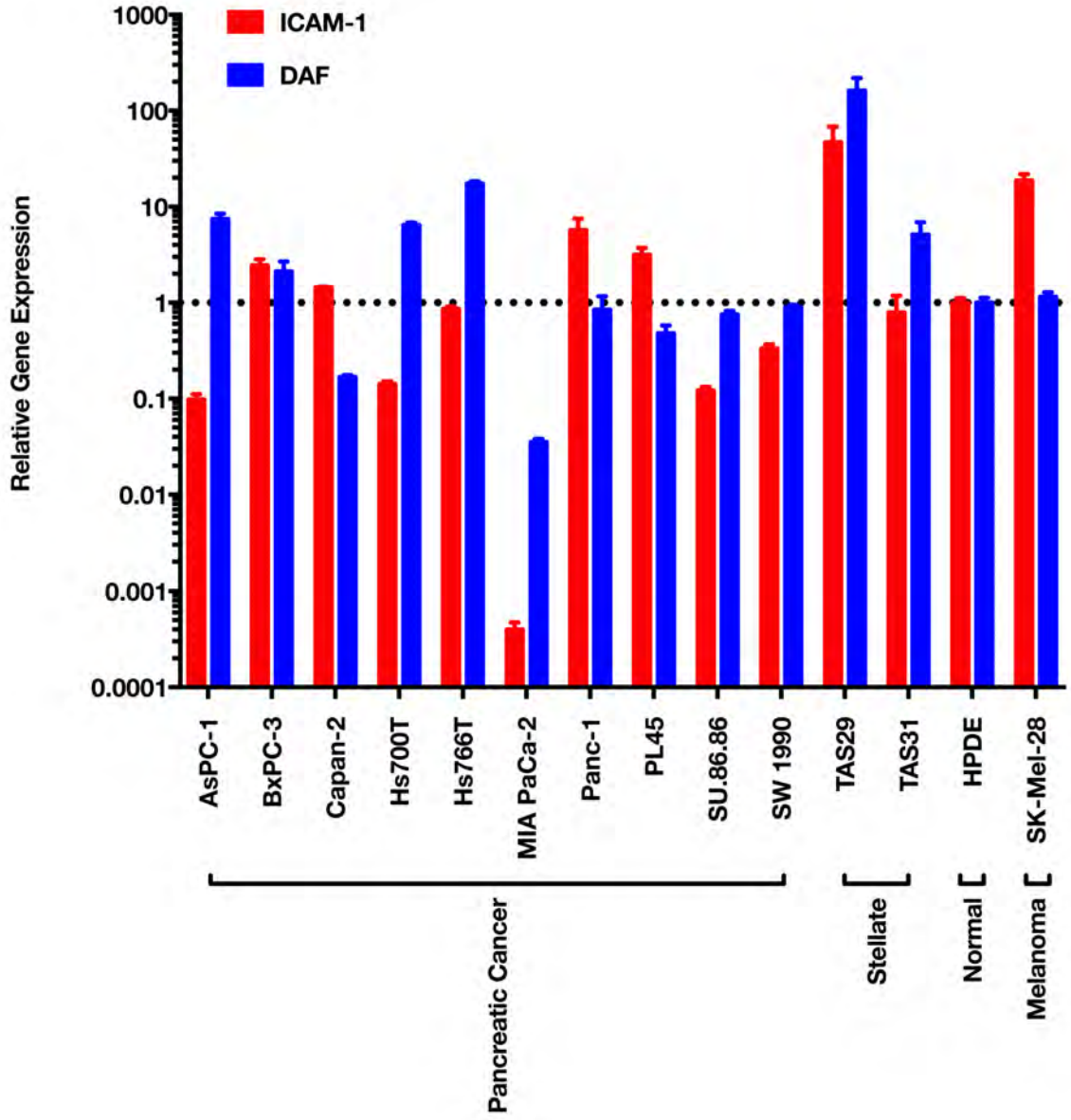

Figure 17: ICAM-1 and DAF gene expression levels from a panel of pancreatic cancer and stellate cells relative to normal pancreas cells. ICAM-1 and DAF gene expression levels were quantified via real time reverse transcription PCR and normalised against the housekeeping genes, ACTB and GAPDH. Data presented relative to normal pancreatic ductal epithelial (HPDE) cells. ICAM-1 and DAF gene expression levels of a highly susceptible melanoma cell line to CVA21 oncolysis, SK-Mel-28, included for comparison. Mean values of three replicates presented +/- SEM.

Table 4: Summary of ICAM-1 and DAF gene expression fold changes relative to normal pancreas cells (HPDE) in a panel of pancreatic cancer and pancreatic stellate cell lines.

		ICAM-1		DAF	
Cell Line	**Cell Type**	**Mean**	**SEM**	**Mean**	**SEM**
AsPC-1	Adenocarcinoma	0.098	0.0131	7.43	1.04
BxPC-3	Adenocarcinoma	2.45	0.388	2.12	0.561
Capan-2	Adenocarcinoma	1.44	0.022	0.168	0.00779
Hs700T	Adenocarcinoma	0.142	0.00928	6.42	0.426
Hs766T	Carcinoma	0.862	0.0479	17.4	0.995
MIA PaCa-2	Carcinoma	0.0004	0.0000747	0.0353	0.00295
Panc-1	Carcinoma	5.69	1.81	0.846	0.316
PL45	Ductal Adenocarcinoma	3.15	0.559	0.481	0.0972
SU.86.86	Ductal Carcinoma	0.122	0.0103	0.754	0.0686
SW 1990	Adenocarcinoma	0.334	0.0336	0.892	0.0596
TAS29	Stellate	46.9	21.5	162	57.2
TAS31	Stellate	0.794	0.389	5.11	1.78
HPDE	Normal Ductal Epithelial	1	0.119	1	0.126
SK-Mel-28	Melanoma	18.8	2.98	1.15	0.132

4.2 ICAM-1 and DAF Cell Surface Expression on a Panel of Human Pancreatic Cancer and Pancreatic Stellate Cell Lines

Following quantification of ICAM-1 and DAF gene expression in the panel of pancreatic cancer and pancreatic stellate cells via real-time PCR, ICAM-1 and DAF cell surface expression was determined for each cell line. Fluorescent cytometric analysis of each cell line labelled with monoclonal antibodies for ICAM-1 or DAF conjugated to phycoerythrin (PE) revealed qualitative ICAM-1 and DAF expression levels (Figure 18). Interpolation of these fluorescence values against a standard curve generated from measurement of Quantibrite™ PE Beads (BD Biosciences) under the same instrument settings allowed for quantification of ICAM-1 and DAF molecules per cell for each cell line (Figure 19). The assumptions for this quantification were that one PE fluorophore is conjugated to one antibody and only one antibody binds per cell surface receptor. Refer to methods section 2.1.5 for a description of the procedure.

In Figure 18 a peak shift to the right of the unlabelled control fluorescence peaks (solid grey) indicates fluorescence for PE corresponding to either ICAM-1 (red peaks) or DAF (blue peaks) expression. The greater the shift to the right indicates the higher the level of receptor per cell. Capan-2, Panc-1, and TAS29 cells expressed noticeably higher levels of cell surface ICAM-1 compared to normal pancreas cells (HPDE). Congruently, each pancreatic cancer cell line (AsPC-1, BxPC-3, Capan-2, Hs700T, Hs766T, MIA PaCa-2, Panc-1, PL45, SU.86.86, and SW 1990) and pancreatic stellate cell line (TAS29, and TAS31) expressed higher levels of DAF than HPDE cells. Melanoma cells, SK-Mel-28 cells expressed high levels of both ICAM-1 and DAF on their cell surface.

The interpolated number of receptor molecules, ICAM-1 or DAF, per cell for each cell line is depicted in Figure 19 and presented in Table 4. Half of the pancreatic cancer cell lines (BxPC-3, Capan-2, Hs766T, Panc-1, and PL45) expressed higher levels of ICAM-1 than normal pancreas cells (HPDE). Panc-1 cells expressed the highest level of ICAM-1 with an average 132,636 ICAM-1 molecules per cell, comparable to CVA21 sensitive melanoma cells (SK-Mel-28) that expressed on average 172,901 ICAM-1 molecules per cell. Both pancreatic stellate cell lines (TAS29, and TAS31) expressed higher levels of ICAM-1 compared to HPDE cells on average.

Interestingly, Panc-1 and TAS29 ICAM-1 cell surface expression did not accurately reflect gene expression data shown in Figure 17 and Table 4. Panc-1 cells had approximately 8-fold less ICAM-1 gene transcript compared to TAS29 cells. Nevertheless, Panc-1 cells had approximately double the number of ICAM-1 molecules per cell. In contrast, the two pancreatic cancer cell lines that expressed the lowest ICAM-1, AsPC-1 (802 molecules per cell), and MIA PaCa-2 (332 molecules per cell) had equally relatively lower gene expression, 0.098-fold, and 0.0004-fold, respectively, compared to HPDE cells. From these data, one observation is gene transcript levels may not always directly correlate with protein translation and receptor translocation to the cell surface.

With regard to DAF expression, AsPC-1, Hs766T, and TAS29 cells expressed the highest levels on average, 579,142, 1,780,426, and 792,963 molecules per cell, respectively. Thus, AsPC-1 cells had lower expression of ICAM-1 but higher expression of DAF compared to HPDE cells. Hs766T had similar ICAM-1 and remarkably higher levels of DAF expression compared to HPDE cells. Finally, TAS29 cells had high levels of both ICAM-1 and DAF expression when compared to HPDE cells. Similarly, BxPC-3, Capan-2, Panc-1, PL45, and TAS31 cells had overexpression of ICAM-1 and DAF compared to HPDE cells.

Based on these data, BxPC-3, Capan-2, Hs766T, Panc-1, PL45, TAS29, and TAS31 cells were suspected of being more susceptible to CVA21 oncolysis due to overexpression of ICAM-1 compared to HPDE cells. Furthermore, although ICAM-1 expression on pancreatic cancer cell lines may be lower compared to normal pancreas cells, the overexpression of DAF on each of the pancreatic cancer and pancreatic stellate cell lines may facilitate virus sequestration to the cell surface, increasing cell entry when a DAF-bound virus particle subsequently binds to ICAM-1. Next, the investigation addressed the susceptibility of the panel of human pancreatic cancer and pancreatic stellate cells to CVA21 oncolysis.

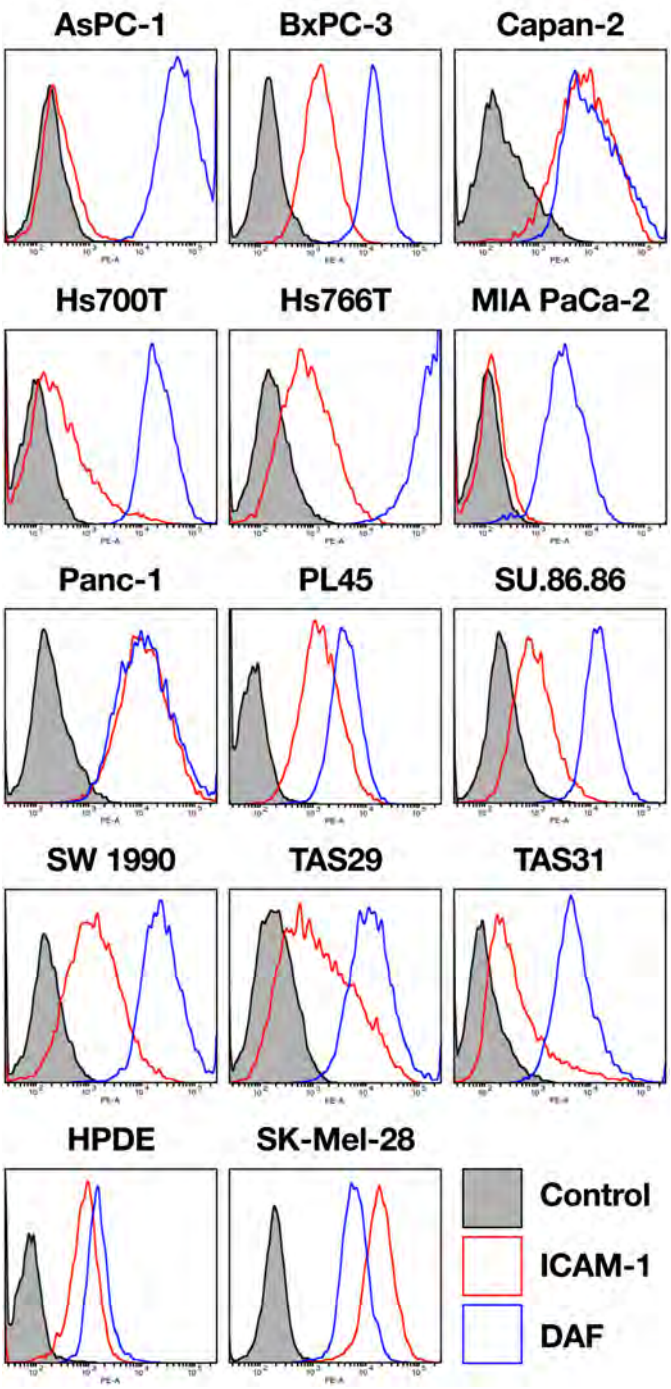

Figure 18: Relative ICAM-1 and DAF expression on a panel of human pancreatic cancer and pancreatic stellate cells. ICAM-1 and DAF cell surface expression was qualitatively determined via flow cytometry of cells labelled with monoclonal anti-ICAM-1 [1H4] (PE), or anti-CD55 [143-30] (PE), compared to unlabelled cells of the same cell line. Solid grey histograms represent the fluorescent intensity of unstained cells (negative control). Red peaks represent ICAM-1 cell surface expression. Blue peaks represent DAF cell surface expression. A shift to the right from the negative control peaks are comparative measures of ICAM-1 and DAF expression. Average of 1 x 10^4 events for each cell line.

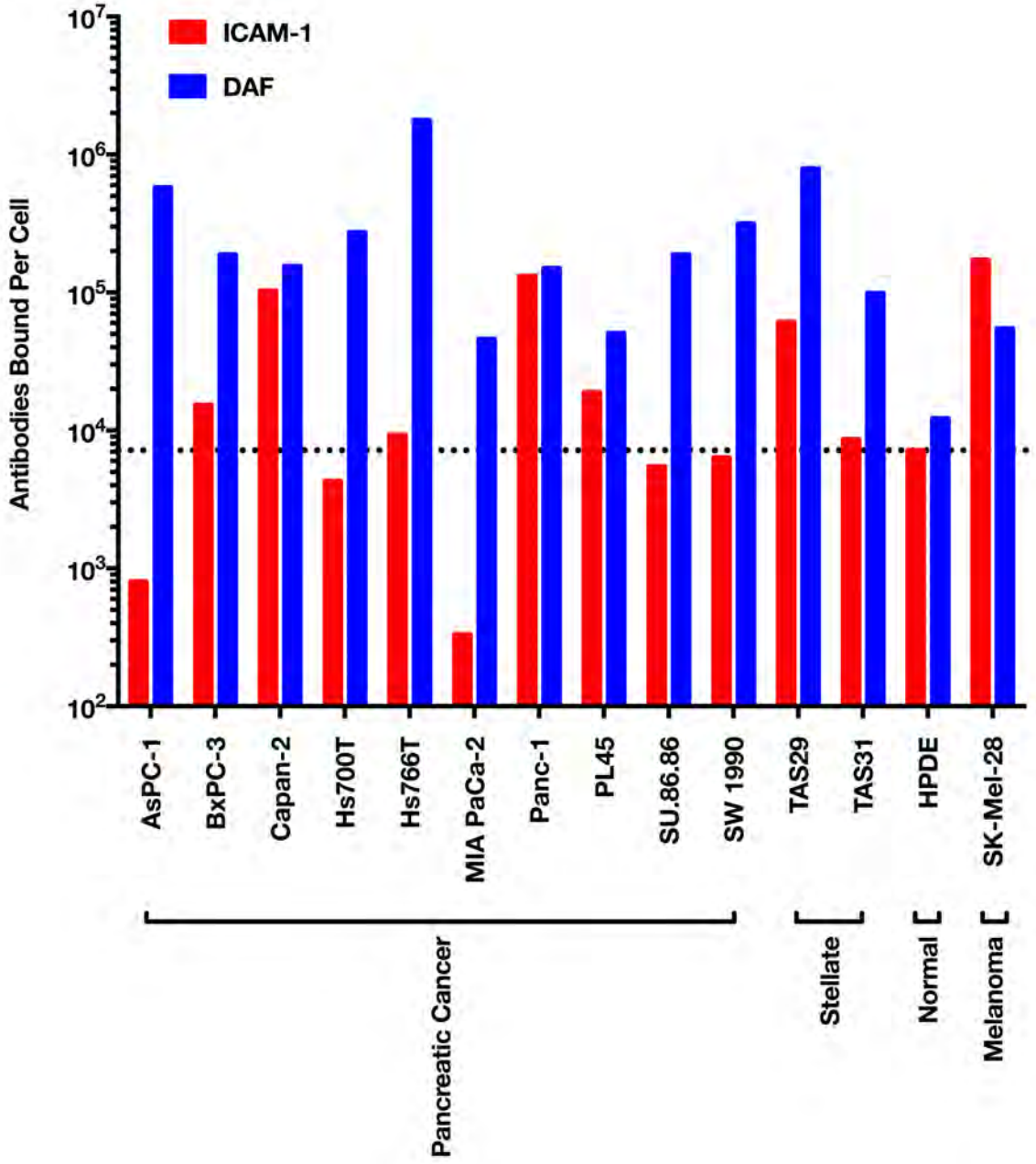

Figure 19: ICAM-1 and DAF cell surface expression on a panel of human pancreatic cancer and pancreatic stellate cells. ICAM-1 and DAF cell surface receptor levels were interpolated from a standard curve generated from measurement of Quantibrite™ PE Beads (BD Biosciences) under the same instrument settings. Red bars represent the number of ICAM-1 molecules per cell. Blue bars represent the number of DAF molecules per cell. Average of 1 x 10^4 events were collected for each cell line.

Table 5: ICAM-1 and DAF molecules per cell on a panel of human pancreatic cancer and pancreatic stellate cell lines. Average of 1 x 10^4 events were collected for each cell line.

Cell Line	Cell Type	ICAM-1	DAF
AsPC-1	Adenocarcinoma	802	579142
BxPC-3	Adenocarcinoma	15349	188835
Capan-2	Adenocarcinoma	102933	155387
Hs700T	Adenocarcinoma	4295	272895
Hs766T	Carcinoma	9295	1780426
MIA PaCa-2	Carcinoma	332	45934
Panc-1	Carcinoma	132636	149911
PL45	Ductal Adenocarcinoma	18918	50599
SU.86.86	Ductal Carcinoma	5478	188819
SW 1990	Adenocarcinoma	6360	316591
TAS29	Pancreatic Stellate	61245	792963
TAS31	Pancreatic Stellate	8626	99361
HPDE	Ductal Epithelial	7164	12217
SK-Mel-28	Melanoma	172901	54693

4.3 Susceptibility of a Panel of Human Pancreatic Cancer and Pancreatic Stellate Cell Lines to CVA21

The susceptibility of each cell line to CVA21 oncolysis was determined by infecting monolayers of cells with 10-fold serial dilutions of CVA21 starting at a constant concentration across each cell line. After 72 hours incubation, the percentage of viable cells was determined via MTT assays and graphed against the log of the dilution of CVA21 ($TCID_{50}$/ml). Non-linear regression curves were generated and the 50% endpoint dilution ($TCID_{50}$/ml values) estimated using Prism v7.0 (GraphPad) for each cell line. Figure 20 illustrates the susceptibility of each cell line to CVA21 oncolysis. Table 6 summarises the effective 50% concentration in $TCID_{50}$/ml values for each cell line. Panc-1 cells were discovered to be the most susceptible pancreatic cancer cell line to CVA21 oncolysis, requiring only 2.28×10^3 $TCID_{50}$/ml to reduce cell viability by 50%. In contrast, MIA PaCa-2 cells were resistant to CVA21 oncolysis as a reduction of 50% cell viability failed to occur during the assay period. Susceptible was defined as a reduction in cell viability by at least 50% within the 72 hour assay timeframe.

Eight of the ten pancreatic cancer cell lines (AsPC-1, BxPC-3, Capan-2, Hs700T, Panc-1, PL45, SU.86.86, and SW 1990) were susceptible to CVA21 oncolysis (Figure 20). Likewise, the two pancreatic stellate cell lines, TAS29 and TAS31, were susceptible to CVA21. Moreover, of these cell lines Panc-1, PL45, SU.86.86, SW 1990, and TAS29 were highly susceptible to CVA21 oncolysis as the percentage of viable cells after 72 hours was reduced to 20% or less. MIA PaCa-2 cells appeared to have increased cell growth in the presence of CVA21. Normal pancreatic ductal epithelial cells (HPDE) were resistant to CVA21 oncolysis indicating CVA21 in general has tropism for pancreatic cancer and pancreatic stellate cells. Compared to the highly susceptible SK-Mel-28 melanoma cell line, pancreatic cancer and pancreatic stellate cell lines were less sensitive to CVA21 oncolysis.

Considering the level of ICAM-1 and DAF cell receptors Figure 19 and the susceptibility of a cell line to CVA21 Figure 20 there are distinct relationships present. ICAM-1 expression is a defining characteristic of a cell lines susceptibility to CVA21 oncolysis. Namely, each cell line that had higher ICAM-1 cell surface expression compared to normal pancreas cells (HPDE), was susceptible to CVA21 oncolysis.

Likewise, DAF expression influences susceptibility of a cell line to CVA21 oncolysis (Newcombe *et al.*, 2004a). For example, AsPC-1 cells expressed lower levels of ICAM-1 compared to HPDE cells, yet due to the high level of DAF on AsPC-1 cells were susceptible to CVA21 oncolysis. Contrastingly, Hs766T cells had the highest level of DAF expression from the panel of tested cell lines but were only mildly sensitive to CVA21. Perhaps, in this situation, the overabundance of DAF on HS766T cells was physically interfering with the binding of CVA21 to ICAM-1 receptors.

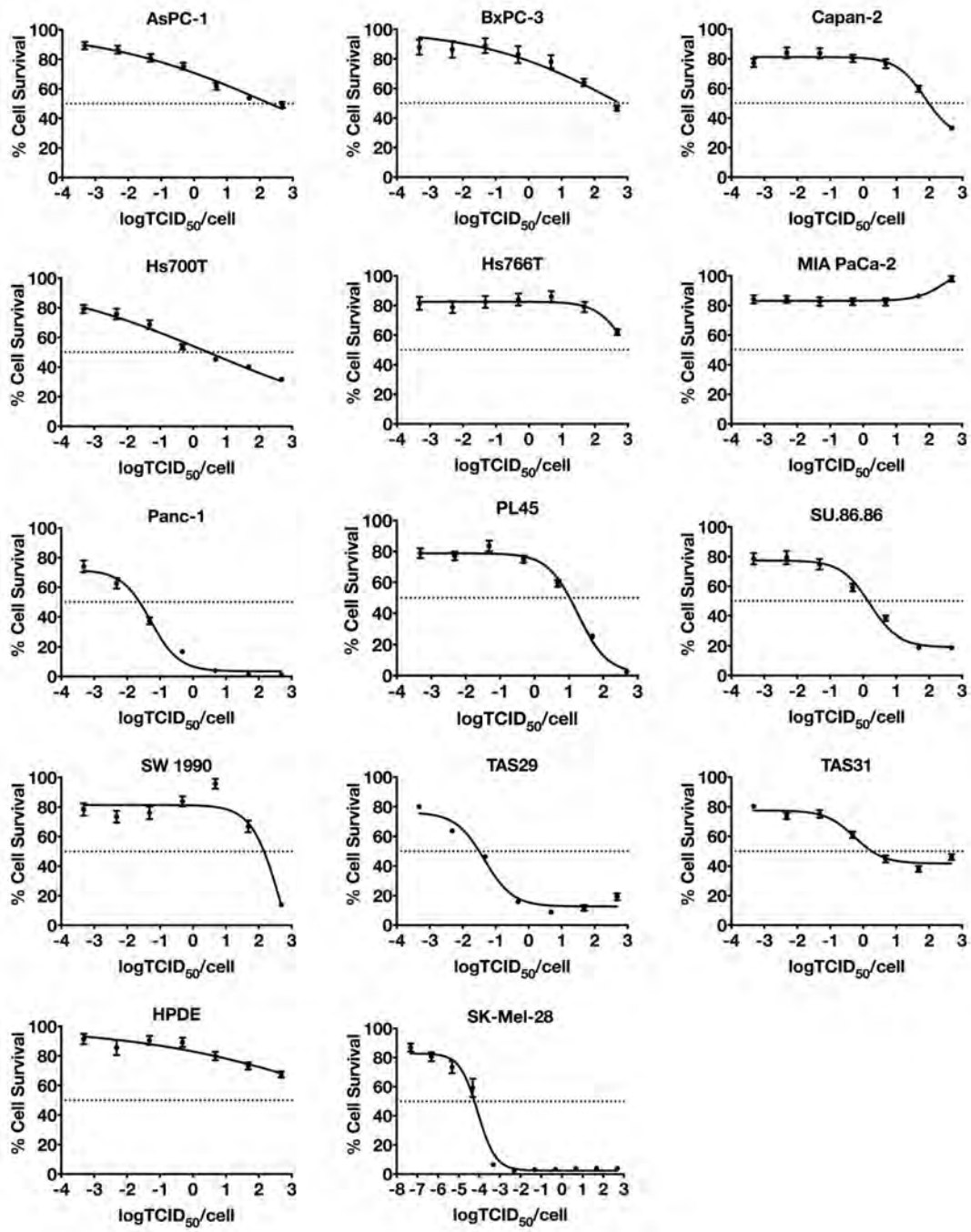

Figure 20: Susceptibility of a panel of human pancreatic cancer and pancreatic stellate cell lines to CVA21 oncolysis. 10-fold serial dilutions of CVA21 starting at a constant concentration were titrated against each cell line and incubated for 72 hours before cell viability measured via MTT assays. Resulting absorbance values were normalised to internal positive and negative controls for each replicate. Average percentage cell survival +/- SEM was plotted against the log of the dilution of CVA21 in $TCID_{50}$/ml. Minimum of three replicates were conducted for each cell line. Non-linear regression curves were generated and $TCID_{50}$/ml concentrations interpolated for each cell line using Prism v7.0 (GraphPad). Dotted line indicates 50% cell survival. N.B. X-axis extended on SK-Mel-28 graph to illustrate susceptibility accurately.

Table 6: Summary of interpolated CVA21 $TCID_{50}$/ml values for each human pancreatic cancer and pancreatic stellate cell line.

Cell Line	Cell Type	log$TCID_{50}$/cell	$TCID_{50}$/ml
AsPC-1	Adenocarcinoma	2.44	2.73E+07
BxPC-3	Adenocarcinoma	2.36	2.29E+07
Capan-2	Adenocarcinoma	1.96	9.09E+06
Hs700T	Adenocarcinoma	0.40	2.52E+05
Hs766T	Carcinoma	2.95	8.82E+07
MIA PaCa-2	Carcinoma	Undefined	Undefined
Panc-1	Carcinoma	-1.64	2.28E+03
PL45	Ductal Adenocarcinoma	1.00	9.92E+05
SU.86.86	Ductal Carcinoma	0.22	1.67E+05
SW 1990	Adenocarcinoma	2.15	1.42E+07
TAS29	Stellate	-1.50	3.15E+03
TAS31	Stellate	0.25	1.80E+05
HPDE	Normal Ductal Epithelial	Undefined	Undefined
SK-Mel-28	Melanoma	-4.24	5.79E+00

4.4 CVA21 Replication Kinetics in a Panel of Human Pancreatic Cancer and Pancreatic Stellate Cell Lines

To determine if pancreatic cancer and pancreatic stellate cells which were susceptible to CVA21 lytic infection could also support viral replication, the kinetics of CVA21 replication was investigated *in vitro* for each cell line. Monolayers of each cell line were infected with a MOI of 10 $TCID_{50}$/cell of CVA21 for one hour, before unbound virus was washed off. Cells were incubated for 0, 2, 4, 6, 8, 24, 48, and 72 hours before three freeze/thaw cycles to burst cells and to collect the total cell lysate. Cell lysates were titrated on SK-Mel-28 cells to determine infectious viral yield. Figure 21 depicts the replication kinetics of CVA21 in each cell line.

Replication of CVA21 within a cell line was observed when an increase in viral titre was present over the course of the assays. Figure 21 depicts the eight pancreatic cancer cell lines (AsPC-1, BxPC-3, Capan-2, Hs700T, Panc-1, PL45, SU.86.86, and SW 1990) that were susceptible to CVA21 (Figure 20), and supported replication of CVA21 as CVA21 concentrations increased over the 72 hour incubation period. Likewise, the two pancreatic stellate cells, TAS29, and TAS31 were susceptible and supported CVA21 replication. Of interest, the pancreatic cancer cell line, Panc-1, yielded on average higher titres of CVA21 compared to the melanoma cell line, SK-Mel-28 (max Panc-1 yield: 2.18×10^9 $TCID_{50}$/ml at 72 hours vs max SK-Mel-28 yield: 1.50×10^9 $TCID_{50}$/ml at 48 hours). Normal pancreas cells, HPDE, supported minimal CVA21 replication. Moreover, viral yield appeared to diminish after 24 hours suggesting that residual virus at the start of the assay degraded over time. Hs766T and MIA PaCa-2 cells supported little, to no, replication of CVA21. For Hs766T cells this could have been due to steric hindrance of cell surface DAF inhibiting virus from invading cells through binding to ICAM-1. In the case of MIA PaCa-2, the low level of ICAM-1 likely did not allow for efficient cell entry by CVA21.

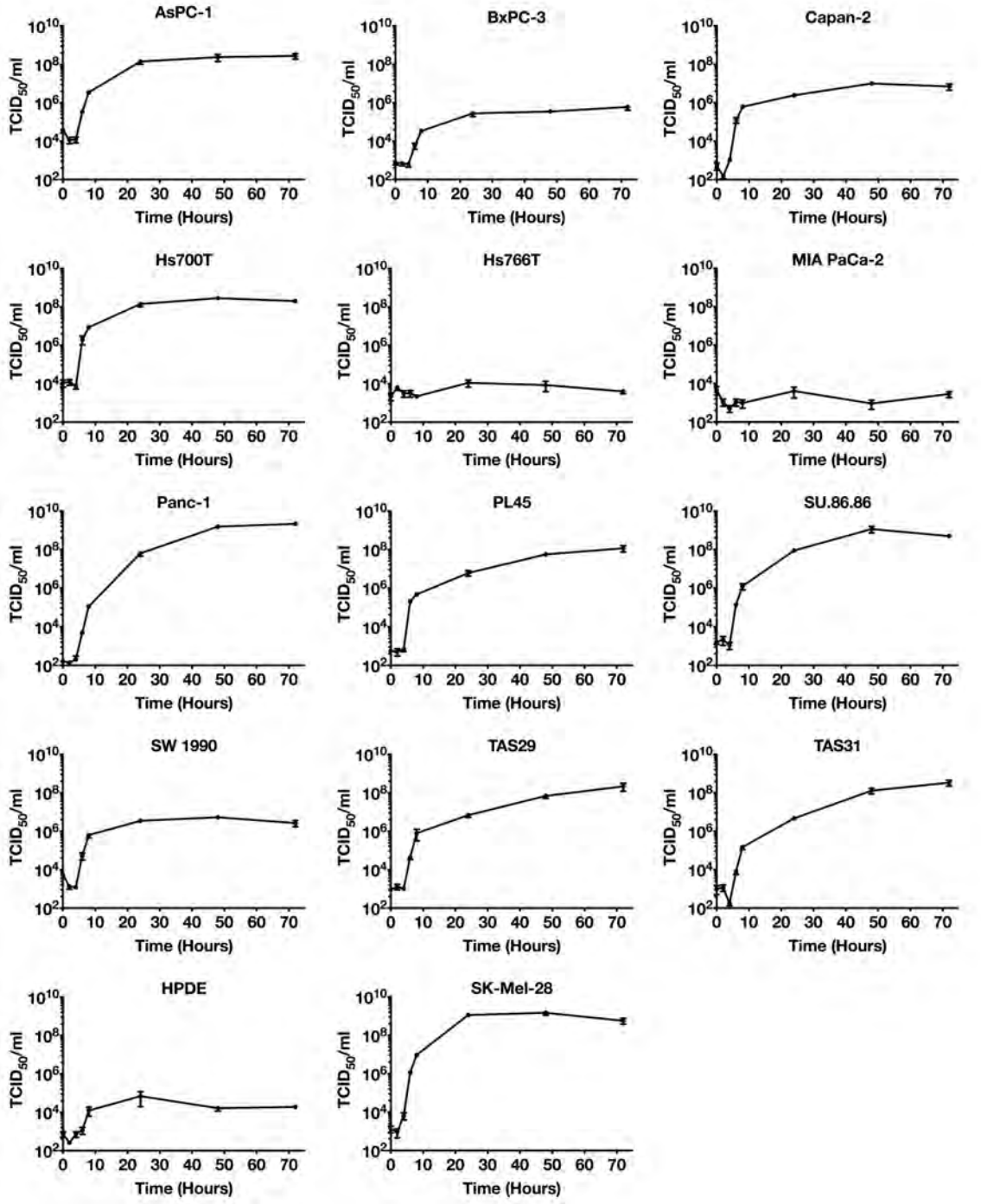

Figure 21: CVA21 replication kinetics in a panel of pancreatic cancer and pancreatic stellate cell lines. Each cell line was infected with an MOI of 10 CVA21 and incubated for 0, 2, 4, 6, 8, 24, 48, and 72 hours before total cell lysate and supernatant was titrated against SK-Mel-28 cells to determine viral yield as $TCID_{50}$/ml. Six replicates were conducted for each cell line. CVA21 replication kinetic graphs were generated for each cell line by plotting the average viral yield +/- SEM for each time point.

4.5 Susceptibility of A Panel of Human Pancreatic Cancer Cell Lines Co-Cultured with Human Pancreatic Stellate Cells

The desmoplastic stromal reaction is a major contribution to the tumour microenvironment in native pancreatic cancer. To simulate the native tumour microenvironment as best as was possible *in vitro*, stellate cells (TAS29, or TAS31) were co-cultured with each pancreatic cancer cell line (AsPC-1, BxPC-3, Capan-2, Hs700T, Hs766T, MIA PaCa-2, Panc-1, PL45, SU.86.86, or SW 1990) at a ratio of four stellate cells to one pancreatic cancer cell. Subsequently, viral infectivity assays were performed to determine the sensitivity of co-cultured cells to CVA21 oncolysis. Cells were exposed to 10-fold serial dilutions of CVA21 and incubated for 72 hours before cell viability assessed by MTT assays. The data displayed in Figure 22 depict the susceptibility of TAS29 cells co-cultured with each pancreatic cancer cell line. Likewise, the graphs in Figure 23 are the susceptibility graphs of TAS31 cells co-cultured with each pancreatic cancer cell line. The susceptibility curves of each stellate cell line, TAS29 or TAS31, and each pancreatic cancer cell line are included on respective graphs for comparison. Unfortunately, the normal pancreas cell line, HPDE, was unable to be co-cultured with either TAS29 or TAS31 cells due to incompatibility of tissue culture mediums.

CVA21 titres required to induce a 50% reduction in cell viability for each pancreatic cancer cell line co-cultured with TAS29 cells were approximately equal in susceptibility to that of TAS29 cells alone (AsPC-1, BxPC-3, Hs700T, and Panc-1), or midway between each pancreatic cancer and TAS29 susceptibility curve (Capan-2, Hs766T, MIA PaCa-2, PL45, SU.86.86 and SW 1990) (Figure 22). Similarly, Figure 23 illustrates TAS31 cells in co-culture with pancreatic cancer cells were approximately equal in susceptibility to TAS31 cells alone (Panc-1, SU.86.86), or between pancreatic cancer and TAS31 susceptibility curves (Capan-2, Hs7766T, and PL45). Thus, TAS29 or TAS31 stellate cells in co-culture with the tested panel of pancreatic cancer cells failed to induce a reduction in CVA21 oncolysis.

Of particular interest, were shifts in susceptibility curves indicating increased sensitivity when TAS31 cells were co-cultured with some of the pancreatic cancer cell

lines (AsPC-1, BxPC-3, Hs700T and SW 1990). The mechanism for this increase cannot definitively be determined from these assays but could be a function of cell proliferation rates that are dissimilar when cultured in isolation and in co-culture at the ratio of 4:1. Alternatively, it may be that oncolysis of highly susceptible stellate cells releases vast numbers of viral progeny that causes the destruction of cancer cells faster than if cancer cells were infected alone. Or, perhaps it is the potential cross-talk between stellate and cancer cells leading to an increase in cell surface ICAM-1 that has mediated the increase in susceptibility. Further testing is required to determine which of these represent the major mode of action. Regardless, taken together these data clearly demonstrated CVA21 is efficient at oncolysing both pancreatic cancer and pancreatic stellate cells when propagated in co-culture.

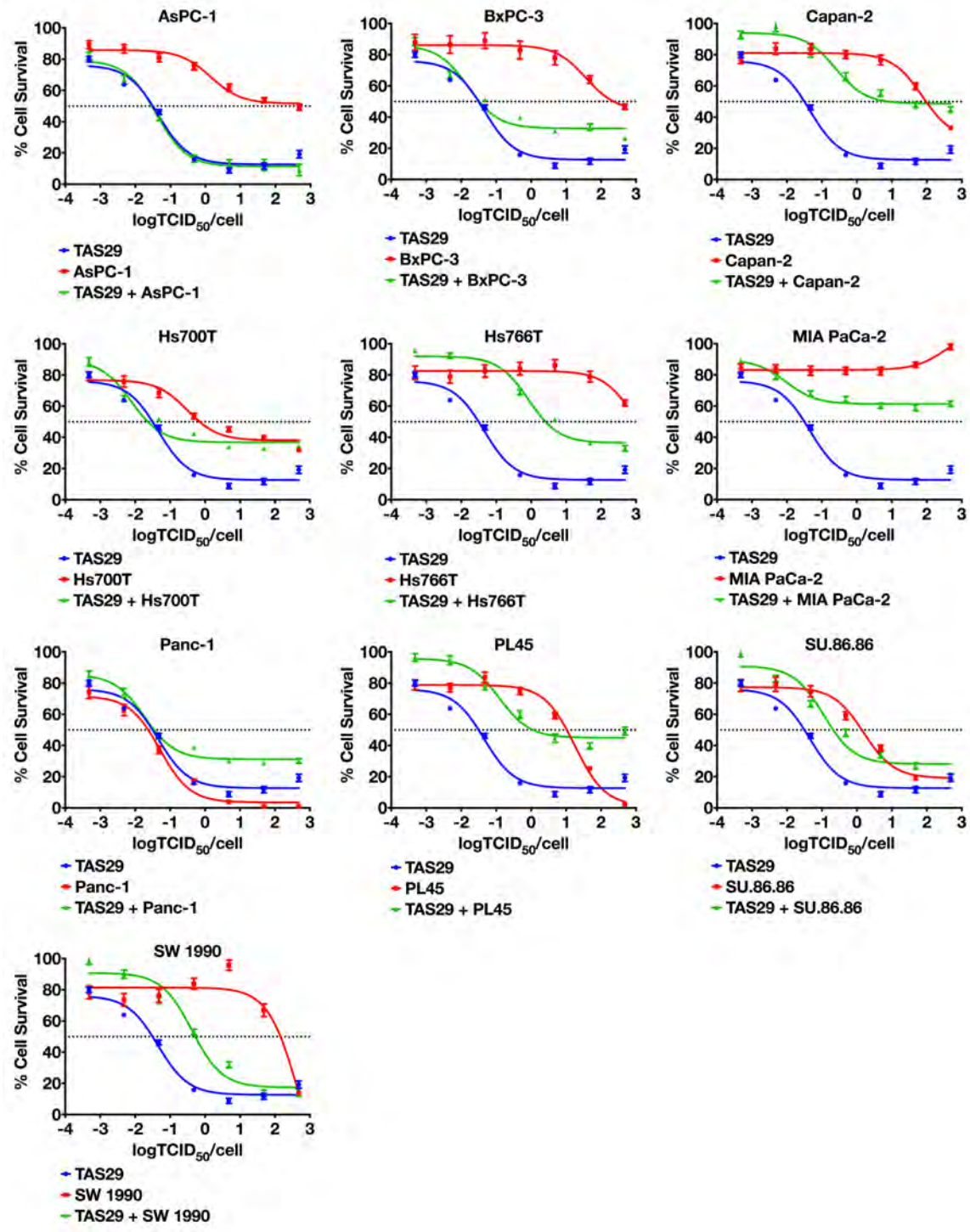

Figure 22: Susceptibility of a panel of human pancreatic cancer cells co-cultured with pancreatic stellate cells (TAS29) to CVA21 oncolysis. Pancreatic cancer cells were cultured together with TAS29 cells at a ratio of 1:4 respectively, and exposed to 10-fold serial dilutions of CVA21. After 72 hours incubation and assessment of cell viability via MTT assays, the resulting absorbance values were normalised to internal positive and negative controls for each replicate. Average percentage cell survival +/- SEM was plotted against the log of the dilution of CVA21 in $TCID_{50}$/ml. Minimum of three replicates were conducted for each cell line. Non-linear regression curves were generated using Prism v7.0 (GraphPad). Dotted line indicates 50% cell survival.

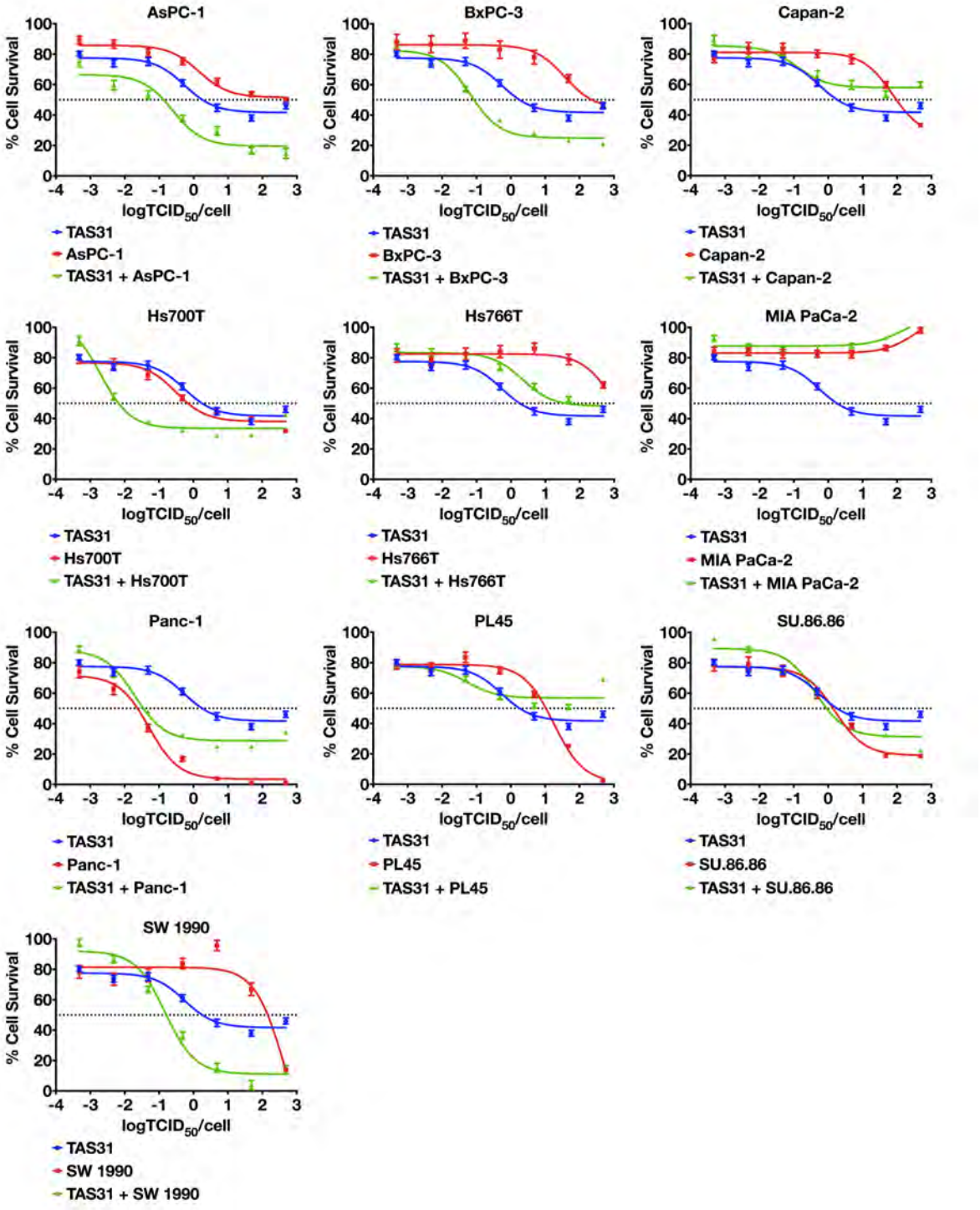

Figure 23: Susceptibility of a panel of human pancreatic cancer cells co-cultured with pancreatic stellate cells (TAS31) to CVA21 oncolysis. Pancreatic cancer cells were cultured together with TAS31 cells at a ratio of 1:4 respectively, and exposed to 10-fold serial dilutions of CVA21. After 72 hours incubation and assessment of cell viability via MTT assays, the resulting absorbance values were normalised to internal positive and negative controls for each replicate. Average percentage cell survival +/- SEM was plotted against the log of the dilution of CVA21 in $TCID_{50}$/ml. Minimum of three replicates were conducted for each cell line. Non-linear regression curves were generated using Prism v7.0 (GraphPad). Dotted line indicates 50% cell survival.

4.6 ICAM-1 Expression on *Ex Vivo* Human Pancreatic Cancer Tissues

The *in vitro* data presented thus far suggests the hypothesis that overexpression of ICAM-1 on a cell surface correlates with increased CVA21 susceptibility. However, the cell lines tested to generate these data are immortalised and have been routinely passaged in laboratory cell culture. Thus, the ICAM-1 levels on these cells may inaccurately reflect the expression levels on native pancreatic cancer. *Ex vivo* patient tissue samples of native pancreatic cancer were analysed to determine if ICAM-1 expression on the panel of cell lines was consistent with native pancreatic cancer. Moreover, determining ICAM-1 expression on native pancreatic cancer allowed prediction of the susceptibility of native pancreatic cancer to CVA21 oncolysis relative to normal pancreas tissue.

Two pancreatic cancer tumour microarrays (TMAs), PA1002a and HPan-A150CS-02, were purchased from US Biomax, Inc. and stained for ICAM-1 according to methods section 2.1.9. Depicted in Figure 24 and Figure 26 are the two pancreatic cancer TMAs analysed for ICAM-1 expression along with positive and negative control stained glioblastoma (GBM) sections #2343 and #2005 (Canadian Virtual Tumour Bank). DAB was used as the substrate for ICAM-1 detection and thus brown staining indicates ICAM-1 expression. The greater the intensity of brown staining on a section correlated to higher expression of ICAM-1 on cells. Haematoxylin and Scott's Tap water counterstaining of tissues resulted in blue nuclei.

Focusing on the PA1002a TMA (Figure 24), and the corresponding TMA legend (Figure 25) and tissue specifications (Table 9), there are a range of grades (1, 2, and 3) and stages (I-IV) of ductal adenocarcinoma tissue sections arranged in rows A through to H, and normal pancreas tissue in rows I and J. There is also a malignant pheochromocytoma tissue section from an adrenal gland at the end of row J as a tissue marker for orientation. The control stained GBM #2343 sections validated the ICAM-1 staining of the PA1002a TMA. GBM #2343 sections have previously been determined to be high in ICAM-1 expression via in-house immunohistochemical analyses (unpublished data). The use of mouse IgG as a negative control with no resulting brown staining confirmed ICAM-1 specific binding when the anti-ICAM-1

(G5) antibody was positive. Generally, the intensity of ICAM-1 staining on the panel of pancreatic cancer tissues compared to normal pancreas tissue was higher.

Observing the HPan-A150CS-02 TMA (Figure 26) and the associated legend (Figure 27) and specification Table 10 there are pancreatic ductal adenocarcinoma and pancreatic adenosquamous carcinoma sections of varying grades (1, 2, and 3) and stages (I-IV) beside corresponding normal matched patient pancreatic tissue. Tissues arranged in uneven numbered columns are pancreatic cancer tissues, while tissues organised in even numbered columns are normal matched tissue. Additionally, the normal tissue section to the right of a pancreatic cancer section is from the same patient. For example, tissue sections, A1 and A2, are from the same patient. Also, Row J is pancreatic ductal adenocarcinoma tissue with no matched patient normal tissue. For full specifications of tissues refer to appendix Table 10. Similar to the staining of GBM #2343 sections as controls alongside the PA1002a TMA, GBM #2005 sections were stained together with HPan-A150CS-02 as positive and negative controls. The lack of brown staining in the mouse IgG negative treated section again validated the brown staining is specific for ICAM-1 in treated sections. Overall there appeared to be an increase in ICAM-1 surface expression on pancreatic cancer tissue sections compared to respective normal matched patient tissue sections.

Depicted in Figure 28 are photomicrographs of representative tissue sections from HPan-A150CS-02 taken at 200x magnification. Panels B, D, and F are grade 1, 2, and 3 ductal adenocarcinomas, respectively. Panel H is an example of adenosquamous carcinoma. Panels A, C, E, and G are the corresponding normal matched pancreas tissue for adjacent sections. On normal pancreas tissue, ICAM-1 expression was localised mainly to supporting septa (black arrows) surrounding acinar cells (yellow arrows), islets of Langherhans (red arrow) and interlobular ducts (green arrow). The example of grade 1 ductal adenocarcinoma in panel B likely originated from a pancreatic intraepithelial neoplasia (PanIN), as the epithelial cells comprising the interlobular duct are well differentiated with papillary architecture and loss of nuclear polarity. Budding of these cells into the lumen appears evident. ICAM-1 did not appear to be expressed on these cells, rather ICAM-1 was expressed on the supporting desmoplastic region. Grade 2 ductal adenocarcinoma (panel D) has moderately differentiated cells which express ICAM-1 as well as the desmoplastic reaction. Grade 3 ductal adenocarcinoma (panel F) highly expresses ICAM-1 on poorly

differentiated cells and the supporting stromal region. Thus, it appeared that ICAM-1 is overexpressed on cancer cells with the progression and metastases of the disease. Of note is adenosquamous carcinoma exhibited high ICAM-1 expression on both glandular and squamous differentiated cells.

To quantify the level of ICAM-1 staining on sections from PA1002a and HPan-A150CS-02 TMAs, the Halo™ Image Analysis Platform (IndicaLabs), was used to generate heat maps of DAB staining intensity and corresponding H score values. Depicted in Figure 29 are representative sections (average DAB staining intensity) of normal pancreas tissue and pancreatic ductal adenocarcinoma sections by grade of disease (1, 2, or 3), along with corresponding heat maps of DAB staining intensity. Again, it appeared that ICAM-1 expression on cells increased during the progression of pancreatic cancer. Namely, there was a progressive increase in ICAM-1 staining from normal pancreas tissue through to grade 3 pancreatic ductal adenocarcinoma.

The calculated H scores of ICAM-1 staining for each section from both the PA1002a and HPan-A150CS-02 TMAs were grouped by cancer cell type and presented in Figure 30. Compared to normal pancreas tissue, pancreatic ductal adenocarcinoma as a whole had a highly statistically significant increase in ICAM-1 expression on cells (Unpaired t-test with Welch's corrections: *** P = 0.00096). Similarly, pancreatic adenosquamous carcinoma had a statistically significant increase in ICAM-1 compared to normal pancreas tissue (Unpaired t-test with Welch's corrections: * P = 0.048). Furthermore, of the 64 ductal adenocarcinoma sections with matched normal tissues on the HPan-A150CS-02 TMA, 47 (73%) patients had higher ICAM-1 expression compared to respective normal matched tissue sections. Likewise, 6 out of the 8 (75%) adenosquamous carcinoma patients displayed higher ICAM-1 expression on cancer tissues compared to respective matched normal tissues. Therefore, the majority of human pancreatic cancers exhibit higher levels of ICAM-1 cell surface expression compared to matched normal pancreas tissue. Of the patients that had lower ICAM-1 expression on cancerous tissues (adenosquamous carcinoma or ductal adenocarcinoma) compared to corresponding normal matched tissue there were no defining characteristics such as age, sex, grade, or stage of disease.

Given the large sample number of pancreatic ductal adenocarcinoma and normal pancreas tissue sections, the associated H scores were presented according to grade

of ductal adenocarcinoma and presented in comparison to normal pancreas tissue. Figure 31 illustrates on average there was a stepwise increase in ICAM-1 expression throughout the progression of the disease resulting in a statistically significant increase in ICAM-1 on grade 2 and grade 3 ductal adenocarcinomas compared to normal pancreas tissue (Unpaired t-tests with Welch's correction: * $P = 0.028$, *** $P = 0.00037$, respectively).

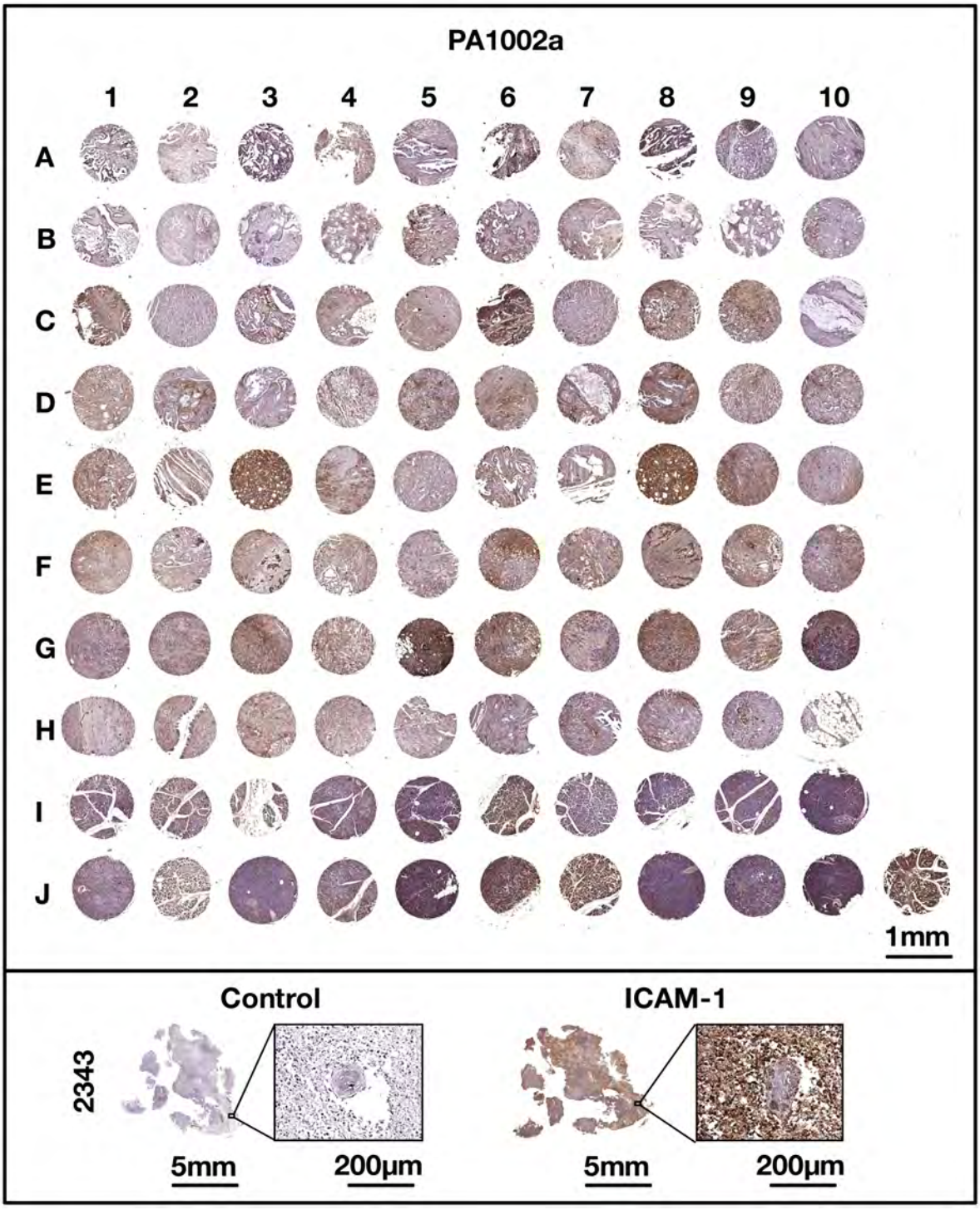

Figure 24: PA1002a Pancreatic Cancer Tumour Microarray (US Biomax, Inc.) along with negative and positive control Glioblastoma sections #2343 (Canadian Virtual Tumour Bank) stained for ICAM-1. The commercially available pancreatic cancer tumour microarray PA1002a, was stained for ICAM-1 with a mouse monoclonal anti-ICAM-1 (G-5) antibody (Santa Cruz Biotechnology). Glioblastoma sections #2343 were stained alongside as negative (Control) and positive (ICAM-1) controls. Mouse IgG negative control (Biocare Medical) was applied to 2343 negative control section. Images captured at 200x magnification using an Aperio AT2 scanner (Leica Biosystems).

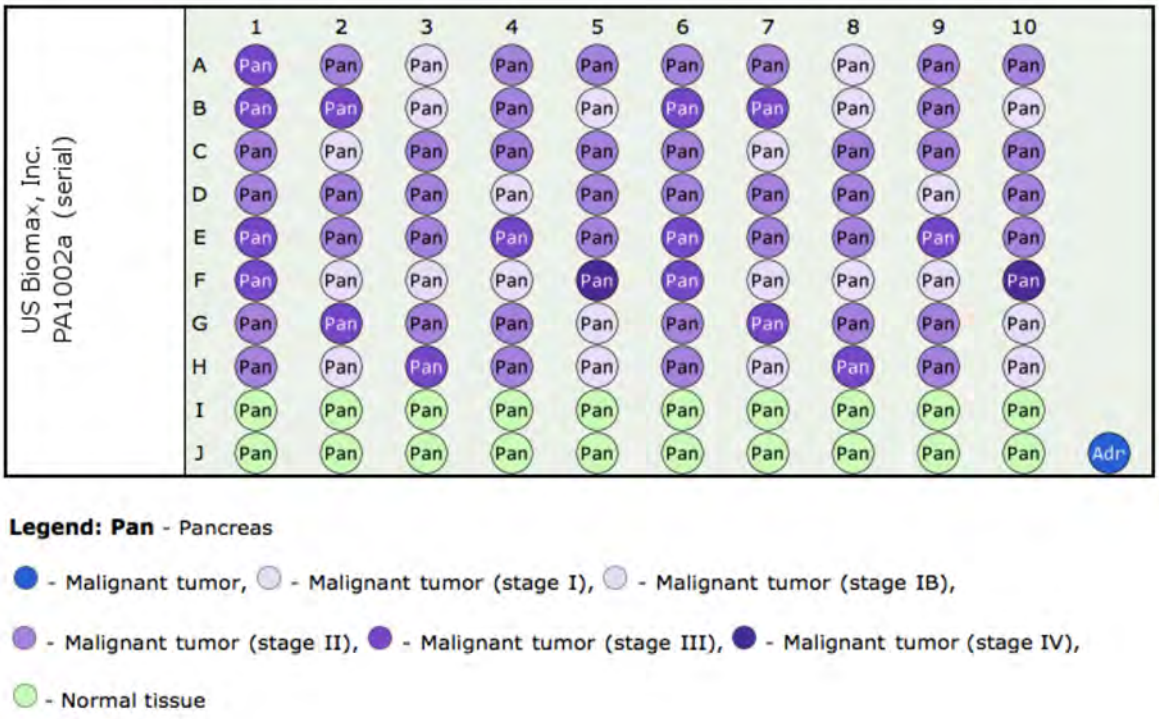

Figure 25: PA1002a Pancreatic Cancer Tumour Microarray Legend Panel. Adapted from US Biomax, Inc. website

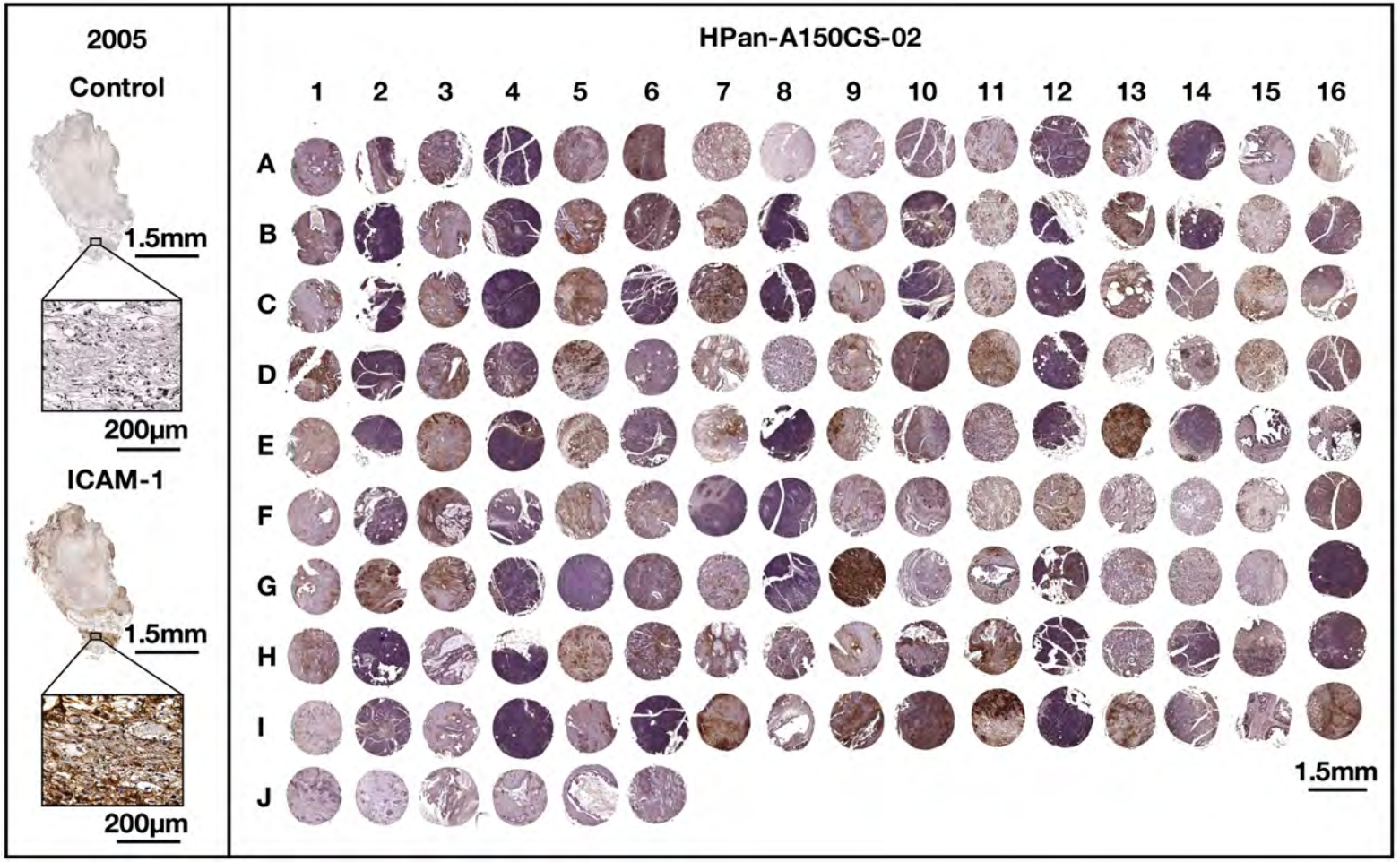

Figure 26: HPan-A150CS-02 Pancreatic Cancer Tumour Microarray (US Biomax, Inc.) along with negative and positive control Glioblastoma sections #2005 (Canadian Virtual Tumour Bank) stained for ICAM-1. The commercially available pancreatic cancer tumour microarray HPan-A150CS-02, was stained for ICAM-1 with a mouse monoclonal anti-ICAM-1 (G-5) antibody (Santa Cruz Biotechnology). Glioblastoma sections #2005 were stained alongside as negative (Control) and positive (ICAM-1) controls. Mouse IgG negative control (Biocare Medical) was applied to negative control section. Images captured at 200x magnification using an Aperio AT2 scanner (Leica Biosystems).

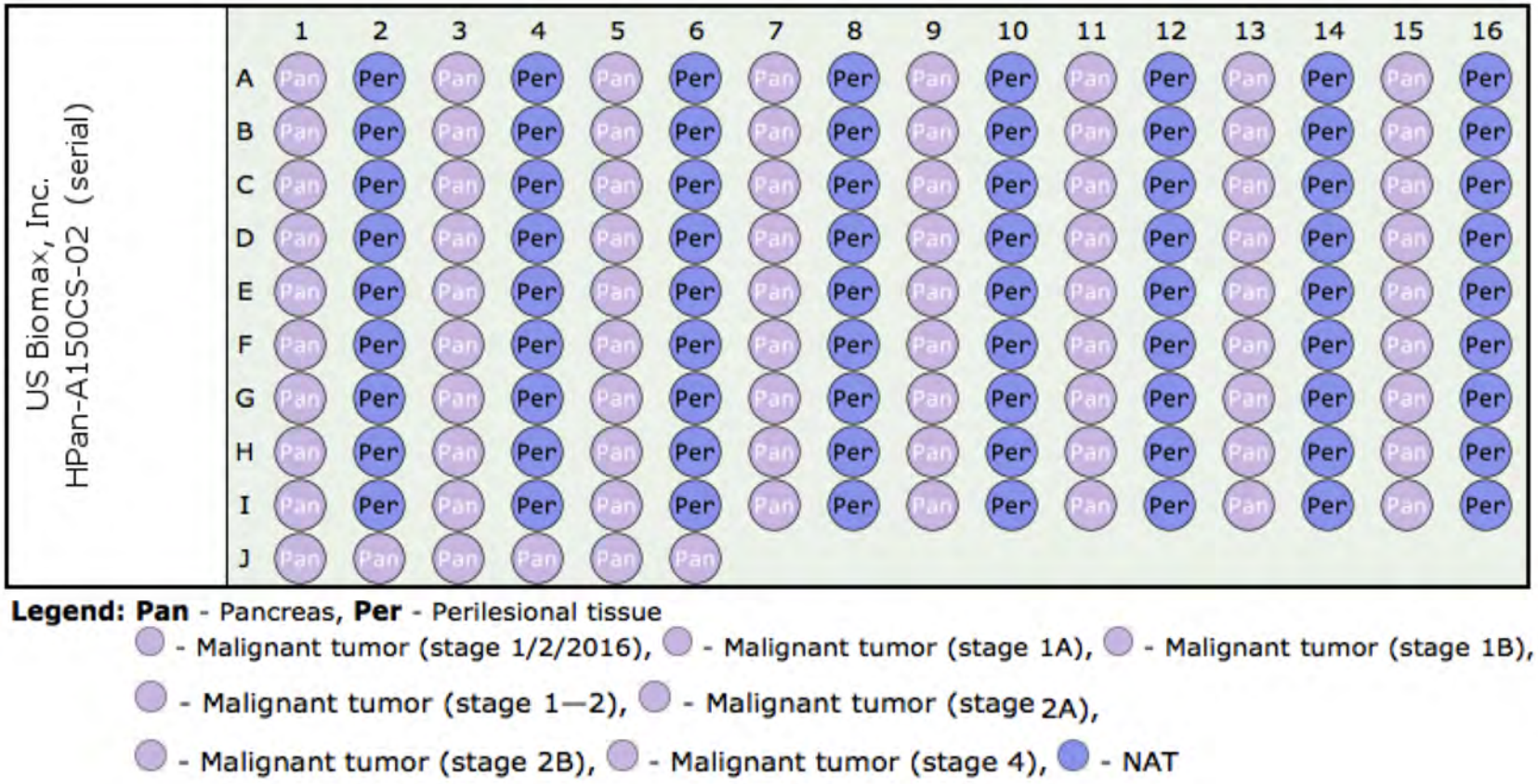

Figure 27: HPan-A150CS-02 Pancreatic Cancer Tumour Microarray Legend Panel. Adapted from US Biomax, Inc. website.

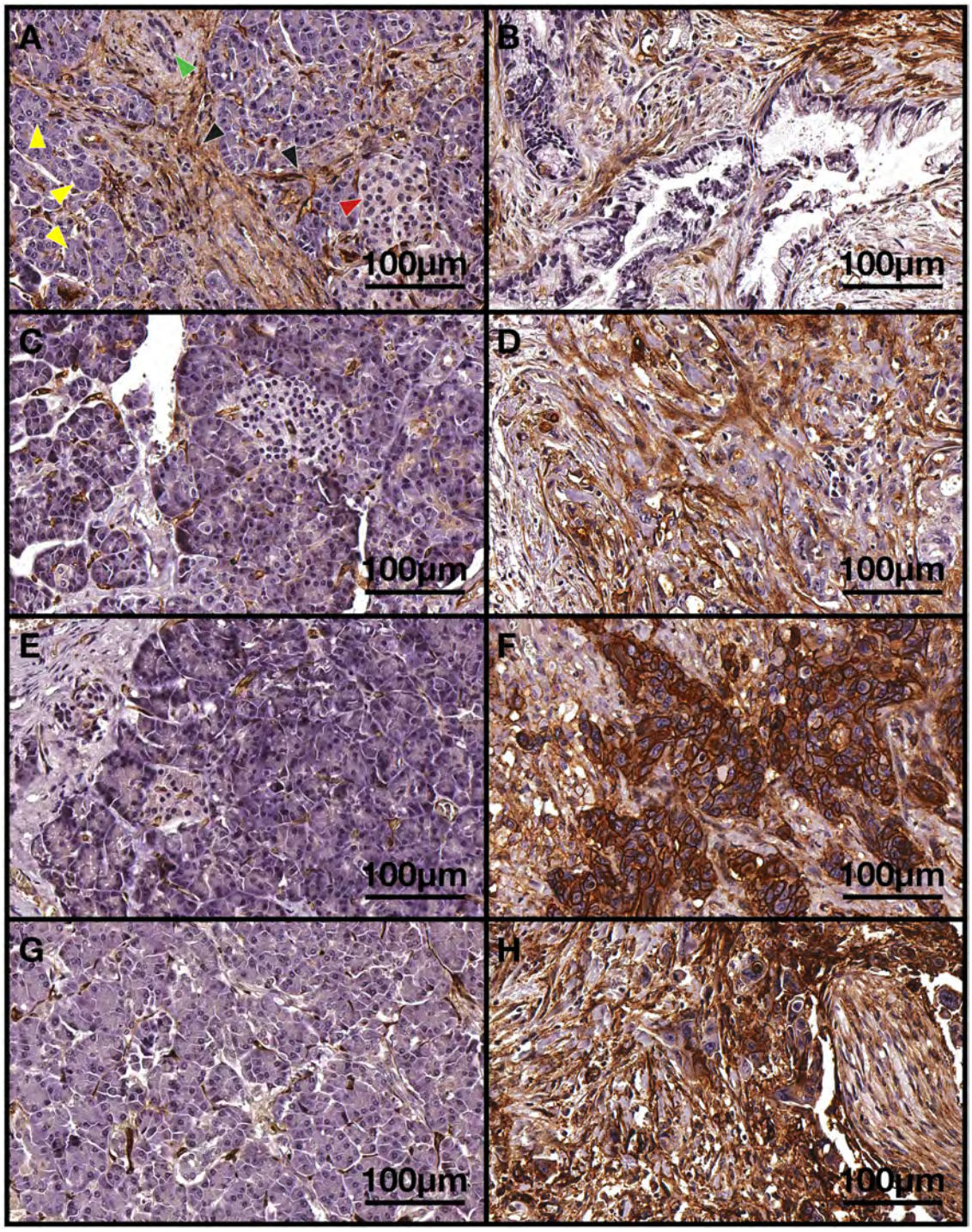

Figure 28: Patient Pancreatic Ductal Adenocarcinoma and Pancreatic Adenosquamous Carcinoma tissues with corresponding normal matched pancreas tissue stained for ICAM-1 at 200x magnification. Normal patient pancreatic tissue stained (A, C, E, and G) alongside corresponding patient ductal adenocarcinoma; grade 1 (B), grade 2 (D), grade 3 (F) and adenosquamous carcinoma (H) stained for ICAM-1. Yellow arrows indicate acinar cells, red arrow, islet of Langerhans, black arrows, septa, green arrow, interlobular duct. Scale bar: 100 µm.

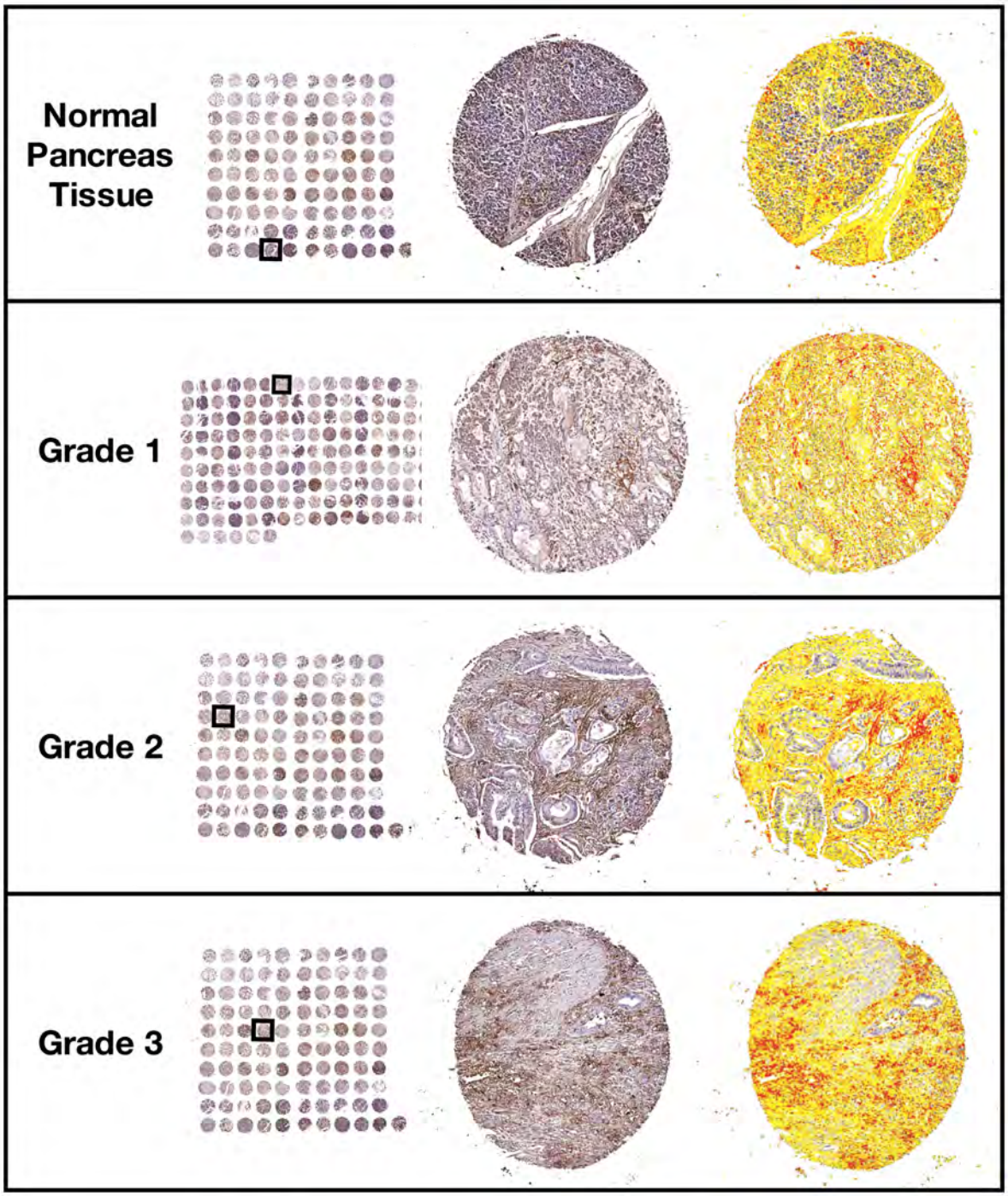

Figure 29: Representative sections from PA1002a and HPan-A150CS-02 Tumour Microarrays stained for ICAM-1 by grade of pancreatic cancer and corresponding heat map (H score) images. Heat maps of DAB staining intensity and corresponding H score values calculated for each section using Halo™ Image Analysis Platform (IndicaLabs).

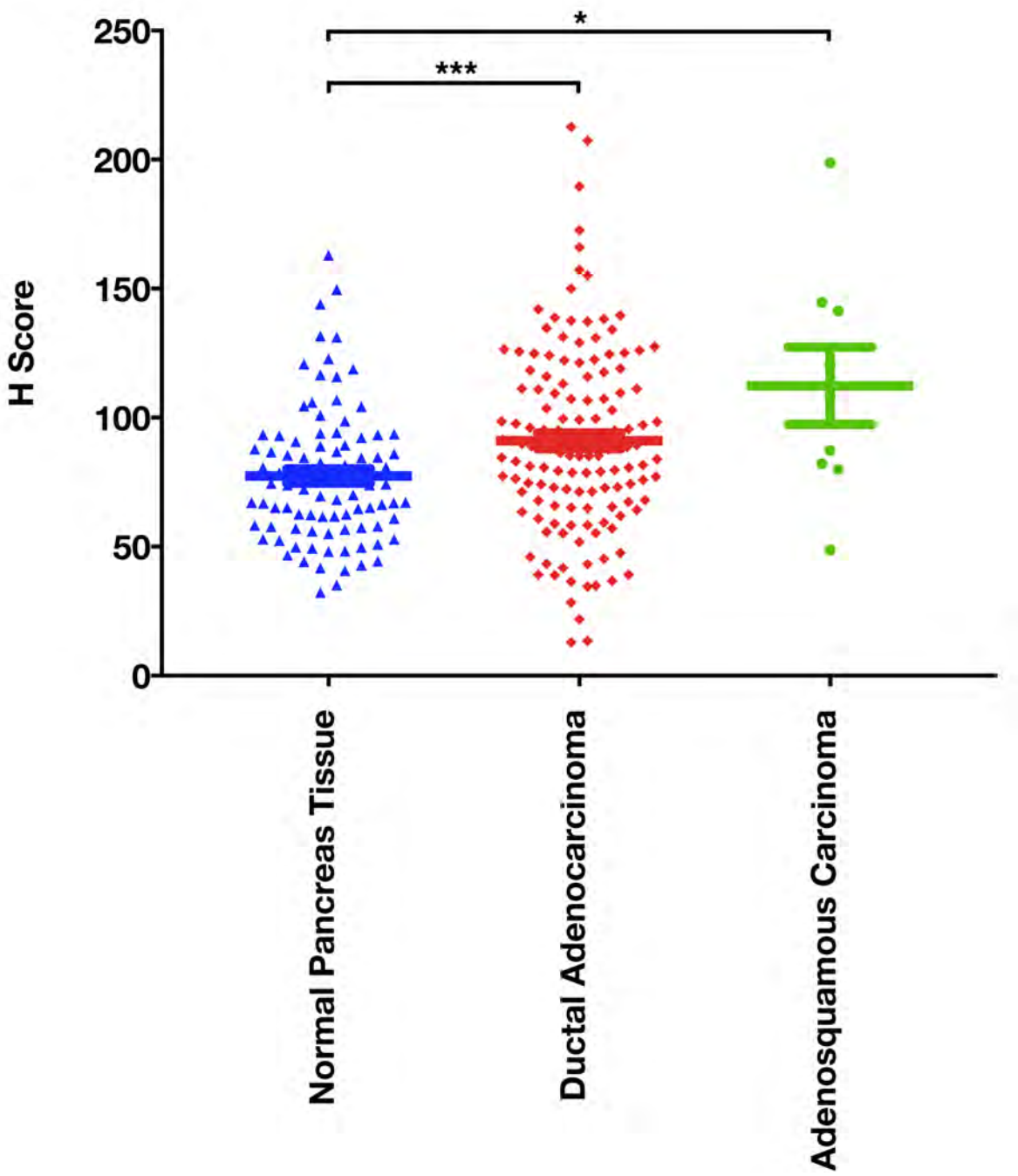

Figure 30: H scores of ICAM-1 staining from PA1002a and HPan-A150CS-02 Tumour Microarrays by type of pancreatic cancer. H scores of DAB staining intensity for ICAM-1 were grouped by type of pancreatic cancer (ductal adenocarcinoma or adenosquamous carcinoma) and compared to normal pancreas tissue. Unpaired t-tests with Welch's correction and a confidence level of 99% were conducted to compare cancer type with normal pancreas tissue using Prism v7.0 (GraphPad). * $P = 0.048$, *** $P = 0.00096$.

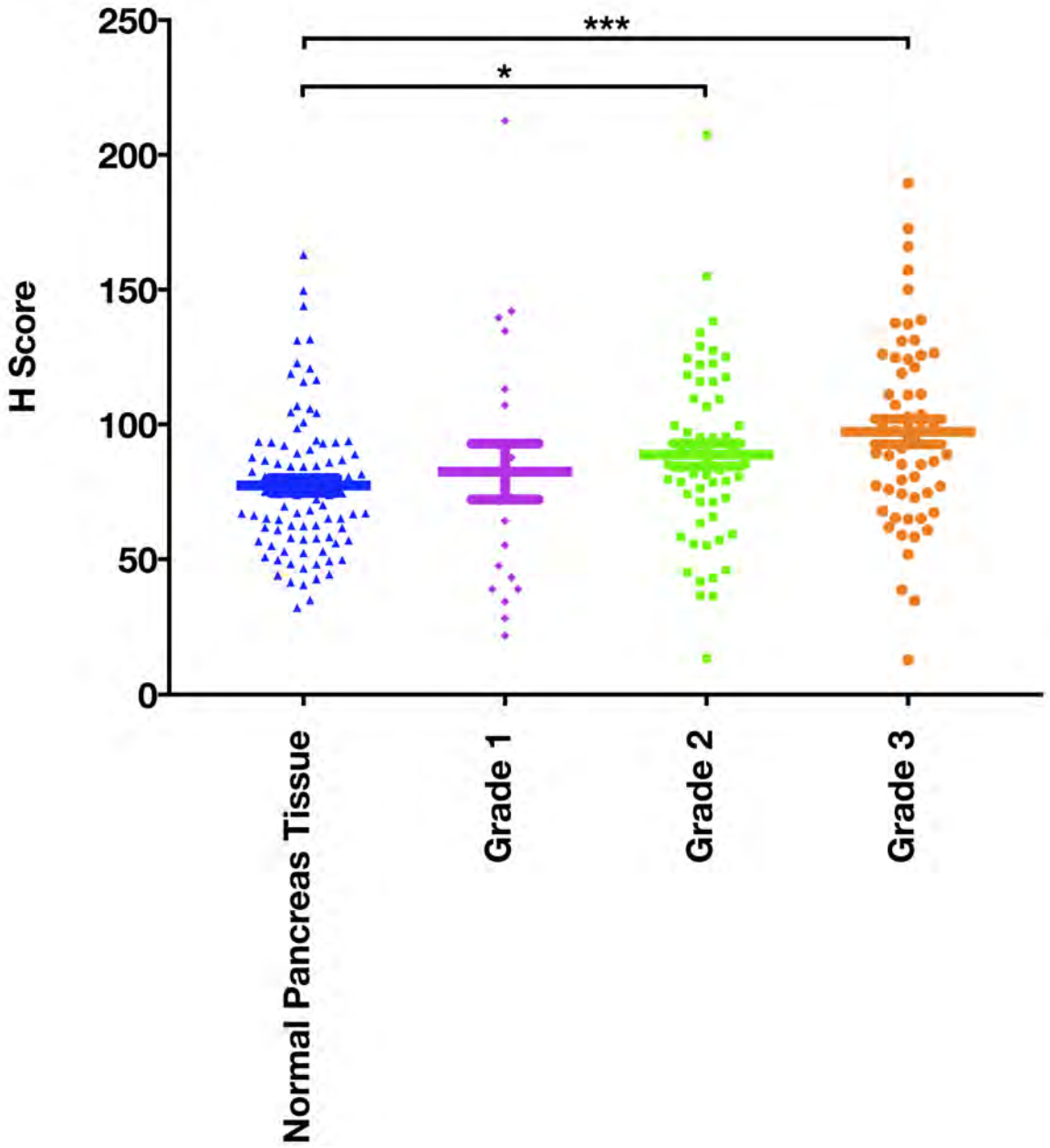

Figure 31: H scores of ICAM-1 staining from PA1002a and HPan-A150CS-02 Tumour Microarrays by grade of pancreatic ductal adenocarcinoma. H scores of DAB staining intensity for ICAM-1 were grouped by grade (1, 2, or 3) of ductal adenocarcinoma or normal pancreas tissue. Unpaired t-tests with Welch's correction and a confidence level of 99% were conducted to compare cancer type with normal pancreas tissue using Prism v7.0 (GraphPad). * $P = 0.028$, *** $P = 0.00037$.

Chapter 5

Coxsackievirus A21 as a Potential Treatment for Pancreatic Cancer in Combination With Conventional Chemotherapy: *In Vitro* and *In Vivo* Investigations

In this chapter, *in vitro* and *in vivo* studies were investigated to determine the potential of CVA21 as a treatment for pancreatic cancer, as a single agent, and in combination with the conventional chemotherapy, gemcitabine. *In vitro* and *in vivo* investigations enabled a direct comparison between a current frontline therapeutic for the treatment of pancreatic cancer with the investigational drug, CAVATAK™. CAVATAK™ is Viralytics Ltd. bio-selected formulation of CVA21. CAVATAK™ was used for *in vivo* studies whereas crude preparations of CVA21 were utilised for *in vitro* studies. Initially, dose-response assays were conducted to determine the effects of gemcitabine on the panel of pancreatic cancer, pancreatic stellate, and normal pancreas cell lines. Following this, the kinetics of CVA21 and gemcitabine in combination were investigated through checkerboard assays to determine if synergy or antagonism was present when used to treat the panel of cell lines. Finally, two mouse models of pancreatic cancer in athymic nude mice were conducted to investigate the two agents in the preclinical setting.

5.1 Susceptibility of a Panel of Human Pancreatic Cancer and Pancreatic Stellate Cells to Gemcitabine.

Before determining the activity of CVA21 in combination with gemcitabine, the potency of gemcitabine on the panel of pancreatic cancer (AsPC-1, BxPC-3, Capan-2, Hs700T, Hs766T, MIA PaCa-2, Panc-1, PL45, SU.86.86, and SW 1990) and pancreatic stellate (TAS29 and TAS31) cells was ascertained. The normal human pancreatic ductal epithelial (HPDE) cell line was also tested alongside as a normal cell control. Similar to the $TCID_{50}$ assays employed to determine the susceptibility of the cell lines to CVA21, 50% effective concentration (EC_{50}) assays were conducted. Ten-fold serial dilutions of gemcitabine starting at four times the reported maximum plasma concentration (C_{max}) in patients (4 x 100 μM) (Mavroudis *et al.*, 2003) were titrated against each cell line and incubated for 72 hours before cell viability assessed by MTT cell viability assays. The resulting absorbance values were normalised against internal positive and negative controls for each replicate and graphs generated using Prism v7.0 (GraphPad).

The susceptibility of pancreatic cancer, pancreatic stellate, and normal pancreas cells to the conventional chemotherapy, gemcitabine, determined through EC_{50} assays are illustrated in Figure 32. Corresponding EC_{50} values have been expressed empirically in Table 7. For the EC_{50} of gemcitabine on a cell line to be calculated accurately, a discrete reduction of 50% cell viability or greater during the 72 hour treatment period with gemcitabine was necessary. Where the EC_{50} of gemcitabine on a cell line could not be interpolated, the EC_{50} was denoted as undefined. Of all the cell lines tested, the most susceptible to gemcitabine were the normal pancreatic ductal epithelial (HPDE) cells, requiring only 2.1 nM of gemcitabine to decrease cell viability by 50%. Moreover, the viability of HPDE cells at concentrations above 40.1 nM were reduced by 85% or greater. Of the ten pancreatic cancer cell lines tested, AsPC-1, BxPC-3, Hs700T, MIA PaCa-2 and PL45 cells were determined to be susceptible to gemcitabine having achieved a reduction of at least 50% cell survival after the 72 hour treatment period with gemcitabine. BxPC-3 and PL45 were considered highly susceptible as cell viability was reduced to $\leq$ 20%. The EC_{50} values for the remaining five pancreatic cancer cell lines (Capan-2, Hs766T, Panc-1, SU.86.86, and SW 1990) were not accurately assessed as 50% cell death was not achieved, or the non-linear

regression curves applied to the data failed to discretely cross the 50% point. The two stellate cell lines, TAS29 and TAS31, were both resistant to the effects of gemcitabine. In fact, TAS29 cells appeared to be entirely refractive to clinically toxic concentrations. In summary, from these findings alone, gemcitabine was regarded as an unsuitable agent for the treatment of pancreatic cancer due to its high toxicity towards healthy pancreas cells, lack of effect on pancreatic stellate cells, and minimal effect on half of the tested pancreatic cancer cell lines.

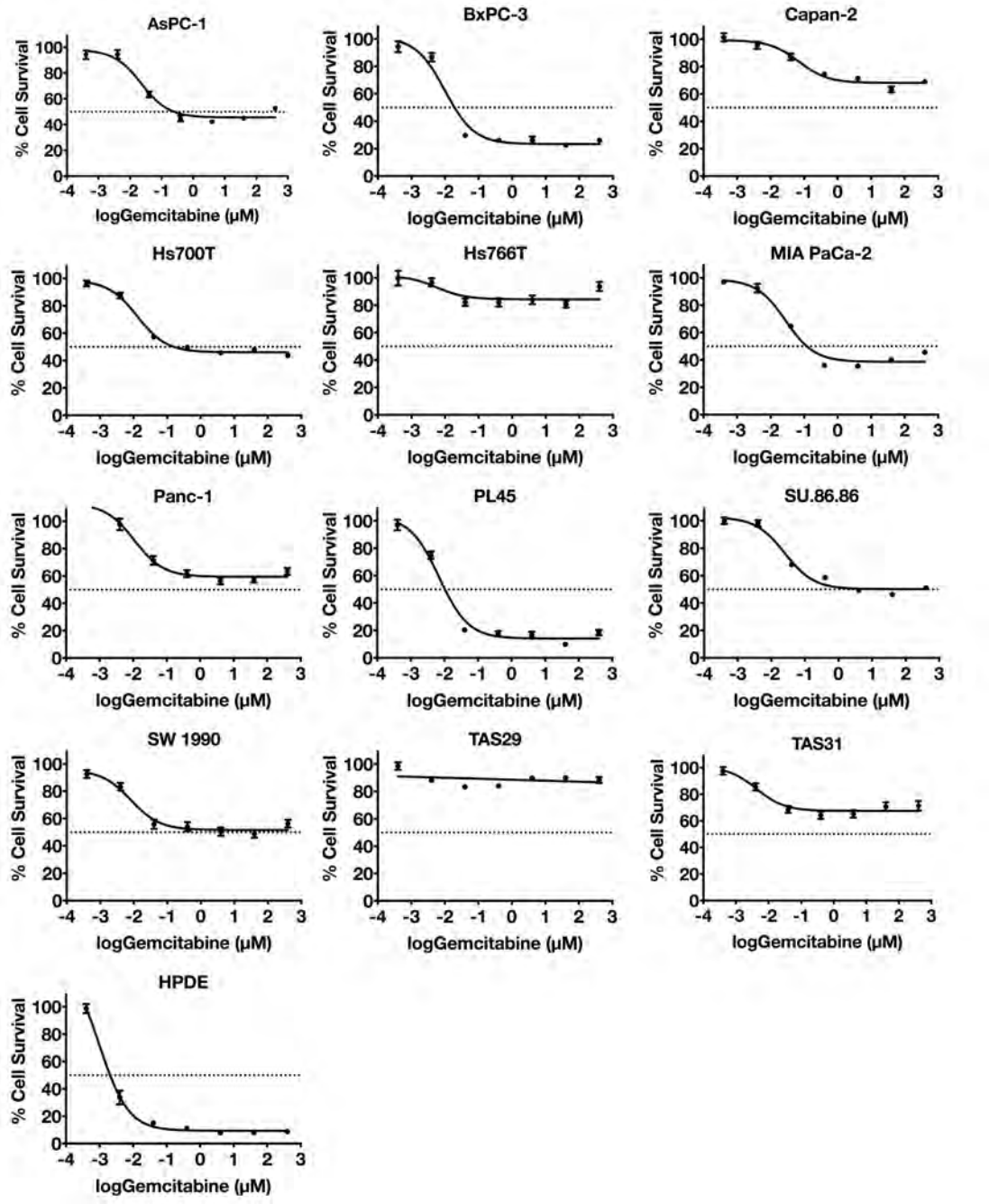

Figure 32: Susceptibility of a panel of human pancreatic cancer and pancreatic stellate cells to gemcitabine. Ten-fold serial dilutions of gemcitabine starting at 400 μM (4 x reported C_{max}) were titrated against each cell line and incubated for 72 hours before cell viability measured via MTT assays. Resulting absorbance values were normalised to internal positive and negative controls for each replicate. Average percentage cell survival +/- SEM was plotted against the log of the dilution of gemcitabine. Minimum of three replicates were conducted for each cell line. Non-linear regression curves were generated and EC_{50} concentrations interpolated for each cell line using Prism v7.0 (GraphPad). Dotted line indicates 50% cell survival.

Table 7: Summary of interpolated gemcitabine EC_{50} values for each human pancreatic cancer and pancreatic stellate cell line.

Cell Line	Cell Type	logEC_{50} (µM)	EC_{50} (nM)
AsPC-1	Adenocarcinoma	-1.14	243.11
BxPC-3	Adenocarcinoma	-2.24	19.12
Capan-2	Adenocarcinoma	Undefined	Undefined
Hs700T	Adenocarcinoma	-1.32	158.20
Hs766T	Carcinoma	Undefined	Undefined
MIA PaCa-2	Carcinoma	-1.44	120.31
Panc-1	Carcinoma	Undefined	Undefined
PL45	Ductal Adenocarcinoma	-2.51	10.43
SU.86.86	Ductal Carcinoma	Undefined	Undefined
SW 1990	Adenocarcinoma	Undefined	Undefined
TAS29	Stellate	Undefined	Undefined
TAS31	Stellate	Undefined	Undefined
HPDE	Normal Ductal Epithelial	-3.21	2.06

5.2 Susceptibility of a Panel of Human Pancreatic Cancer and Pancreatic Stellate Cells to CVA21 in Combination With Gemcitabine

Once the optimal concentrations of CVA21 or gemcitabine to reduce cell viability of each cell line by 50% were determined (Figure 20 and Figure 32) the combined activity of CVA21 and gemcitabine together was investigated. Treating each cell line with the two agents at the optimal concentrations established if synergistic or antagonistic relationships were present between the two agents. Determination of the relationships between the two agents on each cell line was achieved by conducting checkerboard assays. Starting at four times the predetermined respective $TCID_{50}$ and EC_{50} concentrations for each cell line, 2-fold serial dilutions of CVA21 and gemcitabine, alone, and in combination, were titrated against cells and incubated for 72 hours before cell viability was assessed by MTT cell viability assays. If the concentration of CVA21 to elicit a 50% reduction in cell viability was not successfully determined for a cell line, then the highest achievable concentration of CVA21 from working stock virus at 4.06×10^8 $TCID_{50}$/ml was used as the starting concentration for the 2-fold serial dilutions. Likewise, four times the C_{max} of gemcitabine at 400 μM was used as the initial concentration for the 2-fold serial dilution series when the EC_{50} concentration was unable to be interpolated from dose-response curves. Titrating the concentrations around the effective concentrations to elicit a 50% reduction in cell viability also enabled the Chou-Talalay method of drug combination to be calculated based on the median-effect equation using CompuSyn software (CompuSyn, Inc.). Isobolograms and fraction affected vs combination index plots were constructed from calculations.

5.3 Synergy (Checkerboard) Assays on Pancreatic Cancer, Pancreatic Stellate, and Normal Pancreas Cells with CVA21 and Gemcitabine

Data from checkerboard assays of CVA21 and gemcitabine for each pancreatic cancer (AsPC-1, BxPC-3, Capan-2, Hs700T, Hs766T, MIA PaCa-2, Panc-1, PL45,

SU.86.86, and SW 1990), pancreatic stellate (TAS29 and TAS31), and normal pancreatic ductal epithelial (HPDE) cell line were compiled into combination graphs (Figure 33). Within each graph blue lines represent the CVA21 susceptibility curves. Likewise, red lines indicate gemcitabine dose-response curves. Finally, green lines denote susceptibility curves for each cell line when both CVA21 and gemcitabine were applied to cells in combination.

Observing the graph for AsPC-1, concentrations of either agent (CVA21 or gemcitabine) alone resulted in approximately 50% cell death over the 2-fold dilution series applied to the cells. When cells were treated with both agents in combination there was an increased effect observed; the percentage of viable cells after treatment with both agents at the same concentrations were substantially lower than expected, suggesting an additive, or synergistic effect of the two drugs together on AsPC-1 cells. CVA21 in combination with gemcitabine on BxPC-3, Capan-2, Hs700T, Hs766T, PL45 and SW 1990 cells also displayed this trend, suggesting CVA21 and gemcitabine given together has an additive or synergistic effect on pancreatic cancer cells.

Contrastingly there was no increased activity when the two agents were applied to pancreatic stellate cells (TAS29 and TAS31) as the combination susceptibility curves are equal or less than either agent alone. TAS29 and TAS31 cells were resistant to gemcitabine (Figure 32) and susceptible to CVA21 oncolysis (Figure 20). Thus, adding gemcitabine to CVA21 failed to increase cytotoxic activity on pancreatic stellate cells.

With regard to normal pancreatic ductal epithelial (HPDE) cells, the highest concentration of CVA21 achievable from stock virus (9:10 dilution of virus in KSFM) was applied to cells in the checkerboard assay. Stock virus was prepared in DMEM whereas HPDE cells can only grow in KSFM. Therefore, the reduction in cell viability from CVA21 on HPDE cells observed in Figure 33 could have been due to incompatibility of mediums and not viral oncolysis. HPDE cells were resistant to CVA21 when infected with a 1:10 starting dilution of stock virus in KSFM (Figure 20). Combination of CVA21 and gemcitabine on HPDE cells appeared to have an increased effect compared to either agent alone. However, the increased activity may be due to the susceptibility of HPDE cells to gemcitabine and the incompatibility of mediums rather than an actual additive effect of both agents together.

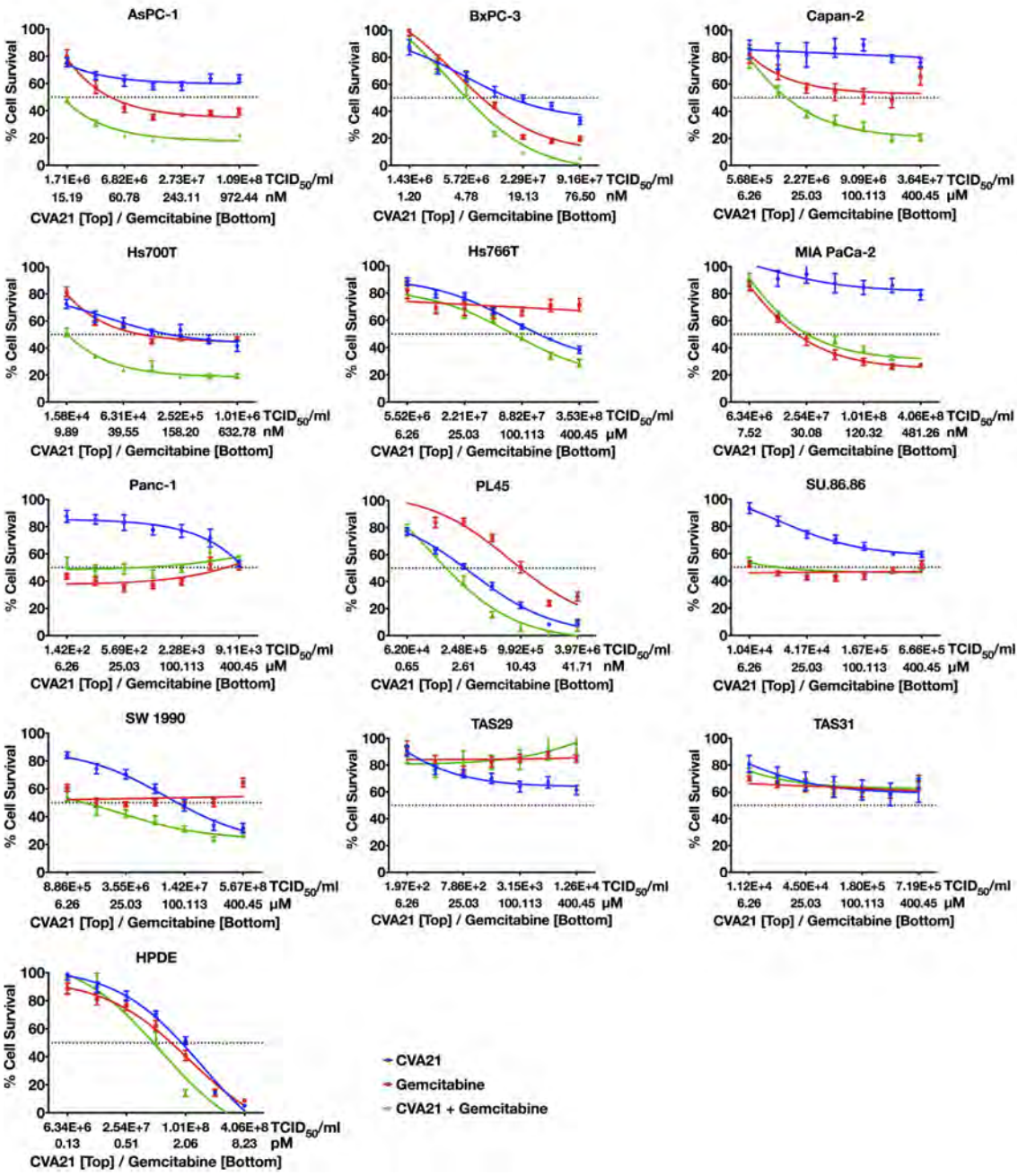

Figure 33: Susceptibility of a panel of human pancreatic cancer and pancreatic stellate cells to CVA21 and gemcitabine in combination. 2-fold serial dilutions of CVA21, or gemcitabine, alone, or in combination were titrated against each cell line starting at 4 x the predetermined $TCID_{50}$/ml/EC_{50} concentrations of CVA21 and gemcitabine and incubated for 72 hours before cell viability assessed via MTT assays. Resulting absorbance values were normalised to internal positive and negative controls for each replicate. Average percentage cell survival +/- SEM was plotted against dilutions. Minimum of three replicates were conducted for each cell line. Non-linear regression curves were generated using Prism v7.0 (GraphPad). Dotted line indicates 50% cell survival.

5.4 Calculating Synergy or Antagonism Between CVA21 and Gemcitabine on Pancreatic Cancer, Pancreatic Stellate, and Normal Pancreas Cells

To further illustrate the kinetics of CVA21 and gemcitabine against pancreatic cancer, pancreatic stellate, and normal pancreas cells, isobolograms and Fraction affected (Fa) vs Combination Index (CI) graphs were constructed using CompuSyn software (CompuSyn, Inc.). Calculations were based off experimental data illustrated in Figure 33. In some of these graphs a 50% reduction of cell viability was not accurately determined over each 2-fold dilution series of CVA21 or gemcitabine. Biological variation, such as confluency of cells in tissue culture plates, cell passage number, and growth rate, may have been the cause of the CVA21 curves not crossing the 50% cell viability point at the interpolated $TCID_{50}$/ml concentrations. Likewise, serial dilutions starting at four times the C_{max} of gemcitabine were applied to several of the cell lines and failed to achieve a 50% reduction in cell viability.

Isobolograms in which the dose requirements for each agent at 50%, 75% and 95% cell inhibition (EC_{50}, EC_{75}, and EC_{95} respectively) were used as a read-out for synergy (Figure 34 and Figure 35). The y-axis on each isobologram represents the concentration of CVA21. Correspondingly, the x-axis is the dose of gemcitabine on each graph. A diagonal line (isobole) is connected between the calculated concentrations of either agents alone to elicit the EC_{50}, EC_{75} or EC_{95} response. The concentrations along each isobole indicate the possible dose combinations that would result in the same response. Thus, the isobole indicates strictly additive combinations of CVA21 and gemcitabine required to achieve either 50%, 75% or 95% cell inhibition. Experimental data from the checkerboard assays (green curves in Figure 33) was used to calculate the concentrations of drug combinations to achieve either 50%, 75% or 95% cell inhibition. If the calculated concentration lies below the isobole then the combination of the two agents is synergistic. Conversely, if the point lies above the isobole, antagonism is present between the two agents. Important to consider also, concentrations above the reported C_{max} (100 μM) are clinically toxic (Mavroudis *et al.*, 2003). In clinical trials, the dose limiting toxicity has not been determined for CAVATAK™ (Andtbacka *et al.*, 2015a). Therefore, the C_{max} of CVA21 is yet unknown.

In general, from the isobolograms depicted in Figure 34 and Figure 33 there was confirmed synergy between CVA21 and gemcitabine at EC_{50}, EC_{75}, and EC_{95} on seven of the ten pancreatic cancer cell lines (AsPC-1, BxPC-3, Capan-2, Hs700T, Hs766T, Panc-1, PL45), one of the two pancreatic stellate cell lines (TAS29), and normal pancreas cells (HPDE). Synergism was confirmed between CVA21 and gemcitabine on SU.86.86 cells to reduce cell viability when EC_{50} concentrations of each agent were used. Contrastingly, antagonism between the two agents was calculated when higher concentrations of these drugs, EC_{75} and EC_{95} were used on SU.86.86 cells with the combination data point plotted to the extreme right of the isobole. Antagonism between CVA21 and gemcitabine was indicated when treating MIA PaCa-2, SW 1990, and TAS31 cells at each combination at EC_{50}, EC_{75} and EC_{95}. Therefore, the kinetics between CVA21 and gemcitabine synergy on pancreatic cells was found to be dependent on both concentration and nature of cell line.

An example of when CVA21 and gemcitabine worked synergistically together to achieve a clinically notable reduction in cell viability (EC_{95}) was when Hs700T were treated with the two agents in combination. The concentration of CVA21 alone required to reduce cell viability by 95% was calculated to be 8.1 x 10^9 $TCID_{50}$/ml. Similarly, 1.3 mM gemcitabine was calculated to reduce cell viability of Hs700T cells to 5%. 1.3 mM gemcitabine would be fatal in patients. However, when added together, to achieve a similar level of cell death the concentrations of each agent required were calculated to be dramatically lower; 4.4 x 10^7 CVA21 $TCID_{50}$/ml and 27.8 μM gemcitabine. Both of these concentrations are clinically achievable. In contrast, an example of when the two agents work synergistically together but failed to result in clinically relevant concentrations at an EC_{95} is on AsPC-1 cells. Although synergistic, the concentration of gemcitabine required when added with CVA21 is clinically toxic (181.1 μM) (Mavroudis *et al.*, 2003). In this instance, if a patients' tumour comprised AsPC-1 like cells, it would be more beneficial to administer CVA21 alone due to its low toxicity profile.

Using the experimental data from the checkerboard assays presented herein, CI vs Fa graphs were also generated using CompuSyn software (CompuSyn, Inc.). As the interactions between CVA21 and gemcitabine may change as a function of concentration or activity, these graphs depict the predicted synergistic or antagonistic effects (CI values) of the two agents together on each cell line over fraction affected

(Fa) values from 5% to 95%. Illustrated in Figure 36, Fa-CI curves (red lines) were applied to the experimental data (blue dots) to extrapolate effects at Fa values that were not achieved through experimentation. CI vs Fa graphs also depict how well the CompuSyn calculations fit the experimental data. Greater accuracy is present when Fa-CI curves fit the experimental data over a wide range of Fa's. Generally depicted in Figure 36, synergy was calculated to be present at higher Fa values across the panel of pancreatic cancer, pancreatic stellate, and normal pancreas cells (CI<1). Thus, CVA21 and gemcitabine were predicted to result in synergistic effects on pancreatic cells when high concentrations of each agent are administered. As previously discussed, higher concentrations (>100 μM) of gemcitabine are clinically toxic (Mavroudis *et al.*, 2003). In summary, based on these findings CVA21 as a single agent towards pancreatic cancer would be the preferred frontline treatment option when compared to gemcitabine alone, and gemcitabine in combination with CVA21.

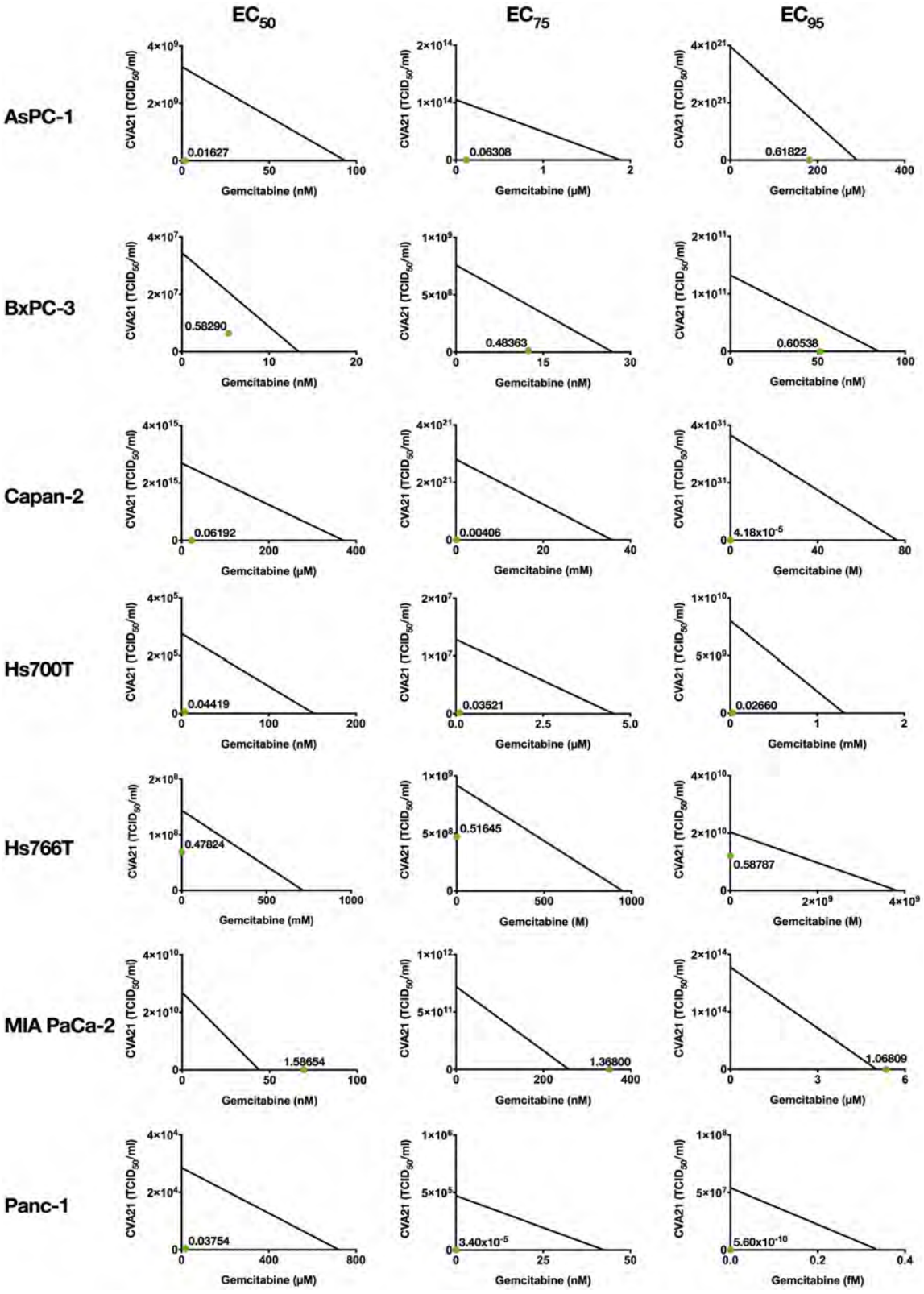

Figure 34: Isobolograms depicting the kinetics between CVA21 and gemcitabine at EC_{50}, EC_{75}, and EC_{95} on pancreatic cancer cell lines (Part 1). Using CompuSyn software (CompuSyn, Inc.) the relationships between CVA21 and gemcitabine on pancreatic cell lines were calculated from the average fraction affected values achieved through experimentation. The calculated values predicted to achieve 50%, 75%, and 95% cell death for each drug alone are indicated by a connecting diagonal line (isobole), and the postulated concentrations of each agent together are depicted as a green dot. Synergy is observed when the green dot lies below the isobole. Antagonism is present when the green dot is situated above the isobole. N.B. gemcitabine concentrations >100 μM are clinically unachievable.

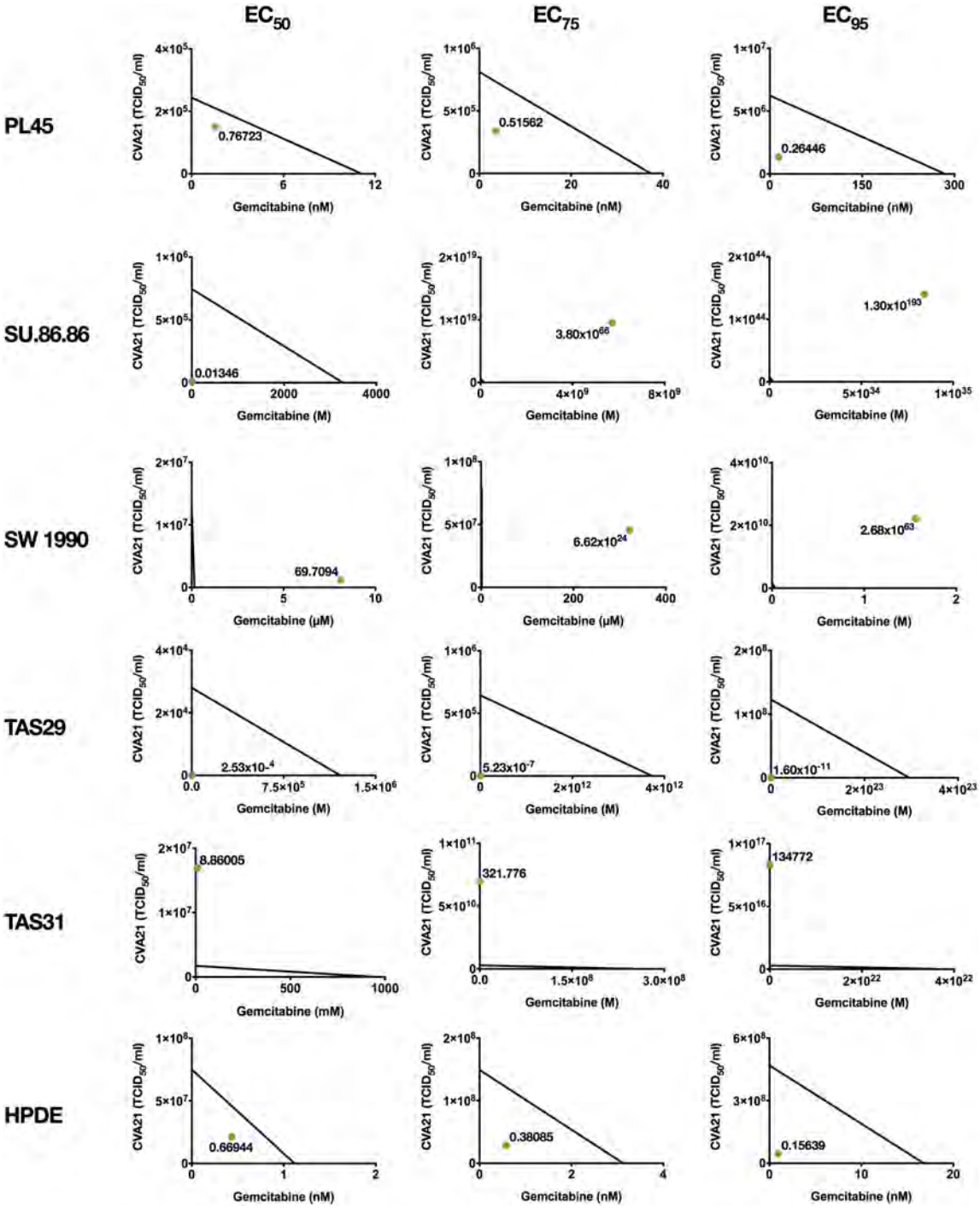

Figure 35: Isobolograms depicting the kinetics between CVA21 and gemcitabine at EC_{50}, EC_{75}, and EC_{95} on pancreatic cancer cell, pancreatic stellate, and normal pancreas cell lines (Part 2). Using CompuSyn software (CompuSyn, Inc.) the relationships between CVA21 and gemcitabine on pancreatic cell lines were calculated from the average fraction affected values achieved through experimentation. The calculated values predicted to achieve 50%, 75%, and 95% cell death for each drug alone are indicated by a connecting diagonal line (isobole), and the postulated concentrations of each agent together are depicted as a green dot. Synergy is observed when the green dot lies below the isobole. Antagonism is present when the green dot is situated above the isobole. N.B. Gemcitabine concentrations >100 μM are clinically unachievable.

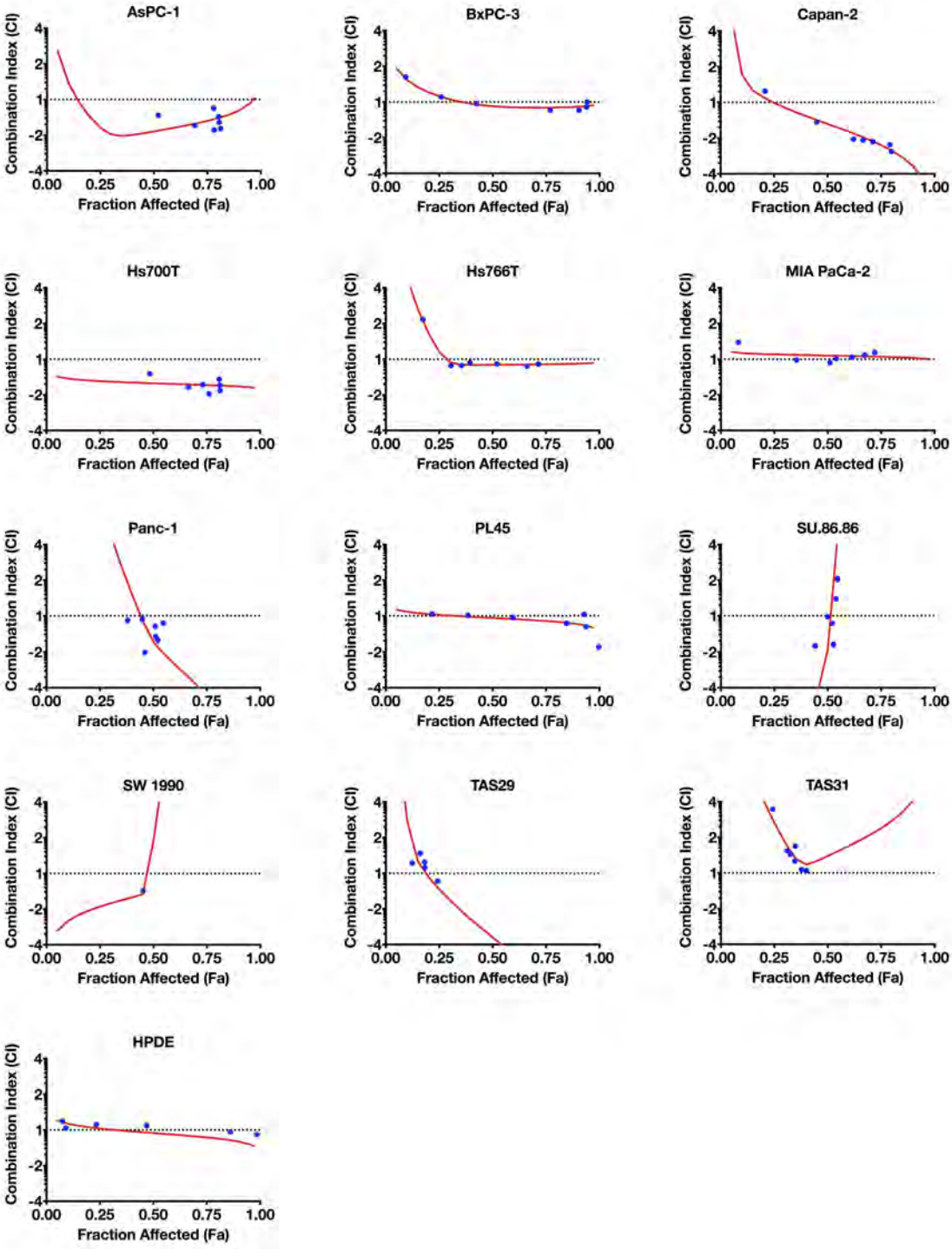

Figure 36: Fraction affected (Fa) vs Combination Index (CI) graphs for each pancreatic cancer, pancreatic stellate, and normal pancreas cell lines. Using CompuSyn software (CompuSyn, Inc.) with the input experimental data from checkerboard assays, the fraction of cells affected (Fa) by the combination of CVA21 and gemcitabine were plotted against the combination index (CI). A Fa-CI curve was applied to data to depict predicted CI values over a Fa of 5% to 95%. A CI below 1 indicates synergy. A CI=1 is additive. A CI above 1 indicates antagonism.

5.5 *In Vivo* Investigation of CVA21 in Combination With Gemcitabine as a Treatment for Pancreatic Cancer

Following characterisation of pancreatic cancer, pancreatic stellate, and normal pancreas cells to the combination of CVA21 oncolysis and gemcitabine *in vitro*, the study advanced into preclinical *in vivo* investigations. Initially a model was developed in immune deficient athymic nude mice to investigate the effects of CVA21 without the influence of the added secondary immune response. Gemcitabine was also investigated in combination with CVA21 as treatments. Briefly, athymic nude mice were inoculated with 1 x 10^6 Panc-1-luc cells directly into the pancreas to generate orthotopic pancreatic cancer. After a tumour development period of 58 days, CAVATAK™ (1 x 10^8 $TCID_{50}$) or saline, was administered intratumourally (I.T.) to mice twice over three weeks on days 58 and 78. Gemcitabine was investigated as a treatment alongside, and in combination with CAVATAK™. Gemcitabine (120 mg/kg), or saline, was administered intraperitoneally (I.P.) on days 81, 85, 89, and 93. Four mice were designated no treatment controls (N.T.C.). Besides recording body mass three times a week, N.T.C. mice were excluded from tumour inoculation and all other procedures. Eight mice were designated to each treatment group: I.T. Saline + I.P. Saline, I.T. Saline + I.P. Gemcitabine, I.T. CAVATAK™ + I.P. Saline, and I.T. CAVATAK™ + I.P. Gemcitabine. Tumour volumes were measured weekly through bioluminescent imaging of tumours using an IVIS™ Imaging System 100 (Xenogen). Sera were collected for analysis of viremia and circulating neutralising antibodies towards CVA21 on a weekly basis commencing two days prior to viral treatment, and weekly thereafter. Mice were euthanised if signs of pain and distress, a weight loss of 10% or more from the maximum weight prior to initial CVA21 treatment, or a tumour burden of 5 x 10^9 flux (photons/second) or greater was observed. Depicted in Figure 37 is a schematic diagram of the mouse model.

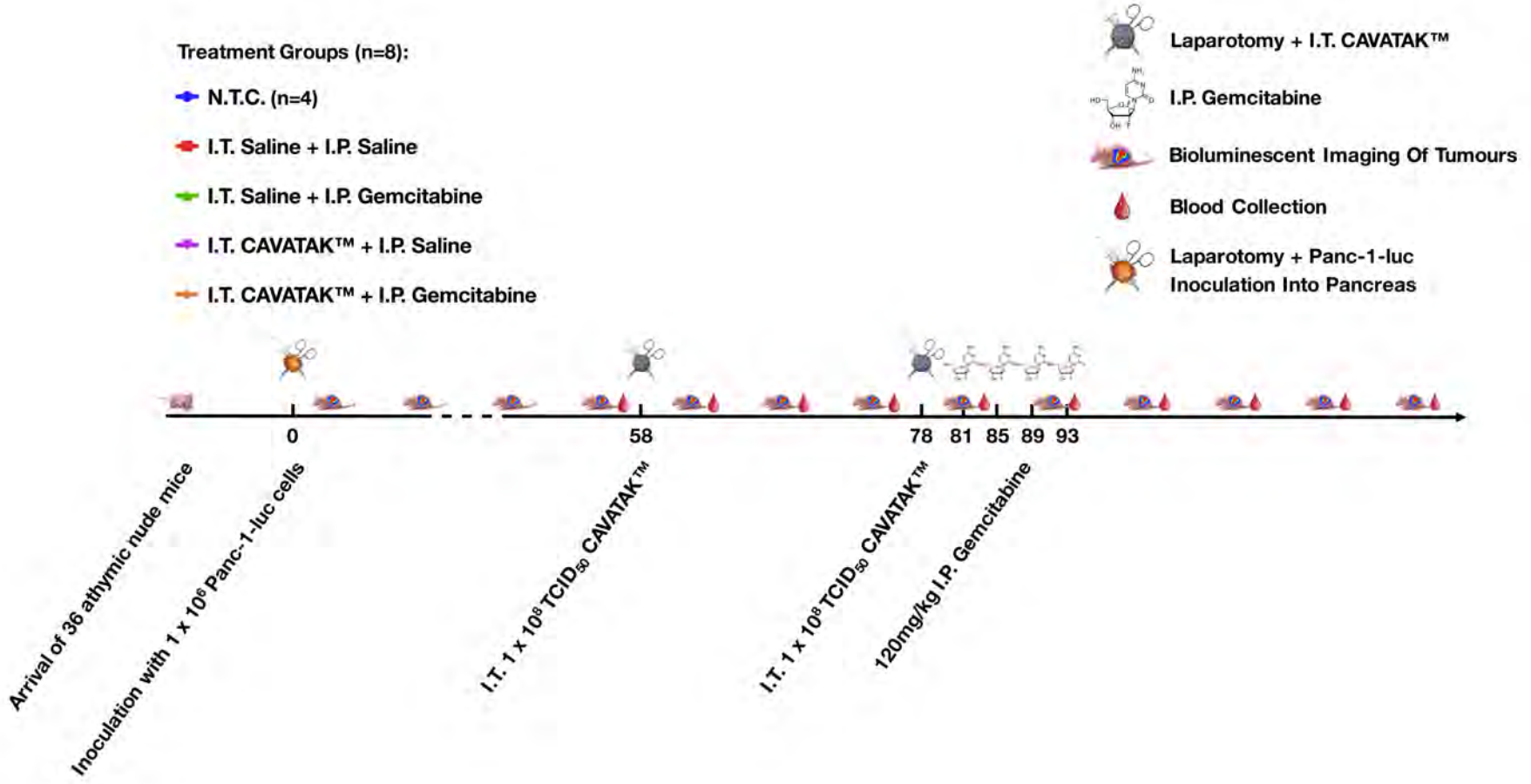

Figure 37: Schematic diagram of orthotopic pancreatic cancer athymic nude mouse model. 32 athymic nude mice were inoculated with 1 x 10^6 Panc-1-luc cells directly into the pancreas and tumours developed for 58 days before intratumoural treatments with CAVATAK™ (1 x 10^8 $TCID_{50}$), or saline, on days 58 and 78. Gemcitabine (120 mg/kg), or saline, was administered intraperitoneally every four days beginning three days after the second CAVATAK™ treatment for a total of four gemcitabine treatments (days 81, 85, 89, and 93). Bloods were collected, and tumours monitored via bioluminescence imaging on a weekly basis.

5.5.1 Welfare of Mice

Body mass is a general indicator of the welfare of a mouse. Mice were weighed three times a week to monitor the wellbeing of each mouse. If a 10% weight loss from the maximum recorded weight was observed prior to the initial surgery to administer viral treatment, then the mouse was humanely euthanised. Weights of treated mice were also compared to N.T.C. mice to assess the effects of the procedures and treatments on the body mass of each mouse. Depicted in Figure 38 are the weights of mice by treatment group and N.T.C. mice over the course of the study. Furthermore, presented in Table 8 is a summary of the differences in weights between each treatment group and N.T.C. mice at intervals of seven days over the course of the project. Significance was calculated with multiple unpaired t-tests without corrections for multiple comparisons using Prism v7.0 (GraphPad).

The greatest factor that affected mice weights over the study were the laparotomies conducted to inoculate the pancreas with tumour cells on day 0, and administer viral treatments on days 58, and 78 (Figure 38). Interestingly, the reduction in weight in N.T.C. mice mirrored that of treatment groups after initial surgery to generate orthotopic pancreatic cancer, despite not being operated on. Thus, there was no statistical significance between each treatment group and N.T.C. mice after the first surgery (Table 8). There was statistical significance between each treatment group and N.T.C. mice after the second two surgical procedures (days 58, and 78). Furthermore, mice treated with gemcitabine had lower weights compared to mice treated with saline and/or virus. Statistical significance in weights was not present present between N.T.C. and I.T. Saline + I.P. Gemcitabine mice as half of the group were euthanised due to dramatic weight loss during and after the gemcitabine treatment schedule. The weight loss was not as drastic in I.T. CAVATAK™ + I.P. Gemcitabine mice suggesting an advantage of CVA21 on the welfare of mice when co-administered with gemcitabine. Statistical significance in weights compared to N.T.C. mice was observed in this group. However, mice gained weight over the remaining duration of the study. Statistical significance could not be calculated for I.T. Saline + I.P. Saline, and I.T. Saline + I.P. Gemcitabine groups when group size was reduced to one mouse. Accordingly, in Table 8 when statistical significance could not be calculated, the time point was denoted undefined.

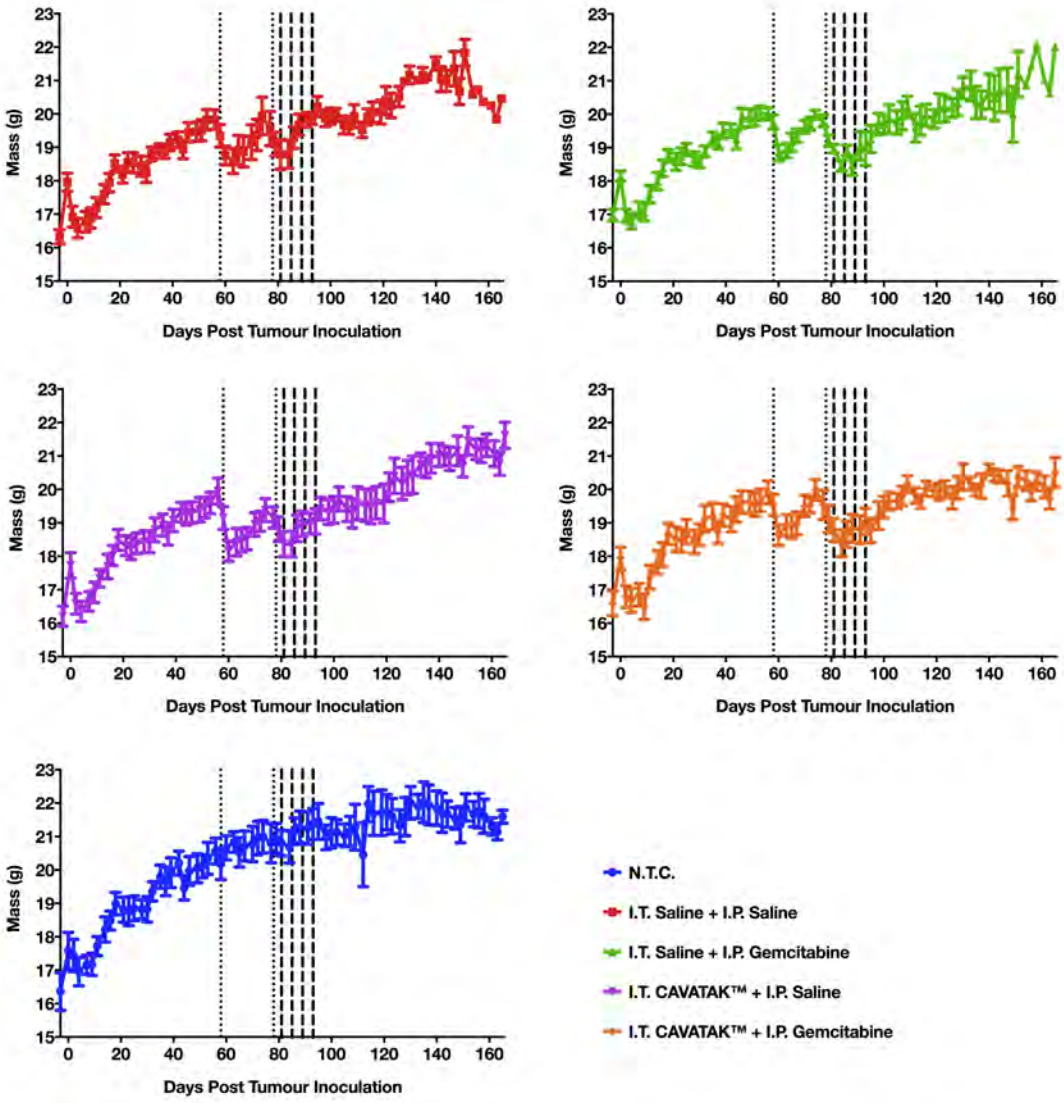

Figure 38: Mouse weights by treatment groups over the course of the study. Mice were weighed three times a week and average weights +/- SEM depicted according to treatment groups. Dotted lines indicate laparotomy and I.T. CAVATAK™ (1 x 10^8 $TCID_{50}$) or saline treatments. Dashed lines indicate I.P. gemcitabine (120 mg/kg) or saline treatments.

Table 8: Summary of differences in weights between treatment groups (n = 8) and N.T.C. mice (n = 4) over the course of the study. Multiple unpaired t-tests without corrections for multiple comparisons were performed using Prism v7.0 (GraphPad) to compare each treatment group (I.T. Saline + I.P. Saline, I.T. Saline + I.P. Gemcitabine, I.T. CAVATAK™ + I.P. Saline, and I.T. CAVATAK™ + I.P. Gemcitabine) with N.T.C. mice for each measurement at intervals of seven days post tumour inoculation (DPTI).

DPTI	I.T. Saline + I.P. Saline	I.T. Saline + I.P. Gemcitabine	I.T. CAVATAK™ + I.P. Saline	I.T. CAVATAK™ + I.P. Gemcitabine
0	N.S.	N.S.	N.S.	N.S.
7	N.S.	N.S.	N.S.	N.S.
14	N.S.	N.S.	N.S.	N.S.
21	N.S.	N.S.	N.S.	N.S.
28	N.S.	N.S.	N.S.	N.S.
35	*	N.S.	N.S.	N.S.
42	*	N.S.	N.S.	N.S.
49	N.S.	N.S.	N.S.	N.S.
56	N.S.	N.S.	N.S.	N.S.
63	**	***	**	**
70	N.S.	*	*	N.S.
77	N.S.	N.S.	*	N.S.
84	*	***	**	**
91	*	*	**	**
98	*	N.S.	*	*
105	*	*	*	**
112	N.S.	N.S.	N.S.	N.S.
119	N.S.	N.S.	N.S.	**
126	N.S.	N.S.	N.S.	*
133	N.S.	N.S.	N.S.	**
140	N.S.	N.S.	N.S.	*
147	N.S.	N.S.	N.S.	*
154	Undefined	Undefined	N.S.	*
161	Undefined	Undefined	N.S.	*
165	Undefined	Undefined	N.S.	N.S.

N.S. = no significance, * $P = < 0.05$, ** $P = < 0.01$, *** $P = < 0.001$, and **** $P = < 0.0001$.

5.5.2 Tumour Burden

Throughout the model, tumour volumes were the greatest indication of treatment efficacy. Presented in Figure 39, Figure 40, Figure 41 and Figure 42 are the bioluminescent overlay images of tumour volumes for each mouse by treatment group for the entire 165 day project. The associated flux values are graphed in Figure 43 by treatment group. Five mice (1808, 1809, 1811, 1814, and 1831) had spontaneous remission of tumours prior to any treatments (indicated by †). Mice with spontaneous remission of tumours were designated to either the I.T. Saline + I.P. Saline, or I.T. Saline + I.P. Gemcitabine, so that the number of mice in I.T. CAVATAK™ + I.P. Saline, and I.T. CAVATAK™ + I.P. Gemcitabine had a group number of eight mice. Furthermore, these mice with spontaneous tumour remission were excluded from all graphical and statistical analyses.

Focusing on the I.T. Saline + I.P. Saline treatment group (Figure 39), there was no effect on tumour burden, as expected, from administration of saline. Mice succumbed to the disease and reached the endpoints previously mentioned of a weight loss greater than 10% prior to the initial laparotomy and administration of I.T. treatments (day 58), or a tumour volume of 5×10^9 flux. Only one mouse (1807) was still on study at the end of the project. Similarly, gemcitabine administered as a single agent (Figure 40) had no effect on tumour burden. In fact, as previously mentioned, the mice had such drastic weight loss due to the administration of the conventional chemotherapy, and also large tumour burden, that two thirds (4/6) of the tumour bearing mice (1835, 1836, 1837 and 1838) in this group could not be maintained on study and had to be euthanised. All mice in the I.T. Saline + I.P. Gemcitabine had reached the designated endpoints and were euthanised by the end of the study on day 165.

Regarding CAVATAK™ as a single agent treatment for pancreatic cancer (Figure 41), 62.5% (5/8) of mice were alive and well at the end of the study on day 165. Mice 1816, and 1826 had stabilisation of disease (indicated by ✦), mouse 1815 had a partial response (portrayed by ★), and mouse 1825 had complete and sustained remission of disease (labelled with ❖). Comparatively, when gemcitabine was added with CAVATAK™ as a combination treatment for pancreatic cancer (Figure 42), 50% (4/8) of mice were alive and well upon completion of the study. Mouse 1828 had stable disease but had to be euthanised due to development of a skin rash and erratic

behavior. The cause of which was unclear but may have been due to administration of gemcitabine. Mouse 1819 had a very small but stable tumour throughout the model. Mouse 1822 had a partial response and mouse 1821 had a complete and sustained response after administration of CAVATAK™ and gemcitabine in combination. In summary, CAVATAK™ proved to be an efficacious treatment for pancreatic cancer in the described setting. Gemcitabine had no effect on tumour burden, and permitted the action of CAVATAK™.

The empirical flux values corresponding to tumour volumes are presented in Figure 43 according to treatment group. Panel A depicts the tumour volumes of each mouse according to treatment group. Panel B illustrates the mean flux values according to treatment group. Two graphs have been depicted in panel B for ease of visualisation of data points and statistical analysis bars comparing groups. The flux values for each individual mouse (Panel A graphs) clearly illustrated the lack of effect of saline and gemcitabine on pancreatic tumours as all tumours progressed until the endpoints previously discussed were reached. Comparatively, CAVATAK™ treated mice and CAVATAK™ in combination with gemcitabine treated mice had delayed tumour progression and several partial and complete responses. Statistical analyses (two-tailed paired t-tests with a confidence level of 95%) were performed on the mean flux values (Panel B graphs) for each measurement interval between each treatment group over the course of the study. Highly statistically significant differences between tumour volumes were achieved between saline or gemcitabine as single agent treated mice and CAVATAK™ treated mice. (I.T. CAVATAK™ + I.P. Saline vs. I.T. Saline + I. P. Saline: **** P = 0.00004. I.T. CAVATAK™ + I.P. Saline vs. I.T. Saline + I. P Gemcitabine: *** P = 0.0002). Congruently, tumour volumes between saline or gemcitabine as single agents treated mice and CAVATAK™ in combination with gemcitabine were similarly statistically significantly different (I.T. CAVATAK™ + I.P. Gemcitabine vs. I.T. Saline + I. P. Saline: *** P = 0.0002. I.T. CAVATAK™ + I.P. Gemcitabine vs. I.T. Saline + I. P. Gemcitabine **** P = 0.00007). There was no statistical significance between mean tumour volumes of mice administered with saline or gemcitabine as monotherapies. Likewise, there was no statistically significant difference in average tumour volumes in mice between CAVATAK™ and CAVATAK™ in combination with gemcitabine. Furthermore, these data highlighted the lack efficacy of gemcitabine as a treatment for pancreatic cancer in this setting, and the strong potential for CAVATAK™ to be a treatment for pancreatic cancer.

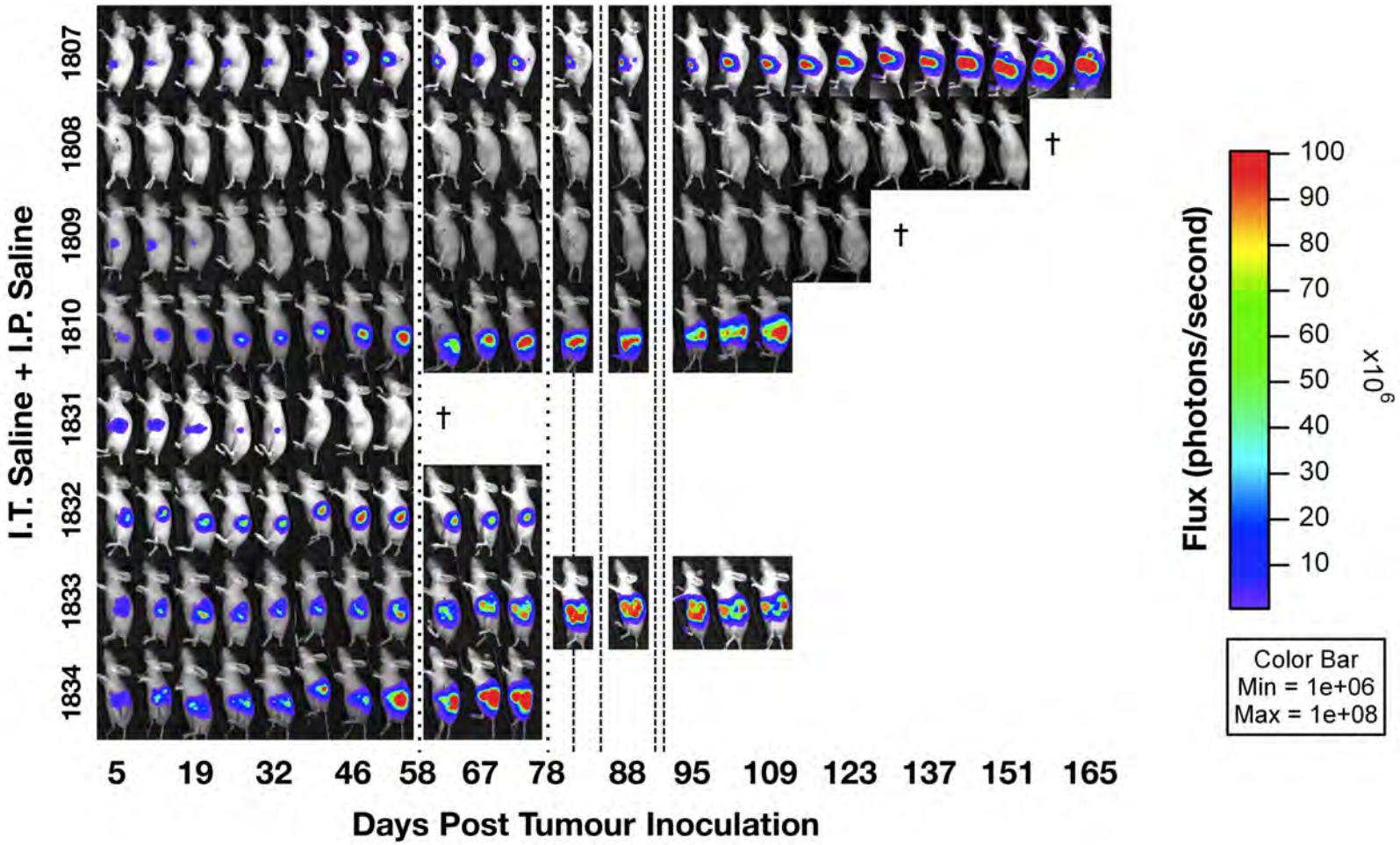

Figure 39: I.T. Saline + I.P. Saline treated mice tumour progression over the course of the study. Weekly bioluminescent imaging of tumours was conducted to measure tumour volume and track progression in each mouse. Dotted lines indicate laparotomy and I.T. CAVATAK™ (1 x 10^8 $TCID_{50}$) or saline treatments. Dashed lines indicate I.P. gemcitabine (120 mg/kg) or saline treatments. † indicates mice that had spontaneous remission of tumours prior to treatments and were excluded from statistical analyses.

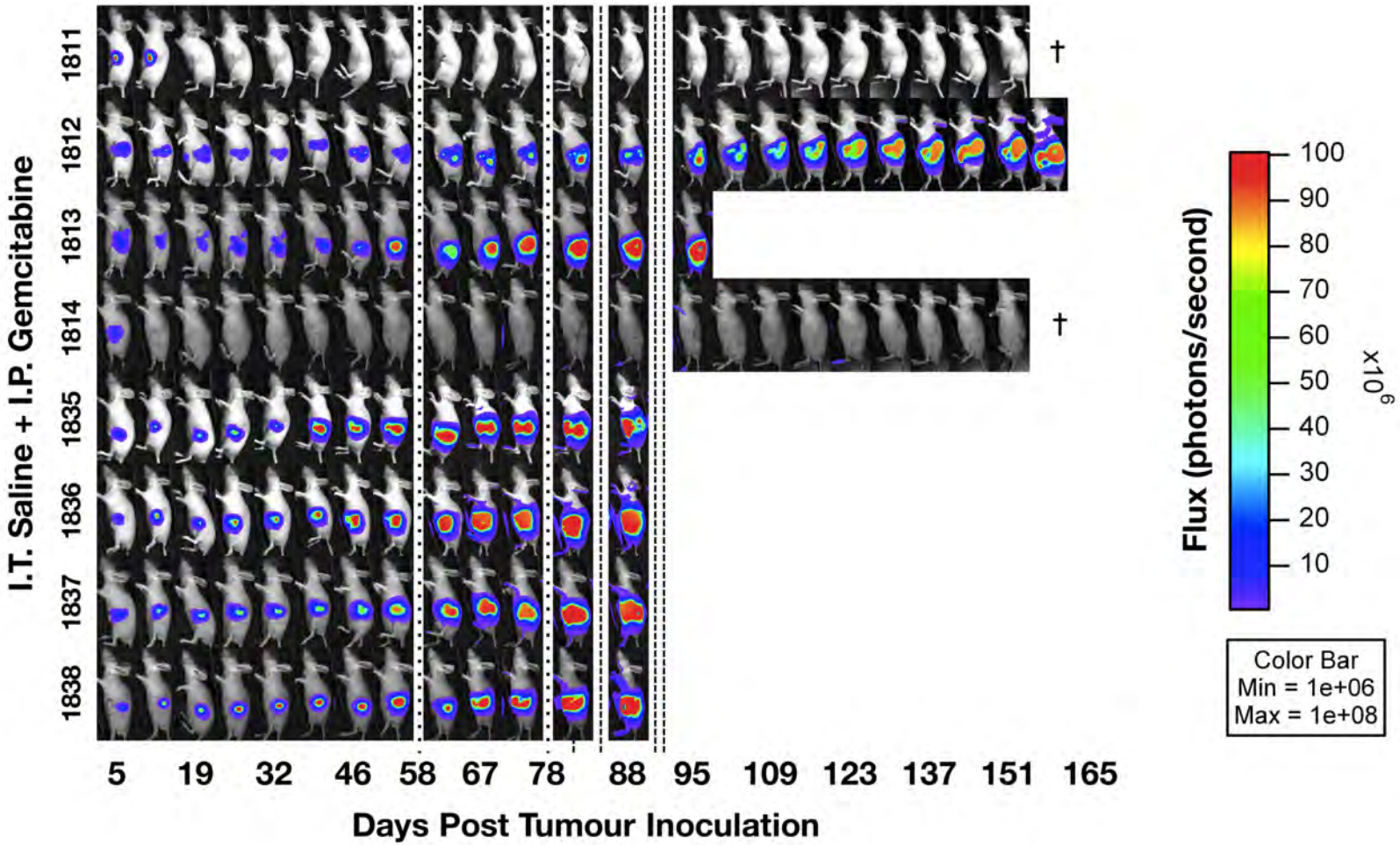

Figure 40: I.T. Saline + I.P. Gemcitabine treated mice tumour progression over the course of the study. Weekly bioluminescent imaging of tumours was conducted to measure tumour volume and track progression in each mouse. Dotted lines indicate laparotomy and I.T. CAVATAK™ (1 x 10^8 $TCID_{50}$) or saline treatments. Dashed lines indicate I.P. gemcitabine (120 mg/kg) or saline treatments. † indicates mice that had spontaneous remission of tumours prior to treatments and were excluded from statistical analyses.

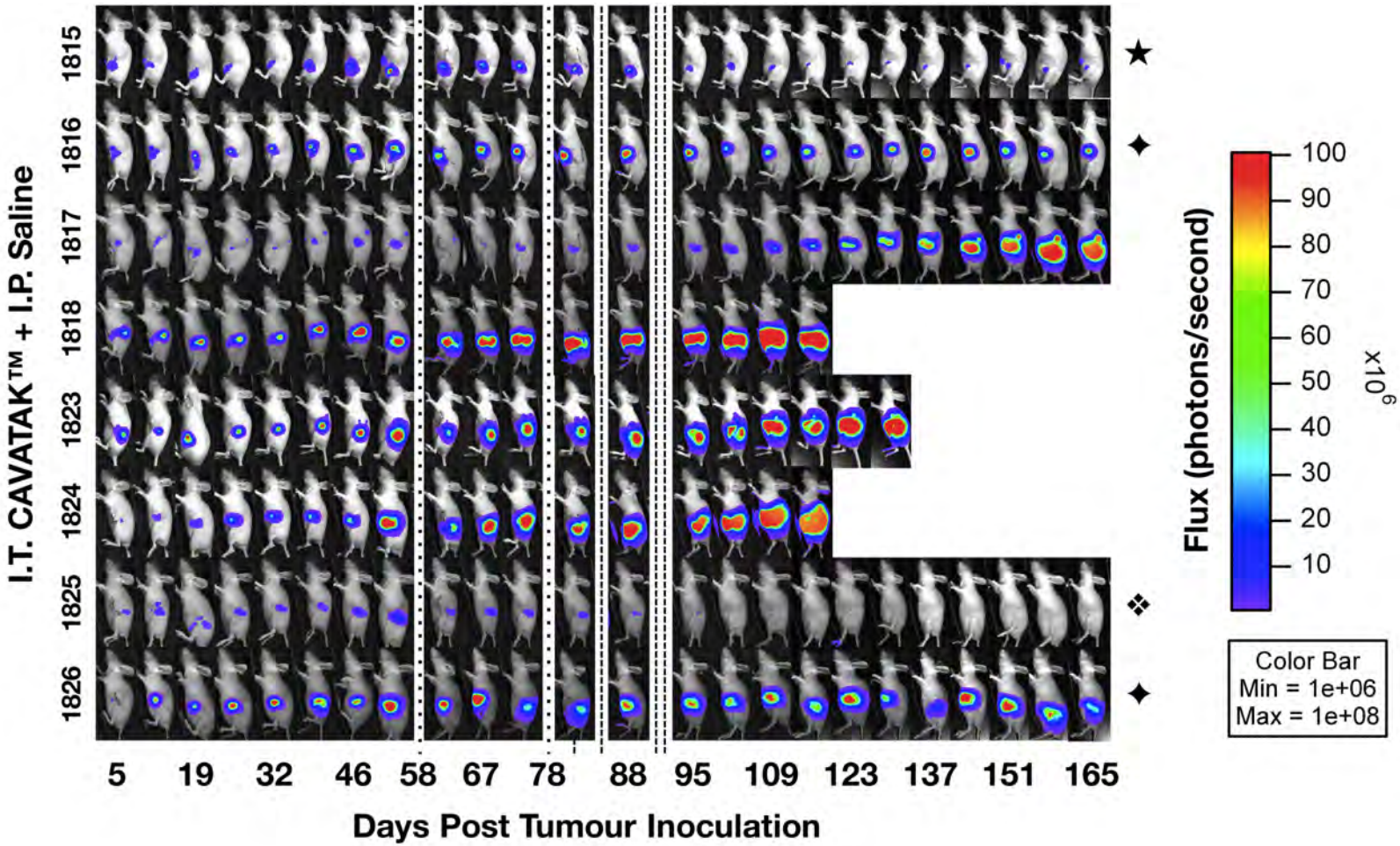

Figure 41: I.T. CAVATAK™ + I.P. Saline treated mice tumour progression over the course of the study. Weekly bioluminescent imaging of tumours was conducted to measure tumour volume and track progression in each mouse. Dotted lines indicate laparotomy and I.T. CAVATAK™ (1×10^8 $TCID_{50}$) or saline treatments. Dashed lines indicate I.P. gemcitabine (120 mg/kg) or saline treatments. ★ indicates mice that had a partial response (P.R.). ✦ indicates mice that had stable disease (S.D.). ❖ indicates mice that had a complete response (C.R.).

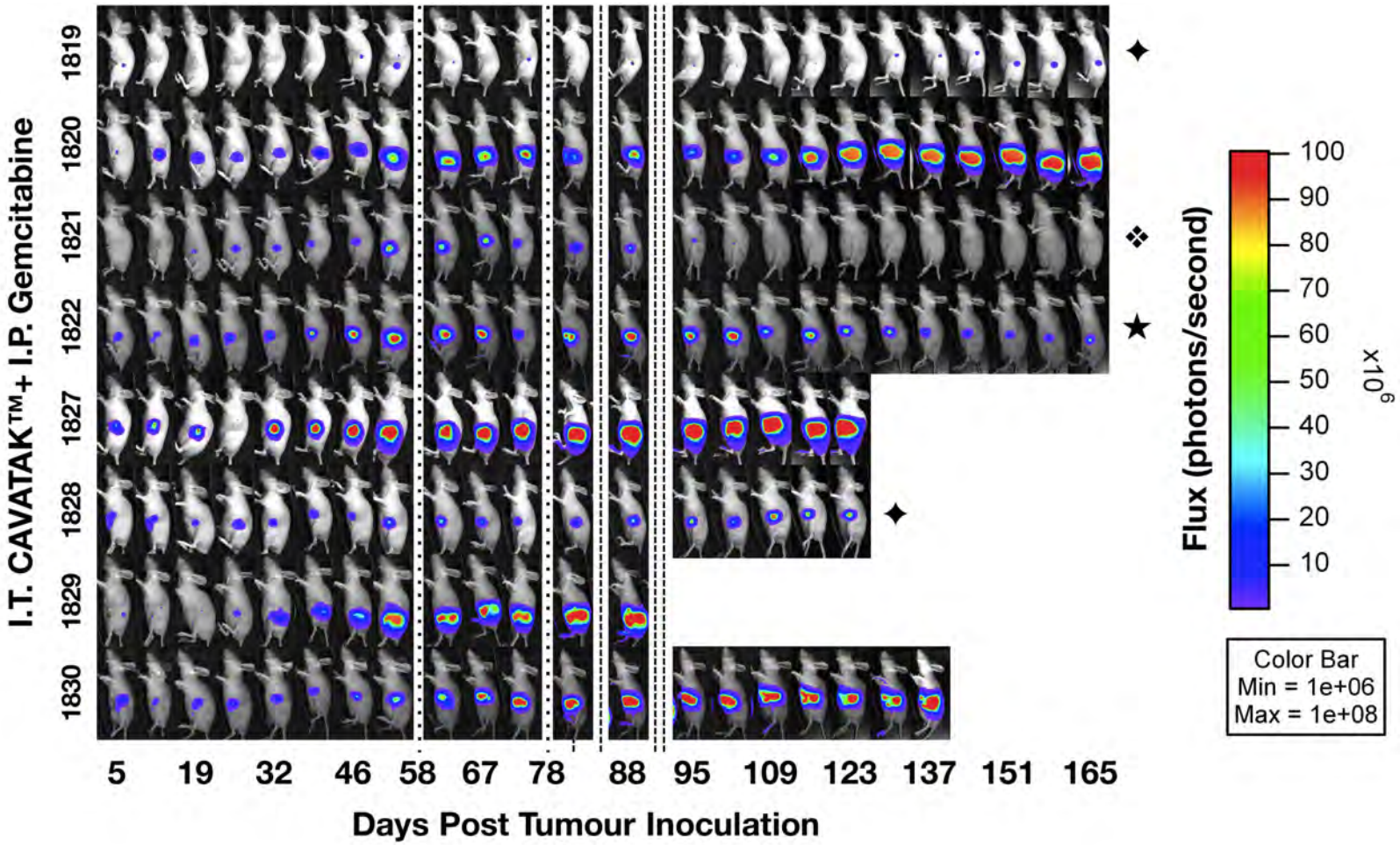

Figure 42: I.T. CAVATAK™ + I.P. Gemcitabine treated mice tumour progression over the course of the study. Weekly bioluminescent imaging of tumours was conducted to measure tumour volume and track progression in each mouse. Dotted lines indicate laparotomy and I.T. CAVATAK™ (1 x 10^8 $TCID_{50}$) or saline treatments. Dashed lines indicate I.P. gemcitabine (120 mg/kg) or saline treatments. ★ indicates mice that had a partial response (P.R.). ✦ indicates mice that had stable disease (S.D.). ❖ indicates mice that had a complete response (C.R.).

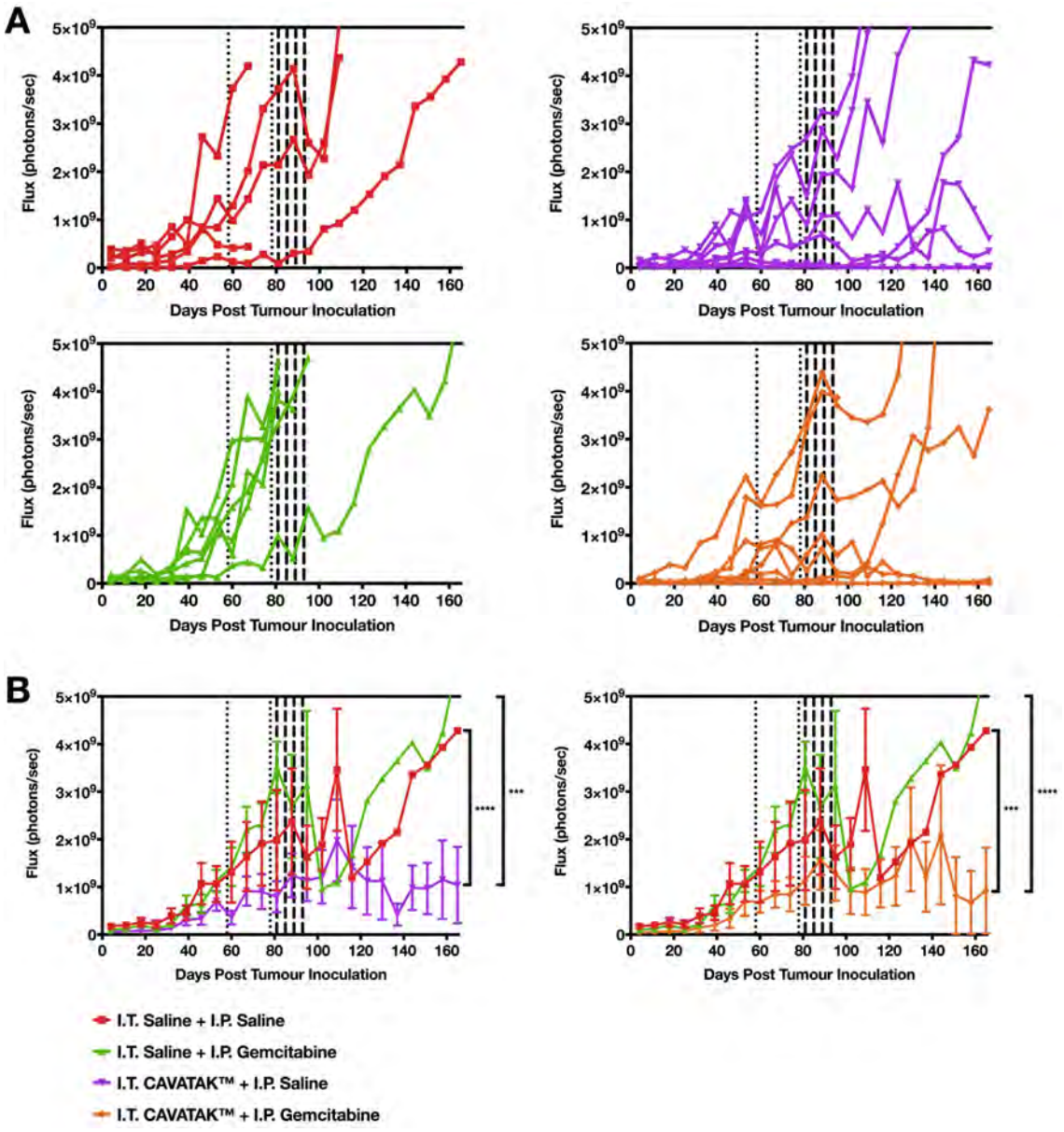

Figure 43: Tumour progression as a measure of flux (photons/second) by treatment groups over the course of the study. Flux values corresponding to tumour size according to treatment group obtained from weekly bioluminescent imaging of tumours were graphed for individual mice (Panel A) and group average +/- SEM (Panel B) for the duration of the model. Dotted lines indicate laparotomy and I.T. CAVATAK™ (1 x 10^8 $TCID_{50}$) or saline treatments. Dashed lines indicate I.P. gemcitabine (120 mg/kg) or saline treatment. Line at 5 x 10^9 flux indicates endpoint as tumour burden was deemed too large. Two-tailed paired t-tests with a confidence level of 95% were conducted to compare the mean flux values for each tumour measurement time point between each treatment group. I.T. CAVATAK™ + I.P. Saline vs. I.T. Saline + I. P. Saline: **** P = 0.00004. I.T. CAVATAK™ + I.P. Saline vs. I.T. Saline + I. P Gemcitabine: *** P = 0.0002. I.T. CAVATAK™ + I.P. Gemcitabine vs. I.T. Saline + I. P. Saline: *** P = 0.0002. I.T. CAVATAK™ + I.P. Gemcitabine vs. I.T. Saline + I. P. Gemcitabine **** P = 0.00007.

5.5.3 Survival Advantage

A Kaplan-Meier plot to portray survival advantage was generated for each treatment group based on the number of days each mouse was on study. Log-rank (Mantel-Cox) tests were performed to determine statistical significance in survival advantage between treatment groups. Figure 44 illustrates CAVATAK™ as a monotherapy treatment for pancreatic cancer provided a statistically significant survival advantage compared to either saline or gemcitabine as single agent treatments (I.T. CAVATAK™ + I.P. Saline vs I.T. Saline + I.P. Saline * $P = 0.033$, I.T. CAVATAK™ + I.P. Saline vs I.T. Saline + I.P. Gemcitabine ** $P = 0.0021$). Similarly, there was a statistically significant increase in survival for mice treated with CAVATAK™ in combination with gemcitabine compared to gemcitabine treated mice (I.T. CAVATAK™ + I.P. Gemcitabine vs. I.T. Saline + I.P. Gemcitabine ** $P = 0.0077$).

In terms of median survival of mice according to treatment group, gemcitabine alone treated mice appeared to be worse off than mice administered with saline alone as the calculated average survival times were 90.5 and 112 days, respectively. Mice treated with the combination of CAVATAK™ and gemcitabine (median survival 154.5 days) had on average 42.5 days increased survival compared to saline treated mice, and an average survival increase of 64 days compared to gemcitabine treated mice. The survival advantage in days could not be calculated for CAVATAK™ alone treated mice as 62.5% (5/8) of mice were still alive at the end of the study on day 165. Therefore, the advantage would have been greater than 53 days compared to saline treated mice, or over 74.5 days compared to gemcitabine treated mice if the study had been prolonged.

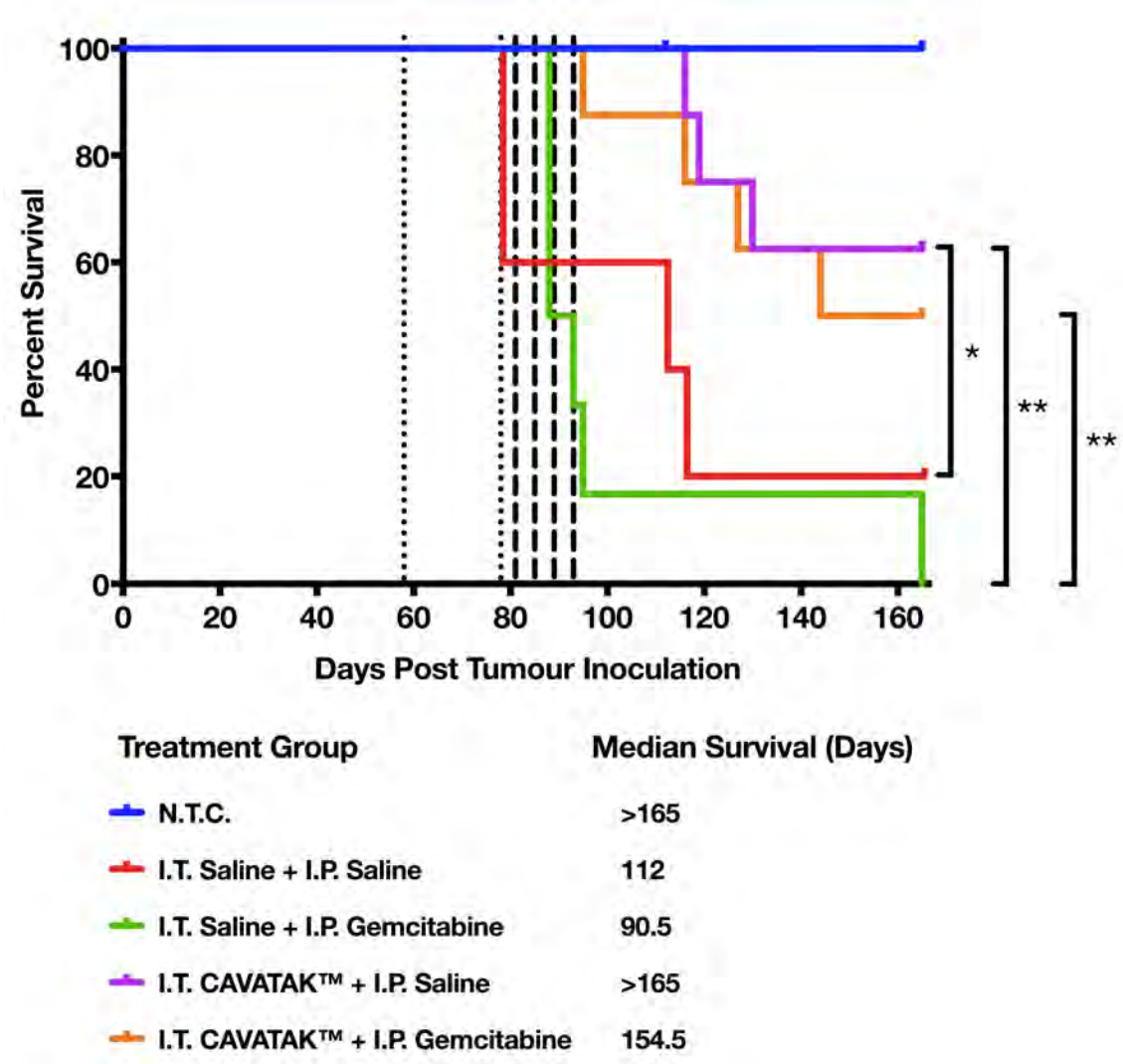

Figure 44: Survival advantage of mice according to treatment groups. Survival periods of mice were graphed as a Kaplan-Meier plot according to treatment groups and the survival advantage calculated through log-rank (Mantel-Cox) tests between treatment groups. I.T. CAVATAK™ + I.P. Saline vs I.T. Saline + I.P. Saline * P = 0.033. I.T. CAVATAK™ + I.P. Saline vs I.T. Saline + I.P. Gemcitabine ** P = 0.0021. I.T. CAVATAK™ + I.P. Gemcitabine vs. I.T. Saline + I.P. Gemcitabine ** P = 0.0077.

5.5.4 Serum Analyses

Sera from treatment group mice were collected weekly commencing two days prior to the initial treatment with CAVATAK™, allowing for characterisation of the anti-CVA21 immune response throughout the model. Shown in Figure 45, viremia (square symbols) was not detected at any collection point in any mouse when titrating 10-fold dilutions of serum samples against SK-Mel-28 cells, most likely due to viral clearance within the five days after treatment administration and before blood collection. Virus may have been present but could not be detected at a 1:100 starting dilution of sera. Therefore, depicted in Figure 45, viremia is presented as below level of detection (B.L.D.) for each treatment group.

Neutralising antibody (nAb) concentrations were successfully measured by titrating 2-fold sera dilutions incubated for 1 hour with 100 $TCID_{50}$ of CVA21, against SK-Mel-28 cells. Depicted in Figure 45 are the nAb profiles (triangle symbols) according to treatment groups over the duration of the model. Prior to initial CAVATAK™ treatments (day 56) there were no detectable nAbs in any mice. A B.L.D. value was depicted for each time point as detection sensitivity was based off 1:32 starting dilutions of sera. nAbs were not detected at any time point in saline, or gemcitabine alone treated mice. CAVATAK™ as a single agent treated mice had a regular increase in nAbs towards CVA21 after both administrations reaching on average a 50% neutralisation titre of 1:288 on day 112. nAbs did not begin to subside on average until approximately 34 days after the second treatment with CAVATAK™ and were not detected after 133 days. Comparatively, the addition of gemcitabine as a treatment with CAVATAK™ resulted in a reduced immune reaction as lower levels of nAbs were produced in mice treated with the combination of the two agents. The highest average 50% neutralising antibody concentration was on day 105 at 1:123, less than half of the maximum nAb recorded from CAVATAK™ alone treated mice. However, unlike the CAVATAK™ treated mice, there was detectable nAbs in one of the four remaining mice in the combination treatment group at the end of the study.

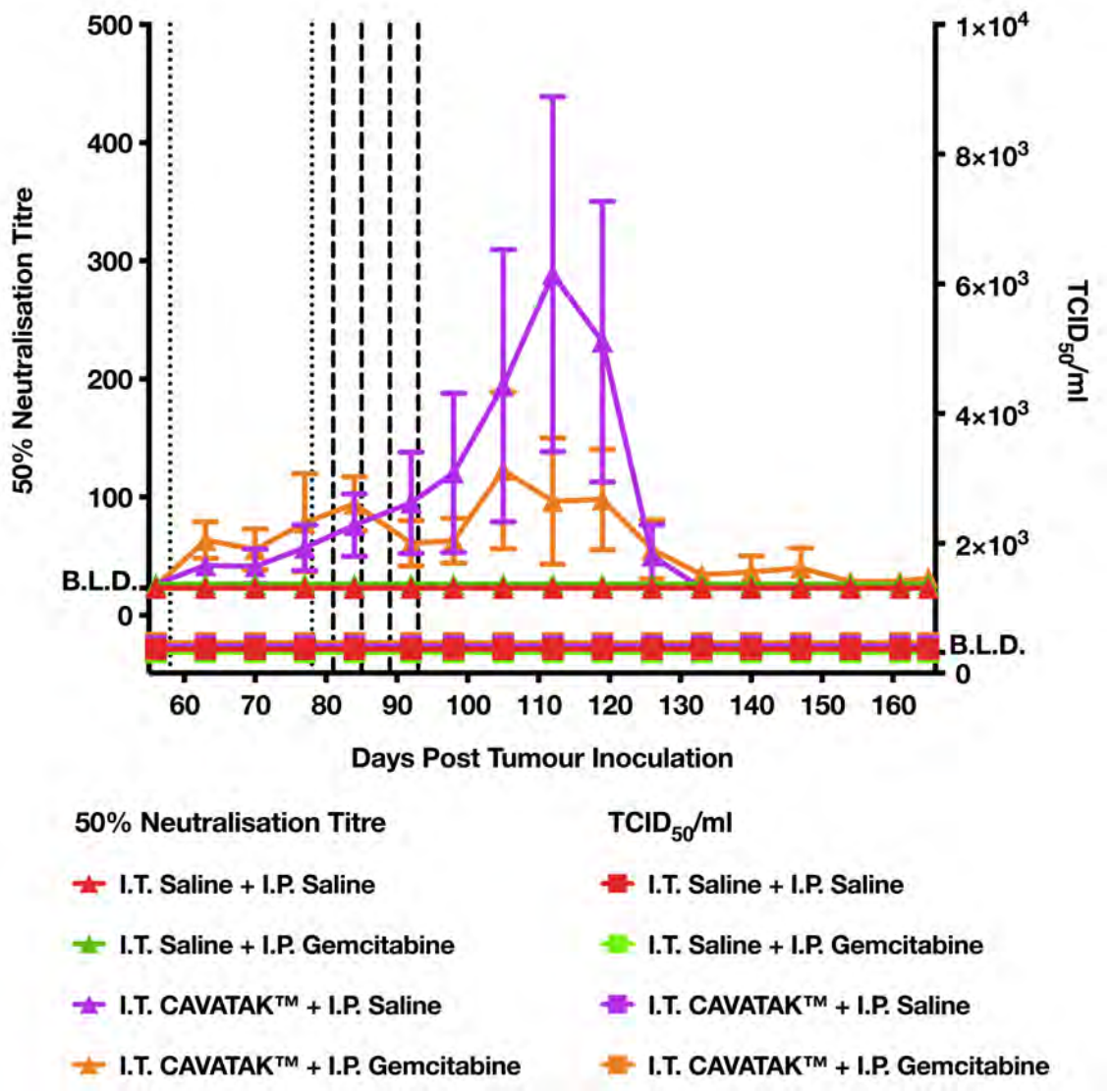

Figure 45: Viremia and neutralising antibodies towards CVA21 concentrations over the course of the study. Sera samples collected weekly from mice were analysed for viremia (square symbols) through $TCID_{50}$ assays and neutralising antibodies (triangle symbols) towards CVA21 via neutralisation assays. Mean values +/- SEM were depicted according to treatment groups and graphed using Prism v7.0 (GraphPad). Dotted lines indicate laparotomy and I.T. CAVATAK™ (1×10^8 $TCID_{50}$) or saline treatments. Dashed lines indicate I.P. gemcitabine (120 mg/kg) or saline treatment. B.L.D. indicates the below level of detection value for either assay. N.B. Overlapping data points were nudged to better visualise.

5.6 *In Vivo* Investigation of CVA21 in Combination With Gemcitabine as a Treatment for Pancreatic Cancer Incorporating Pancreatic Stellate Cells

At this point in the study two pancreatic stellate cell (PSC) lines, TAS29 and TAS31, were obtained for investigation. A mouse model was developed to incorporate stellate cells into the tumour progression model of pancreatic cancer. Presented in Figure 46 is a schematic diagram of the designed model. Treatment groups were consistent with the previous mouse model: I.T. Saline + I.P. Saline, I.T. Saline + I.P. Gemcitabine, I.T. CAVATAK™ + I.P. Saline, and I.T. CAVATAK™ + I.P. Gemcitabine. Sixteen tumour bearing mice were allocated to each treatment group. Four mice were again designated as N.T.C.s and excluded from all procedures besides routine monitoring of body mass throughout the model. 64 athymic nude mice were inoculated with a cell mixture of 1 x 10^5 Panc-1 and 5 x 10^5 TAS29 cells (1:5 ratio of PC:PSC) subcutaneously (S.C.) into the left hind flank of each mouse. A mixture of 1 x 10^5 Panc-1 plus 5 x 10^5 TAS29 cells (1:5 ratio of PC:PSC) were also injected S.C. into the right hind flank of each mouse to develop a second tumour. After a tumour development period of eight days, mice were administered CAVATAK™ (7.5 x 10^6 $TCID_{50}$) or saline I.T into the left hind flank tumour. Concurrently, gemcitabine (120 mg/kg) or saline was administered I.P. to relevant treatment groups. Treatments were repeated on days 11, 14, and 17 days post tumour inoculation for a total of four treatments. Tumour volumes of left and right hind flank tumours were measured weekly using Vernier calipers. Sera were collected for analysis of viremia and circulating neutralising antibodies towards CVA21 on a weekly basis commencing approximately one hour after the initial viral treatment, and weekly thereafter. Mice were euthanised if a weight loss of 10% or more from the maximum weight, or a tumour volume of 2500 mm^3 or greater was measured. The model was designed to give greater weight to the results of the previous model given that a larger treatment group number of 16 was employed enabling greater statistical significance. Additionally, the incorporation of pancreatic stellate cells into the tumour progression model would better recapitulate native pancreatic cancer. Furthermore, a lower dose of CAVATAK™ was investigated to determine if the same effect could be achieved. Finally, the model also aimed to determine if the virus could systemically migrate to

distant tumours (non-injected right hind flank tumour) and have an effect on tumour progression.

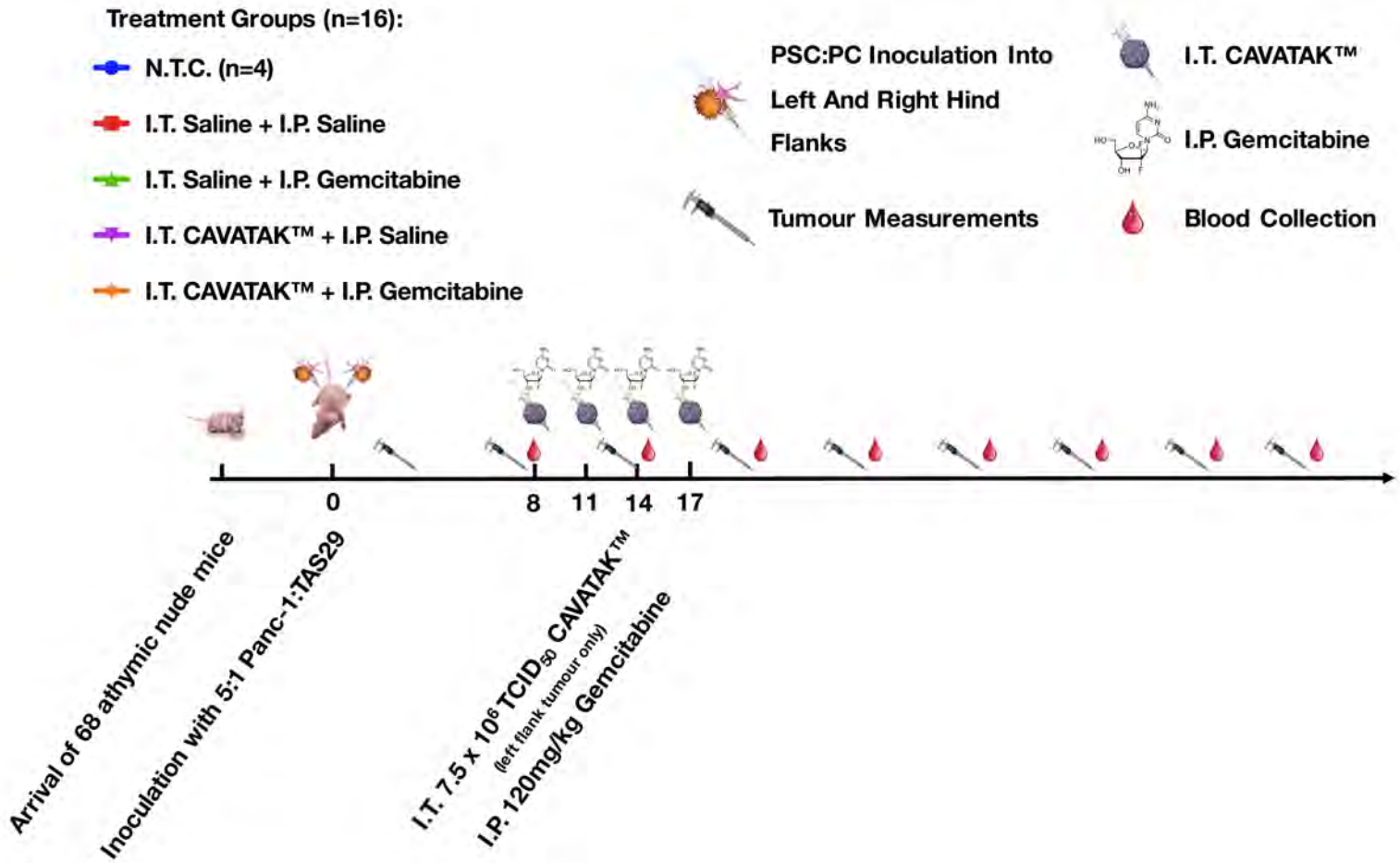

Figure 46: Schematic diagram of subcutaneous pancreatic cancer athymic nude mouse model. 64 athymic nude mice were inoculated with 1 x 10^5 Panc-1 + 5 x 10^5 TAS29 cells subcutaneously into both the left and right hind flanks. Beginning 8 days post tumour inoculation the left flank tumour was injected with CAVATAK™ (7.5 x 10^6 $TCID_{50}$), or saline, on days 8, 11, 14 and 17. Gemcitabine (120 mg/kg), or saline, was administered I.P. concurrently to relevant treatment groups. Bloods were collected, and tumours measured with Vernier calipers on a weekly basis.

5.6.1 Tumour Volumes

Tumour volumes of left and right hind flank tumours were to be measured weekly using Vernier calipers to monitor tumour progression. However, unfortunately the pancreatic stellate cells (TAS29) injected in combination with the pancreatic cancer cells (Panc-1) entered into senescence shortly after inoculation in mice. An observation that was mirrored in maintenance of cells in tissue culture flasks after approximately 10 cell passages. Therefore, as can be seen in Figure 47, both the left (injected tumour) and right hind flank (non-injected tumour) tumours spontaneously regressed. The 1 x 10^5 Panc-1 cells co-injected with the stellate cells did not take and develop tumours. Tumour reduction was not a result of treatments as the non-injected right hind flank tumours in the I.T. Saline + I.P. Saline treated mice had tumour remission.

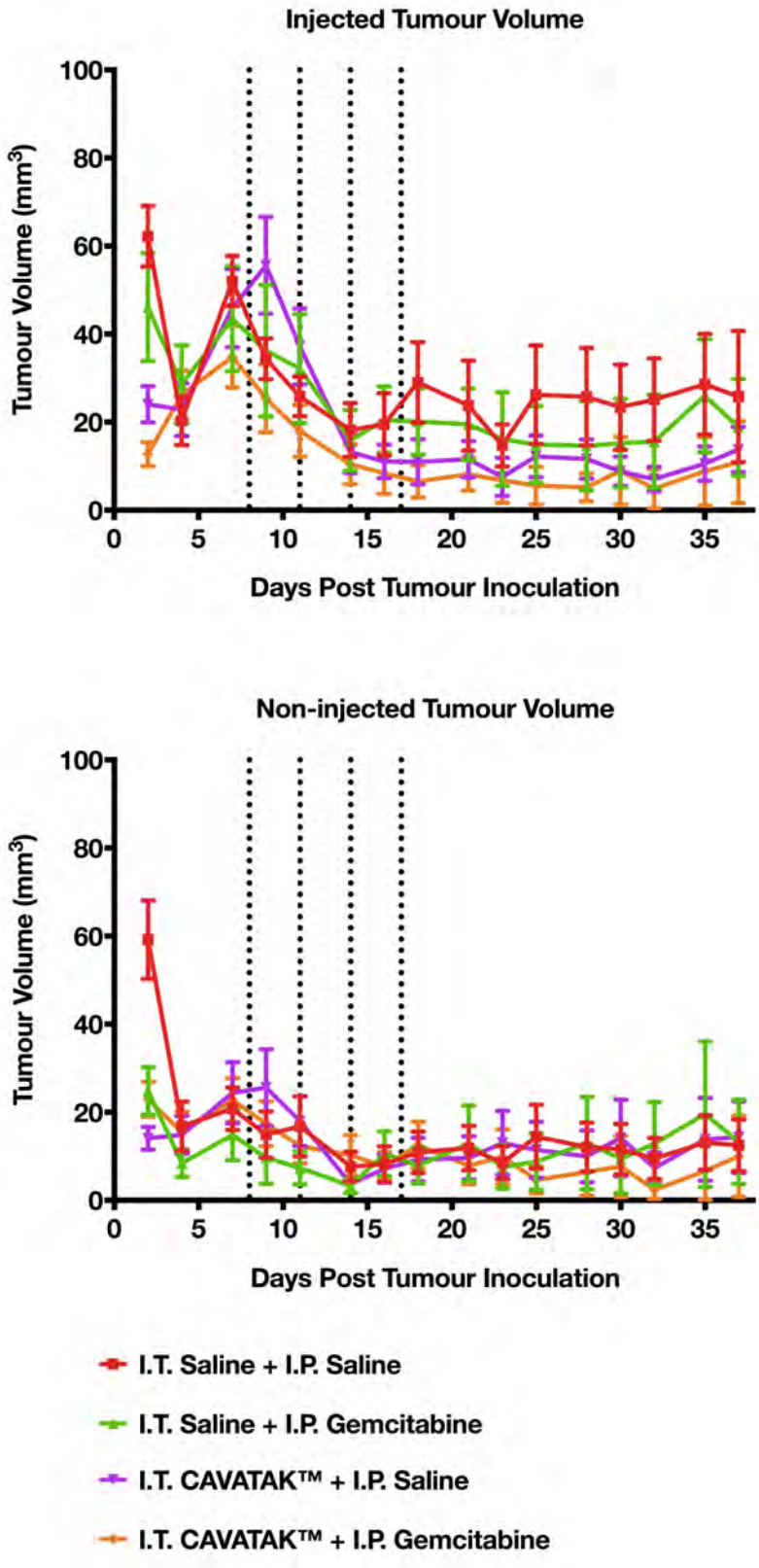

Figure 47: Tumour progression as a measure of tumour volume (mm^3) by treatment groups over the course of the study. Left hind flank tumours (injected tumours) and right hind flank (non-injected tumours) were measured using Vernier calipers on a weekly basis and graphed using Prism v7.0 (GraphPad). Dotted lines indicate treatments with either CAVATAK™ (7.5×10^6 $TCID_{50}$) or saline treatments I.T. and I.P. gemcitabine (120 mg/kg) or saline treatments.

5.6.2 Sera Analyses

The presented model enabled viremia and circulating neutralising antibody profiles to be determined from weekly sera collections. Depicted in Figure 48 CVA21 viremia (square symbols) was detected on average in CAVATAK™, and CAVATAK™ plus gemcitabine, treated mice shortly after the initial and final treatments. Mice treated with the combination of CAVATAK™ and gemcitabine appeared to have higher viremia at each time point suggesting that gemcitabine reduced the immune reaction towards and clearance of virus. Reduction of the immune reaction to CVA21 was further supported by the nAb titres (triangle symbols) between the two CAVATAK™ treated groups. Gemcitabine in addition with CAVATAK™ appeared to minimise the level of nAbs initially generated towards CVA21. Moreover, the nAb titres dropped earlier than CAVATAK™ alone treated mice. No viremia or circulating nAbs were detected in saline, or gemcitabine alone treated mice.

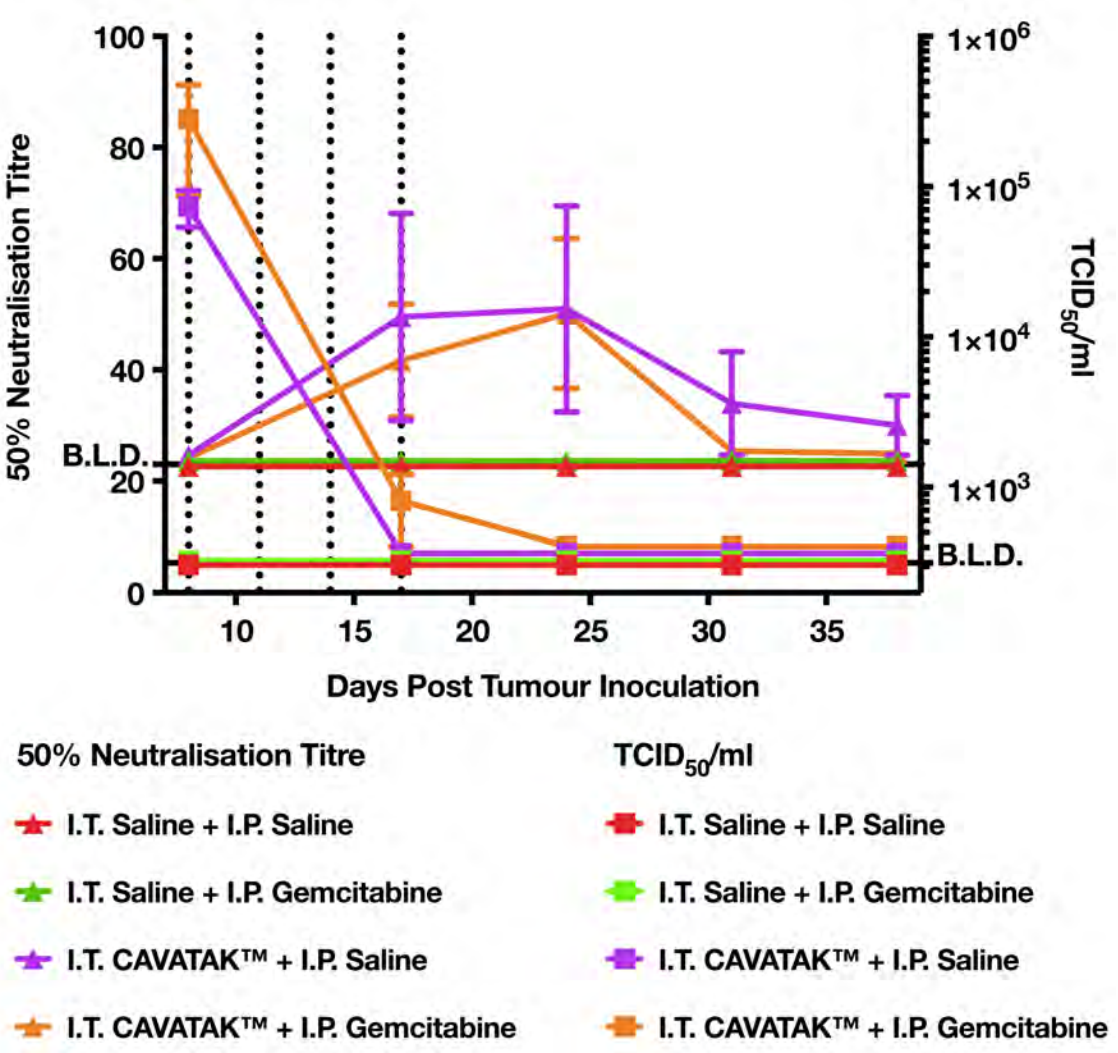

Figure 48: Viremia and neutralising antibodies towards CVA21 concentrations over the course of the study. Sera samples collected weekly from mice were analysed for viremia (square symbols) through $TCID_{50}$ assays and neutralising antibodies (triangle symbols) towards CVA21 via neutralisation assays. Mean values +/- SEM were depicted according to treatment groups and graphed using Prism v7.0 (GraphPad). Dotted lines indicate treatments with either CAVATAK™ (7.5×10^6 $TCID_{50}$) or saline treatments I.T. and I.P. gemcitabine (120 mg/kg) or saline treatments. B.L.D. indicates the below level of detection value for either assay. N.B. Overlapping data points were nudged to better visualise.

Chapter 6

Generation of an Immune Competent Mouse Model of Orthotopic Pancreatic Cancer Susceptible to CVA21 Oncolysis

Presented herein are the attempts to generate a model of orthotopic pancreatic cancer, susceptible to CVA21 oncolysis, in an immune competent strain of mouse. Initially, the manipulation of mouse pancreatic cancer cells, UN-KPC-961, and mouse pancreatic stellate cells, ImPSCc2, to express human ICAM-1 and firefly luciferase through transfection and transduction experiments are discussed. Characterisation of CVA21 oncolysis of the resulting cell lines, UN-KPC-961-ICAM-1-luc and ImPSCc2-ICAM-1 was achieved through viral infectivity and viral growth kinetics assays. Finally, three pilot mouse models to generate orthotopic pancreatic cancer in BALB/c or C57BL/6 mice were investigated.

If successful, the model would allow investigation of CVA21 as a treatment for pancreatic cancer in an immune competent setting. Thus, the secondary anti-cancer immune response potentially generated by CVA21 oncolysis could be more readily observed. Moreover, investigations could be conducted to determine the potential efficacy of CVA21 in combination with immune checkpoint inhibitors. Immune checkpoint inhibitors require a functional immune system, namely the presence of CD8 T cells. Unfortunately, there were a number of hurdles to overcome in generating this model and finalising all the aims could not be completed within the timeframe of the project.

6.1 Transfection and Transduction of Mouse Pancreatic Cancer and Pancreatic Stellate Cells for Use In *In Vivo* Models

To sensitise the mouse pancreatic cancer cell line, UN-KPC-961, and the mouse pancreatic stellate cell line, ImPSCc2, to CVA21 oncolysis, the two cell lines were transfected with a plasmid, pEF-BOS, containing the gene for human ICAM-1 (huICAM-1). pEF-BOS-ICAM-1 had no positive selection marker for transfected cells. Therefore, to achieve stably transfected, pure populations of transfected cells, each cell line underwent multiple rounds of cell sorting to enrich for huICAM-1 expressing cells, and numerous subsequent single cell dilutions and expansions to select stable single clone populations over consecutive cell passages. The transfected cell lines were denoted UN-KPC-961-ICAM-1, and ImPSCc2-ICAM-1. Additionally, to enable bioluminescent imaging of tumours, UN-KPC-961-ICAM-1 cells were transduced with a lentiviral vector to express the firefly luciferase gene. Thus, when the substrate D-luciferin was added to these cells an enzymatic reaction resulting in bioluminescence occurred. The transfected and transduced mouse pancreatic cancer cell line was designated UN-KPC-961-ICAM-1-luc.

Once each cell line was successfully transfected, transduced, and stable colonies selected, expression of huICAM-1 was measured through flow cytometry. Presented in Figure 49 are the flow cytometric analyses for huICAM-1 expression on the generated cell lines, ImPSCc2-ICAM-1, and UN-KPC-961-ICAM-1-luc, along with corresponding wild-type (WT) cell lines, ImPSCc2 and UN-KPC-961. Panel A illustrates the qualitative analyses of ICAM-1 expression (red histogram) on the WT cells and the genetically modified cell lines. Background staining for huICAM-1 was not present on the WT cells, as a quantifiable shift from the unstained controls was absent (solid grey histogram). There are discrete peaks of high ICAM-1 expression on both ImPSCc2-ICAM-1 and UN-KPC-961-ICAM-1-luc cell lines. Fluorescent gating for huICAM-1 expression revealed 95.84% of ImPSCc2-ICAM-1 and 98.20% of UN-KPC-961-ICAM-1-luc cells expressed huICAM-1.

Quantibrite™ PE beads (BD Biosciences) were measured alongside the cell lines under the same instrument settings to allow quantification of the number of antibodies

bound per cell, and thus, the approximate number of ICAM-1 receptors per cell on ImPSCc2-ICAM-1 and UN-KPC-961-ICAM-1-luc cells to be interpolated. Depicted in Figure 49 Panel B are the interpolated ICAM-1 molecules per cell for each of the genetically modified and WT cell lines. Low, non-specific background ICAM-1 levels were recorded from unstained cells and non-specific binding of the anti-ICAM-1 antibody on WT cells. Discounting such levels, ImPSCc2-ICAM-1 cells expressed approximately 206,745 huICAM-1 molecules per cell, and UN-KPC-961-ICAM-1-luc cells displayed approximately 790,720 huICAM-1 molecules per cell.

To measure the bioluminescence produced from the enzymatic reaction within UN-KPC-961-ICAM-1-luc cells, D-luciferin was added to 2-fold dilutions of cells in a 96-well black plate and the flux values recorded using an IVIS™ Imaging System 100 (Xenogen). Portrayed in Figure 50 Panel A are the flux heatmaps within each well over the dilution series starting at 1 x 10^6 UN-KPC-961-ICAM-1-luc cells. Panel B is a graphical representation of the flux values corresponding to cell number. The linear regression curve applied to these data points indicated a clear linear correlation between cell number and bioluminescence.

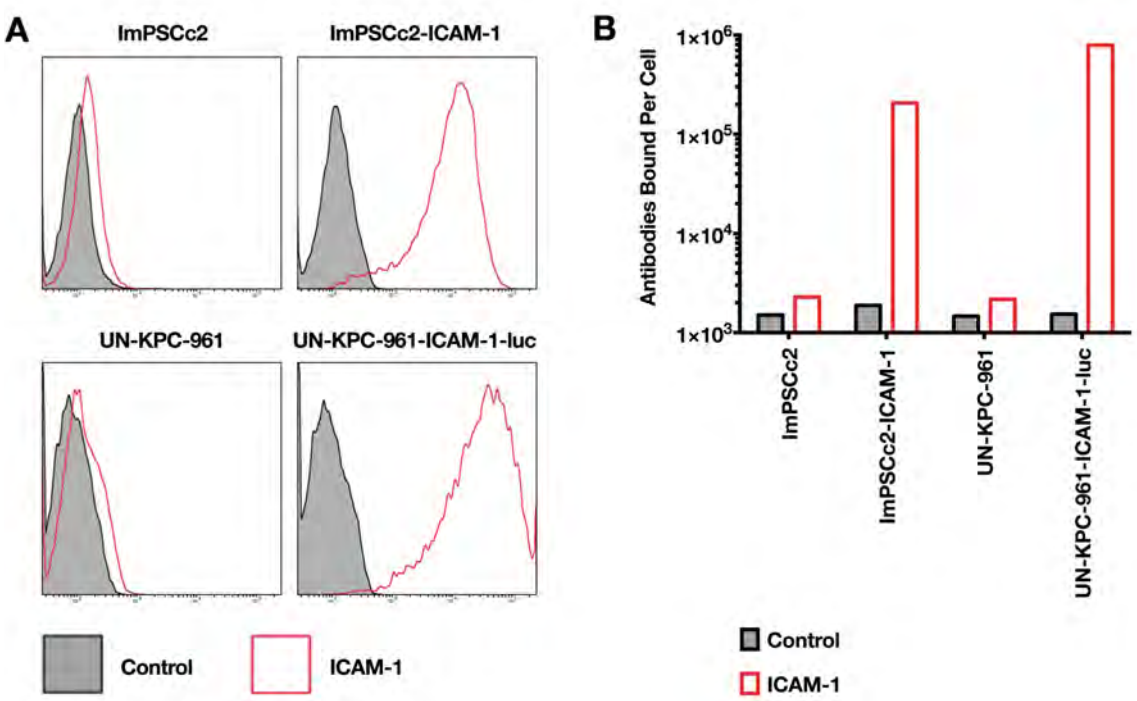

Figure 49: Human ICAM-1 cell surface expression on transfected mouse pancreatic cancer and mouse pancreatic stellate cells. Mouse pancreatic cancer (UN-KPC-961) and mouse pancreatic stellate (ImPSCc2) cells were transfected with pEF-BOS-ICAM-1 to express human ICAM-1. After multiple cell sorts to enrich for transfected populations of cells, and subsequent single cell isolations to select for stably transfected cells, the level of human ICAM-1 expression was measured via flow cytometry. Panel A depicts qualitative FACS overlay graphs of human ICAM-1 expression on transfected, and non-transfected cells. Panel B is the number of ICAM-1 molecules per cell extrapolated from BD QuantiBrite PE Beads run alongside each cell line under the same instrument settings. Average of 1 x 10^4 recorded events for each cell line.

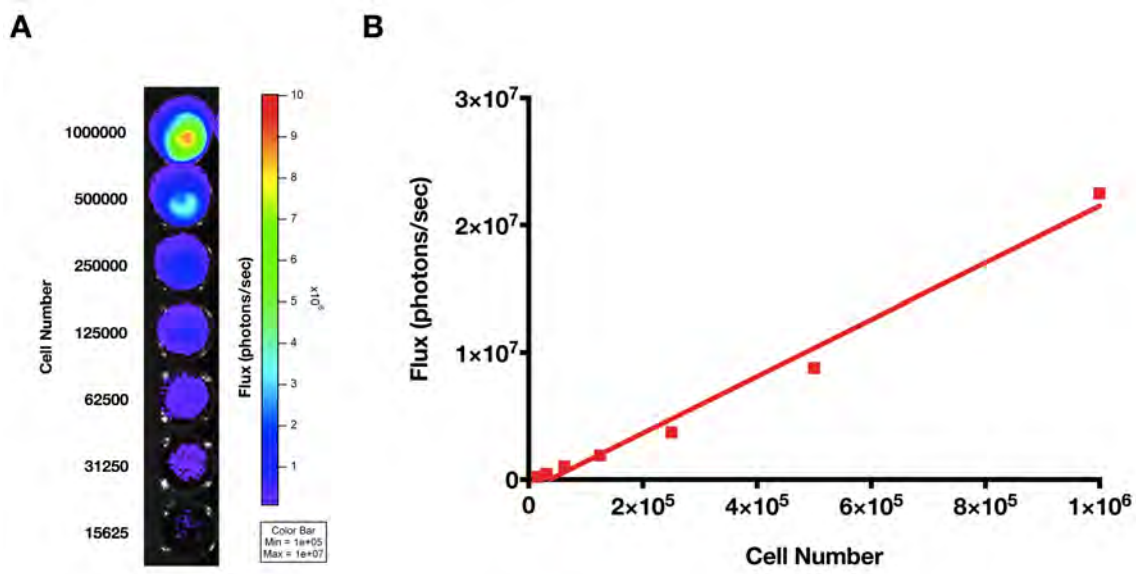

Figure 50: Bioluminescence of luciferase transduced mouse pancreatic cancer cells. Mouse pancreatic cancer cells transfected to express human ICAM-1, UN-KPC-961-ICAM-1, were transduced with a lentiviral vector to express the firefly luciferase gene. Panel A depicts the bioluminescence produced by UN-KPC-961-ICAM-1-luc cells when exposed to D-luciferin over 2-fold dilutions of cells. Panel B graphs the associated flux values within each well by number of cells with a linear regression curve applied.

6.1.1 Characterisation of Transfected and Transduced Mouse Pancreatic Cancer and Pancreatic Stellate Cells to CVA21 Oncolysis

The susceptibility of the manipulated mouse pancreatic cancer cells, UN-KPC-961-ICAM-1-luc, and pancreatic stellate cells, ImPSCc2-ICAM-1, to CVA21 oncolysis was determined through viral infectivity and viral growth kinetic assays. Results from these assays ensured the cells were susceptible, and supported CVA21 replication over consecutive passages, prior to generating an *in vivo* model of orthotopic pancreatic cancer in an immune competent strain of mouse. Figure 51 illustrates the susceptibility of each of the generated, and corresponding WT cell lines to CVA21 oncolysis. Likewise, Figure 52 displays the growth kinetics of CVA21 within the two modified cell lines and their WT counterparts.

Both ImPSCc2-ICAM-1 and UN-KPC-961-ICAM-1-luc cells were susceptible to CVA21 oncolysis (Figure 51). As expected, both the WT mouse cell lines, ImPSCc2 and UN-KPC-961 were resistant to CVA21. The infection titre of CVA21 required to lyse 50% of ImPSCc2-ICAM-1 cells was interpolated to be 6.22 x 10^3 CVA21 $TCID_{50}$/ml (log1.206 $TCID_{50}$/cell). Likewise, 1.48 x 10^6 $TCID_{50}$/ml (log1.17 $TCID_{50}$/cell) was the calculated $TCID_{50}$/ml concentration for CVA21 on UN-KPC-961-ICAM-1-luc cells. Interestingly, UN-KPC-961-ICAM-1-luc cells were less susceptible to CVA21 compared to ImPSCc2-ICAM-1 cells, despite UN-KPC-961-ICAM-1-luc cells expressing more cell surface ICAM-1 (Figure 49). Steric hindrance of high levels of ICAM-1 molecules on UN-KPC-961-ICAM-1-luc cells may have impeded efficient binding and uncoating of CVA21.

To determine if the transfected cell lines supported CVA21 replication, viral growth kinetic assays were performed on the two cell lines. CVA21 viral growth kinetics depicted in Figure 52 demonstrate ImPSCc2-ICAM-1, and UN-KPC-961-ICAM-1-luc cells supported multiple cycles of CVA21 replication. Likewise, Figure 52 displays the WT counterparts, ImPSCc2 and UN-KPC-961, supported little replication of CVA21 as there was rarely CPE evident in SK-Mel-28 cells titrated with harvested supernatant from the two WT cell lines treated with CVA21 at each time point. Therefore, once inside a cell through binding to huICAM-1, CVA21 can hijack mouse host cellular

replication machinery to propagate. Thus, the two ICAM-1 transfected mouse cell lines were deemed suitable for investigations to develop an *in vivo* model of orthotopic pancreatic cancer in an immune competent strain of mouse.

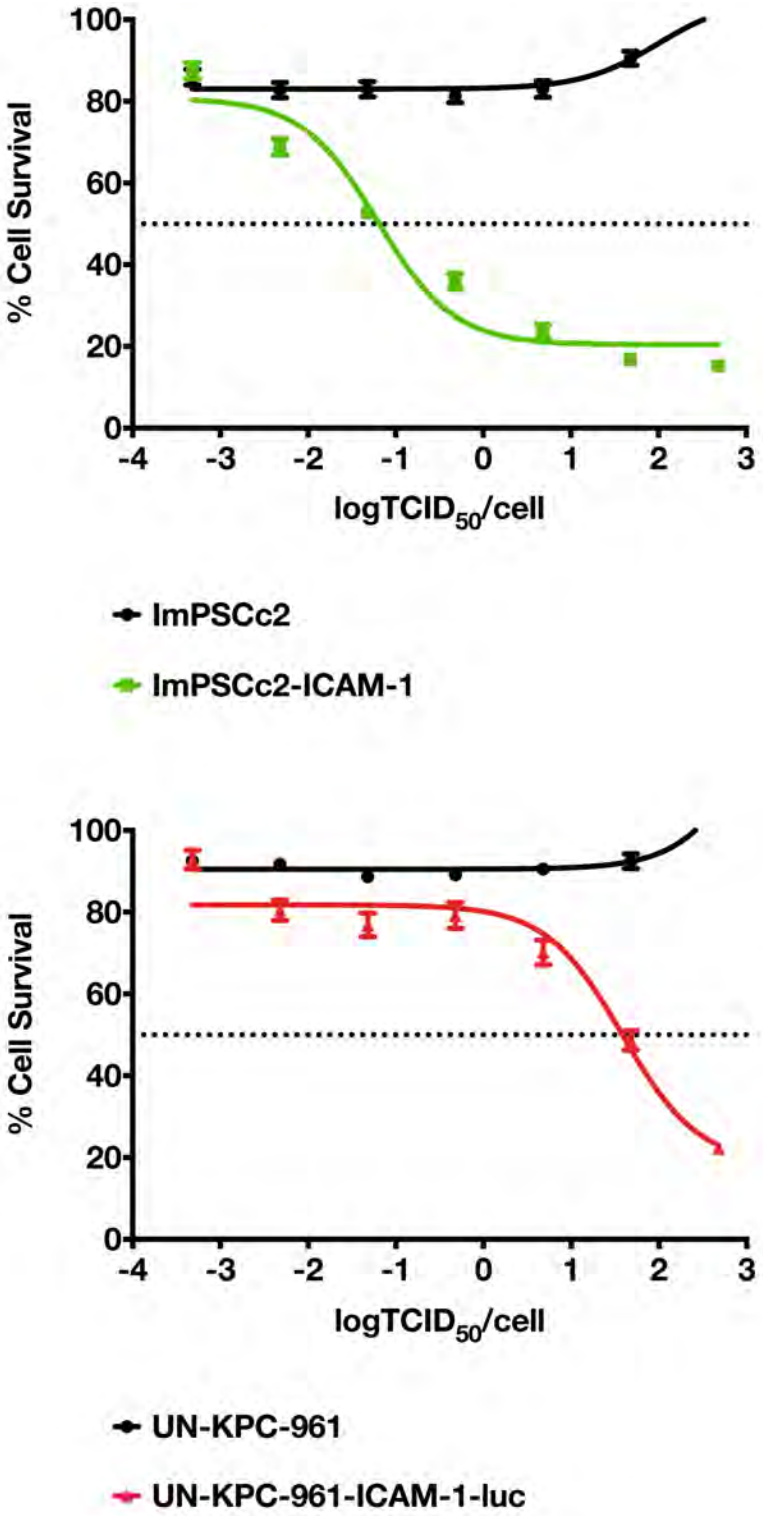

Figure 51: Susceptibility of transfected and transduced mouse pancreatic cancer cells, UN-KPC-961-ICAM-1-luc, and transfected mouse pancreatic stellate cells, ImPSCc2-ICAM-1 to CVA21 oncolysis. 10-fold serial dilutions of CVA21 starting at a constant concentration was titrated against each cell line and incubated for 72 hours before cell viability measured via MTT assays. Resulting absorbance values were normalised to internal positive and negative controls for each replicate. Average percentage cell survival +/- SEM was plotted against the log of the dilution of CVA21 in $TCID_{50}$/ml. Minimum of three replicates were conducted for each cell line. Non-linear regression curves were generated, and $TCID_{50}$/ml concentrations interpolated for each cell line using Prism v7.0 (GraphPad). Dotted line indicates 50% cell survival.

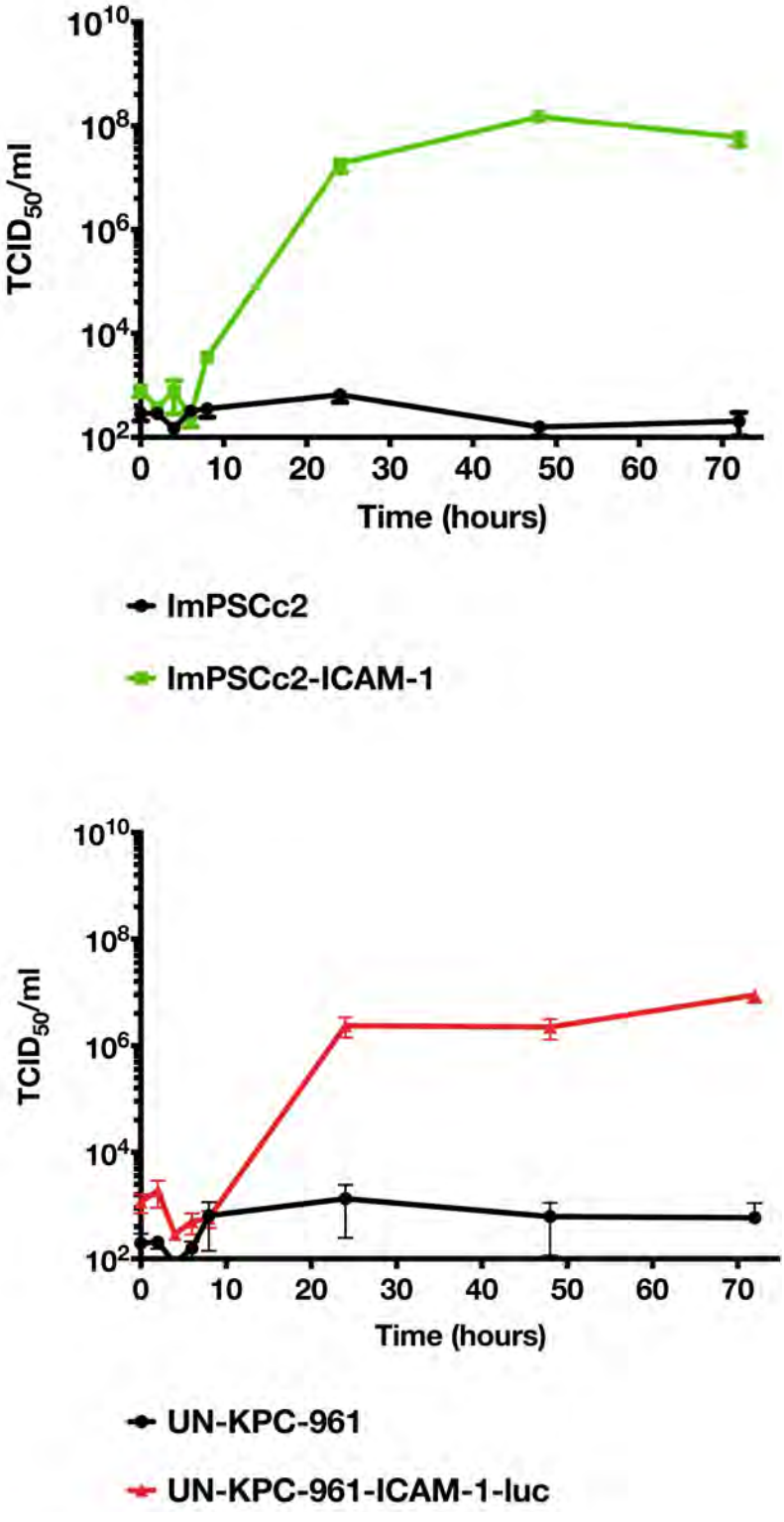

Figure 52: CVA21 viral growth kinetics within mouse transfected and transduced pancreatic cancer cells, UN-KPC-961-ICAM-1-luc, and transfected mouse pancreatic stellate cells, ImPSCc2-ICAM-1. Each cell line was infected with an MOI of 10 CVA21 and incubated for 0, 2, 4, 6, 8, 24, 48, and 72 hours before total supernatant was titrated against SK-Mel-28 cells to determine viral yield as $TCID_{50}$/ml. Six replicates were conducted for each cell line. CVA21 replication kinetic graphs were generated for each cell line by plotting the average viral yield +/- SEM for each time point using Prism v7.0 (GraphPad).

6.2 Generation of an Orthotopic Pancreatic Cancer Immune Competent Mouse Model

Based on prior preclinical experience, it was presumed that tumours would develop in C57BL/6 mice without issue due to the lineage of ImPSCc2 (Mathison *et al.*, 2010) and UN-KPC-961 (Torres *et al.*, 2013) cell lines originating from C57BL/6, and KPC mice (mixed background of 129/SvJae/C57BL/6), respectively. Unfortunately, this absolutely was not the case. Four pilot mouse models were investigated prior to the following three models discussed in this chapter that revealed tumours did not grow in C57BL/6 or BALB/c mice due to the immune system.

To overcome the issue of tumour rejection due to an immune reaction, investigations into depletion of NK1.1, CD4, and CD8 immune cells in mice were conducted to establish tumours. The hypothesis being that once tumours had established, they would have developed a niche. Such a tumour niche would prohibit the immune reaction towards tumours when the depleted immune cells recovered. Tumours would progress in the presence of a functional immune system and CVA21 as a treatment for pancreatic cancer in an immune competent setting could be investigated.

From the four previous failed models, it was discovered that generation of tumours from UN-KPC-961-ICAM-1-luc in combination with ImPSCc2-ICAM-1 remained slightly longer than tumours generated from UN-KPC-961-ICAM-1-luc cells alone (data not shown). That is, the pancreatic stellate cells facilitated tumour establishment when injected in combination with the pancreatic cancer cells compared to tumour establishment of pancreatic cancer cells alone. Thus, tumours in the following models were established from a combination of ImPSCc2-ICAM-1 and UN-KPC-961-ICAM-1-luc cells.

6.2.1 Pilot Model #1: Determination of Optimal Mouse Strain and Tumour Cell Inoculate

The first model denoted pilot model #1, aimed to establish tumours in BALB/c and C57BL/6 mice when NK1.1, CD4, and CD8 immune cells were depleted for the duration of the model to identify the optimal strain for future studies. Depleting the immune cells enabled ImPSCc2-ICAM-1 and UN-KPC-961-ICAM-1-luc cells to establish tumours. Observation of tumour progression, metastases, and hallmark characteristics of PC such as ascites, in each strain enabled the optimal strain of mouse for future models to be identified. Presented in Figure 53 is a schematic diagram of pilot model #1. BALB/c and C57BL/6 mice were injected via I.P. route of administration with anti-NK1.1, anti-CD4, and anti-CD8α antibodies at 100 µg/antibody/mouse on days -2, 3, 5, 8, and 11 post tumour inoculation. Surgery was performed on day 0 to inoculate the pancreas of mice with 5 x 10^5 cells of a mixture of UN-KPC-961-ICAM-1-luc and ImPSCc2-ICAM-1, at a ratio of either 1:1, or 1:4, respectively. Four BALB/c and four C57BL/6 mice were designated no tumour control (N.T.C.). Besides recording body mass three times a week, N.T.C. mice were excluded from all other procedures. Four mice were designated to each tumour group: BALB/c 1:1 PC:PSC, BALB/c 1:4 PC:PSC, C57BL/6 1:1 PC:PSC, and C57BL/6 1:4 PC:PSC. Tumour volumes were measured weekly through bioluminescent imaging of tumours using an IVIS™ Imaging System 100 (Xenogen). Mice were euthanised if pain and distress and/or a weight loss of 15% was observed.

Welfare of mice was monitored routinely by observing for signs of pain and distress and routine measurements of body mass. Mouse weights over the course of pilot model #1 are presented in Figure 54. Minimal disruption to the wellbeing of mice that had surgery was observed as there was only minor reductions in weights on average. Additionally, tumour burden failed to induce a reduction in body mass even when mice required euthanasia due to succumbing to the disease.

Tumour burden in mice over the course of pilot model #1 was measured weekly via an IVIS™ Imaging System 100 (Xenogen). Bioluminescent overlay images portrayed in Figure 55 and the flux graphs in Figure 56 indicated no difference in tumour progression between a 1:1 or a 1:4 ratio of pancreatic cancer to pancreatic stellate cells in either strain of mouse. A 1:4 PC:PSC ratio was chosen for all future models to

emphasise the contribution of the stromal environment in native pancreatic cancer. Five of the eight tumour bearing BALB/c mice had profound and rapid tumour progression. On the other hand, the remaining three tumour bearing BALB/c mice appeared to have a reduction in tumour volume between days 13 and 20 post tumour inoculation. All BALB/c mice were euthanised by day 21 due to moribund appearance and tumour burden in the mice with tumour progression. Comparatively, tumours in C57BL/6 mice were notably smaller upon initial tumour measurement yet progressed at a similar rate as BALB/c mice. All tumours within C57BL/6 mice progressed. Furthermore, tumour burden localisation was noticeably different to BALB/c mice as the flux heatmaps appeared to indicate metastatic spread throughout the bodies of C57BL/6 mice.

Necropsies were performed on mice when euthanised to monitor tumour burden and metastatic spread. Pictured in Figure 57 are representative tumour burdens of BALB/c and C57BL/6 mice. Ascites regularly formed in both BALB/c (A) and C57BL/6 (B) mice. Swollen abdomens indicating ascites were deemed an appropriate endpoint as mice quickly declined in following days. Upon necropsies of BALB/c mice, mice were commonly burdened with a very large pancreatic tumour engulfing the adjacent spleen. Occasionally metastases (red and yellow arrows) were observed in the liver of BALB/c mice. Contrastingly, pancreatic tumours fused to adjacent spleens with secondary peritoneal tumours and frequently observable metastases throughout organs in the peritoneal cavity was characteristic in C57BL/6 mice upon necropsies.

To better visualise metastatic formation in tumour bearing mice, organs and tumour masses (pancreatic tumour/spleen mass, secondary tumour, lungs, brain, right kidney, a section of diaphragm, the small and large intestines, and liver) were harvested and incubated in D-luciferin shortly after euthanasia. Tissues were arranged on a petri dish and imaged using an IVIS™ Imaging System 100 (Xenogen). Figure 58 illustrates representative tumour burden and metastases. BALB/c mice would occasionally have metastases to organs situated in close proximity to the pancreas such as the spleen, liver, and diaphragm. Whereas metastases to nearby and distant organs were common in C57BL/6 mice. Recorded in Figure 58 for the representative C57BL/6 mouse were prolific metastases to the spleen, peritoneal wall, liver, intestines, and diaphragm. Metastases were also observed to the kidney, lungs, and brain.

It is necessary to highlight that the kinetics of tumour development in C57BL/6 and BALB/c mice were not consistent. BALB/c mice required euthanasia by day 21 of the model due to decline in welfare and tumour burden, whereas C57BL/6 mice on average were able to tolerate tumour burden for longer. However, for this reason, and that C57BL/6 better reflected the aetiology of pancreatic cancer, it was concluded that C57BL/6 was the superior mouse strain for developing a model of pancreatic cancer.

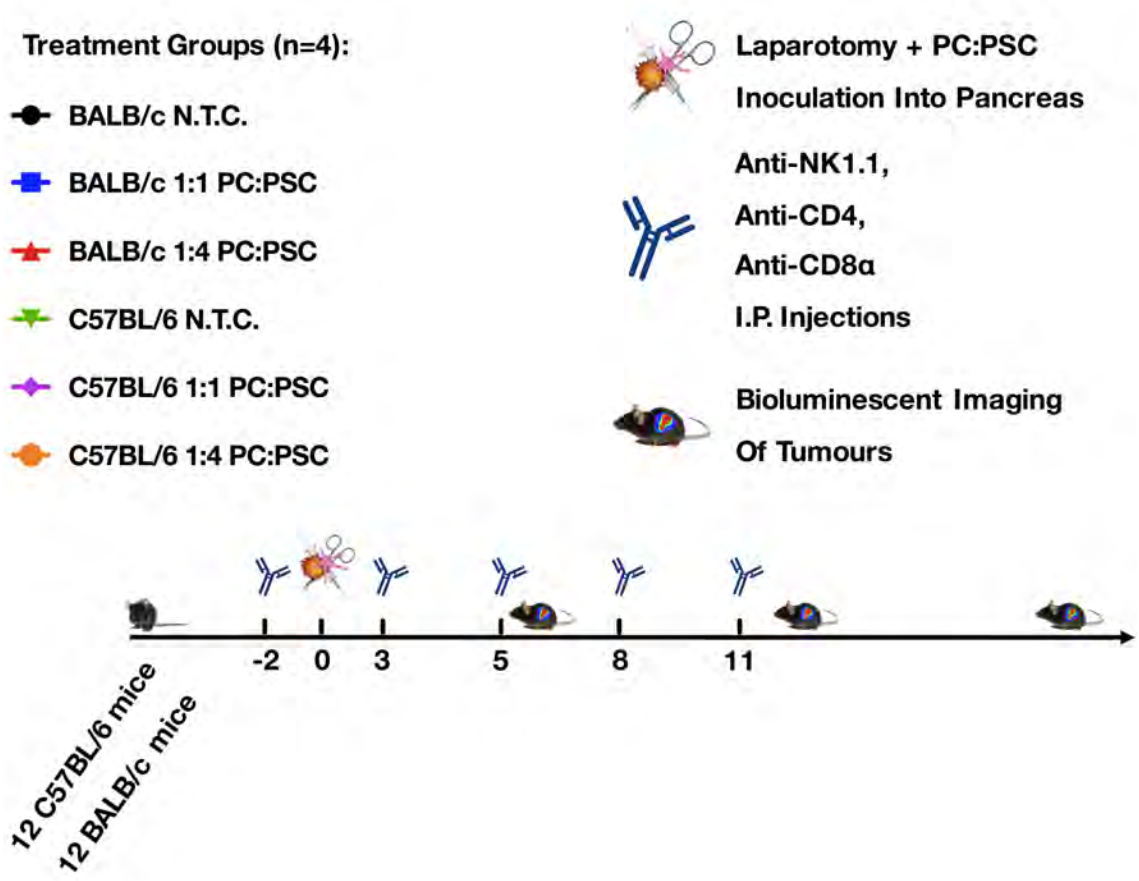

Figure 53: Schematic diagram of pilot orthotopic pancreatic cancer immune competent mouse model #1. Eight BALB/c and eight C57BL/6 mice were depleted of NK1.1, CD4, and CD8 cells by I.P. injection with 200 µg anti-CD4 + 200 µg anti-NK1.1, 200 µg anti-CD8α/mouse on days -2, 3, 5, 8, and 11 post tumour inoculation. 5 x 10^5 cells of either a 1:1 or 1:4 ratio of UN-KPC-961-ICAM-1-luc:ImPSCc2-ICAM-1 cells were injected directly into the pancreas of mice to generate orthotopic pancreatic cancer on day 0. Tumour progression was monitored via bioluminescence imaging on a weekly basis.

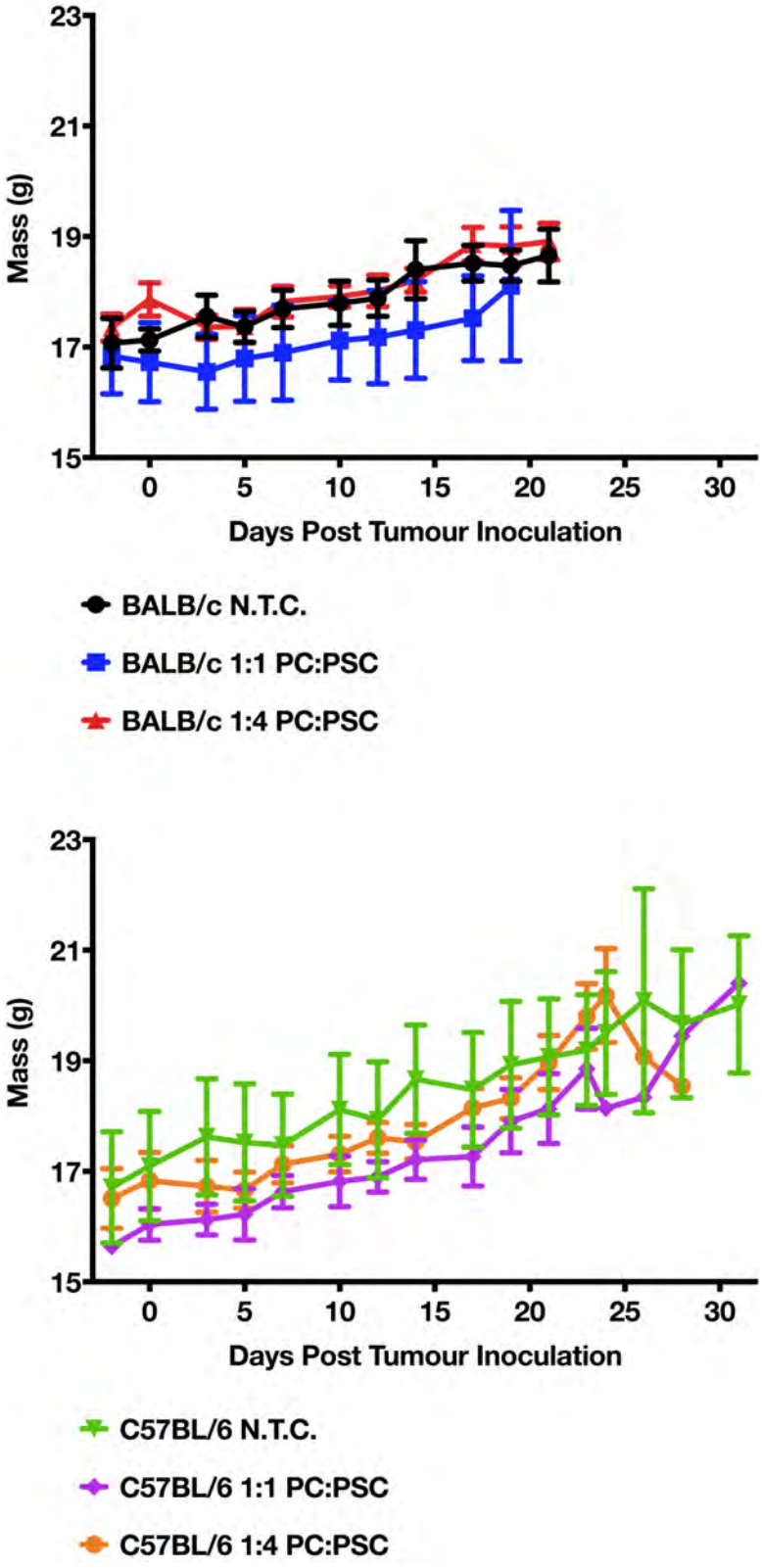

Figure 54: BALB/c and C57BL/6 mouse weights over the course of pilot model #1 according to mouse strain and tumour type. Mice were weighed three times a week to monitor welfare. Weights were graphed using Prism v7.0 (GraphPad) according to species and tumour type +/- SEM for each time point.

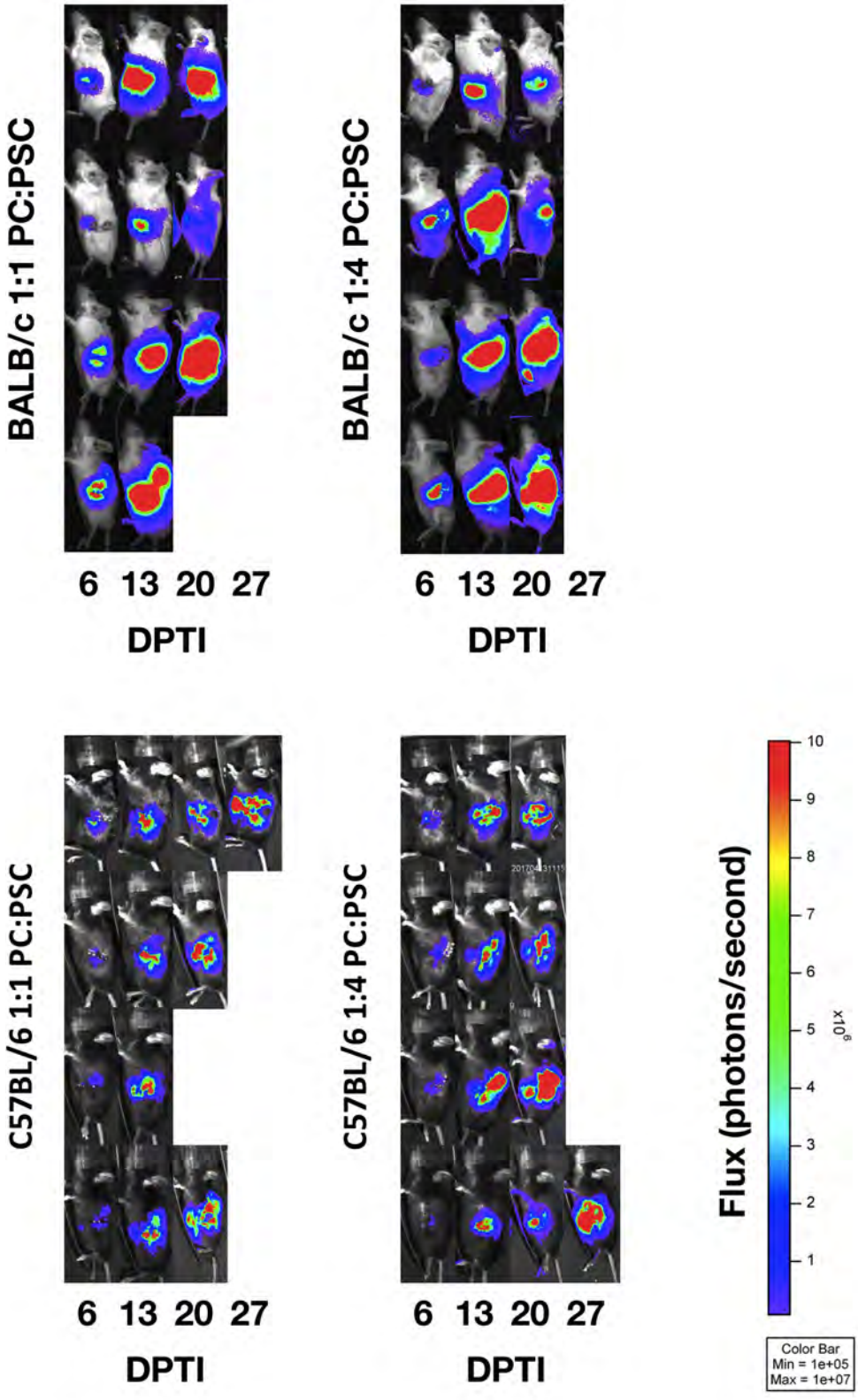

Figure 55: Tumour progression of BALB/c and C57BL/6 mice bearing UN-KPC-961-ICAM-1-luc + ImPSCc2-ICAM-1 pancreatic tumours over the course of pilot model #1. Weekly bioluminescent imaging of tumours using an IVIS™ Imaging System 100 (Xenogen) was conducted to measure tumour volume and track progression in each mouse.

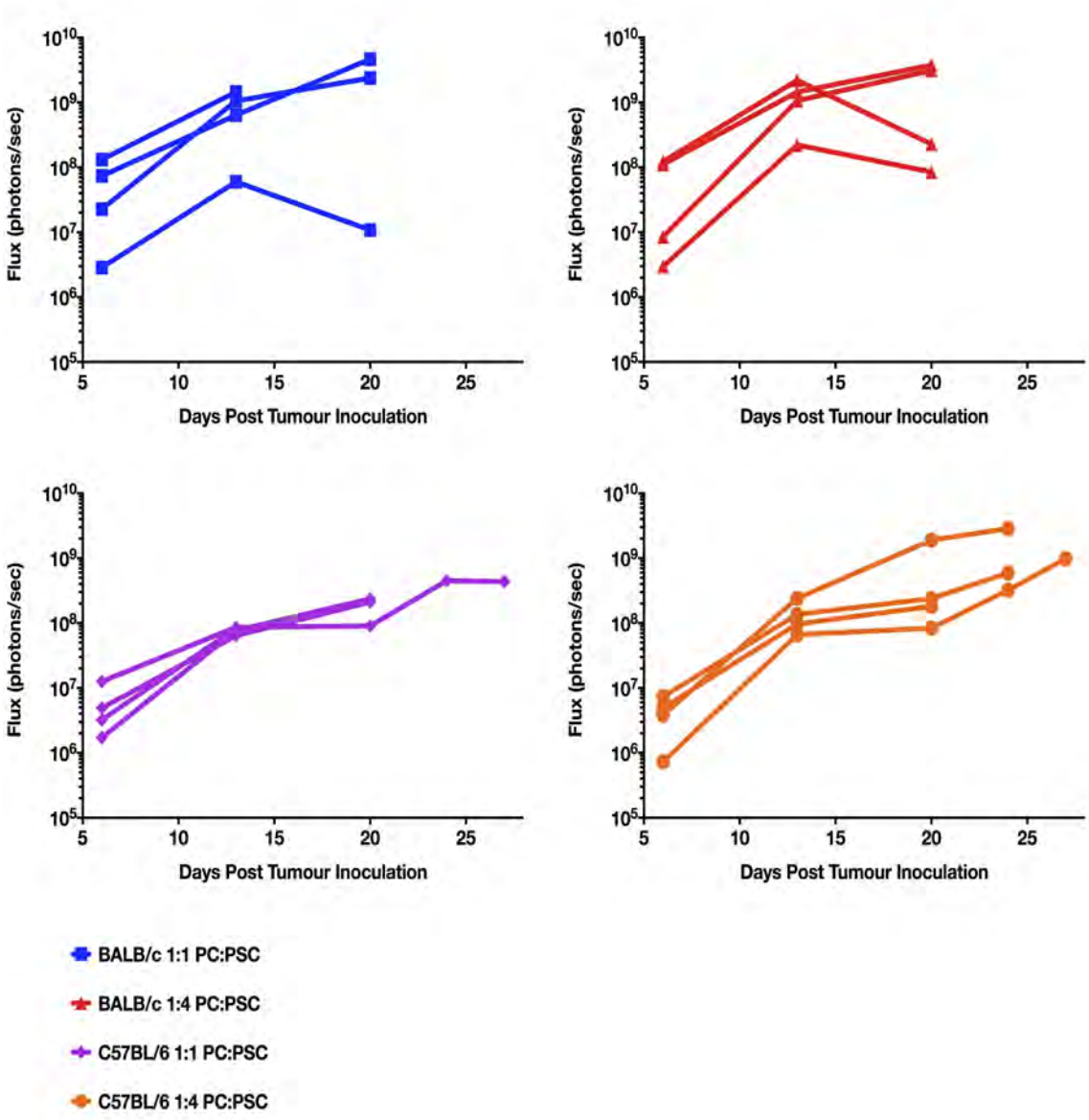

Figure 56: Tumour progression as a measure of flux (photons/second) by treatment group over the course of pilot model #1. Flux values corresponding to tumour size according to group obtained from weekly bioluminescent imaging of tumours using an IVIS™ Imaging System 100 (Xenogen) were graphed for individual mice using Prism v7.0 (GraphPad).

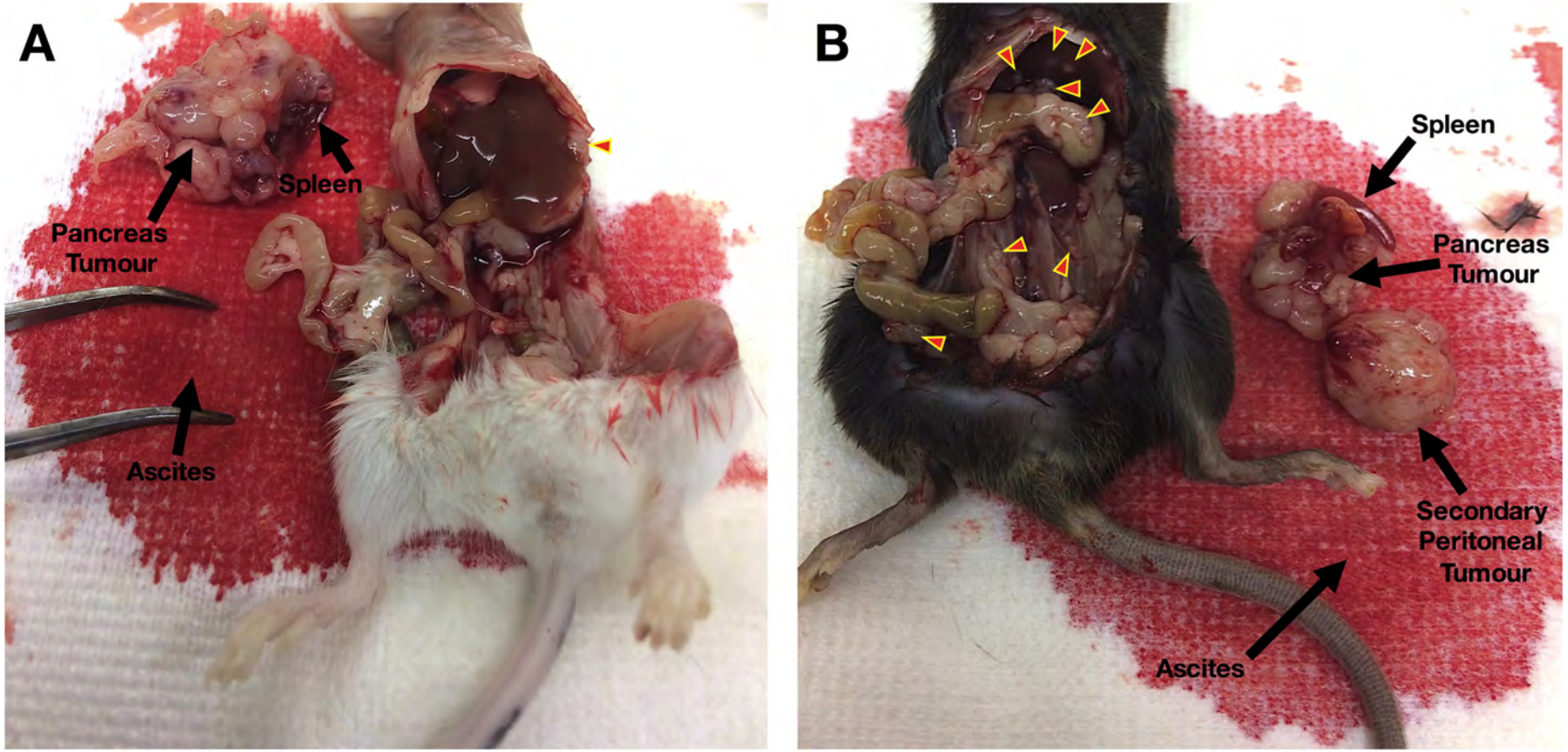

Figure 57: Representative tumour burden of A: BALB/c and B: C57BL/6 mice from pilot model #1 upon necropsy 18 days post tumour inoculation. Necropsies were performed on euthanised BALB/c and C57L/6 mice 18 days post tumour inoculation to observe tumour burden and metastases. Tumours in both mice originated from a 1:1 ratio of UN-KPC-961-ICAM-1-luc:ImPSCc2-ICAM-1 cells. Red and yellow arrows indicate metastases.

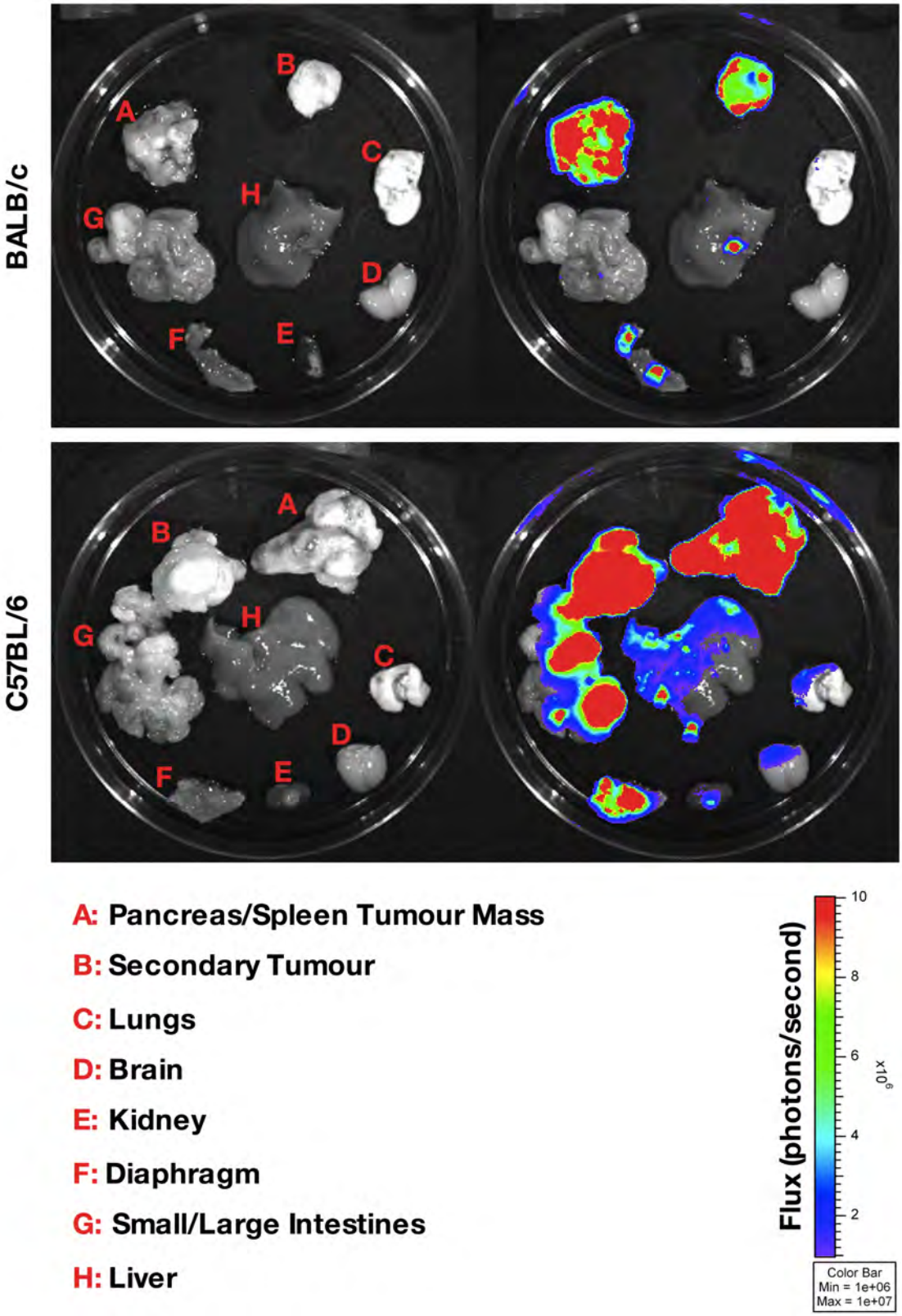

Figure 58: Representative bioluminescent imaging of organs upon necropsy from BALB/c and C57BL/6 mice from pilot model #1. Organs were harvested from euthanised BALB/c and C57BL/6 mice and incubated in D-luciferin before imaged in a petri dish using an IVIS™ Imaging System 100 (Xenogen).

6.2.2 Pilot Model #2: Recovery of A Functional Immune System While Maintaining Tumour Progression

The second mouse model discussed herein, denoted pilot model #2, aimed to establish and maintain progression of orthotopic pancreatic tumours while observing recovery of the depleted immune system. Also, in an attempt to increase the duration of the model, a lower cell inoculate concentration was employed to generate smaller orthotopic pancreatic cancers. Additionally, treatments were attempted to gauge the optimal timing for treatment administration. Briefly, 16 C57BL/6 mice were given a single I.P. injection of 200 µg/antibody/mouse: anti-NK1.1, anti-CD4, and anti-CD8α three days prior to surgery. Next, 2 x 10^5 cells of a mixture of 1:4 UN-KPC-961-ICAM-1-luc and ImPSCc2-ICAM-1 were injected into the pancreas of mice to generate orthotopic pancreatic cancer. Four C57BL/6 mice were again designated N.T.C. Besides recording body mass three times a week, N.T.C. mice were excluded from all other procedures. Eight tumour bearing mice were designated to each treatment group: I.T. Saline or I.T. CAVATAK™. Tumour volumes were measured weekly via bioluminescent imaging of tumours using an IVIS™ Imaging System 100 (Xenogen). A single injection of CAVATAK™ (7.5 x 10^6 $TCID_{50}$), or saline, was administered I.T. to respective mice on day 22. Surgery was not required to inject tumours as they were clearly palpable by day 22. Thus, I.T. treatments were administered simply by injecting directly into palpated tumours. Mice were euthanised if pain and distress and/or a weight loss of 15% was observed. Presented in Figure 59 is a schematic diagram of pilot model #2.

The welfare of mice throughout pilot model #2 was reflected by body mass. Displayed in Figure 60 are the mean body weights of C57BL/6 mice according to treatment group. Surgery to generate orthotopic pancreatic tumours had minimal impact on mice and recovery was short. Treatment administration did not affect the welfare of mice as body weights continued to increase after delivery. Subsequently, it was discovered that a large body weight increase, rather than decrease, in tumour bearing mice was indicative of decline in welfare of a mouse over the following days. Consequently, body weight was closely monitored, and mice were euthanised accordingly.

Weekly bioluminescent imaging of mice enabled tumour progression to be measured. Presented in Figure 61 are the bioluminescent overlay images of each mouse during the course of pilot model #2 according to treatment group. The corresponding flux values are graphically represented for each mouse in Figure 62. Unfortunately, one mouse failed to recover from the surgical procedure to generate orthotopic pancreas cancer. As a low cell inoculate of 2 x 10^5 cells was injected to establish tumours the initial tumour measurement three days post tumour inoculation displayed minimal tumour development. However, by day 10 tumours had rapidly progressed in the majority of mice displaying an average bioluminescence of approximately 1 x 10^8 flux (photons/second). A flux value of 1 x 10^8 was the average tumour size of C57BL/6 mice in pilot model #1 13 days post tumour inoculation when 5 x 10^5 cells were injected to generate tumours (Figure 56). Additionally, there were four mice that had spontaneous remission of tumours in pilot model #2 after 10 days post tumour inoculation, likely because of the low cell number used to generate tumours. Using a lower cell concentration did not increase the duration of the model due to the rapid early progression. However, it did allow for some tumours to spontaneously regress. Therefore, for the above two reasons a cell inoculate concentration of 5 x 10^5 was deemed the optimal concentration for generating orthotopic pancreatic cancer in C57BL/6 mice for future models. Additionally, a flux value of 1 x 10^9 (photons/second) was deemed a necessary endpoint as tumour burden was so large that mice shortly succumbed to the disease.

In an attempt to gauge the opportune timing for treatment administration, treatments of CAVATAK™ (7.5 x 10^6 $TCID_{50}$), or saline, were administered on day 22. Demonstrated in Figure 61 and Figure 62, administration of treatments proved ineffective when tumour burden corresponded to a flux value of ~1 x 10^9 photons/second. Tumours in CAVATAK™ treated mice increased in size, possibly because of viral oncolysis resulting in inflammation by immune cells. Tumours in saline treated mice were stable, likely due to the physical disruption of the tumour mass when the needle and saline solution were injected directly into the tumour. Tumour progression was anticipated in saline treated mice. However, as tumour burden was considered too great in CAVATAK™ treated mice, the model was ended to analyse CD4 and CD8 cell levels in circulating blood from the remaining mice.

Mouse blood from terminal heart bleeds were measured for CD4 and CD8 cell levels via flow cytometry. Presented in Figure 63 are qualitative measures of CD4 and CD8 T cell levels in circulating blood from mice on days 22 and 23 post tumour inoculation. T cell levels in N.T.C. mice bloods were quantified alongside as a measure of normal cell concentrations. In hindsight, addition of counting beads to enumerate the number of CD4 or CD8 cells per microliter of blood may have improved the accuracy of the comparison. Thus, cell concentrations are presented as percentages of each recorded leukocyte population. Secondly, an antibody for the measurement of NK1.1 cell concentrations was not available at this point. Despite these oversights (absence of counting beads and anti-NK1.1 antibody in experimental protocol), CD4 and CD8 cell concentrations were measured, and partial recovery of CD4 and CD8 cells were observed in mice at 22 and 23 days post tumour inoculation. No statistically significant difference in CD4 and CD8 cell percentages between saline or CAVATAK™ treated mice was observed. Statistical significance was calculated from ordinary one-way ANOVA analyses in CD4 levels between N.T.C. and I.T. Saline mice (CD4 N.T.C. vs. I.T. Saline ** $P = 0.0054$), and CD8 levels in N.T.C. mice compared to both I.T. Saline and I.T. CAVATAK™ mice (CD8 N.T.C. vs. I.T. Saline ** $P = 0.0095$. CD8 N.T.C. vs. I.T. CAVATAK™ ** $P = 0.0055$).

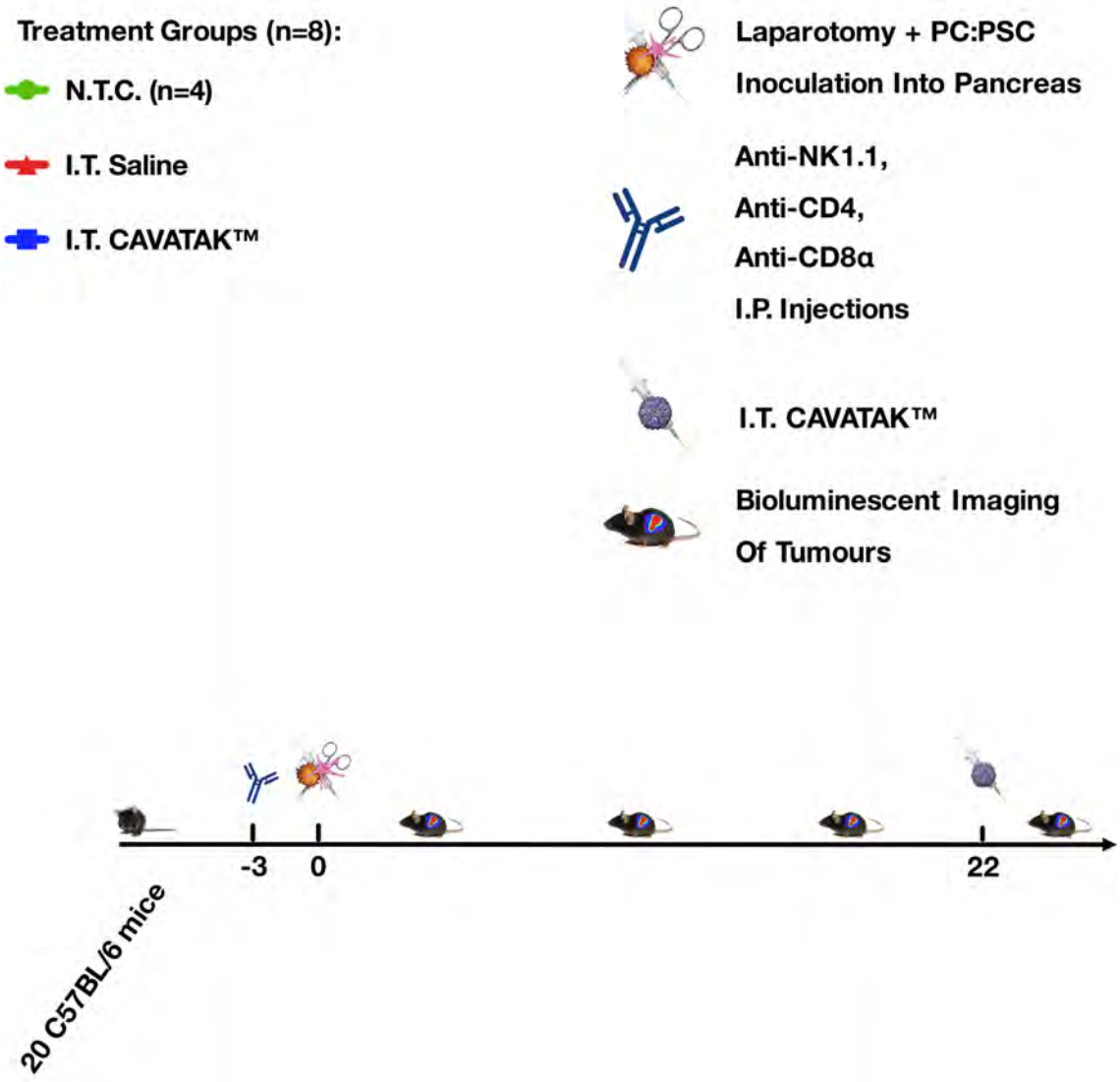

Figure 59: Schematic diagram of pilot orthotopic pancreatic cancer immune competent mouse model #2. Sixteen C57BL/6 mice were depleted of NK1.1, CD4, and CD8 cells by I.P. injection with 200 µg anti-CD4 + 200 µg anti-NK1.1, 200 µg anti-CD8α/mouse three days prior to tumour inoculation. A mixture of 4 x 10^4 UN-KPC-961-ICAM-1-luc + 1.6 x 10^5 ImPSCc2-ICAM-1 cells was injected directly into the pancreas of mice to generate orthotopic pancreatic cancer on day 0. Tumour progression was monitored via bioluminescence imaging on a weekly basis. CAVATAK™ (7.5 x 10^6 $TCID_{50}$) or saline was administered I.T. to mice on day 22.

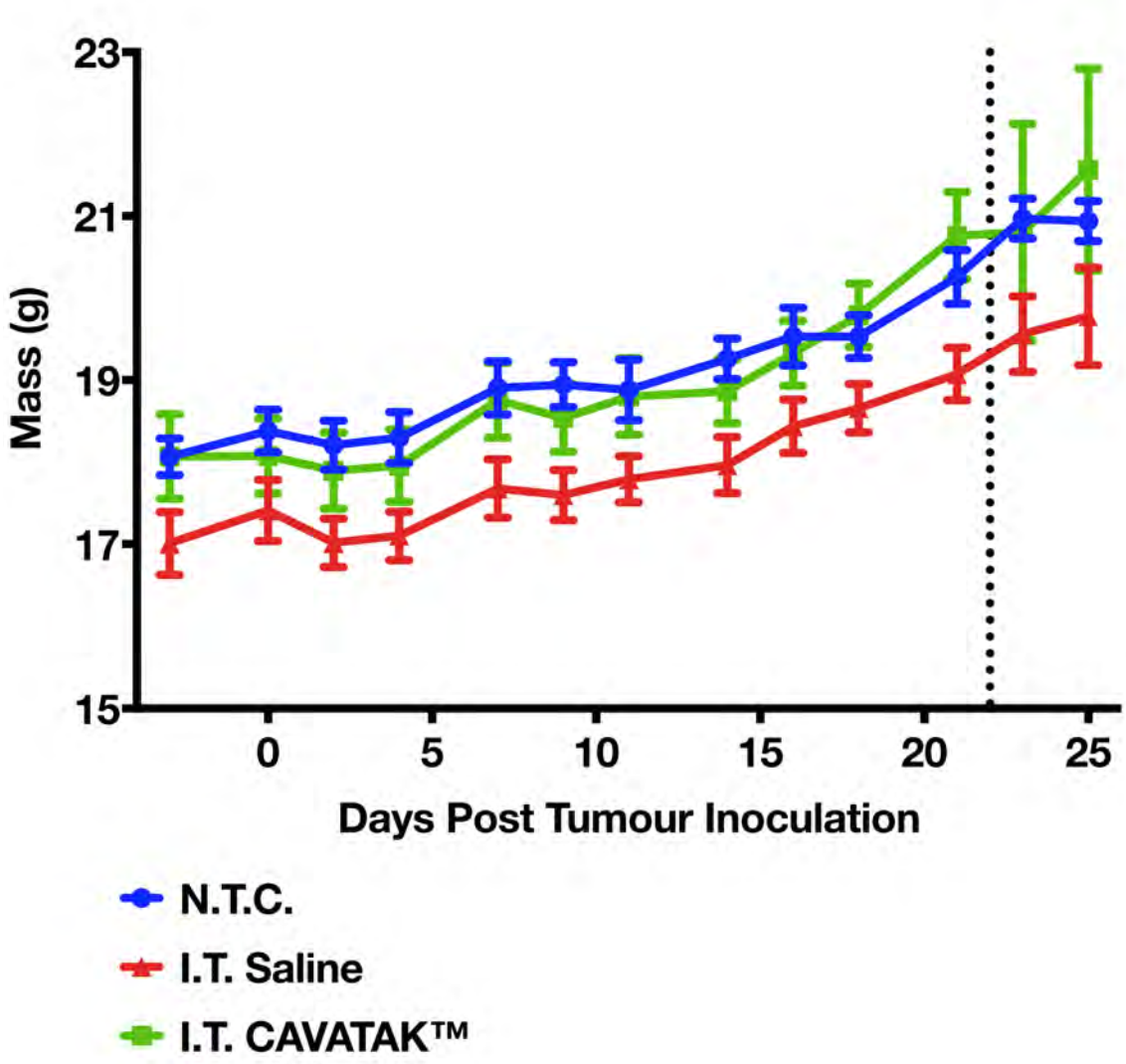

Figure 60: C57BL/6 mouse weights over the course of pilot model #2 according to treatment groups. Mice were weighed three times a week to monitor welfare. Weights were graphed using Prism v7.0 (GraphPad) according treatment group +/- SEM for each time point.

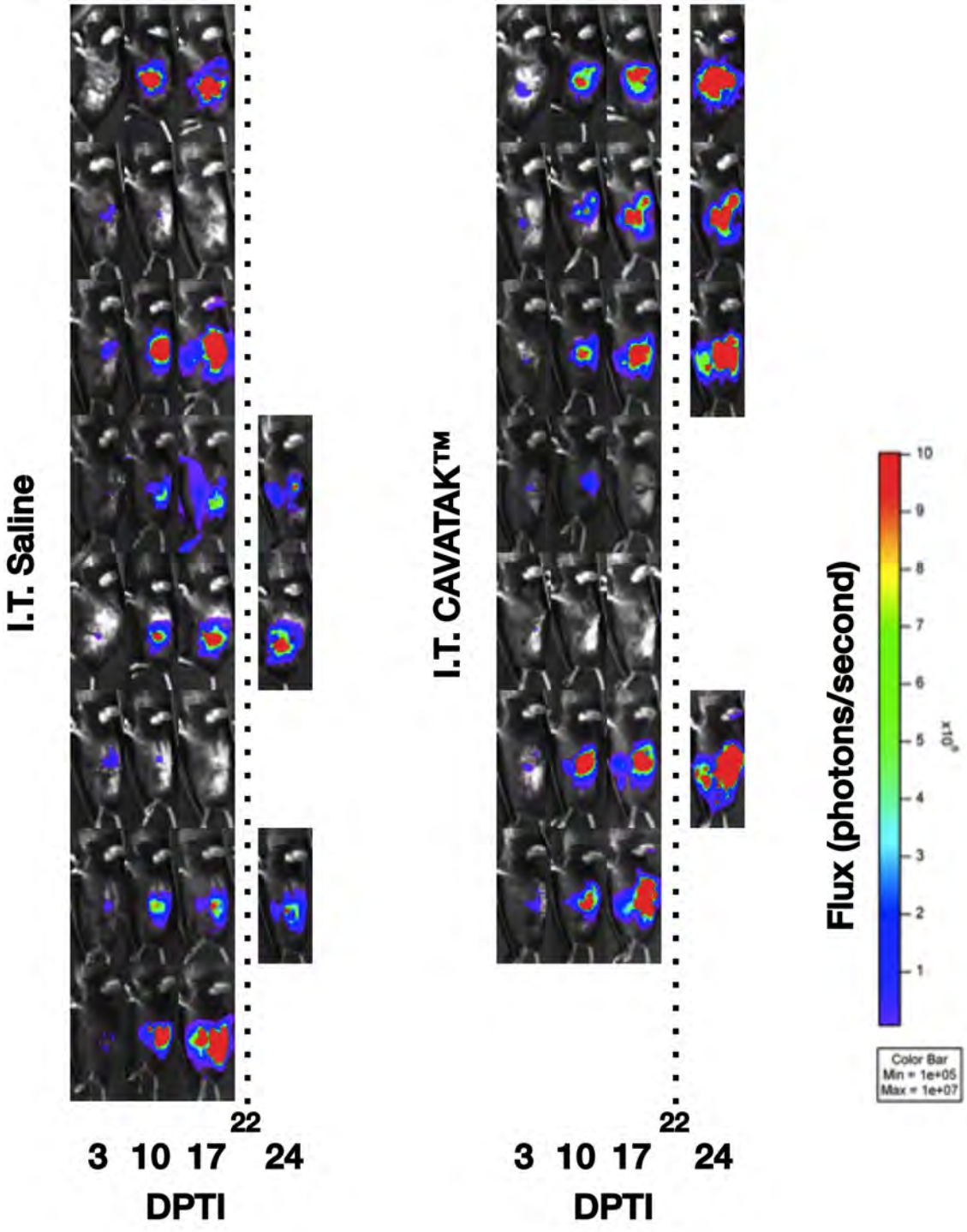

Figure 61: Tumour progression of C57BL/6 mice bearing UN-KPC-961-ICAM-1-luc + ImPSCc2-ICAM-1 pancreatic tumours over the course of pilot model #2. Weekly bioluminescent imaging of tumours using an IVIS™ Imaging System 100 (Xenogen) was conducted to measure tumour volume and track progression in each mouse. Dotted line indicates I.T. treatments with either saline or CAVATAK™ (7.5 x 10^6 $TCID_{50}$) 22 days post tumour inoculation (DPTI).

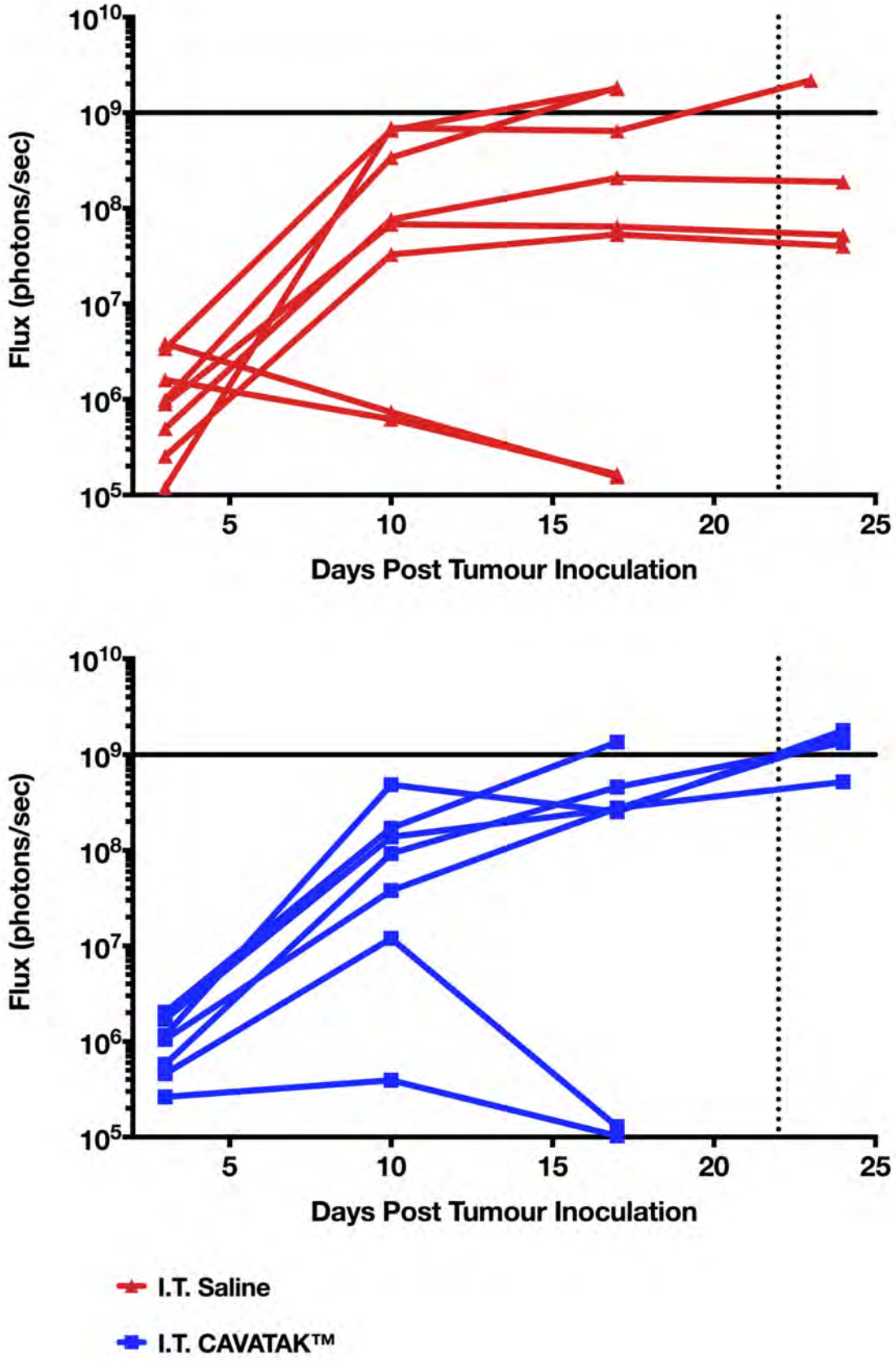

Figure 62: Tumour progression as a measure of flux (photons/second) by group over the course of pilot model #2. Flux values corresponding to tumour size obtained from weekly bioluminescent imaging of tumours using an IVIS™ Imaging System 100 (Xenogen) were graphed for individual mice using Prism v7.0 (GraphPad). Dotted line indicates I.T. treatments with either saline or CAVATAK™ (7.5×10^6 $TCID_{50}$).

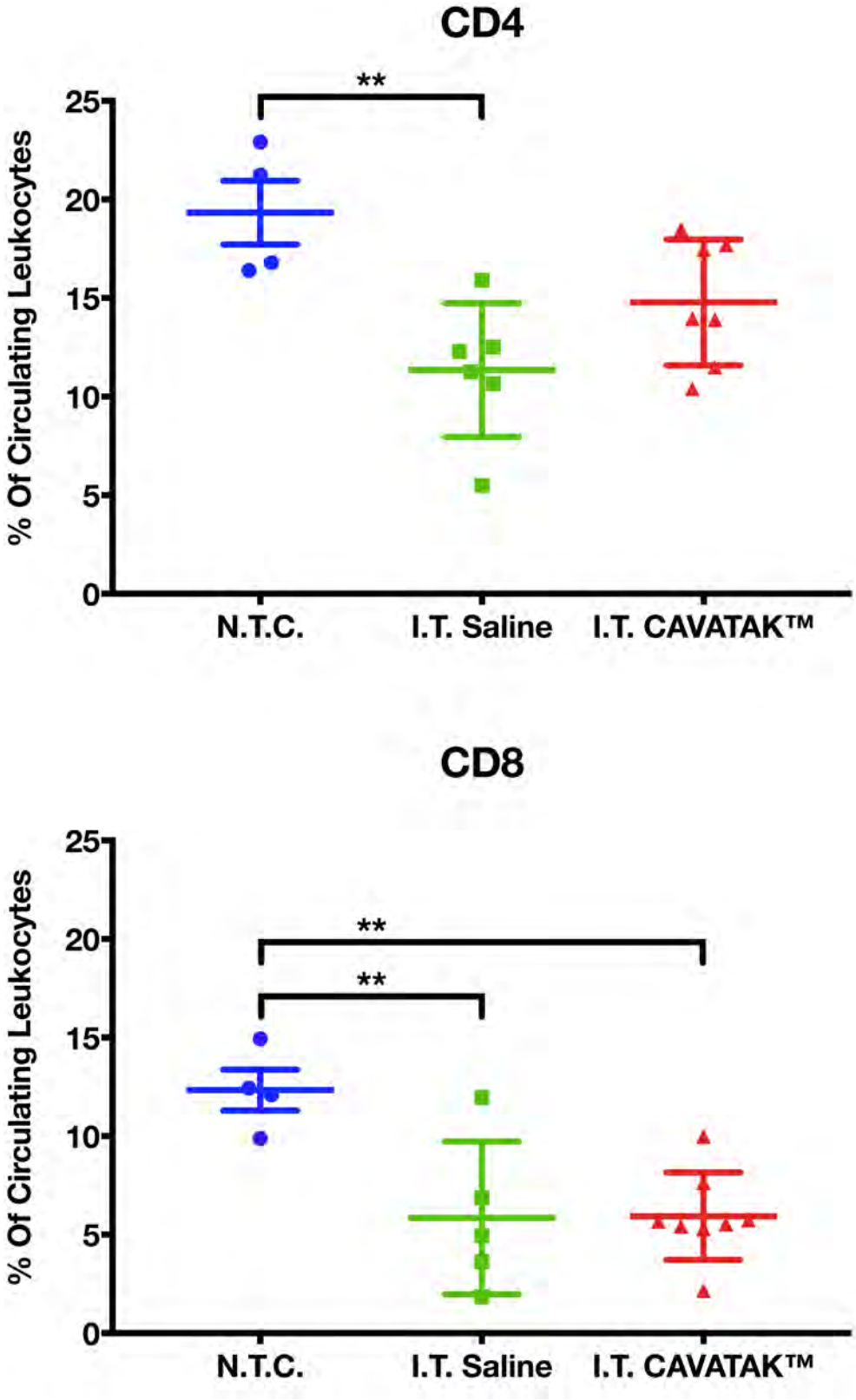

Figure 63: T cell levels in terminal heart bleeds according to treatment groups from pilot model #2. CD4 and CD8 cell levels from red blood cell lysed whole blood collected upon euthanasia of mice on days 22 and 23 post tumour inoculation were measured via flow cytometry. Cell levels presented as percentage of circulating leukocytes according to treatment group +/- SEM and ordinary one-way ANOVA analyses conducted using Prism v7.0 (GraphPad). CD4 N.T.C. vs. I.T. Saline ** P = 0.0054. CD8 N.T.C. vs. I.T. Saline ** P = 0.0095. CD8 N.T.C. vs. I.T. CAVATAK™ ** P = 0.0055.

6.2.3 Pilot Model #3: Optimisation of Tumour Progression and Immune Cell Recovery

Pilot model #3 aimed to elucidate the delicate balance between tumour establishment, maintenance and progression of tumours, and recovery of immune cells at an early stage. Secondly, to profile the recovery of NK1.1, CD4, and CD8 immune cells over the course of the study. Thirdly, the central goal of the study was to determine the activity of CAVATAK™ on tumours. Finally, to determine cytokine and chemokine signalling in mice as a result of treatments.

In an attempt to have recovery of the immune system earlier in pilot model #3, a lower dose of the antibody cocktail was used. Twenty-four C57BL/6 mice were administered with a single I.P. injection of 50 µg/antibody/mouse: anti-NK1.1, anti-CD4, and anti-CD8α three days prior to surgery. A cell mixture of 5 x 10^5 cells of UN-KPC-961-ICAM-1-luc and ImPSCc2-ICAM-1 at a ratio of 1:4 was injected into the pancreas of mice to generate an orthotopic model of pancreatic cancer. Four C57BL/6 mice were selected as N.T.C. Besides recording body weights three times a week, and weekly blood collections, N.T.C. mice were excluded from all other procedures. Twelve tumour bearing mice were designated to each treatment group: I.T. Saline or I.T. CAVATAK™. Tumour volumes were measured weekly through bioluminescent imaging of tumours using an IVIS™ Imaging System 100 (Xenogen). CAVATAK™ (7.5 x 10^6 $TCID_{50}$) or saline was administered I.T. to respective mice on day eight. I.T. administration of treatments were performed by palpation and injection of tumours. Blood was collected for analysis of NK1.1, CD4, and CD8 cells on a weekly basis starting one day prior to treatments. Mice were euthanised if pain and distress and/or a weight loss of 15% was observed. Presented in Figure 64 is a schematic diagram of pilot model #3.

Mouse weights were routinely measured in the same manner as previous pilot models to monitor welfare. Graphed in Figure 65 are the weights of mice by treatment group from pilot model #3. As with each previous model, the welfare of mice was minimally affected by the laparotomies to establish pancreatic tumours. Additionally, administration of treatments had no effect on mice welfare.

Unfortunately, shortly after treatments with either CAVATAK™ or saline, tumours spontaneously regressed in all but one mouse, likely due to immune cell recovery too early in the model. Specifically, the 50 µg/antibody/mouse concentration of anti-NK1.1, anti-CD4, and anti-CD8α was too low to successfully deplete all, or at least enough, of these immune cells to facilitate tumour establishment and progression until the tumour niche was achieved. Similarly, the physical disruption of tumours with either saline or CAVATAK™ may have promoted inflammation and migration of immune cells inside the tumours. Presented in Figure 66 are the bioluminescent overlay images of tumour progression for pilot model #3. Similarly, the corresponding flux values are graphed in Figure 67 according to treatment group for each individual mouse. The one mouse that displayed tumour progression had a massive tumour burden and metastases to the liver. Potentially, tumour progression had advanced too rapidly before administration of CAVATAK™ for there to be an effect. Regarding the remaining mice, it appears that in some saline treated mice tumours had progressed marginally by the end of the model. Speculatively, there appeared to be a trend towards tumour regression in some of the CAVATAK™ treated mice.

Blood was routinely collected from mice and measured for NK1.1, CD4, and CD8 cells via flow cytometry. Represented in Figure 68 are the NK1.1, CD4, and CD8 profiles throughout pilot model #3. There was little to no recovery of NK1.1 cells in both saline and virus treated mice. N.T.C. mice had a low 3-4% NK1.1 cells out of the total leukocyte population at each measurement. Approximately 5% of the leukocyte population was CD4 cells in antibody depleted mice prior to treatments. Complete recovery of CD4 cells was detectable in saline and CAVATAK™ treated mice by day 28. Moreover, there was no difference in CD4 levels at each point between saline and virus treated mice. Similarly, roughly 2% of circulating leukocytes were CD8 cells in antibody depleted mice prior to treatments on day eight. Again, CD8 cell recovery reached similar levels to N.T.C. mice by the end of the study on day 28. Likewise, the two treatments failed to cause a difference in CD8 levels as similar levels were recorded in circulating blood from saline and virus treated mice at each measurement. The partial and continued recovery of CD4 and CD8 cells prior to and shortly after treatments is more than likely the cause of spontaneous tumour remission in both saline and virus treated mice.

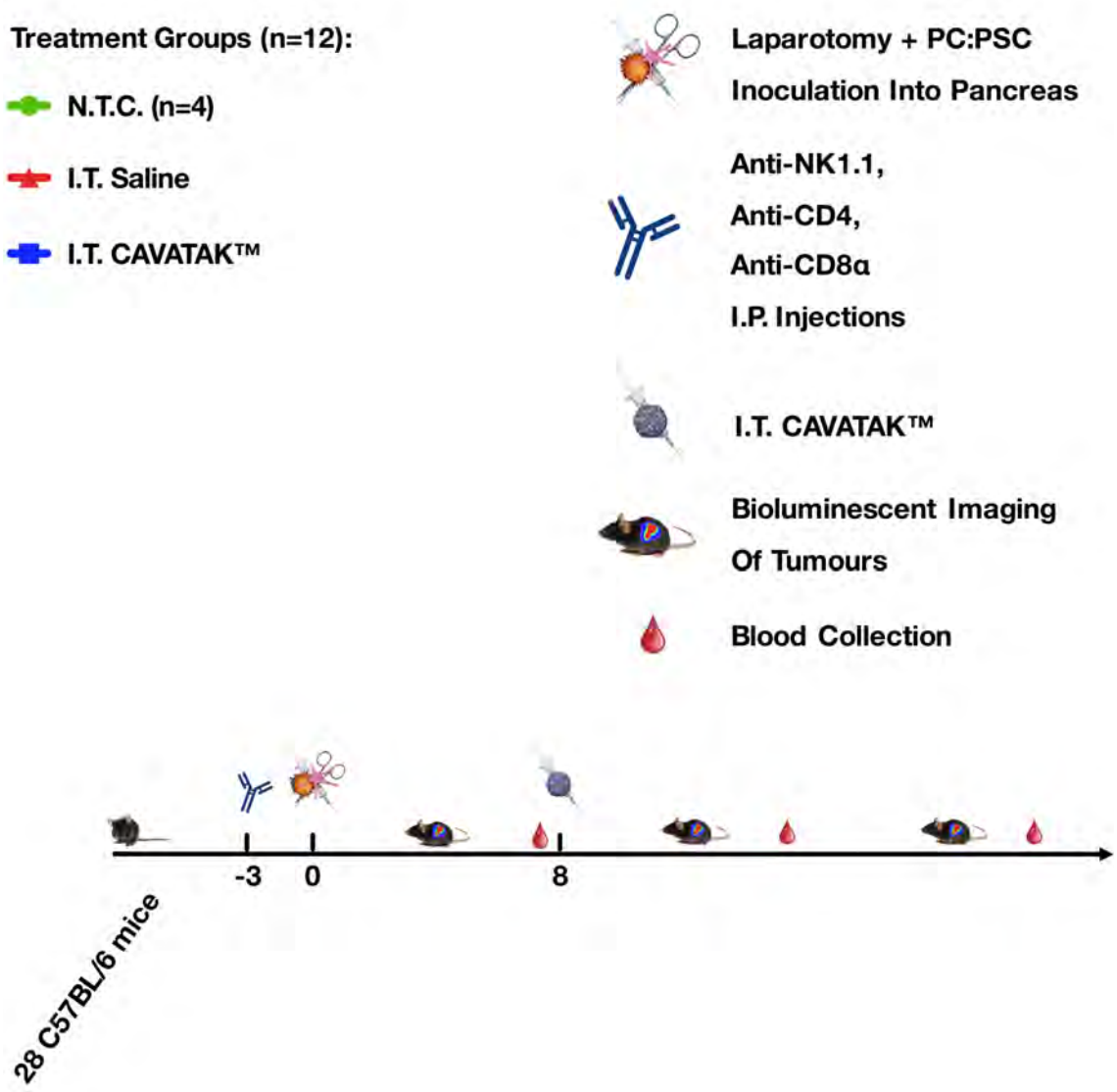

Figure 64: Schematic diagram of pilot orthotopic pancreatic cancer immune competent mouse model #3. Twenty-Four C57BL/6 mice were depleted of NK1.1, CD4, and CD8 cells by I.P. injection with 50 µg anti-CD4 + 50 µg anti-NK1.1, 50 µg anti-CD8α/mouse three days prior to tumour inoculation. A cell mixture of 1 x 10^5 UN-KPC-961-ICAM-1-luc + 4 x 10^5 ImPSCc2-ICAM-1 cells were injected directly into the pancreas of mice to generate orthotopic pancreatic cancer on day 0. Tumour progression was monitored via bioluminescence imaging on a weekly basis Blood was collected on a weekly basis commencing one day prior to administration of treatments. CAVATAK™ (7.5 x 10^6 $TCID_{50}$) or saline was administered I.T. to mice on day 8.

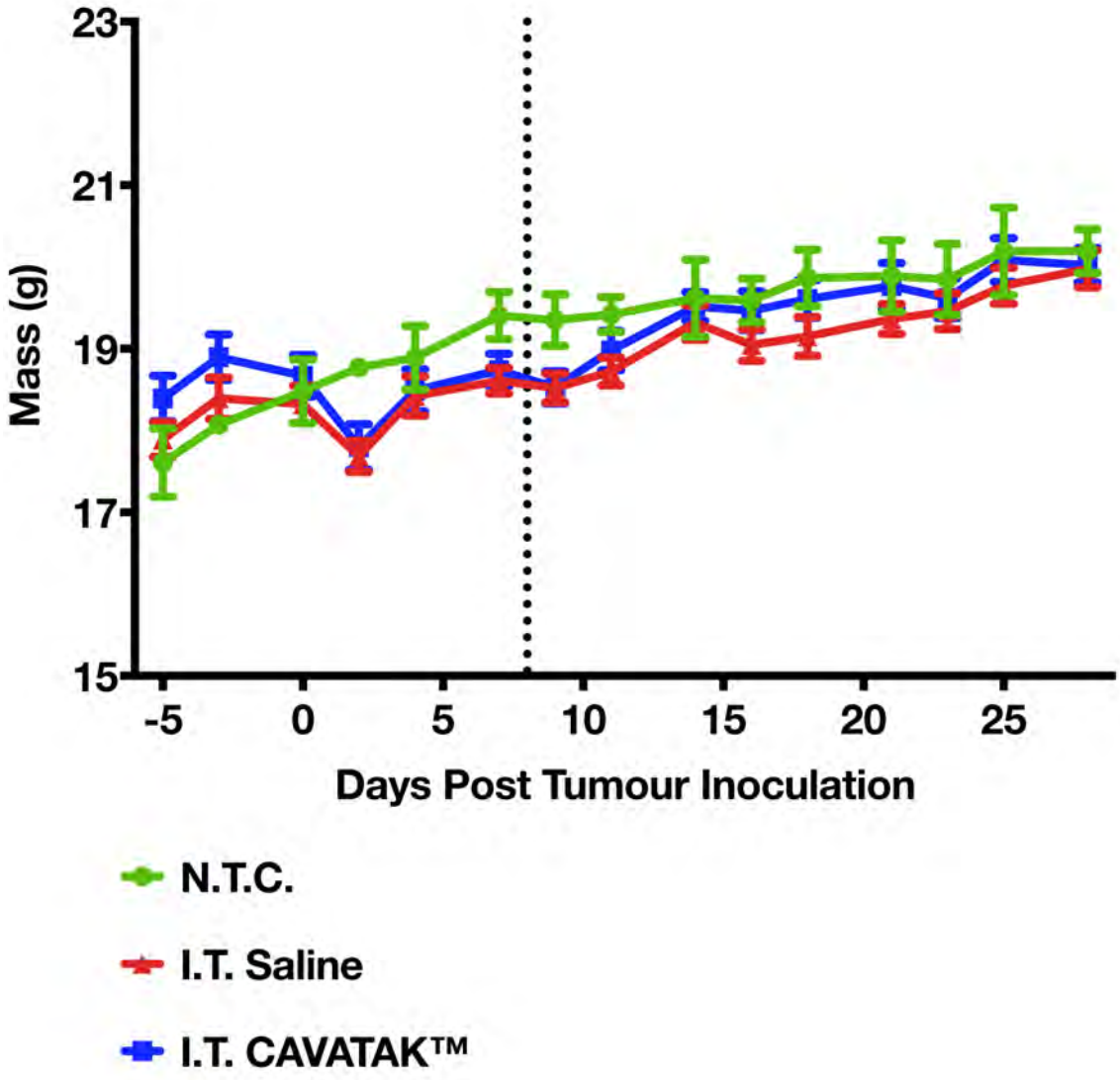

Figure 65: C57BL/6 mouse weights over the course of pilot model #3 according to treatment groups. Mice were weighed three times a week to monitor welfare. Weights were graphed using Prism v7.0 (GraphPad) according treatment group +/- SEM for each time point.

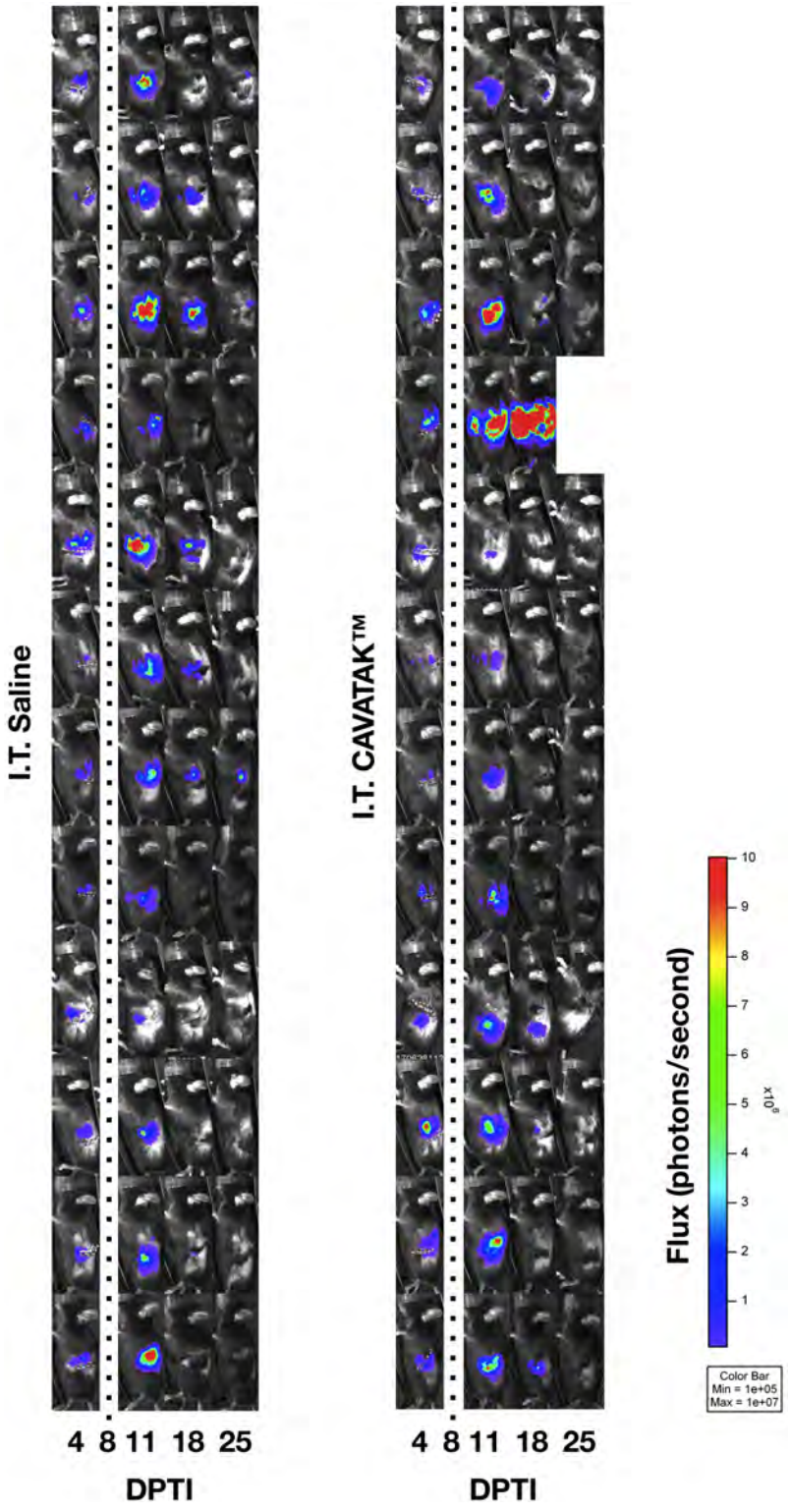

Figure 66: Tumour progression of C57BL/6 mice bearing UN-KPC-961-ICAM-1-luc + ImPSCc2-ICAM-1 pancreatic tumours over the course of pilot model #3. Weekly bioluminescent imaging of tumours using an IVIS™ Imaging System 100 (Xenogen) was conducted to measure tumour volume and track progression in each mouse. Dotted line indicates I.T. treatments with either saline or CAVATAK™ (7.5 x 10^6 $TCID_{50}$) 8 days post tumour inoculation (DPTI).

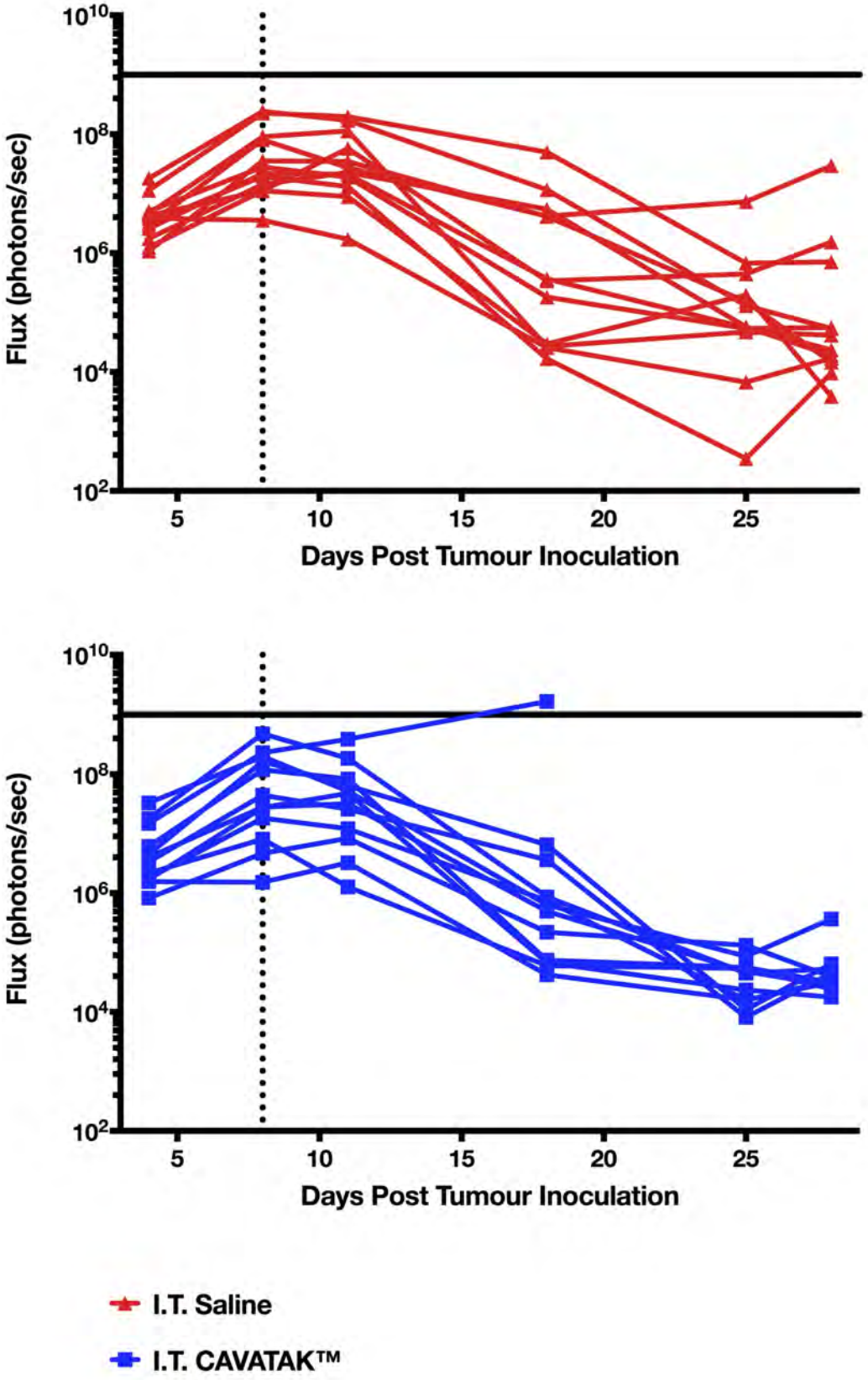

Figure 67: Tumour progression as a measure of flux (photons/second) by group over the course of pilot model #3. Flux values corresponding to tumour size obtained from weekly bioluminescent imaging of tumours using an IVIS™ Imaging System 100 (Xenogen) were graphed for individual mice using Prism v7.0 (GraphPad). Dotted line indicates I.T. treatments with either saline or CAVATAK™ (7.5×10^6 $TCID_{50}$).

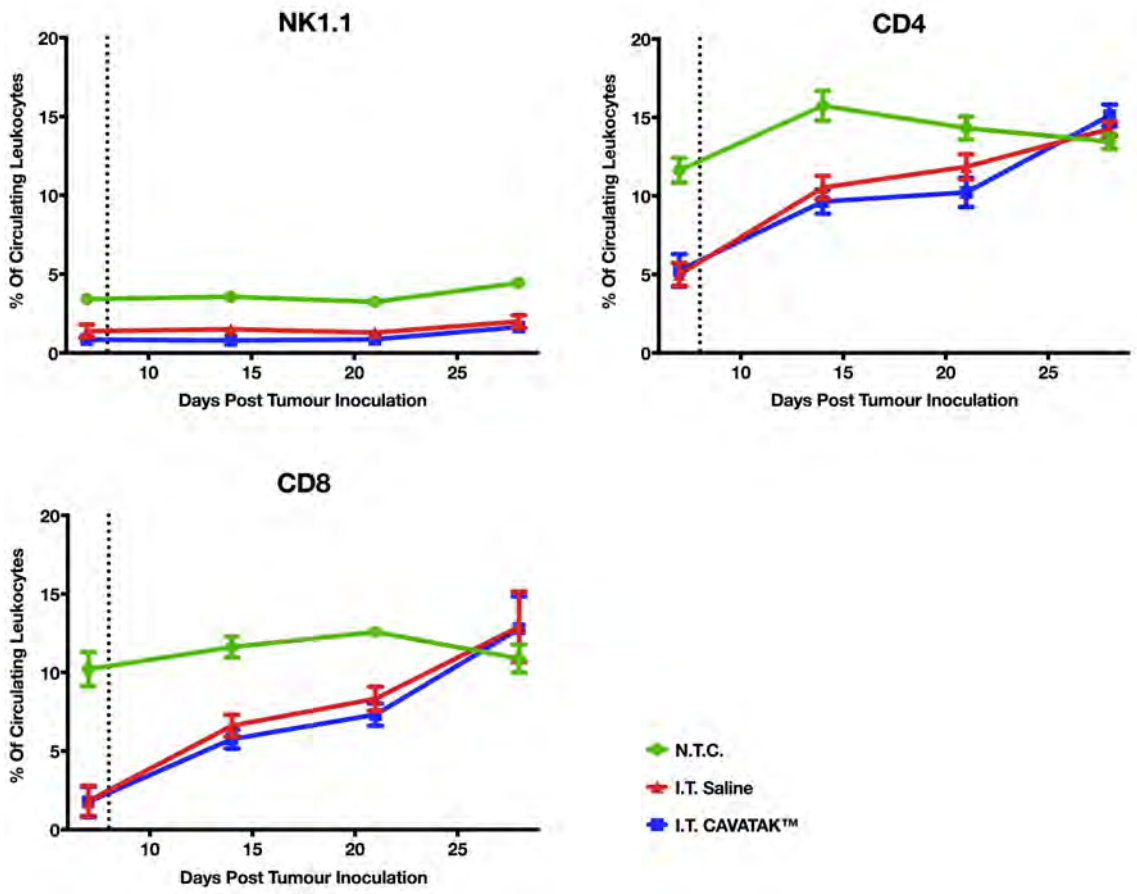

Figure 68: NK1.1 and CD4, CD8 T cell levels in mice according to treatment groups from pilot model #3. NK1.1, CD4 and CD8 cell levels from red blood cell lysed whole blood collected weekly from mice were measured via flow cytometry. Cell levels presented as percentage of circulating leukocytes according to treatment group +/- SEM. Dotted line indicates I.T. treatments with either saline or CAVATAK™ (7.5×10^6 $TCID_{50}$).

Chapter 7

Discussion and Future Directions

PC is the most lethal of all cancer types (Lennon *et al.*, 2014). PC has the lowest survival rates of any cancer type and incidence continues to increase annually (Siegel *et al.*, 2017). Even though the genomic aberration profiles and molecular pathogenesis of PC are well documented there are still no early detection mechanisms for PC (Apte *et al.*, 2015b; Biankin *et al.*, 2012; Masamune and Shimosegawa, 2015; Scarlett *et al.*, 2011b). PC is characterised by a dense desmoplastic reaction that is highly tumour promoting. Thus, the progression of PC is incredibly rapid. Currently, there are no treatments that can control the disease. Furthermore, treatment options provide unsatisfactory toxicity and quality of life to suffering patients (Borazanci *et al.*, 2017; Lau and Cheung, 2017). Efficacious treatment options are rapidly needed. The oncolytic virus, CVA21, has great potential as a treatment for PC. The capacity to directly oncolyse tumour cells as well as prompt an adaptive anti-tumour immune response while proving to exert minimal side effects makes CVA21 an ideal, potential anti-cancer agent (Bradley *et al.*, 2014).

The aim of the project was to investigate CVA21 as a potential treatment for PC in the preclinical setting. The hypotheses for this project were CVA21 would be an effective anti-cancer agent against pancreatic cancer due to high expression of viral entry receptors, ICAM-1 and/or DAF on PC and PSCs. Furthermore, CVA21 would have a synergistic effect in combination with standard of care chemotherapeutic, or immunotherapeutic agents. Hypotheses were tested through *in vitro* tissue culture and immunohistochemical analyses, and *in vivo* mouse models.

7.1 Chapter Four Discussion

The initial aim of the study was to determine the expression levels of CVA21 cell entry receptors, ICAM-1 and DAF, on the surface of PC and PSCs compared to normal pancreatic cells. Expression levels were measured through quantitative real-time PCR and flow cytometric analyses of a panel of PC, PSC, and normal pancreatic ductal epithelial cells. Furthermore, ICAM-1 cell surface expression on *ex vivo* patient PC tissues was measured through immunohistochemical analyses. The second aim of the project was to screen the sensitivity of human PC cells and PSCs to CVA21 in comparison to normal pancreatic cells. Sensitivity to CVA21 was defined through viral infectivity and viral growth kinetic assays on the same panel of PC, PSC, and normal pancreatic ductal epithelial cell lines.

The findings presented in chapter four demonstrate CVA21 to be an efficacious and appropriate treatment for PC. ICAM-1 and DAF, gene, and cell receptor expression showed that PC and PSCs, in general, overexpressed ICAM-1 and/or DAF compared to normal pancreatic ductal epithelial cells (Figure 17, Figure 18 and Figure 19). A convincing oncolytic effect of CVA21 on PC and PSCs was observed. Thus, the hypothesis that CVA21 will be a potential effective anti-cancer agent against PC due to overexpression of ICAM-1 and/or DAF was confirmed. Moreover, the minimal oncolytic effect of CVA21 on normal pancreatic ductal epithelial cells is promising when considering translation to a clinical setting (Figure 20 and Figure 21). Furthermore, the ability of CVA21 to oncolyse both PC and PSCs alone, and when co-cultured implicated CVA21 as a strong candidate for oncolysis of PC cells and the major stromal desmoplastic reaction observed in native PC (Figure 22 and Figure 23). Finally, the observation of a stepwise increase in ICAM-1 cell surface expression over the progression of PC from clinical samples attests CVA21 as a specific and potential candidate for the treatment of PC (Figure 31).

The use of immortalised cell lines was a limitation of *in vitro* experimental findings throughout this project. After long-term passage of cells, the genomic and proteomic expression profiles would unlikely reflect those of their WT counterpart cells *in situ*. Thus, the ICAM-1 and DAF expression on the tested cell lines may not mirror the normal physiological situation in PC and the pancreas. Likewise, the susceptibility and viral growth kinetics of CVA21 in the tested cell lines may not mirror the situation in

native PC or normal pancreatic tissue. However, analyses of *ex vivo* patient derived PC tissues and investigation into *in vivo* mouse models that agreed with findings from tissue culture assays, reinforces the results accuracy and reflection of PC and the pancreas. That is, overexpression of ICAM-1 was observed on *ex vivo* tissue sections of PC but not on normal pancreatic tissue, and CVA21 was a well-tolerated and efficacious anti-cancer agent for the treatment of PC in an orthotopic model of PC (Figure 24 and Figure 26).

The observation of an increase in ICAM-1 on PC compared to normal pancreatic tissue is in agreement with the literature. Hayes *et al.*, observed ICAM-1 expression on pancreatic cancer tissues, but absent from normal pancreas tissue through immunohistochemical analyses (Hayes and Seigel, 2009). Liu *et al.*, showed high ICAM-1 expression on BxPC-3 and Panc-1 cells, but not MIA PaCa-2 cells through FACS analysis (Liu *et al.*, 2009). Such results agree with the findings from FACS analyses of ICAM-1 expression in this thesis (Figure 19). Furthermore, Tempia-Caliera *et al.*, concluded a 5.4-fold increase in ICAM-1 in PC samples compared to normal pancreas samples via northern blot analysis ($P = <0.01$) (Tempia-Caliera *et al.*, 2002). Finally, ICAM-1 has been shown to have potential as a serum biomarker for PC due to overexpression. Brand *et al.*, found a highly statistically significant increase in serum ICAM-1 in PC patients compared to healthy controls (1011.3 ng/ml vs. 177.1 ng/ml, respectively. $P = 0.001$) (Brand *et al.*, 2011). Along with these discoveries, the stepwise increase of ICAM-1 on patient PC tissues over the progression of disease (Figure 31), directly implicates and highlights the role of ICAM-1 in the progression and metastasis of PC. Therefore, CVA21 is a uniquely suitable anti-cancer agent for the treatment of PC as the viral cell entry receptor, ICAM-1, is a key molecule in PC pathogenesis.

A major novel finding of this research has been the oncolysis of not only PC cells but also PSCs (Figure 22 and Figure 22) suggesting that CVA21 alone could destroy PC tumours as a whole. The major hurdle to achieving an efficacious treatment for PC is overcoming the dense stromal reaction that prohibits infiltration of anti-cancer agents. Currently, the paradigm in PC research is to combine agents that individually target either PC cells or the desmoplastic reaction to remodel the TME allowing access of anti-cancer agents to reach and kill PC cells (Kota *et al.*, 2017). Administration of multiple agents would likely increase toxicity and cost to patients. Thus, CVA21 is not

only a suitable, but also an optimal agent for the treatment of PC because of the ability to oncolyse PC, and the major contributing cell type to the stromal reaction, PSCs. Furthermore, the lack of oncolytic effect on normal pancreas cells (Figure 20) along with the low pathogenicity of CVA21 which causes only common cold symptoms, suggests CVA21 would have less side effects than a combination treatment modality.

Admittedly, co-culturing of PC and PSCs as monolayers in tissue culture plates does not recapitulate the protective characteristics of native PC desmoplasia. The three-dimensional, intricate structural and biochemical relationship between stromal cells, ECM constituents, and PC cells was not well replicated. Involvement of PSCs in a mouse model of PC was attempted (Figure 47) to better mimic native PC and substantiate *in vitro* results. However, the PSCs used entered into senescence and ultimately tumours did not establish in mice. Therefore, future studies could utilise 3D tissue culture technologies to better reflect PC. Likewise, utilising immortalised PSCs that maintained an activated phenotype reflective of native PSCs in a mouse model of PC could be conducted. Alternatively, the best way to replicate the PC TME would be to generate an immunocompetent mouse strain expressing human ICAM-1 ubiquitously, that spontaneously generated PC (discussed later). Although flawed, the *in vitro* analyses of PSCs with PC cells do prove the concept that CVA21 can eliminate PSC cells when cultured alongside PC cells.

A recent study by Man and colleagues investigating genetically modified adenoviruses (Ad5A20 and Ad5A20-477dlTAYT) as treatments for pancreatic cancer utilised a sophisticated organotypic 3D co-culture model. Briefly, a mixture of matrigel and collagen type I was used as a gel medium for seeding PC cells and PSCs onto. After an incubation period of up to four days, organoids formed exhibiting characteristics similar to native PC TME; epithelial layers on top of the gel medium with duct like structures invading the medium. After treatment with the modified adenoviruses, the organoids were formalin fixed, sectioned, and analysed through immunohistochemistry. The investigators found co-culturing PC cells with PSCs greatly increased growth rate and invasion into the gel medium. Finally, after treatment with the modified adenoviruses, the investigators concluded the modified adenoviruses infected both the PC and PSCs, and was able to spread between cells in the gel medium (Man *et al.*, 2018). This organotypic 3D co-culture model that better

replicates the TME of PC than the described model within this project could be utilised in future studies investigating CVA21.

To summarise the findings and discussion of results from chapter four, ICAM-1 is a key directing molecule in the progression of PC. Thus, CVA21 is a very suitable candidate for treatment of PC. Moreover, CVA21 is an optimal anti-cancer agent for PC due to the ability to oncolyse PC cells and the major cell type contributing the stromal desmoplastic reaction, PSCs. Furthermore, the absence of viral lysis on, and replication within normal pancreas cells suggests CVA21 would have minimal toxic effects in patients. Based on these findings, there is substantial cause to progress investigations further with *in vitro* and *in vivo* studies, and even potentially into the clinic.

7.2 Chapter Five Discussion

The third aim of the study was to determine the synergistic or antagonistic relationship between CVA21 and conventional chemotherapy on human PC and PSCs, compared to normal pancreatic cells. The sensitivity of the panel of pancreatic cell lines to gemcitabine was investigated through dose-response assays. Checkerboard assays employing the respective experimentally determined concentrations of CVA21 and gemcitabine required to reduce cell viability by 50% were titrated in combination against each cell line to observe the relationship. Computational analyses based off the Chou-Talalay method of drug calculation using the experimentally recorded values enabled the synergistic or antagonistic relationship between the two agents to be empirically calculated. The fourth aim of the study was to establish an orthotopic mouse model of human PC and investigate CVA21 as a treatment, alone, and in combination with conventional chemotherapy. Investigation of CVA21 as a treatment was successfully conducted in an athymic nude mouse model of orthotopic PC generated from human Panc-1-luc cells.

The results detailed in chapter five further enforce the hypothesis that CVA21 would be an effective anti-cancer agent against PC. Furthermore, the findings illustrate the frequent high-grade toxicity that gemcitabine causes to PC patients. Dose-response assays of gemcitabine on the panel of PC, PSC, and normal pancreas cells showed normal pancreatic ductal epithelial cells to be incredibly susceptible, PSCs to be almost entirely refractive, and varying degrees of sensitivity on PC cells (Figure 32). Combination checkerboard assays of CVA21 and gemcitabine on the panel of cell lines revealed a synergistic relationship between the two agents when calculated from accurate experimental data (Figure 33, Figure 34, Figure 35 and Figure 36). Thus, the hypothesis that CVA21 in combination with a chemotherapeutic agent would have a synergistic effect was confirmed in some instances. Furthermore, gemcitabine does not have an inhibitory or antiviral effect on CVA21 *in vitro*, or *in vivo*. However, in many examples the calculated concentrations of gemcitabine were not clinically achievable. Moreover, there was a lack of sensitisation of stellate cells to gemcitabine, and increased toxicity towards normal pancreas cells. Therefore, CVA21 and gemcitabine should be considered with extreme caution as a combination treatment in the clinical setting.

The athymic nude mouse model of orthotopic PC generated from Panc-1-luc cells demonstrated CVA21 to be an efficacious and well tolerated treatment for PC when administered intratumourally (Figure 39, Figure 40, Figure 41, Figure 42 and Figure 43). Furthermore, there was a definite increase in survival time of mice treated with CVA21 compared to saline, or gemcitabine treated mice ($P = 0.0021$) (Figure 44). Gemcitabine proved ineffective at controlling PC either as a single agent, or when combined with CVA21. Moreover, the profound toxic effects of gemcitabine reduced the welfare of mice such that the majority had to be euthanised due to weight loss (Figure 38). Additionally, there was a diminishing effect of gemcitabine towards the anti-viral immune response generated towards CVA21 when considering the neutralising antibody profiles of CVA21 treated, and CVA21 plus gemcitabine treated mice (Figure 45). Dampening of an immune reaction to CVA21 was also observed in mice from the second athymic nude mouse model (Figure 48).

Gemcitabine was initially investigated as an antiviral drug after its synthesis and patenting during the AIDS epidemic in the 1980's (Hertel, 1985). It was found to have activity against herpes simplex virus (HSV) types 1 and 2, and human immunodeficiency virus (HIV) in cell culture assays. However, the therapeutic effect was insufficient in *in vivo* models (Hertel *et al.*, 1990; Martin *et al.*, 1990; Mitchell *et al.*, 1986). It appears from the literature that several investigations were conducted to find potential uses for the newly patented drug gemcitabine. Subsequently, gemcitabine was found to have a cytotoxic effect on the human leukaemia cell line CCRF-CEM (Heinemann *et al.*, 1990; Hertel *et al.*, 1990). Accordingly, gemcitabine was investigated in a range of cancer types including PC.

Prior to clinical investigation, gemcitabine was examined in a PC xenograft mouse model. The study generated tumours subcutaneously in the axillary region of athymic nude mice from either Panc-1 or MIA PaCa-2 cell lines. Treatments with gemcitabine started after seven days tumour development. A range of gemcitabine concentrations (40 mg/kg, 80 mg/kg, or 160 mg/kg) were administered I.P. to groups of ten mice on days 7, 10, 13, and 16. It is not reported if the control group mice received mock treatments (e.g. saline). The duration of the studies is not reported. Response to treatment (inhibition) as an empirical value is not defined. Moreover, duration of responses is not specified. Empirical tumour volumes for gemcitabine treated or control mice are not reported for either MIA PaCa-2 or Panc-1 xenograft models.

Endpoints such as 10% weight loss, or death as an endpoint, are not indicated. The exact number of deaths in treatment groups are not stated. Statistical analyses, if any were conducted, are not described. Data reported regarding gemcitabine from the models in the paper is pictured below in Figure 69. In summary, Gemcitabine at 160 mg/kg caused greater than two deaths out of the ten mice bearing subcutaneous MIA PaCa-2 tumours. Comparatively, gemcitabine at 160 mg/kg given to mice bearing Panc-1 tumours allegedly caused over 60% inhibition. Likewise, greater than 60% inhibition was recorded for either xenograft model at a concentration of 80 mg/kg gemcitabine. Less than 60% inhibition was observed at a dose of 40 mg/kg. From these data the authors concluded response rates for gemcitabine of 69% inhibition in MIA PaCa-2, and 76% inhibition in Panc-1 xenografts (Schultz *et al.*, 1993). Data from this preclinical study was the basis for translating gemcitabine into clinical investigations.

Table 2. Antitumor activity of various drugs against MIA PaCa-2 and PANC-1 human pancreatic carcinoma xenografts.

			Antitumor Activity**	
Drug	Schedule*	Dose (mg/kg)	PaCa-2	PANC-1
Adriamycin	D7,11,15;IP	15.0	Toxic***	Toxic
		7.5	–	–
CisPlatin	D7,11,15;IP	15.0	Toxic	Toxic
		7.5	–	–
5–FU	Daily(D7–16);IP	40.0	Toxic	Toxic
		20.0	–	–
		10.0	–	–
Gemcitabine	D7,10,13,16;IP	160.0	Toxic	+
		80.0	+	+
		40.0	–	–
Sulofenur	Daily(D7–16);PO	600.0	+++	Toxic
		300.00	+++	–
		150.0	–	–
LY295501	Daily(D7–16);PO	1200.0	+++	Toxic
		600.0	+++	–
		300.0	–	–
Taxol	D7,9,11,13,15;IV	24.0	Toxic	++
		12.0	–	+

*Therapy was delayed for 7 days after tumor implantation.
**Antitumor Activity: +++, 95–100% Inh.; ++, 80–94% Inh.; +, 60–79% Inh.; –, <60% inhibition of tumor weight.
***Toxic represents >20% deaths in treated groups.

Figure 69: Data presented by Schultz, *et al.* regarding efficacy of gemcitabine as a treatment in subcutaneous xenograft Panc-1 or MIA PaCa-2 models. Table from: **Schultz, R. M., Merriman, R. L., Toth, J. E., Zimmermann, J. E., Hertel, L. W., Andis, S. L., Dudley, D. E., Rutherford, P. G., Tanzer, L. R. and Grindey, G. B.** (1993). Evaluation of new anticancer agents against the MIA PaCa-2 and PANC-1 human pancreatic carcinoma xenografts. Oncol. Res. **5**, 223–228.

As is still the case, there was a desperate need for improved treatments for PC. This may explain the irrational advancement into clinical trials investigating gemcitabine as a treatment for PC. Perhaps the patenting of gemcitabine also inspired the advancement. At the time, 5-FU had been the standard treatment for PC for over 30 years. 5-FU and gemcitabine were directly compared in a phase II clinical trial which demonstrated a significant increase in clinical benefit: 23.8% (15/63) in gemcitabine treated patients vs. 4.8% (3/63) in 5-FU treated patients (P = 0.0022). Clinical benefit was a subjective measure, defined as improvement in one or more parameters for a minimum of 4 weeks: pain (assessed by pain intensity and administration of morphine), functional impairment (assessed by Karnofsky performance status) and weight (assessed by body weight). Objective tumour response was a secondary measurement of efficacy. Only three of the 63 gemcitabine treated patients (5.4%) achieved a partial response in tumour reduction (≥50% reduction in measurable lesions for a minimum of four weeks). The technique of tumour measurement and definition of measurable lesions were not reported. Forty-one of the 63 gemcitabine treated patients (65.1%) discontinued treatment because of progressive disease and toxicity. Higher incidence of grade 3 and 4 neutropenia was observed in gemcitabine treated patients (25.9% vs 4.9% P = <0.001). Likewise, higher incidence of grade 3 and 4 leukopenia (9.7% vs. 1.6%) and thrombocytopenia (9.7% vs. 1.6%) was observed in gemcitabine treated patients (no grade 4 observed in either group). Grade 3 elevated liver enzyme related adverse events were higher in gemcitabine patients: alkaline phosphatase (16.4% vs. 9.5%), aspartate transaminase (9.8% vs. 1.6%), and alanine transaminase (8.2% vs. 0%). Finally, retrospective survival analyses showed a minor median survival increase: 5.65 months for the gemcitabine cohort, compared to 4.41 months in 5-FU treated patients (P = 0.0025), a difference of 5 weeks. However, eight of the 63 gemcitabine treated patients (12.7%), and three 5-FU patients (4.8%) were omitted from survival analyses. The reasons for which are not described. The study concluded that gemcitabine alleviated some disease related symptoms and confers a modest survival advantage in patients with advanced, symptomatic PC (Burris *et al.*, 1997). Subsequently, gemcitabine was approved by the USFDA in 1996 for the frontline treatment of PC (USFDA, 1996).

The substantial involvement of the desmoplastic reaction in the progression of PC had not been characterised at the time gemcitabine was investigated in clinical trials as a treatment for PC. The importance of stellate cells in disease progression and

chemoresistance in PC has only begun to be explored in the last two decades (Apte *et al.*, 1999; Bachem *et al.*, 2005; Bachem *et al.*, 2008; Hwang *et al.*, 2008; Jaster, 2004; Masamune and Shimosegawa, 2009; Masamune *et al.*, 2002; Masamune *et al.*, 2009; Mews *et al.*, 2002; Omary *et al.*, 2007; Schneider *et al.*, 2001; Vonlaufen *et al.*, 2008). A current review by Cannon *et. al.* highlights the lack of comprehension of PC desmoplasia by reporting on contradictions within the literature. The authors conclude that greater research is needed in this area to fully elucidate PC TME mechanisms and discover areas of therapeutic potential (Cannon *et al.*, 2018). Indeed, it has only been in the last few years that pancreatic stellate cell lines maintaining an activated WT phenotype have been isolated for scientific research. The characterisation of the two pancreatic stellate cell lines, TAS29 and TAS31, investigated in this dissertation was not published until 2015 (Han *et al.*, 2015). Similarly, characterisation of the normal pancreatic ductal epithelial cell line, HPDE, studied throughout this project was not reported until 1996; the year gemcitabine was approved by the USFDA for frontline treatment of PC (Furukawa *et al.*, 1996). If these cell lines had been available and tested when gemcitabine was investigated *in vitro* and in *in vivo* mouse models as an anti-cancer agent against PC, there is no doubt that gemcitabine would have been disregarded as a candidate. Therefore, gemcitabine would not, and should not, have ever been considered for clinical investigation.

Advances in treatments considered to be major since the approval of gemcitabine have been the addition of nab-paclitaxel to gemcitabine as a combination treatment, and FOLFIRINOX. Both treatment regimens are only appropriate for patients with good performance status due to a marked increase in toxicity. There are significantly higher incidences of grade 3 and 4 neutropenia, febrile neutropenia, thrombocytopenia, diarrhoea, and sensory neuropathy in patients treated with FOLFIRINOX compared to gemcitabine. Likewise, the incidence of grade 3 and 4 neutropenia, leukopenia, fatigue, and peripheral neuropathy is higher in gemcitabine plus nab-paclitaxel treated patients compared to gemcitabine alone treated patients. The addition of nab-paclitaxel to gemcitabine increased median survival by 1.8 months compared to gemcitabine alone. FOLFIRINOX was found to give a median survival of 11.1 months (Conroy *et al.*, 2011; Hoff *et al.*, 2013). Still to this day, the current frontline treatments for PC provide poor survival advantage and frequent high-grade toxicity to patients.

CVA21 has been well characterised as causing common cold symptoms: fever, chills, malaise, and coryza in humans. (Magee and Miller, 1970; Patel *et al.*, 1964; Spickard *et al.*, 1963; Xiang *et al.*, 2012; Yin-Murphy and Almond, 1996; Zou *et al.*, 2017). Additionally, the administration of the clinical formulation of CVA21, CAVATAK™, via multiple routes (intralesional, intravenous, intravesicular) for the treatment of multiple cancer types and stages (melanoma, bladder, non-small cell lung) has been generally well tolerated by patients in numerous clinical trials (Andtbacka *et al.*, 2015a; Kaufman *et al.*, 2015). The proven low pathogenicity and tolerability of CVA21 in patients burdened with late stage cancers, strongly suggests CVA21 would potentially be a similarly well-tolerated treatment in patients with PC. Furthermore, the findings from this project, both *in vitro* and *in vivo*, infer that CVA21 would be a better tolerated and more efficacious treatment, and provide greater survival advantage compared to gemcitabine, in patients with PC.

Endoscopic ultrasound (EUS) fine needle aspiration (FNA) is a routine method for diagnosis and staging PC. An echoendoscope is inserted through the gastrointestinal tract to obtain detailed images of the pancreas. Simultaneously, a retractable needle is used to collect sample areas of interest for analyses. EUS fine needle injection (FNI) utilises this minimally invasive and well tolerated procedure to directly inject and administer drugs into pancreatic tumours (Bartel and Raimondo, 2017; Han and Chang, 2017; Hecht *et al.*, 2003; Yoo *et al.*, 2016). ONYX-015, an oncolytic adenovirus, was investigated in clinical trials in combination with gemcitabine for the treatment of PC through administration by EUS-FNI. ONYX-015 in combination with gemcitabine was found to have a partial response in two out of 21 patients and provided a median survival time of 7.5 months. Although the treatments were not significant, delivery of an OV via EUS-FNI into pancreatic tumours was very well tolerated by patients (Hecht *et al.*, 2003).

Although successful in non-small cell lung cancer and bladder cancer, I.V. administration of CVA21 is not thought to be effective at delivering the virus to, and infiltration of, PC tumours. Preliminary mouse models investigating CVA21 as a treatment administered virus I.V. and I.P. in athymic nude mice bearing orthotopic pancreatic tumours. Administration of CVA21 via these routes failed to show an effect on tumour burden at the administered doses. Thus, the direct infiltration of the virus into a pancreatic tumour was concluded necessary to initiate a direct oncolytic effect,

establish a cradle for inter-tumour viral replication, and launchpad for future systemic spread. CVA21 via EUS-FNI for the treatment of PC is posited to be the optimal route of administration when studies advance into the clinical setting. Not only is this technique minimally invasive, it enables real-time imaging of the tumour while the injection is performed to ensure successful delivery of the agent into the tumour. Moreover, the agent can be disseminated throughout the tumour by fanning the needle in and out around the tumour mass. CT-guided injection of tumours is another option for delivery. However, this procedure is cumbersome and requires multiple CT scans to pinpoint and ensure the needle has been injected into the tumour. Abdominal ultrasound (US)-guided injection is yet another option. Using this method does provide real-time imaging of the tumour when injected. However, there is a longer injection and imaging pathway compared to EUS resulting in less sensitivity, particularly with tumours smaller than 10 mm (Bartel and Raimondo, 2017; Yoo *et al.*, 2016).

One of the greatest limitations to systemic spread of an OV are neutralising antibodies (nAbs). An influx of nAbs were observed in both mouse models presented in chapter five (Figure 45 and Figure 48) and are consistently detected in patient sera samples. nAbs disable virus particles by binding to virions, blocking the interaction of virus with cell receptors and subsequent internalisation of host cells. Thus, it would seem that once an antibody response towards an OV is generated, the potential for systemic spread to regional and distant tumour sites is reduced. However, there is a growing body of evidence that OVs utilise immune cells to deliver functional virus particles to distant tumour sites while evading neutralising antibodies (Adair *et al.*, 2012; Ilett *et al.*, 2011; Ilett *et al.*, 2009; Jennings *et al.*, 2014; Roy and Bell, 2013; Zhao *et al.*, 2017). Through phagocytosis of reovirus by dendritic cells, the systemic delivery of reovirus to distant tumour sites, induction of a cytokine storm (IFNγ, IL-12, IFNα and TNFα) and adaptive immune response was observed in the presence of nAbs. (Jennings *et al.*, 2014). IFNγ and TNFα lead to the expression of ICAM-1 (Hubbard and Rothlein, 2000). Thus, ICAM-1 in the TME would likely increase. Therefore, even in the presence of nAbs, it is posited that CVA21 is delivered to distant tumour sites by immune cells. Moreover, the tumour becomes more susceptible to CVA21 oncolysis because of upregulated ICAM-1 expression on cancer and stromal cells. Finally, the associated influx in cytokines leads to an adaptive anti-tumour immune response.

To summarise the results from chapter five and discussion of findings, CAVATAK™ would likely be a superior treatment for PC compared to gemcitabine and possibly other approved treatments. CAVATAK™ can potentially be administered intratumourally in a minimally invasive manner (EUS-FNI), tolerated well, provide better anti-tumour response and disease control, increase patient survival and quality of life, and finally initiate an adaptive anti-tumour immune response in patients. CAVATAK™ should be considered for immediate clinical investigation to replace gemcitabine as a treatment for PC. Combination of CAVATAK™ with gemcitabine is not warranted. With ever increasing means of palliative care, gemcitabine is long overdue to be removed as a treatment for PC. Gemcitabine's place in the treatment of PC is a final hope for patients. Unfortunately, it is a false hope. Gemcitabine leads to mortality quicker than PC would otherwise.

7.3 Chapter Six Discussion

The final aim of this project was to establish an immune competent mouse model of orthotopic, human ICAM-1 expressing, PC and investigate CVA21 as a treatment, alone, and in combination with immunotherapeutic agents. Unfortunately, this aim was not achieved. Generation of the model proved harder than anticipated and due to time constraints a reliable and well characterised model was not finalised. Consequently, investigations of CVA21 in combination with immune checkpoint inhibitors could not be conducted. Thus, the hypothesis that CVA21 will have a synergistic effect in combination with immunotherapeutic agents could not be confirmed.

Findings from the three pilot models conducted indicated C57BL/6 mice were the optimal strain for generation of an orthotopic PC model that showed hallmark metastatic characteristics of native PC; for example metastases to liver, spleen, and lung (Figure 57 and Figure 58) Secondly, both the surgical procedures to generate orthotopic PC and administration of CAVATAK™ were well tolerated by mice (Figure 54, Figure 60 and Figure 65). Finally, immune cell recovery was observed late in pilot model #2 while tumours were maintained and progressed in C57BL/6 mice (Figure 63). Mice were administered 200 µg/antibody/mouse three days prior to tumour inoculation to suppress NK1.1, CD4, and CD8 cells. Contrastingly, in pilot model #3, when mice were administered 50 µg/antibody/mouse three days prior to tumour

inoculation, immune cell recovery occurred earlier in the model and subsequent spontaneous remission of tumours in mice was observed (Figure 66 and Figure 68).

In future, to achieve immune system recovery while maintaining tumour burden and progression, double the antibody dose used in pilot model #3 will be administered to mice in pilot model #4. Refer to Figure 70 for a schematic of the proposed mouse model. Briefly, 24 C57BL/6 mice will be given a single I.P. injection of 100 µg/antibody/mouse: anti-NK1.1, anti-CD4, and anti-CD8α three days prior to surgery. The pancreas of mice will be injected with 5 x 10^5 cells of a mixture of 1:4 UN-KPC-961-ICAM-1-luc and ImPSCc2-ICAM-1 to generate orthotopic PC. Four C57BL/6 mice will be selected as N.T.C. Besides recording body weights three times a week, and weekly blood collections, N.T.C. mice will be excluded from all other procedures. Twelve tumour bearing mice will be designated to each treatment group: I.T. Saline or I.T. CAVATAK™. Tumour volumes will be measured weekly through bioluminescent imaging of tumours using an IVIS™ Imaging System 100 (Xenogen). CAVATAK™ (7.5 x 10^6 $TCID_{50}$) or saline will be administered I.T. to respective mice on day eight. I.T. administration of treatments will be performed by palpation and injection of tumours. Blood will be collected for analysis of NK1.1, CD4, and CD8 cells on a weekly basis starting one day prior to treatments. Quantitation beads will also be measured alongside to determine immune cell levels quantitatively. Sera fractions will also be collected at the same time for chemokine and cytokine profiling. Mice will be euthanised if pain and distress and/or a weight loss of 15% is observed.

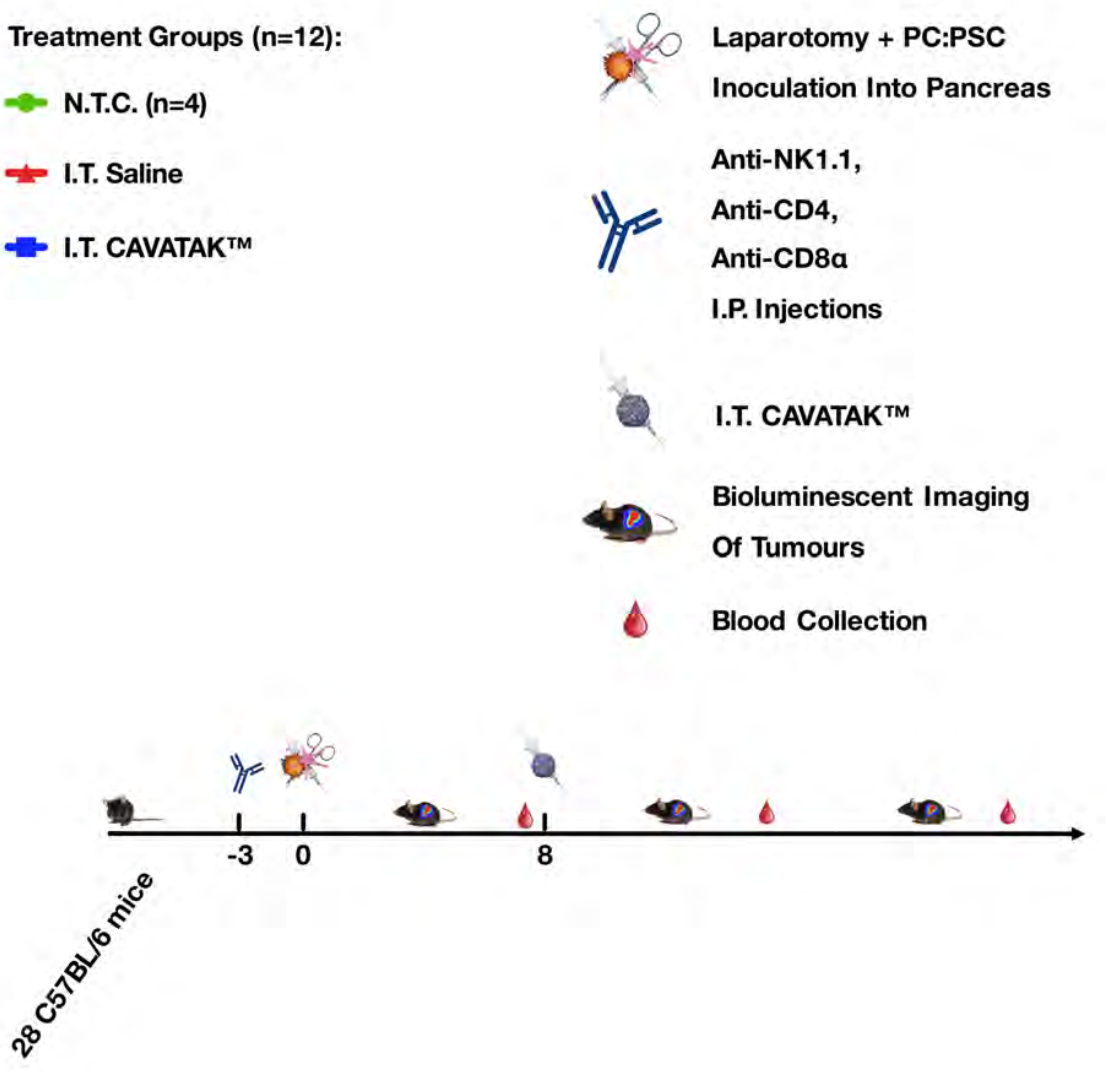

Figure 70: Proposed orthotopic PC immune competent mouse model (pilot model #4). 100 µg/antibody/mouse will be administered in an attempt to maintain tumour progression while observing recovery of a functional immune system.

Complete recovery of NK1.1, CD4, and CD8 cells appeared to occur by the end of pilot model #3 after administration of 50 µg/antibody/mouse three days prior to tumour inoculation (Figure 68). CD4 depletion studies in C57BL/6 and BALB/c mice by Rice and Bucy found that CD4 cells took up to 100 days to recover fully when administered 100 µg anti-CD4/mouse. Furthermore, CD4 cells recovered faster in younger mice (4-6 months) than in aged mice (> 2 years) (Rice and Bucy, 1995). When quantitation beads are utilised in future models, the exact recovery rates and levels will be ascertained. With aging comes an inherent reduction in the effectiveness of the immune system in humans (Bektas *et al.*, 2017). The majority of PC patients are aged between 60 and 80 years of age (Siegel and Jemal, 2017; Siegel *et al.*, 2017). Thus, it

could be argued that only a partial recovery of the immune system in a mouse model would better recapitulate that of an elderly PC patient. There is increasing evidence that efficacy of immune checkpoint inhibitors are lower in elderly patients than younger, fitter patients that have overrepresented patient populations in clinical trials (Daste *et al.*, 2017). Therefore, the efficacy of immune checkpoint inhibitors in combination with CAVATAK™ in future models would likely better reflect patient populations if only partial recovery of immune cells is observed in mice. This may be the case when a concentration of 100 µg/antibody/mouse is administered.

There are evident limitations to the immune competent mouse model. Primarily, determining the intricate balance between tumour establishment and progression during recovery of a functional immune system may not be achieved. Maintenance and progression of tumours was observed after recovery of immune cells in pilot model #2 (Figure 62 and Figure 63). Thus, the assumption that there is a balance between tumour growth and immune cell recovery is likely. However, achieving the precise concentrations and timing of administration of antibodies to deplete immune cells may never be achieved and/or be reproducible due to biological variation among mice. Secondly, the cancer cells and stellate cells used to establish tumours are susceptible to CVA21 oncolysis because they express a plasmid containing the gene for human ICAM-1. Thus, the expression of human ICAM-1 will only be present on the cancer and stellate cells, and the level of expression will unlikely mimic that of the normal physiological situation in PC. Moreover, as CVA21 will not infect mouse cells, any toxic effects to mice will not be observed. Furthermore, loss of plasmid from cells could occur spontaneously, rendering the model inadequate for investigating CVA21 as a treatment. Numerous consecutive isolations of stably transfected single cell colonies were conducted in the generation of the two cells lines. Thus, loss of plasmid from cells is less likely to occur. Finally, only PC and PSC cells are used to establish tumours. The cross-talk between the two cell lines was not experimentally determined and thus may not replicate the native situation in PC. Likewise, the influence of other CAFs, immune cells, adipocytes, pericytes and endothelial cells present in native PC desmoplasia will not be represented, unless, recruitment of these cells into the TME occurs from the mouse.

KPC mice (LSL-Kras^{G12D}; LSL-Trp53^{R172H}; Pdx1-Cre) are an ideal, well characterised mouse model of PC that closely mimics human PC (Colvin and Scarlett, 2014). KPC

mice could possibly be genetically modified through CRISPR/Cas9 technology (Kaboli and Babazada, 2017) to ubiquitously express human ICAM-1 instead of mouse ICAM-1. However, this option was outside the scope of this project and so the current approach was embarked upon. The model would also have one major disadvantage compared to the current approach. Expression of firefly luciferase by tumour cells and routine monitoring of tumour progression via non-invasive bioluminescent imaging of tumours could not be achieved. Thus, efficacy of treatments would primarily be based on survival advantage, unless cohorts of mice were routinely sacrificed, and tumours measured and weighed to determine average tumour burden over the course of studies. Routine euthanasia would dramatically increase the number of mice required, cost, and ethical considerations.

Once the model has been well characterised and vetted for reproducibility, investigations of CAVATAK™ in combination with immune checkpoint inhibitors can be undertaken. Immune checkpoint inhibitors have proven to be ineffective as treatments for PC due to the immunosuppressive nature of the tumour microenvironment, low mutational load of PC and minimal expression of neoantigens on PC cells, and basal levels of immune checkpoint molecules on PC cells (Guo *et al.*, 2017; Johansson *et al.*, 2016). It is hypothesised that the immune inflammatory characteristic of CVA21 to generate an adaptive anti-tumour immune response will also lead to upregulated expression of neoantigens and immune checkpoint molecules on PC cells. Upregulation of neoantigens, along with direct lysis of PC, and PSCs (bulk of the desmoplastic reaction) would likely result in a synergistic effect against PC when CVA21 is administered in combination with immune checkpoint inhibitors. Essentially, along with direct tumour lysis, CVA21 is postulated to turn PC from an immune desert into a 'heated' immunological environment permitting possible increase of immune checkpoint inhibitor function.

Cytotoxic T lymphocyte antigen 4 (CTLA-4) and cluster of differentiation (CD28) are expressed on T cells. The ligands for both CTLA-4 and CD28 are B7.1 and B7.2 which are expressed on APCs. In the situation where CD28 binds to either B7.1 or B7.2 on APCs, activation of tumour specific T cells and an anti-tumour inflammatory response occurs. However, if CTLA-4 binds to B7.1 or B7.2 then T cell activation and proliferation is inhibited. CTLA-4 has greater affinity for its ligands than CD28. Thus, in the normal physiological situation a T cell response is prohibited by competitive

binding of CTLA-4 with B7.1 or B7.2 (Brunet *et al.*, 1987; Krummel and Allison, 1995). Ipilimumab (Yervoy®) is a monoclonal antibody specific for CTLA-4 (anti-CTLA-4) that permits unimpeded binding of CD28 to B7.1 or B7.2 leading to an anti-tumour immune response. Ipilimumab was the first immune checkpoint inhibitor approved by the USFDA in 2011 for the treatment of melanoma (Lipson and Drake, 2011; Mansh, 2011).

Programmed cell death protein 1 (PD-1) expressed on T cells binds to programmed death ligand 1 (PD-L1) on cancer cells recognising them as self, or PD-L2 on APCs suppressing T cell function. Blockade of PD-1 binding to its ligands with monoclonal anti-PD-1 or anti-PD-L1/anti-PD-L2 antibodies reverses the tumour protective effects allowing T cell proliferation and an anti-tumour response (Fife and Pauken, 2011; Pardoll, 2012; Topalian *et al.*, 2014; Topalian *et al.*, 2012). Currently there are two anti-PD-1 immune checkpoint inhibitors approved by the USFDA, Pembrolizumab (Keytruda®) and Nivolumab (Opdivo®), for the treatment of melanoma (Chuk *et al.*, 2017; Hazarika *et al.*, 2017).

The use of immune checkpoint inhibitors for the treatment of advanced cancer patients has some disadvantages. Along with fatigue, grade 3 and 4 adverse events affecting the gastrointestinal tract (abdominal pain, nausea, vomiting, diarrhoea), and skin (pruritus, rash) are consistently observed (Borghaei *et al.*, 2015; Brahmer *et al.*, 2012; Camacho, 2015; Chuk *et al.*, 2017; Hazarika *et al.*, 2017; Lipson and Drake, 2011; Topalian *et al.*, 2014). Importantly, due to the immune stimulatory action of immune checkpoint inhibitors, immune related adverse events (irAEs) need to be identified and appropriate action taken early to avoid serious irAEs. Immune related adverse events include pneumonitis, hypothyroidism, hyperthyroidism, colitis, nephritis, hypophysitis and hepatitis. Guidelines have been implemented when using immune checkpoint inhibitors including administration of corticosteroids when an irAE is suspected or cessation of treatment. Patients with underlying autoimmune disorders should be treated with extreme caution, if at all (Camacho, 2015; Lipson and Drake, 2011).

Along with anti-CTLA-4 and anti-PD-1 as suitable immune checkpoint inhibitors for PC, lymphocyte activation gene-3 (LAG-3) would concomitantly be an appropriate target molecule in PC. LAG-3 binds to MHC class II molecules on dendritic cells

leading to maturation into APCs and an increased antigen specific CD8 T cell response. LAG-3 also negatively regulates CD8 T cell function by binding to T cell receptors (Triebel, 2003). LAG-3 is a particularly suitable target in PC due to the high level of Tregs and MDSCs within the TME that suppress CD8 T cell function (Zhan *et al.*, 2017). Thus, if Treg and MDSC binding is blocked, CD8 T cell activation and proliferation would be permitted. There are currently no LAG-3 immune checkpoint inhibitors approved by the USFDA for the treatment of malignancies.

IMP321 is a LAG-3 immune checkpoint inhibitor currently undergoing clinical investigation by Immutep Ltd. with significant promise in malignancies including breast, renal cell carcinoma, and advanced PC. IMP321 binds to MHC class II molecules on dendritic cells causing dendritic cell maturation into APCs and production of tumour specific CD8 T cells. The binding of IMP321 to MHC class II molecules on dendritic cells also inhibits binding of CD8 T cells to dendritic cells, and thus, allows perpetual CD8 T cell proliferation and an anti-tumour response (Fougeray *et al.*, 2006; Li *et al.*, 2015b). Unlike other immune checkpoint inhibitors, IMP321 has a low toxicity profile. From three clinical trials involving a total of 68 evaluable patients there were no grade 3 or 4 IMP321 related adverse events recorded (Brignone *et al.*, 2009; Brignone *et al.*, 2010; Wang-Gillam *et al.*, 2012).

Investigation of CVA21 in combination with anti-CTLA-4, anti-PD-1, and anti-LAG-3 checkpoint inhibitors in the established mouse model is proposed. If increased activity is observed when CAVATAK™ is administered in combination with these agents as doublet, triplet, or even quadruplet treatment regimens, there would be substantial indication to translate investigations into the clinical setting. CVA21 may turn PC into a 'heated' immunological environment allowing the checkpoint inhibitors to have their intended effect on PC. It would be particularly interesting to investigate CAVATAK™ in combination with a mouse homolog of IMP321. Both CAVATAK™ and IMP321 are suitable treatments for PC that have shown anti-tumour efficacy, excellent tolerability, and stimulation of an anti-tumour immune response in neoplasms.

In summary, substantial progress towards developing an immune competent mouse model of orthotopic PC susceptible to CVA21 has been achieved. Future studies will optimise and verify the model to allow for combination studies of CAVATAK™ with immune checkpoint inhibitors. Although there are several limitations to the mouse

model, if results are promising from combination studies, there would be considerable indication to translate research into a combination clinical trial.

7.4 Concluding Remarks

Taken together, this body of work has highlighted CVA21 is a suitable, generally well tolerated and potentially efficacious anti-cancer agent for the treatment of pancreatic cancer. Further detailed investigations are required to overcome immune-competent animal model limitations and optimise experimental protocols. However, the data presented in this dissertation already provides evidence to translate research into the clinical setting. A clinical trial could be initiated to investigate CVA21 (in combination with immune checkpoint inhibitors) in comparison with gemcitabine as a treatment for PC. Redundancy of gemcitabine as a treatment could be accomplished and improvement in treatment options for PC could potentially be achieved for society.

Chapter 8

References

Abraham, S. C., Klimstra, D. S., Wilentz, R. E., Yeo, C. J., Conlon, K., Brennan, M., Cameron, J. L., Wu, T.-T. and Hruban, R. H. (2002). Solid-pseudopapillary tumors of the pancreas are genetically distinct from pancreatic ductal adenocarcinomas and almost always harbor beta-catenin mutations. *Am. J. Pathol.* **160**, 1361–1369.

Abratt, R. P., Bezwoda, W. R., Falkson, G., Goedhals, L., Hacking, D. and Rugg, T. A. (1994). Efficacy and safety profile of gemcitabine in non-small-cell lung cancer: a phase II study. *J. Clin. Oncol.* **12**, 1535–1540.

Adair, R. A., Roulstone, V., Scott, K. J., Morgan, R., Nuovo, G. J., Fuller, M., Beirne, D., West, E. J., Jennings, V. A., Rose, A., et al. (2012). Cell carriage, delivery, and selective replication of an oncolytic virus in tumor in patients. *Science Translational Medicine* **4**, 138ra77.

Adamek, H. E., Albert, J., Breer, H., Weitz, M., Schilling, D. and Riemann, J. F. (2000). Pancreatic cancer detection with magnetic resonance cholangiopancreatography and endoscopic retrograde cholangiopancreatography: a prospective controlled study. *Lancet* **356**, 190–193.

Adams, M. J., Lefkowitz, E. J., King, A. M. Q., Harrach, B., Harrison, R. L., Knowles, N. J., Kropinski, A. M., Krupovic, M., Kuhn, J. H., Mushegian, A. R., et al. (2017). Changes to taxonomy and the International Code of Virus Classification and Nomenclature ratified by the International Committee on Taxonomy of Viruses (2017). *Arch Virol* **162**, 2505–2538.

Adamska, A., Domenichini, A. and Falasca, M. (2017). Pancreatic Ductal Adenocarcinoma: Current and Evolving Therapies. *international journal of molecular sciences* **18**, 1–43.

Ahlgren, J. D. (1996). Epidemiology and risk factors in pancreatic cancer. *Semin Oncol* **23**, 241–250.

Ahlquist, P. and Kaesberg, P. (1979). Determination of the length distribution of poly(A) at the 3′ terminus of the virion RNAs of EMC virus, poliovirus, rhinovirus, RAV-61 and CPMV and of mouse globin mRNA. *Nucleic Acids Res.* **7**, 1195–1204.

AIHW (2017). *Australian Institute of Health and Welfare: Cancer in Australia 2017. Cancer Series no. 101. Cat. no. CAN 100*. Canberra: aihw.gov.au.

Al-Hawary, M. M., Francis, I. R. and Anderson, M. A. (2015). Pancreatic Solid and Cystic Neoplasms: Diagnostic Evaluation and Intervention. *Radiol. Clin. North Am.* **53**, 1037–1048.

Aldabe, R. and Carrasco, L. (1995). Induction of membrane proliferation by poliovirus proteins 2C and 2BC. *Biochem. Biophys. Res. Commun.* **206**, 64–76.

Alexandrov, L. B., Nik-Zainal, S., Wedge, D. C., Aparicio, S. A. J. R., Behjati, S., Biankin, A. V., Bignell, G. R., Bolli, N., Borg, A., Børresen-Dale, A.-L., et al. (2013). Signatures of mutational processes in human cancer. *Nature* **500**, 415–421.

Almoguera, C., Shibata, D., Forrester, K., Martin, J., Arnheim, N. and Perucho, M. (1988). Most human carcinomas of the exocrine pancreas contain mutant c-K-ras genes. *Cell* **53**, 549–554.

Altieri, B., Grant, W. B., Casa, Della, S., Orio, F., Pontecorvi, A., Colao, A., Sarno, G. and Muscogiuri, G. (2017). Vitamin D and pancreas: The role of sunshine vitamin in the pathogenesis of diabetes mellitus and pancreatic cancer. *Crit Rev Food Sci Nutr* **57**, 3472–3488.

Ambros, V. and Baltimore, D. (1978). Protein is linked to the 5' end of poliovirus RNA by a phosphodiester linkage to tyrosine. *J. Biol. Chem.* **253**, 5263–5266.

Amin, M. B., Edge, S., Greene, F. L., Byrd, D. R., Brookland, R. K., Washington, M. K., Gershenwald, J. E., Compton, C. C., Hess, K. R., Sullivan, D. C., et al. (2016). *AJCC Cancer Staging Manual*. Springer.

Amundadottir, L., Kraft, P., Stolzenberg-Solomon, R. Z., Fuchs, C. S., Petersen, G. M., Arslan, A. A., Bueno-de-Mesquita, H. B., Gross, M., Helzlsouer, K., Jacobs, E. J., et al. (2009). Genome-wide association study identifies variants in

the ABO locus associated with susceptibility to pancreatic cancer. *Nat. Genet.* **41**, 986–990.

Andtbacka, R. H. I., Curti, B. D., Kaufman, H., Daniels, G. A., Nemunaitis, J. J., Spitler, L. E., Hallmeyer, S., Lutzky, J., Schultz, S. M., Whitman, E. D., et al. (2015a). Final data from CALM: A phase II study of Coxsackievirus A21 (CVA21) oncolytic virus immunotherapy in patients with advanced melanoma. *J. Clin. Oncol.* **33**, 9030.

Andtbacka, R. H. I., Kaufman, H. L., Collichio, F., Amatruda, T., Senzer, N., Chesney, J., Delman, K. A., Spitler, L. E., Puzanov, I., Agarwala, S. S., et al. (2015b). Talimogene Laherparepvec Improves Durable Response Rate in Patients With Advanced Melanoma. *J. Clin. Oncol.* **33**, 2780–2788.

Ansardi, D. C., Porter, D. C. and Morrow, C. D. (1992). Myristylation of poliovirus capsid precursor P1 is required for assembly of subviral particles. *J. Virol.* **66**, 4556–4563.

Aoki, K. and Ogawa, H. (1978). Cancer of the pancreas international mortality trends. *World Health Statistics Report* **31**, 2–27.

Apte, M. V., Haber, P. S., Applegate, T. L., Norton, I. D., McCaughan, G. W., Korsten, M. A., Pirola, R. C. and Wilson, J. S. (1998). Periacinar stellate shaped cells in rat pancreas: identification, isolation, and culture. *Gut* **43**, 128–133.

Apte, M. V., Haber, P. S., Darby, S. J., Rodgers, S. C., McCaughan, G. W., Korsten, M. A., Pirola, R. C. and Wilson, J. S. (1999). Pancreatic stellate cells are activated by proinflammatory cytokines: implications for pancreatic fibrogenesis. *Gut* **44**, 534–541.

Apte, M. V., Pirola, R. C. and Wilson, J. S. (2012). Pancreatic stellate cells: a starring role in normal and diseased pancreas. *Front Physiol* **3**, 344.

Apte, M. V., Wilson, J. S., Lugea, A. and Pandol, S. J. (2013). A starring role for stellate cells in the pancreatic cancer microenvironment. *Gastroenterology* **144**, 1210–1219.

Apte, M. V., Xu, Z., Pothula, S., Goldstein, D., Pirola, R. C. and Wilson, J. S.

(2015a). Pancreatic cancer: The microenvironment needs attention too! *Pancreatology* **15**, S32–8.

Apte, M., Pirola, R. C. and Wilson, J. S. (2015b). Pancreatic stellate cell: physiologic role, role in fibrosis and cancer. *Current Opinion in Gastroenterology* **31**, 416–423.

Armulik, A., Genové, G. and Betsholtz, C. (2011). Pericytes: developmental, physiological, and pathological perspectives, problems, and promises. *Dev. Cell* **21**, 193–215.

Aronsson, L., Andersson, R. and Ansari, D. (2017). Intraductal papillary mucinous neoplasm of the pancreas - epidemiology, risk factors, diagnosis, and management. *Scand. J. Gastroenterol.* **52**, 803–815.

Arsene, D., Ardeleanu, C. and care, C. F. T. U. O. T. G. F. T. (2014). Adhesion cell molecules as potential markers of aggressiveness in meningiomas. *Rom J Morphol Embryol* **55**, 585–589.

Asagi, A., Ohta, K., Nasu, J., Tanada, M., Nadano, S., Nishimura, R., Teramoto, N., Yamamoto, K., Inoue, T. and Iguchi, H. (2013). Utility of Contrast-Enhanced FDG-PET/CT in the Clinical Management of Pancreatic Cancer. *Pancreas* **42**, 11–19.

Au, G. G., Beagley, L. G., Haley, E. S., Barry, R. D. and Shafren, D. R. (2011). Oncolysis of malignant human melanoma tumors by Coxsackieviruses A13, A15 and A18. *Virology Journal 2011 8:1* **8**, 22.

Au, G. G., Lincz, L. F., Enno, A. and Shafren, D. R. (2007). Oncolytic Coxsackievirus A21 as a novel therapy for multiple myeloma. *Br. J. Haematol.* **137**, 133–141.

Au, G. G., Lindberg, A. M., Barry, R. D. and Shafren, D. R. (2005). Oncolysis of vascular malignant human melanoma tumors by Coxsackievirus A21. *Int. J. Oncol.* **26**, 1471–1476.

Bachem, M. G., Schneider, E., Groß, H., Weidenbach, H., Schmid, R. M., Menke, A., Siech, M., Beger, H., Grünert, A. and Adler, G. (1998). Identification, culture, and characterization of pancreatic stellate cells in rats and humans. *Gastroenterology* **115**, 421–432.

Bachem, M. G., Schünemann, M., Ramadani, M., Siech, M., Beger, H., Buck, A., Zhou, S., Schmid-Kotsas, A. and Adler, G. (2005). Pancreatic carcinoma cells induce fibrosis by stimulating proliferation and matrix synthesis of stellate cells. *Gastroenterology* **128**, 907–921.

Bachem, M. G., Zhou, S., Buck, K., Schneiderhan, W. and Siech, M. (2008). Pancreatic stellate cells—role in pancreas cancer. *Langenbecks Arch Surg* **393**, 891–900.

Baghurst, P. A., McMichael, A. J., Slavotinek, A. H., Baghurst, K. I., Boyle, P. and Walker, A. M. (1991). A Case-Control Study of Diet and Cancer of the Pancreas. *Am. J. Epidemiol.* **134**, 167–179.

Bagnardi, V., Rota, M., Botteri, E., Tramacere, I., Islami, F., Fedirko, V., Scotti, L., Jenab, M., Turati, F., Pasquali, E., et al. (2014). Alcohol consumption and site-specific cancer risk: a comprehensive dose–response meta-analysis. *British Journal of Cancer* **112**, 580–593.

Bailey, P., Chang, D. K., Nones, K., Johns, A. L., Patch, A.-M., Gingras, M.-C., Miller, D. K., Christ, A. N., Bruxner, T. J. C., Quinn, M. C., et al. (2016). Genomic analyses identify molecular subtypes of pancreatic cancer. *Nature* **531**, 47–52.

Ballehaninna, U. K. and Chamberlain, R. S. (2012). The clinical utility of serum CA 19-9 in the diagnosis, prognosis and management of pancreatic adenocarcinoma: An evidence based appraisal. *J Gastrointest Oncol* **3**, 105–119.

Banks, R. E., Gearing, A. J., Hemingway, I. K., Norfolk, D. R., Perren, T. J. and Selby, P. J. (1993). Circulating intercellular adhesion molecule-1 (ICAM-1), E-selectin and vascular cell adhesion molecule-1 (VCAM-1) in human malignancies. *British Journal of Cancer* **68**, 122–124.

Bao, Y., Ng, K., Wolpin, B. M., Michaud, D. S., Giovannucci, E. and Fuchs, C. S. (2010). Predicted vitamin D status and pancreatic cancer risk in two prospective cohort studies. *British Journal of Cancer* **102**, 1422–1427.

Barish, M. A., Yucel, E. K. and Ferrucci, J. T. (1999). Magnetic Resonance Cholangiopancreatography. *N Engl J Med* **341**, 258–264.

Barone, E., Corrado, A., Gemignani, F. and Landi, S. (2016). Environmental risk factors for pancreatic cancer: an update. *Archives of Toxicology* **90**, 2617–2642.

Barreto, S. G. (2016). How does cigarette smoking cause acute pancreatitis? *Pancreatology* **16**, 157–163.

Bartel, M. J. and Raimondo, M. (2017). Endoscopic Management of Pancreatic Cysts. *Dig. Dis. Sci.* **62**, 1808–1815.

Barton, D. J. and Flanegan, J. B. (1997). Synchronous replication of poliovirus RNA: initiation of negative-strand RNA synthesis requires the guanidine-inhibited activity of protein 2C. *J. Virol.* **71**, 8482–8489.

Barugola, G., Falconi, M., Bettini, R., Boninsegna, L., Casarotto, A., Salvia, R., Bassi, C. and Pederzoli, P. (2007). The determinant factors of recurrence following resection for ductal pancreatic cancer. *JOP* **8**, 132–140.

Basavappa, R., Syed, R., Flore, O., Icenogle, J. P., Filman, D. J. and Hogle, J. M. (1994). Role and mechanism of the maturation cleavage of VP0 in poliovirus assembly: structure of the empty capsid assembly intermediate at 2.9 A resolution. *Protein Sci.* **3**, 1651–1669.

Basturk, O., Zamboni, G., Klimstra, D. S., Capelli, P., Andea, A., Kamel, N. S. and Adsay, N. V. (2007). Intraductal and Papillary Variants of Acinar Cell Carcinomas. *The American Journal of Surgical Pathology* **31**, 363–370.

Bausch, D., Pausch, T., Krauss, T., Hopt, U. T., Fernandez-del-Castillo, C., Warshaw, A. L., Thayer, S. P. and Keck, T. (2011). Neutrophil granulocyte derived MMP-9 is a VEGF independent functional component of the angiogenic switch in pancreatic ductal adenocarcinoma. *Angiogenesis* **14**, 235–243.

Bayne, L. J., Beatty, G. L., Jhala, N., Clark, C. E., Rhim, A. D., Stanger, B. Z. and Vonderheide, R. H. (2012). Tumor-derived granulocyte-macrophage colony-stimulating factor regulates myeloid inflammation and T cell immunity in pancreatic cancer. *Cancer Cell* **21**, 822–835.

Bayo-Puxan, N., Gimenez-Alejandre, M., Lavilla-Alonso, S., Gros, A., Cascallo, M., Hemminki, A. and Alemany, R. (2009). Replacement of adenovirus type 5 fiber

shaft heparan sulfate proteoglycan-binding domain with RGD for improved tumor infectivity and targeting. *Hum. Gene Ther.* **20**, 1214–1221.

Bektas, A., Schuman, S. H., Sen, R. and Ferrucci, L. (2017). Human T cell immunosenescence and inflammation in aging. *J Leukoc Biol.* **102**, 977–988.

Bergamini, G., Preiss, T. and Hentze, M. W. (2000). Picornavirus IRESes and the poly(A) tail jointly promote cap-independent translation in a mammalian cell-free system. *RNA* **6**, 1781–1790.

Berry, L. J., Au, G. G., Barry, R. D. and Shafren, D. R. (2008). Potent oncolytic activity of human enteroviruses against human prostate cancer. *Prostate* **68**, 577–587.

Bhella, D., Goodfellow, I. G., Roversi, P., Pettigrew, D., Chaudhry, Y., Evans, D. J. and Lea, S. M. (2004). The Structure of Echovirus Type 12 Bound to a Two-domain Fragment of Its Cellular Attachment Protein Decay-accelerating Factor (CD 55). *J. Biol. Chem.* **279**, 8325–8332.

Biankin, A. V., Waddell, N., Kassahn, K. S., Gingras, M.-C., Muthuswamy, L. B., Johns, A. L., Miller, D. K., Wilson, P. J., Patch, A.-M., Wu, J., et al. (2012). Pancreatic cancer genomes reveal aberrations in axon guidance pathway genes. *Nature* **491**, 399–405.

Bien, E., Godzinski, J., Dall'igna, P., Defachelles, A.-S., Stachowicz-Stencel, T., Orbach, D., Bisogno, G., Cecchetto, G., Warmann, S., Ellerkamp, V., et al. (2011). Pancreatoblastoma: a report from the European cooperative study group for paediatric rare tumours (EXPeRT). *Eur. J. Cancer* **47**, 2347–2352.

Bierman, H. R., Crile, D. M., Dod, K. S., Kelly, K. H., Petrakis, N. L., White, L. P. and Shimkin, M. B. (1953). Remissions in leukemia of childhood following acute infectious disease: staphylococcus and streptococcus, varicella, and feline panleukopenia. *Cancer* **6**, 591–605.

Binnerts, M. E., van Kooyk, Y., Simmons, D. L. and Figdor, C. G. (1994). Distinct binding of T lymphocytes to ICAM-1, -2 or -3 upon activation of LFA-1. *Eur. J. Immunol.* **24**, 2155–2160.

Bischoff, J. R., Kirn, D. H., Williams, A., Heise, C., Horn, S., Muna, M., Ng, L., Nye, J. A., Sampson-Johannes, A., Fattaey, A., et al. (1996). An adenovirus mutant that replicates selectively in p53-deficient human tumor cells. *Science* **274**, 373–376.

Blackford, A., Parmigiani, G., Kensler, T. W., Wolfgang, C., Jones, S., Zhang, X., Parsons, D. W., Lin, J. C.-H., Leary, R. J., Eshleman, J. R., et al. (2009). Genetic mutations associated with cigarette smoking in pancreatic cancer. *Cancer Research* **69**, 3681–3688.

Blank, H. (1949). Virus diseases affecting the skin. *Acta Derm Venereol* **29**, 77–107.

Bluming, A. Z. and Ziegler, J. L. (1971). Regression of Burkitt's lymphoma in association with measles infection. *The Lancet* **2**, 105–106.

Bolm, L., Cigolla, S., Wittel, U. A., Hopt, U. T., Keck, T., Rades, D., Bronsert, P. and Wellner, U. F. (2017). The Role of Fibroblasts in Pancreatic Cancer: Extracellular Matrix Versus Paracrine Factors. *Transl Oncol* **10**, 578–588.

Boon, den, J. A., Diaz, A. and Ahlquist, P. (2010). Cytoplasmic viral replication complexes. *Cell Host & Microbe* **8**, 77–85.

Borazanci, E., Dang, C. V., Robey, R. W., Bates, S. E., Chabot, J. A. and Hoff, Von, D. D. (2017). Pancreatic Cancer: “A Riddle Wrapped in a Mystery inside an Enigma.” *Clinical Cancer Research* **23**, 1629–1637.

Borghaei, H., Paz-Ares, L., Horn, L., Spigel, D. R., Steins, M., Ready, N. E., Chow, L. Q., Vokes, E. E., Felip, E., Holgado, E., et al. (2015). Nivolumab versus Docetaxel in Advanced Nonsquamous Non-Small-Cell Lung Cancer. *N Engl J Med* **373**, 1627–1639.

Bosetti, C., Lucenteforte, E., Silverman, D. T., Petersen, G., Bracci, P. M., Ji, B. T., Negri, E., Li, D., Risch, H. A., Olson, S. H., et al. (2012). Cigarette smoking and pancreatic cancer: an analysis from the International Pancreatic Cancer Case-Control Consortium (Panc4). *Ann. Oncol.* **23**, 1880–1888.

Bosman, F. T., Carneiro, F. and Hruban, R. H. (2010). *WHO Classification of Tumours of the Digestive System*. 4 ed. World Health Organization.

Boulay, B. R. and Parepally, M. (2014). Managing malignant biliary obstruction in pancreas cancer: choosing the appropriate strategy. *World Journal of Gastroenterology : WJG* **20**, 9345–9353.

Bournet, B., Gayral, M., Torrisani, J., Selves, J., Cordelier, P. and Buscail, L. (2014). Role of endoscopic ultrasound in the molecular diagnosis of pancreatic cancer. *World Journal of Gastroenterology : WJG* **20**, 10758–10768.

Bradley, S., Jakes, A. D., Harrington, K., Pandha, H., Melcher, A. and Errington-Mais, F. (2014). Applications of coxsackievirus A21 in oncology. *Oncolytic Virotherapy* **3**, 47–55.

Brahmer, J. R., Tykodi, S. S., Chow, L. Q. M., Hwu, W.-J., Topalian, S. L., Hwu, P., Drake, C. G., Camacho, L. H., Kauh, J., Odunsi, K., et al. (2012). Safety and activity of anti-PD-L1 antibody in patients with advanced cancer. *N Engl J Med* **366**, 2455–2465.

Brand, R. E., Nolen, B. M., Zeh, H. J., Allen, P. J., Eloubeidi, M. A., Goldberg, M., Elton, E., Arnoletti, J. P., Christein, J. D., Vickers, S. M., et al. (2011). Serum biomarker panels for the detection of pancreatic cancer. *Clin. Cancer Res.* **17**, 805–816.

Brignone, C., Escudier, B., Grygar, C., Marcu, M. and Triebel, F. (2009). A phase I pharmacokinetic and biological correlative study of IMP321, a novel MHC class II agonist, in patients with advanced renal cell carcinoma. *Clin. Cancer Res.* **15**, 6225–6231.

Brignone, C., Gutierrez, M., Mefti, F., Brain, E., Jarcau, R., Cvitkovic, F., Bousetta, N., Medioni, J., Gligorov, J., Grygar, C., et al. (2010). First-line chemoimmunotherapy in metastatic breast carcinoma: combination of paclitaxel and IMP321 (LAG-3Ig) enhances immune responses and antitumor activity. *J Transl Med* **8**, 71.

Brodbeck, W. G., Liu, D., Sperry, J., Mold, C. and Medof, M. E. (1996). Localization of classical and alternative pathway regulatory activity within the decay-accelerating factor. *J. Immunol.* **156**, 2528–2533.

Brown, B. A., Maher, K., Flemister, M. R., Naraghi-Arani, P., Uddin, M., Oberste,

M. S. and Pallansch, M. A. (2009). Resolving ambiguities in genetic typing of human enterovirus species C clinical isolates and identification of enterovirus 96, 99 and 102. *J. Gen. Virol.* **90**, 1713–1723.

Brown, B., Oberste, M. S., Maher, K. and Pallansch, M. A. (2003). Complete genomic sequencing shows that polioviruses and members of human enterovirus species C are closely related in the noncapsid coding region. *J. Virol.* **77**, 8973–8984.

Broz, M. L., Binnewies, M., Boldajipour, B., Nelson, A. E., Pollack, J. L., Erle, D. J., Barczak, A., Rosenblum, M. D., Daud, A., Barber, D. L., et al. (2014). Dissecting the Tumor Myeloid Compartment Reveals Rare Activating Antigen-Presenting Cells Critical for T Cell Immunity. *Cancer Cell* **26**, 638–652.

Brunet, J. F., Denizot, F., Luciani, M. F., Roux-Dosseto, M., Suzan, M., Mattei, M. G. and Golstein, P. (1987). A new member of the immunoglobulin superfamily--CTLA-4. *Nature* **328**, 267–270.

Bryant, K. L., Mancias, J. D., Kimmelman, A. C. and Der, C. J. (2014). KRAS: feeding pancreatic cancer proliferation. *Trends Biochem. Sci.* **39**, 91–100.

Burris, H. A., Moore, M. J., Andersen, J., Green, M. R., Rothenberg, M. L., Modiano, M. R., Cripps, M. C., Portenoy, R. K., Storniolo, A. M., Tarassoff, P., et al. (1997). Improvements in survival and clinical benefit with gemcitabine as first-line therapy for patients with advanced pancreas cancer: a randomized trial. *J. Clin. Oncol.*

Bynigeri, R. R., Jakkampudi, A., Jangala, R., Subramanyam, C., Sasikala, M., Rao, G. V., Reddy, D. N. and Talukdar, R. (2017). Pancreatic stellate cell: Pandora's box for pancreatic disease biology. *World Journal of Gastroenterology : WJG* **23**, 382–405.

Caldas, C., Hahn, S. A., Da Costa, L. T., Redston, M. S., Schutte, M., Seymour, A. B., Weinstein, C. L., Hruban, R. H., Yeo, C. J. and Kern, S. E. (1994). Frequent somatic mutations and homozygous deletions of the p16 (MTS1) gene in pancreatic adenocarcinoma. *Nat. Genet.* **8**, 27–32.

Callender, G. G., Rich, T. A. and Perrier, N. D. (2008). Multiple Endocrine Neoplasia

Syndromes. *Surgical Clinics of North America* **88**, 863–895.

Camacho, L. H. (2015). CTLA-4 blockade with ipilimumab: biology, safety, efficacy, and future considerations. *Cancer Med* **4**, 661–672.

Cannon, A., Thompson, C., Hall, B. R., Jain, M., Kumar, S. and Batra, S. K. (2018). Desmoplasia in pancreatic ductal adenocarcinoma: insight into pathological function and therapeutic potential. *Genes Cancer* **9**, 78–86.

Carew, J. S., Espitia, C. M., Zhao, W., Kelly, K. R., Coffey, M., Freeman, J. W. and Nawrocki, S. T. (2013). Reolysin is a novel reovirus-based agent that induces endoplasmic reticular stress-mediated apoptosis in pancreatic cancer. *Cell Death Dis* **4**, e728.

Carey, T. E., Takahashi, T., Resnick, L. A., Oettgen, H. F. and Old, L. J. (1976). Cell surface antigens of human malignant melanoma: mixed hemadsorption assays for humoral immunity to cultured autologous melanoma cells. *Proc. Natl. Acad. Sci. U.S.A.* **73**, 3278–3282.

Casper, E. S., Green, M. R., Kelsen, D. P., Heelan, R. T., Brown, T. D., Flombaum, C. D., Trochanowski, B. and Tarassoff, P. G. (1994). Phase II trial of gemcitabine (2,2'-difluorodeoxycytidine) in patients with adenocarcinoma of the pancreas. *Invest New Drugs* **12**, 29–34.

Cassel, W. A. and Murray, D. R. (1992). A ten-year follow-up on stage II malignant melanoma patients treated postsurgically with Newcastle disease virus oncolysate. *Med Oncol Tumor Pharmacother* **9**, 169–171.

Chang, D. Z., Ma, Y., Ji, B., Wang, H., Deng, D., Liu, Y., Abbruzzese, J. L., Liu, Y.-J., Logsdon, C. D. and Hwu, P. (2011). Mast cells in tumor microenvironment promotes the in vivo growth of pancreatic ductal adenocarcinoma. *Clin. Cancer Res.* **17**, 7015–7023.

Chang, J. H., Jiang, Y. and Pillarisetty, V. G. (2016). Role of immune cells in pancreatic cancer from bench to clinical application: An updated review. *Medicine (Baltimore)* **95**, e5541.

Chang, K. J., Senzer, N. N., Binmoeller, K., Goldsweig, H. and Coffin, R. (2012).

Phase I dose-escalation study of talimogene laherparepvec (T-VEC) for advanced pancreatic cancer (ca). *J. Clin. Oncol.* **30**, e14546.

Chang, M.-C., Wong, J.-M. and Chang, Y.-T. (2014). Screening and early detection of pancreatic cancer in high risk population. *World Journal of Gastroenterology : WJG* **20**, 2358–2364.

Chen, J., Yang, R., Lu, Y., Xia, Y. and Zhou, H. (2012). Diagnostic accuracy of endoscopic ultrasound-guided fine-needle aspiration for solid pancreatic lesion: a systematic review. *J. Cancer Res. Clin. Oncol.* **138**, 1433–1441.

Chen, W. H., Horoszewicz, J. S., Leong, S. S., Shimano, T., Penetrante, R., Sanders, W. H., Berjian, R., Douglass, H. O., Martin, E. W. and Chu, T. M. (1982). Human pancreatic adenocarcinoma: in vitro and in vivo morphology of a new tumor line established from ascites. *In Vitro* **18**, 24–34.

Cheng, X.-B., Kohi, S., Koga, A., Hirata, K. and Sato, N. (2016). Hyaluronan stimulates pancreatic cancer cell motility. *Oncotarget* **7**, 4829–4840.

Cho, I.-R., Kaowinn, S., Moon, J., Soh, J., Kang, H. Y., Jung, C.-R., Oh, S., Song, H., Koh, S. S. and Chung, Y.-H. (2015). Oncotropic H-1 parvovirus infection degrades HIF-1α protein in human pancreatic cancer cells independently of VHL and RACK1. *Int. J. Oncol.* **46**, 2076–2082.

Cho, M. W., Teterina, N., Egger, D., Bienz, K. and Ehrenfeld, E. (1994). Membrane rearrangement and vesicle induction by recombinant poliovirus 2C and 2BC in human cells. *Virology* **202**, 129–145.

Chuk, M. K., Chang, J. T., Theoret, M. R., Sampene, E., He, K., Weis, S. L., Helms, W. S., Jin, R., Li, H., Yu, J., et al. (2017). FDA Approval Summary: Accelerated Approval of Pembrolizumab for Second-Line Treatment of Metastatic Melanoma. *Clin. Cancer Res.* **23**, 5666–5670.

Chun, Y. S., Pawlik, T. M. and Vauthey, J.-N. (2017). 8th Edition of the AJCC Cancer Staging Manual: Pancreas and Hepatobiliary Cancers. *Ann Surg Oncol*.

Cicenas, J., Kvederaviciute, K., Meskinyte, I., Meskinyte-Kausiliene, E., Skeberdyte, A. and Cicenas, J. (2017). KRAS, TP53, CDKN2A, SMAD4, BRCA1,

and BRCA2 Mutations in Pancreatic Cancer. *Cancers (Basel)* **9**.

Cingolani, N., Shaco-Levy, R., Farruggio, A. and Klimstra, D. S. (2000). Alpha-fetoprotein production by pancreatic tumors exhibiting acinar cell differentiation: Study of five cases, one arising in a mediastinal teratoma. *Hum. Pathol.* **31**, 938–944.

Clark, C. E., Hingorani, S. R., Mick, R., Combs, C., Tuveson, D. A. and Vonderheide, R. H. (2007). Dynamics of the Immune Reaction to Pancreatic Cancer from Inception to Invasion. *Cancer Research* **67**, 9518–9527.

Coakley, F. V. and Schwartz, L. H. (1999). Magnetic resonance cholangiopancreatography. *J. Magn. Reson. Imaging* **9**, 157–162.

Coffey, M. C., Strong, J. E., Forsyth, P. A. and Lee, P. W. (1998). Reovirus therapy of tumors with activated Ras pathway. *Science* **282**, 1332–1334.

Colvin, E. K. and Scarlett, C. J. (2014). A historical perspective of pancreatic cancer mouse models. *Semin. Cell Dev. Biol.* **27**, 96–105.

Conroy, T., Bachet, J.-B., Ayav, A., Huguet, F., Lambert, A., Caramella, C., Maréchal, R., Van Laethem, J.-L. and Ducreux, M. (2016). Current standards and new innovative approaches for treatment of pancreatic cancer. *European Journal of Cancer* **57**, 10–22.

Conroy, T., Desseigne, F., Ychou, M., Bouché, O., Guimbaud, R., Bécouarn, Y., Adenis, A., Raoul, J.-L., Gourgou-Bourgade, S., la Fouchardière, de, C., et al. (2011). FOLFIRINOX versus Gemcitabine for Metastatic Pancreatic Cancer. *N Engl J Med* **364**, 1817–1825.

Corrigan, P. A., Beaulieu, C., Patel, R. B. and Lowe, D. K. (2017). Talimogene Laherparepvec: An Oncolytic Virus Therapy for Melanoma. *Ann Pharmacother* **51**, 675–681.

Cowley, M. J., Chang, D. K., Pajic, M., Johns, A. L., Waddell, N., Grimmond, S. M. and Biankin, A. V. (2013). Understanding pancreatic cancer genomes. *J Hepatobiliary Pancreat Sci* **20**, 549–556.

Crivellato, E., Nico, B. and Ribatti, D. (2008). Mast cells and tumour angiogenesis:

new insight from experimental carcinogenesis. *Cancer Lett.* **269**, 1–6.

Cui, R., Yue, W., Lattime, E. C., Stein, M. N., Xu, Q. and Tan, X.-L. (2016). Targeting tumor-associated macrophages to combat pancreatic cancer. *Oncotarget* **7**, 50735–50754.

Curti, B., Richards, J., Hallmeyer, S., Faries, M., Andtbacka, R., Daniels, G., Grose, M. and Shafren, D. R. (2017). Abstract CT114: The MITCI (Phase 1b) study: A novel immunotherapy combination of intralesional Coxsackievirus A21 and systemic ipilimumab in advanced melanoma patients with or without previous immune checkpoint therapy treatment. *Cancer Res* **77**, CT114–CT114.

Daste, A., Domblides, C., Gross-Goupil, M., Chakiba, C., Quivy, A., Cochin, V., de Mones, E., Larmonier, N., Soubeyran, P. and Ravaud, A. (2017). Immune checkpoint inhibitors and elderly people: A review. *Eur. J. Cancer* **82**, 155–166.

De Monte, L., Reni, M., Tassi, E., Clavenna, D., Papa, I., Recalde, H., Braga, M., Di Carlo, V., Doglioni, C. and Protti, M. P. (2011). Intratumor T helper type 2 cell infiltrate correlates with cancer-associated fibroblast thymic stromal lymphopoietin production and reduced survival in pancreatic cancer. *Journal of Experimental Medicine* **208**, 469–478.

De Vita, F., Ventriglia, J., Febbraro, A., Laterza, M. M., Fabozzi, A., Savastano, B., Petrillo, A., Diana, A., Giordano, G., Troiani, T., et al. (2016). NAB-paclitaxel and gemcitabine in metastatic pancreatic ductal adenocarcinoma (PDAC): from clinical trials to clinical practice. *BMC Cancer* **16**, 709.

Dekel, B., Yoeli, R., Shulman, L., Padeh, S. and Passwell, J. H. (2002). Localized thigh swelling mimicking a neoplastic process: involvement of coxsackie virus type A21. *Acta Paediatr.* **91**, 357–359.

Deng, T., Lyon, C. J., Bergin, S., Caligiuri, M. A. and Hsueh, W. A. (2016). Obesity, Inflammation, and Cancer. *Annu Rev Pathol* **11**, 421–449.

DePace, N. (1912). Sulla scomparsa di un enome canco vegetante del collo dell'utero senza cura chirurgica. *La Genecologia* **9**, 82–88.

Dhebri, A. R., Connor, S., Campbell, F., Ghaneh, P. and Sutton, R. (2004).

Diagnosis, treatment and outcome of pancreatoblastoma. *Pancreatology* **4**, 441–453.

Diaconu, I., Cerullo, V., Hirvinen, M. L. M., Escutenaire, S., Ugolini, M., Pesonen, S. K., Bramante, S., Parviainen, S., Kanerva, A., Loskog, A. S. I., et al. (2012). Immune Response Is an Important Aspect of the Antitumor Effect Produced by a CD40L-Encoding Oncolytic Adenovirus. *Cancer Research* **72**, 2327–2338.

Diamond, M. S. and Springer, T. A. (1993). A subpopulation of Mac-1 (CD11b/CD18) molecules mediates neutrophil adhesion to ICAM-1 and fibrinogen. *The Journal of Cell Biology* **120**, 545–556.

Diamond, M. S., Staunton, D. E., de Fougerolles, A. R., Stacker, S. A., Garcia-Aguilar, J., Hibbs, M. L. and Springer, T. A. (1990). ICAM-1 (CD54): a counter-receptor for Mac-1 (CD11b/CD18). *The Journal of Cell Biology* **111**, 3129–3139.

Diamond, M. S., Staunton, D. E., Marlin, S. D. and Springer, T. A. (1991). Binding of the integrin Mac-1 (CD11b/CD18) to the third immunoglobulin-like domain of ICAM-1 (CD54) and its regulation by glycosylation. *Cell* **65**, 961–971.

Dimastromatteo, J., Brentnall, T. and Kelly, K. A. (2017). Imaging in pancreatic disease. *Nat Rev Gastroenterol Hepatol* **14**, 97–109.

Dineen, S. P., Lynn, K. D., Holloway, S. E., Miller, A. F., Sullivan, J. P., Shames, D. S., Beck, A. W., Barnett, C. C., Fleming, J. B. and Brekken, R. A. (2008). Vascular Endothelial Growth Factor Receptor 2 Mediates Macrophage Infiltration into Orthotopic Pancreatic Tumors in Mice. *Cancer Research* **68**, 4340–4346.

Distler, M., Aust, D., Weitz, J., Pilarsky, C. and Grützmann, R. (2014). Precursor Lesions for Sporadic Pancreatic Cancer: PanIN, IPMN, and MCN. *Biomed Res Int* **2014**, 1–11.

Dock, G. (1904). *The Influence of Complicating Diseases Upon Leukaemia*. Lea Brothers & Company.

Drucker, B. J., Marincola, F. M., Siao, D. Y., Donlon, T. A., Bangs, C. D. and Holder, W. D. (1988). A new human pancreatic carcinoma cell line developed for adoptive immunotherapy studies with lymphokine-activated killer cells in nude

mice. *In Vitro Cell. Dev. Biol.* **24**, 1179–1187.

Durbec, J. P., Chevillotte, G., Bidart, J. M., Berthezene, P. and Sarles, H. (1983). Diet, alcohol, tobacco and risk of cancer of the pancreas: a case-control study. *British Journal of Cancer* **47**, 463–470.

Eissa, I. R., Naoe, Y., Bustos-Villalobos, I., Ichinose, T., Tanaka, M., Zhiwen, W., Mukoyama, N., Morimoto, T., Miyajima, N., Hitoki, H., et al. (2017). Genomic Signature of the Natural Oncolytic Herpes Simplex Virus HF10 and Its Therapeutic Role in Preclinical and Clinical Trials. *Front Oncol* **7**, 149.

Ene-Obong, A., Clear, A. J., Watt, J., Wang, J., Fatah, R., Riches, J. C., Marshall, J. F., Chin-Aleong, J., Chelala, C., Gribben, J. G., et al. (2013). Activated pancreatic stellate cells sequester CD8+ T cells to reduce their infiltration of the juxtatumoral compartment of pancreatic ductal adenocarcinoma. *Gastroenterology* **145**, 1121–1132.

Engblom, C., Pfirschke, C. and Pittet, M. J. (2016). The role of myeloid cells in cancer therapies. *Nat Rev Cancer* **16**, 447–462.

Erf, L. A. (1950). Human leukemia, with emphasis upon recent therapeutic experiences. *Pa Med J* **53**, 1172–1181.

Eriksson, E., Milenova, I., Wenthe, J., Ståhle, M., Leja-Jarblad, J., Ullenhag, G., Dimberg, A., Moreno, R., Alemany, R. and Loskog, A. (2017a). Shaping the Tumor Stroma and Sparking Immune Activation by CD40 and 4-1BB Signaling Induced by an Armed Oncolytic Virus. *Clin. Cancer Res.*

Eriksson, E., Moreno, R., Milenova, I., Liljenfeldt, L., Dieterich, L. C., Christiansson, L., Karlsson, H., Ullenhag, G., Mangsbo, S. M., Dimberg, A., et al. (2017b). Activation of myeloid and endothelial cells by CD40L gene therapy supports T-cell expansion and migration into the tumor microenvironment. *Gene Therapy* **24**, 92–103.

Erkan, M., Adler, G., Apte, M. V., Bachem, M. G., Buchholz, M., Detlefsen, S., Esposito, I., Friess, H., Gress, T. M., Habisch, H.-J., et al. (2012a). StellaTUM: current consensus and discussion on pancreatic stellate cell research.pp. 172–178.

Erkan, M., Hausmann, S., Michalski, C. W., Fingerle, A. A., Dobritz, M., Kleeff, J. and Friess, H. (2012b). The role of stroma in pancreatic cancer: diagnostic and therapeutic implications. *Nat Rev Gastroenterol Hepatol* **9**, 454–467.

Esposito, I. (2004). Inflammatory cells contribute to the generation of an angiogenic phenotype in pancreatic ductal adenocarcinoma. *Journal of Clinical Pathology* **57**, 630–636.

Etoh, T., Himeno, Y., Matsumoto, T., Aramaki, M., Kawano, K., Nishizono, A. and Kitano, S. (2003). Oncolytic Viral Therapy for Human Pancreatic Cancer Cells by Reovirus. *Clinical Cancer Research* **9**, 1218–1223.

Evans, J., Chapple, A., Salisbury, H., Corrie, P. and Ziebland, S. (2014). "It can't be very important because it comes and goes"--patients' accounts of intermittent symptoms preceding a pancreatic cancer diagnosis: a qualitative study. *BMJ Open* **4**, e004215.

Fabre, A., Sauvanet, A., Flejou, J.-F., Belghiti, J., Palazzo, L., Ruzniewski, P., Degott, C. and Terris, B. (2001). Intraductal acinar cell carcinoma of the pancreas. *Virchows Arch* **438**, 312–315.

Fain, J. N., Madan, A. K., Hiler, M. L., Cheema, P. and Bahouth, S. W. (2004). Comparison of the Release of Adipokines by Adipose Tissue, Adipose Tissue Matrix, and Adipocytes from Visceral and Subcutaneous Abdominal Adipose Tissues of Obese Humans. *Endocrinology* **145**, 2273–2282.

Felix, K. and Gaida, M. M. (2016). Neutrophil-Derived Proteases in the Microenvironment of Pancreatic Cancer -Active Players in Tumor Progression. *Int. J. Biol. Sci.* **12**, 302–313.

Ferdek, P. E. and Jakubowska, M. A. (2017). Biology of pancreatic stellate cells-more than just pancreatic cancer. *Eur J Physiol* **469**, 1039–1050.

Ferlay, J., Soerjomataram, I., Dikshit, R., Eser, S., Mathers, C., Rebelo, M., Parkin, D. M., Forman, D. and Bray, F. (2015). Cancer incidence and mortality worldwide: sources, methods and major patterns in GLOBOCAN 2012. *Int. J. Cancer* **136**, E359–86.

Fernandez-Miragall, O., López de Quinto, S. and Martinez-Salas, E. (2009). Relevance of RNA structure for the activity of picornavirus IRES elements. *Virus Res.* **139**, 172–182.

Ferrer-Orta, C., Arias, A., Agudo, R., Pérez-Luque, R., Escarmís, C., Domingo, E. and Verdaguer, N. (2006). The structure of a protein primer–polymerase complex in the initiation of genome replication. *EMBO J* **25**, 880–888.

Fields, B. N., Knipe, D. M. and Howley, P. M. (1996). *Fields Virology. Enteroviruses: Polioviruses, Coxsackie Viruses, Echoviruses, and Newer Enteroviruses*. Third. Philadelphia. PA. USA: Lippincott-Raven Publishers.

Fife, B. T. and Pauken, K. E. (2011). The role of the PD-1 pathway in autoimmunity and peripheral tolerance. *Ann. N. Y. Acad. Sci.* **1217**, 45–59.

Figura, von, G., Morris, J. P., Wright, C. V. E. and Hebrok, M. (2014). Nr5a2 maintains acinar cell differentiation and constrains oncogenic Kras-mediated pancreatic neoplastic initiation. *Gut* **63**, 656–664.

Fougeray, S., Brignone, C. and Triebel, F. (2006). A soluble LAG-3 protein as an immunopotentiator for therapeutic vaccines: Preclinical evaluation of IMP321. *Vaccine* **24**, 5426–5433.

Franco, O. E., Shaw, A. K., Strand, D. W. and Hayward, S. W. (2010). Cancer associated fibroblasts in cancer pathogenesis. *Semin. Cell Dev. Biol.* **21**, 33–39.

Frič, P., Škrha, J., Šedo, A., Bušek, P., Laclav, M., Bunganič, B. and Zavoral, M. (2017). Precursors of pancreatic cancer. *Eur J Gastroenterol Hepatol* **29**, e13–e18.

Friedman, G. K., Nan, L., Haas, M. C., Kelly, V. M., Moore, B. P., Langford, C. P., Xu, H., Han, X., Beierle, E. A., Markert, J. M., et al. (2015). γ134.5-deleted HSV-1-expressing human cytomegalovirus IRS1 gene kills human glioblastoma cells as efficiently as wild-type HSV-1 in normoxia or hypoxia. *Gene Therapy* **22**, 348–355.

Fujikura, K., Akita, M., Abe-Suzuki, S., Itoh, T. and Zen, Y. (2017). Mucinous cystic neoplasms of the liver and pancreas: relationship between KRAS driver mutations and disease progression. *Histopathology* **71**, 591–600.

Fujimoto, Y., Mizuno, T., Sugiura, S., Goshima, F., Kohno, S.-I., Nakashima, T.

and Nishiyama, Y. (2006). Intratumoral injection of herpes simplex virus HF10 in recurrent head and neck squamous cell carcinoma. *Acta Otolaryngol.* **126**, 1115–1117.

Furukawa, T., Duguid, W. P., Rosenberg, L., Viallet, J., Galloway, D. A. and Tsao, M. S. (1996). Long-term culture and immortalization of epithelial cells from normal adult human pancreatic ducts transfected by the E6E7 gene of human papilloma virus 16. *Am. J. Pathol.* **148**, 1763–1770.

Furukawa, T., Kuboki, Y., Tanji, E., Yoshida, S., Hatori, T., Yamamoto, M., Shibata, N., Shimizu, K., Kamatani, N. and Shiratori, K. (2011). Whole-exome sequencing uncovers frequent GNAS mutations in intraductal papillary mucinous neoplasms of the pancreas. *Scientific Reports* **1**, 161.

Gabrilovich, D. I. and Nagaraj, S. (2009). Myeloid-derived suppressor cells as regulators of the immune system. *Nat Rev Immunol* **9**, 162–174.

Gaida, M. M., Steffen, T. G., Günther, F., Tschaharganeh, D. F., Felix, K., Bergmann, F., Schirmacher, P. and Hänsch, G. M. (2012). Polymorphonuclear neutrophils promote dyshesion of tumor cells and elastase-mediated degradation of E-cadherin in pancreatic tumors. *Eur. J. Immunol.* **42**, 3369–3380.

Gall, T. M. H., Wasan, H. and Jiao, L. R. (2015). Pancreatic cancer: current understanding of molecular and genetic aetiologies. *Postgrad Med J* **91**, 594–600.

Gebauer, F., Kemper, M., Sauter, G., Prehm, P. and Schumacher, U. (2017). Is hyaluronan deposition in the stroma of pancreatic ductal adenocarcinoma of prognostic significance? *PLoS ONE* **12**, e0178703.

Geletneky, K., Huesing, J., Rommelaere, J., Schlehofer, J. R., Leuchs, B., Dahm, M., Krebs, O., Knebel Doeberitz, von, M., Huber, B. and Hajda, J. (2012). Phase I/IIa study of intratumoral/intracerebral or intravenous/intracerebral administration of Parvovirus H-1 (ParvOryx) in patients with progressive primary or recurrent glioblastoma multiforme: ParvOryx01 protocol. *BMC Cancer* **12**, 99.

GenBank Human coxsackievirus A21 strain Kuykendall, complete genome - Nucleotide - NCBI.

Ghadirian, P., Baillargeon, J., Simard, A. and Perret, C. (1995). Food habits and pancreatic cancer: a case-control study of the Francophone community in Montreal, Canada. *Cancer Epidemiol Biomarkers Prev* **4**, 895–899.

Ghadirian, P., Lynch, H. T. and Krewski, D. (2003). Epidemiology of pancreatic cancer: an overview. *Cancer Detect. Prev.* **27**, 87–93.

Ghiorzo, P. (2014). Genetic predisposition to pancreatic cancer. *World Journal of Gastroenterology : WJG* **20**, 10778–10789.

Gobbi, P. G., Bergonzi, M., Comelli, M., Villano, L., Pozzoli, D., Vanoli, A. and Dionigi, P. (2013). The prognostic role of time to diagnosis and presenting symptoms in patients with pancreatic cancer. *Cancer Epidemiol* **37**, 186–190.

Goedegebuure, P., Mitchem, J. B., Porembka, M. R., Tan, M. C. B., Belt, B. A., Wang-Gillam, A., Gillanders, W. E., Hawkins, W. G. and Linehan, D. C. (2011). Myeloid-derived suppressor cells: general characteristics and relevance to clinical management of pancreatic cancer. *Curr Cancer Drug Targets* **11**, 734–751.

Goh, B. K. P., Ooi, L. L. P. J., Tan, Y. M., Cheow, P. C., Chung, Y. F. A., Chow, P. K. H. and Wong, W. K. (2006). Clinico-pathological features of cystic pancreatic endocrine neoplasms and a comparison with their solid counterparts. *Eur J Surg Oncol* **32**, 553–556.

Gold, E. B. (1995). Epidemiology of and Risk Factors for Pancreatic Cancer. *Surgical Clinics of North America* **75**, 819–843.

Goldufsky, J., Sivendran, S., Harcharik, S., Pan, M., Bernardo, S., Stern, R. H., Friedlander, P., Ruby, C. E., Saenger, Y. and Kaufman, H. L. (2013). Oncolytic virus therapy for cancer. *Oncolytic Virotherapy* **2**, 31–46.

Gollamudi, R., Ghalib, M. H., Desai, K. K., Chaudhary, I., Wong, B., Einstein, M., Coffey, M., Gill, G. M., Mettinger, K., Mariadason, J. M., et al. (2009). Intravenous administration of Reolysin®, a live replication competent RNA virus is safe in patients with advanced solid tumors. *Invest New Drugs* **28**, 641–649.

Goodwin, S., Tuthill, T. J., Arias, A., Killington, R. A. and Rowlands, D. J. (2009). Foot-and-mouth disease virus assembly: processing of recombinant capsid

precursor by exogenous protease induces self-assembly of pentamers in vitro in a myristoylation-dependent manner. *J. Virol.* **83**, 11275–11282.

Goonetilleke, K. S. and Siriwardena, A. K. (2007). Systematic review of carbohydrate antigen (CA 19-9) as a biochemical marker in the diagnosis of pancreatic cancer - ScienceDirect. *European Journal of Surgical Oncology …* **33**, 266–270.

Graham, J. S., Jamieson, N. B., Rulach, R., Grimmond, S. M., Chang, D. K. and Biankin, A. V. (2015). Pancreatic cancer genomics: where can the science take us? *Clin. Genet.* **88**, 213–219.

Gross, S. (1971). Measles and leukaemia. *The Lancet* **1**, 397–398.

Grosse-Steffen, T., Giese, T., Giese, N., Longerich, T., Schirmacher, P., Hänsch, G. M. and Gaida, M. M. (2012). Epithelial-to-mesenchymal transition in pancreatic ductal adenocarcinoma and pancreatic tumor cell lines: the role of neutrophils and neutrophil-derived elastase. *Clin. Dev. Immunol.* **2012**, 720768.

Grünewald, K., Lyons, J., Fröhlich, A., Feichtinger, H., Weger, R. A., Schwab, G., Janssen, J. W. G. and Bartram, C. R. (1989). High frequency of Ki-ras codon 12 mutations in pancreatic adenocarcinomas. *Int. J. Cancer* **43**, 1037–1041.

Gubin, M. M. and Schreiber, R. D. (2015). CANCER. The odds of immunotherapy success. *Science* **350**, 158–159.

Guchelaar, H. J., Richel, D. J. and van Knapen, A. (1996). Clinical, toxicological and pharmacological aspects of gemcitabine. *Cancer Treat. Rev.* **22**, 15–31.

Guedan, S., Rojas, J. J., Gros, A., Mercade, E., Cascallo, M. and Alemany, R. (2010). Hyaluronidase expression by an oncolytic adenovirus enhances its intratumoral spread and suppresses tumor growth. *Mol Ther* **18**, 1275–1283.

Gullo, L., Tomassetti, P., Migliori, M., Casadei, R. and Marrano, D. (2001). Do Early Symptoms of Pancreatic Cancer Exist that Can Allow an Earlier Diagnosis? *Pancreas* **22**, 210–213.

Guo, S., Contratto, M., Miller, G., Leichman, L. and Wu, J. (2017). Immunotherapy in pancreatic cancer: Unleash its potential through novel combinations. *WJCO* **8**,

230–240.

Halberg, N., Wernstedt-Asterholm, I. and Scherer, P. E. (2008). The Adipocyte as an Endocrine Cell. *Endocrinology and …* **37**, 753–768.

Hale, M. A., Kagami, H., Shi, L., Holland, A. M., Elsässer, H.-P., Hammer, R. E. and MacDonald, R. J. (2005). The homeodomain protein PDX1 is required at mid-pancreatic development for the formation of the exocrine pancreas. *Dev. Biol.* **286**, 225–237.

Hale, M. A., Swift, G. H., Hoang, C. Q., Deering, T. G., Masui, T., Lee, Y. K., Xue, J. and MacDonald, R. J. (2014). The nuclear hormone receptor family member NR5A2 controls aspects of multipotent progenitor cell formation and acinar differentiation during pancreatic organogenesis. *Development* **141**, 3123–3133.

Hamada, S., Masamune, A. and Shimosegawa, T. (2014). Inflammation and pancreatic cancer: disease promoter and new therapeutic target. *J. Gastroenterol.* **49**, 605–617.

Hamada, S., Masamune, A., Takikawa, T., Suzuki, N., Kikuta, K., Hirota, M., Hamada, H., Kobune, M., Satoh, K. and Shimosegawa, T. (2012). Pancreatic stellate cells enhance stem cell-like phenotypes in pancreatic cancer cells. *Biochem. Biophys. Res. Commun.* **421**, 349–354.

Hamid, O., Hoffner, B., Gasal, E., Hong, J. and Carvajal, R. D. (2017). Oncolytic immunotherapy: unlocking the potential of viruses to help target cancer. *Cancer Immunol. Immunother.*

Han, J. and Chang, K. J. (2017). Endoscopic Ultrasound-Guided Direct Intervention for Solid Pancreatic Tumors. *Clin Endosc* **50**, 126–137.

Han, S., Delitto, D., Zhang, D., Sorenson, H. L., Sarosi, G. A., Thomas, R. M., Behrns, K. E., Wallet, S. M., Trevino, J. G. and Hughes, S. J. (2015). Primary outgrowth cultures are a reliable source of human pancreatic stellate cells. *Lab. Invest.* **95**, 1331–1340.

Hanahan, D. and Weinberg, R. A. (2011). Hallmarks of cancer: the next generation. *Cell* **144**, 646–674.

Haqq, J., Howells, L. M., Garcea, G., Metcalfe, M. S., Steward, W. P. and Dennison, A. R. (2014). Pancreatic stellate cells and pancreas cancer: current perspectives and future strategies. *Eur. J. Cancer* **50**, 2570–2582.

Harada, J. N. and Berk, A. J. (1999). p53-Independent and -dependent requirements for E1B-55K in adenovirus type 5 replication. *J. Virol.* **73**, 5333–5344.

Harak, C. and Lohmann, V. (2015). Ultrastructure of the replication sites of positive-strand RNA viruses. *Virology* **479-480**, 418–433.

Hayes, S. H. and Seigel, G. M. (2009). Immunoreactivity of ICAM-1 in human tumors, metastases and normal tissues. *Int J Clin Exp Pathol* **2**, 553–560.

Hazarika, M., Chuk, M. K., Theoret, M. R., Mushti, S., He, K., Weis, S. L., Putman, A. H., Helms, W. S., Cao, X., Li, H., et al. (2017). U.S. FDA Approval Summary: Nivolumab for Treatment of Unresectable or Metastatic Melanoma Following Progression on Ipilimumab. *Clin. Cancer Res.* **23**, 3484–3488.

Hecht, J. R., Bedford, R., Abbruzzese, J. L., Lahoti, S., Reid, T. R., Soetikno, R. M., Kirn, D. H. and Freeman, S. M. (2003). A phase I/II trial of intratumoral endoscopic ultrasound injection of ONYX-015 with intravenous gemcitabine in unresectable pancreatic carcinoma. *Clin. Cancer Res.* **9**, 555–561.

Heinemann, V., Xu, Y. Z., Chubb, S., Sen, R., Hertel, L. W., Grindey, G. B. and Plunkett, W. (1990). Inhibition of ribonucleotide reduction in CCRF-CEM cells by 2“,2-”difluorodeoxycytidine. *Mol Pharmacol* **38**, 567–572.

Heinrich, B., Goepfert, K., Delic, M., Galle, P. R. and Moehler, M. (2013). Influence of the oncolytic parvovirus H-1, CTLA-4 antibody tremelimumab and cytostatic drugs on the human immune system in a human in vitro model of colorectal cancer cells. *Onco Targets Ther* **6**, 1119–1127.

Heinrich, S., Goerres, G. W., Schäfer, M., Sagmeister, M., Bauerfeind, P., Pestalozzi, B. C., Hany, T., Schulthess, von, G. K. and Clavien, P.-A. (2006). Positron Emission Tomography/Computed Tomography Influences on the Management of Resectable Pancreatic Cancer and Its Cost-Effectiveness. *Ann. Surg.* **242**, 235–243.

Hertel, L. W. (1985). Difluoro Antivirals and Intermediate Therefor US4526988. *docs.google.com*.

Hertel, L. W., Boder, G. B., Kroin, J. S., Rinzel, S. M., Poore, G. A., Todd, G. C. and Grindey, G. B. (1990). Evaluation of the antitumor activity of gemcitabine (2',2'-difluoro-2'-deoxycytidine). *Cancer Research* **50**, 4417–4422.

Hewat, E. A., Neumann, E., Conway, J. F., Moser, R., Ronacher, B., Marlovits, T. C. and Blaas, D. (2000). The cellular receptor to human rhinovirus 2 binds around the 5-fold axis and not in the canyon: a structural view. *EMBO J* **19**, 6317–6325.

Higgins, G. K. and Pack, G. T. (1951). Virus therapy in the treatment of tumors. *Bull Hosp Joint Dis* **12**, 379–382.

Hill, A., Jugovic, P., York, I., Russ, G., Bennink, J., Yewdell, J., Ploegh, H. and Johnson, D. (1995). Herpes simplex virus turns off the TAP to evade host immunity. *Nature* **375**, 411–415.

Hippisley-Cox, J. and Coupland, C. (2012). Identifying patients with suspected pancreatic cancer in primary care: derivation and validation of an algorithm. *Br J Gen Pract* **62**, e38–45.

Hiraoka, N., Onozato, K., Kosuge, T. and Hirohashi, S. (2006). Prevalence of FOXP3+ Regulatory T Cells Increases During the Progression of Pancreatic Ductal Adenocarcinoma and Its Premalignant Lesions. *Clinical Cancer Research* **12**, 5423–5434.

Hirata, K., Sato, T. and Mukaiya, M. (1997). Results of 1001 Pancreatic Resections for Invasive Ductal Adenocarcinoma of the Pancreas. *Arch Surg* **132**, 771–776.

Hishinuma, S., Ogata, Y., Tomikawa, M., Ozawa, I., Hirabayashi, K. and Igarashi, S. (2006). Patterns of recurrence after curative resection of pancreatic cancer, based on autopsy findings. *J Gastrointest Surg* **10**, 511–518.

Ho, M. Y., Kennecke, H. F., Renouf, D. J., Cheung, W. Y., Lim, H. J. and Gill, S. (2015). Defining Eligibility of FOLFIRINOX for First-Line Metastatic Pancreatic Adenocarcinoma (MPC) in the Province of British Columbia: A Population-based Retrospective Study. *American Journal of Clinical Oncology*.

Hoff, Von, D. D., Ervin, T., Arena, F. P., Chiorean, E. G., Infante, J., Moore, M., Seay, T., Tjulandin, S. A., Ma, W. W., Saleh, M. N., et al. (2013). Increased survival in pancreatic cancer with nab-paclitaxel plus gemcitabine. *N Engl J Med* **369**, 1691–1703.

Hogle, J. M., Chow, M. and Filman, D. J. (1985). Three-dimensional structure of poliovirus at 2.9 A resolution. *Science* **229**, 1358–1365.

Holly, E. A., Chaliha, I., Bracci, P. M. and Gautam, M. (2004). Signs and symptoms of pancreatic cancer: a population-based case-control study in the San Francisco Bay area. *Clin. Gastroenterol. Hepatol.* **2**, 510–517.

Hori, M., Takahashi, M., Hiraoka, N., Yamaji, T., Mutoh, M., Ishigamori, R., Furuta, K., Okusaka, T., Shimada, K., Kosuge, T., et al. (2014). Association of pancreatic Fatty infiltration with pancreatic ductal adenocarcinoma. *Clin Transl Gastroenterol* **5**, e53.

Horiuchi, M., Goto, H., Ishiguro, N. and Shinagawa, M. (1994). Mapping of determinants of the host range for canine cells in the genome of canine parvovirus using canine parvovirus/mink enteritis virus chimeric viruses. *Journal of General Virology* **75**, 1319–1328.

Hosaka, K., Yang, Y., Seki, T., Fischer, C., Dubey, O., Fredlund, E., Hartman, J., Religa, P., Morikawa, H., Ishii, Y., et al. (2016). Pericyte-fibroblast transition promotes tumor growth and metastasis. *Proc. Natl. Acad. Sci. U.S.A.* **113**, E5618–27.

Hosoda, W. and Wood, L. D. (2016). Molecular Genetics of Pancreatic Neoplasms. *Surgical Pathology* **9**, 685–703.

Hoster, H. A., Zanes, R. P. and Haam, von, E. (1949). Studies in Hodgkin“s syndrome; the association of viral hepatitis and Hodgkin”s disease; a preliminary report. *Cancer Research* **9**, 473–480.

Hotta, Y., Kasuya, H., Bustos, I. and Naoe, Y. (2017). Curative effect of HF10 on liver and peritoneal metastasis mediated by host antitumor immunity. *Oncolytic Virotherapy* **6**, 31–38.

Howard, K., Lo, K. K., Ao, L., Gamboni, F., Edil, B. H., Schulick, R. and Barnett, C. C. (2014). Intercellular adhesion molecule-1 mediates murine colon adenocarcinoma invasion. *J. Surg. Res.* **187**, 19–23.

Howlader, N., Noone, A. M., Krapcho, M., Miller, D., Bishop, K., Kosary, C. L., Yu, M., Ruhl, J., Tatalovich, Z., Mariotto, A., et al. (2017). *SEER Cancer Statistics Review, 1975–2014. Bethesda, MD: National Cancer Institute; 2016*. https://seer.cancer.gov/csr/1975_2014/.

Hruban, R. H., Maitra, A., Kern, S. E. and Goggins, M. (2007a). Precursors to pancreatic cancer. *Gastroenterol. Clin. North Am.* **36**, 831–49– vi.

Hruban, R. H., Pitman, M. B. and Klimstra, D. S. (2007b). Tumours of the Pancreas, 4th ed. *Atlas of tumor pathology*.

Huang, P., Chubb, S., Hertel, L. W., Grindey, G. B. and Plunkett, W. (1991). Action of 2“,2-”difluorodeoxycytidine on DNA synthesis. *Cancer Research* **51**, 6110–6117.

Hubbard, A. K. and Rothlein, R. (2000). Intercellular adhesion molecule-1 (ICAM-1) expression and cell signaling cascades. *Free Radic. Biol. Med.* **28**, 1379–1386.

Hwang, R. F., Moore, T., Arumugam, T., Ramachandran, V., Amos, K. D., Rivera, A., Ji, B., Evans, D. B. and Logsdon, C. D. (2008). Cancer-associated stromal fibroblasts promote pancreatic tumor progression. *Cancer Research* **68**, 918–926.

Hyypiä, T., Hovi, T., Knowles, N. J. and Stanway, G. (1997). Classification of enteroviruses based on molecular and biological properties. *J. Gen. Virol.* **78 (Pt 1)**, 1–11.

Ikerjiri, N. (1990). The vitamin A-storing cells in the human and rat pancreas. *Kurume Med. J.* **37**, 67–81.

Ilett, E. J., Bárcena, M., Errington-Mais, F., Griffin, S., Harrington, K. J., Pandha, H. S., Coffey, M., Selby, P. J., Limpens, R. W. A. L., Mommaas, M., et al. (2011). Internalization of oncolytic reovirus by human dendritic cell carriers protects the virus from neutralization. *Clin. Cancer Res.* **17**, 2767–2776.

Ilett, E. J., Prestwich, R. J., Kottke, T., Errington, F., Thompson, J. M., Harrington,

K. J., Pandha, H. S., Coffey, M., Selby, P. J., Vile, R. G., et al. (2009). Dendritic cells and T cells deliver oncolytic reovirus for tumour killing despite pre-existing anti-viral immunity. *Gene Therapy* **16**, 689–699.

Ilic, M. and Ilic, I. (2016). Epidemiology of pancreatic cancer. *World Journal of Gastroenterology : WJG* **22**, 9694–9705.

Inoue, K., Ohuchida, J., Ohtsuka, T., Nabae, T., Yokohata, K., Ogawa, Y., Yamaguchi, K. and Tanaka, M. (2003). Severe localized stenosis and marked dilatation of the main pancreatic duct are indicators of pancreatic cancer instead of chronic pancreatitis on endoscopic retrograde balloon pancreatography. *Gastrointest. Endosc.* **58**, 510–515.

Iodice, S., Gandini, S., Maisonneuve, P. and Lowenfels, A. B. (2008). Tobacco and the risk of pancreatic cancer: a review and meta-analysis. *Langenbecks Arch Surg* **393**, 535–545.

Jang, S. K. (2006). Internal initiation: IRES elements of picornaviruses and hepatitis c virus. *Virus Res.* **119**, 2–15.

Jang, S. K., Pestova, T. V., Hellen, C. U. T., Witherell, G. W. and Wimmer, E. (2017). Cap-Independent Translation of Picornavirus RN As: Structure and Function of the Internal Ribosomal Entry Site. *Enzyme* **44**, 292–309.

Jaster, R. (2004). Molecular regulation of pancreatic stellate cell function. *Mol Cancer* **3**, 26.

Jenkinson, C., Elliott, V., Menon, U., Apostolidou, S., Fourkala, O. E., Gentry-Maharaj, A., Pereira, S. P., Jacobs, I., Cox, T. F., Greenhalf, W., et al. (2015). Evaluation in pre-diagnosis samples discounts ICAM-1 and TIMP-1 as biomarkers for earlier diagnosis of pancreatic cancer. *J Proteomics* **113**, 400–402.

Jennings, V. A., Ilett, E. J., Scott, K. J., West, E. J., Vile, R., Pandha, H., Harrington, K., Young, A., Hall, G. D., Coffey, M., et al. (2014). Lymphokine-activated killer and dendritic cell carriage enhances oncolytic reovirus therapy for ovarian cancer by overcoming antibody neutralization in ascites. *Int. J. Cancer* **134**, 1091–1101.

Jiang, H., Hegde, S. and DeNardo, D. G. (2017). Tumor-associated fibrosis as a regulator of tumor immunity and response to immunotherapy. *Cancer Immunol. Immunother.* **66**, 1037–1048.

Jiang, P., Liu, Y., Ma, H. C., Paul, A. V. and Wimmer, E. (2014). Picornavirus Morphogenesis. *Microbiology and Molecular Biology Reviews* **78**, 418–437.

Jin, H., Wu, Y. and Tan, X. (2017). The role of pancreatic cancer-derived exosomes in cancer progress and their potential application as biomarkers. *Clinical and Translational Oncology* **19**, 921–930.

Johansson, H., Andersson, R., Bauden, M., Hammes, S., Holdenrieder, S. and Ansari, D. (2016). Immune checkpoint therapy for pancreatic cancer. *World Journal of Gastroenterology : WJG* **22**, 9457–9476.

Jones, S., Zhang, X., Parsons, D. W., Lin, J. C.-H., Leary, R. J., Angenendt, P., Mankoo, P., Carter, H., Kamiyama, H., Jimeno, A., et al. (2008). Core signaling pathways in human pancreatic cancers revealed by global genomic analyses. *Science* **321**, 1801–1806.

Jordan, W. S. (1960). Stability characteristics of Coe virus. *Proc. Soc. Exp. Biol. Med.* **103**, 506–509.

Jun, S.-Y. and Hong, S.-M. (2016). Nonductal Pancreatic Cancers. *Surgical Pathology* **9**, 581–593.

Kaboli, S. and Babazada, H. (2017). CRISPR Mediated Genome Engineering and its Application in Industry. *Curr Issues Mol Biol* **26**, 81–92.

Kadayifci, A., Atar, M., Basar, O., Forcione, D. G. and Brugge, W. R. (2017). Needle-Based Confocal Laser Endomicroscopy for Evaluation of Cystic Neoplasms of the Pancreas. *Dig. Dis. Sci.* **62**, 1346–1353.

Kalluri, R. and Zeisberg, M. (2006). Fibroblasts in cancer. *Nat Rev Cancer* **6**, 392–401.

Kaowinn, S., Cho, I.-R., Moon, J., Jun, S. W., Kim, C. S., Kang, H. Y., Kim, M., Koh, S. S. and Chung, Y.-H. (2015). Pancreatic adenocarcinoma upregulated factor (PAUF) confers resistance to pancreatic cancer cells against oncolytic

parvovirus H-1 infection through IFNA receptor-mediated signaling. *Biochem. Biophys. Res. Commun.* **459**, 313–318.

Kaufman, H. L., Kohlhapp, F. J. and Zloza, A. (2015). Oncolytic viruses: a new class of immunotherapy drugs. *Nat Rev Drug Discov* **14**, 642–662.

Kaufman, H. L., Ruby, C. E., Hughes, T. and Slingluff, C. L. (2014). Current status of granulocyte-macrophage colony-stimulating factor in the immunotherapy of melanoma. *J Immunother Cancer* **2**, 11.

Kauhanen, S. P., Komar, G., Seppänen, M. P., Dean, K. I., Minn, H. R., Kajander, S. A., Rinta-kiikka, I., Alanen, K., Borra, R. J., Puolakkainen, P. A., et al. (2009). A Prospective Diagnostic Accuracy Study of 18f-fluorodeoxyglucose Positron Emission Tomography/computed Tomography, Multidetector Row Computed Tomography, and Magnetic Resonance Imaging in Primary Diagnosis and Staging of Pancreatic Cancer. *Ann. Surg.* **250**, 957–963.

Keane, M. G., Horsfall, L., Rait, G. and Pereira, S. P. (2014). A case–control study comparing the incidence of early symptoms in pancreatic and biliary tract cancer. *BMJ Open* **4**, e005720.

Kelly, E. and Russell, S. J. (2007). History of oncolytic viruses: genesis to genetic engineering. *Mol Ther* **15**, 651–659.

King, A. M. Q., Adams, M. J. and Lefkowitz, E. J. (2011). *Virus Taxonomy*. Elsevier.

Klimstra, D. S., Modlin, I. R., Coppola, D., Lloyd, R. V. and Suster, S. (2010). The Pathologic Classification of Neuroendocrine Tumors. *Pancreas* **39**, 707–712.

Kohlhapp, F. J. and Kaufman, H. L. (2016). Molecular Pathways: Mechanism of Action for Talimogene Laherparepvec, a New Oncolytic Virus Immunotherapy. *Clin. Cancer Res.* **22**, 1048–1054.

Kohno, S.-I., Luo, C., Goshima, F., Nishiyama, Y., Sata, T. and Ono, Y. (2005). Herpes simplex virus type 1 mutant HF10 oncolytic viral therapy for bladder cancer. *Urology* **66**, 1116–1121.

Konda, V. J. A., Meining, A., Jamil, L. H., Giovannini, M., Hwang, J. H., Wallace, M. B., Chang, K. J., Siddiqui, U. D., Hart, J., Lo, S. K., et al. (2013). A pilot study of

in vivo identification of pancreatic cystic neoplasms with needle-based confocal laser endomicroscopy under endosonographic guidance. *Endoscopy* **45**, 1006–1013.

Koprowska, I. (1953). Morphologic changes of exfoliated cells in effusions of cancer patients following induced viral infections; preliminary observations. *Am. J. Pathol.* **29**, 1105–1121.

Kota, J., Hancock, J., Kwon, J. and Korc, M. (2017). Pancreatic cancer: Stroma and its current and emerging targeted therapies. *Cancer Lett.* **391**, 38–49.

Kotteas, E., Saif, M. W. and Syrigos, K. (2016). Immunotherapy for pancreatic cancer. *J. Cancer Res. Clin. Oncol.* **142**, 1795–1805.

Krishna, S. G., Brugge, W. R., Dewitt, J. M., Kongkam, P., Napoléon, B., Robles-Medranda, C., Tan, D., El-Dika, S., McCarthy, S., Walker, J., et al. (2017). Needle-based confocal laser endomicroscopy for the diagnosis of pancreatic cystic lesions: an international external interobserver and intraobserver study (with videos). *Gastrointest. Endosc.* **86**, 644–654.e2.

Krummel, M. F. and Allison, J. P. (1995). CD28 and CTLA-4 have opposing effects on the response of T cells to stimulation. *J. Exp. Med.* **182**, 459–465.

Kulke, M. H., Bendell, J., Kvols, L., Picus, J., Pommier, R. and Yao, J. (2011). Evolving diagnostic and treatment strategies for pancreatic neuroendocrine tumors. *Journal of Hematology & Oncology* **4**, 29.

Kunk, P. R., Bauer, T. W., Slingluff, C. L. and Rahma, O. E. (2016). From bench to bedside a comprehensive review of pancreatic cancer immunotherapy. *J Immunother Cancer* **4**, 14.

Kyriazis, A. A., Kyriazis, A. P., Sternberg, C. N., Sloane, N. H. and Loveless, J. D. (1986). Morphological, biological, biochemical, and karyotypic characteristics of human pancreatic ductal adenocarcinoma Capan-2 in tissue culture and the nude mouse. *Cancer Research* **46**, 5810–5815.

Kyriazis, A. P., McCombs, W. B., Sandberg, A. A., Kyriazis, A. A., Sloane, N. H. and Lepera, R. (1983). Establishment and characterization of human pancreatic

adenocarcinoma cell line SW-1990 in tissue culture and the nude mouse. *Cancer Research* **43**, 4393–4401.

La Rosa, S., Adsay, V., Albarello, L., Asioli, S., Casnedi, S., Franzi, F., Marando, A., Notohara, K., Sessa, F., Vanoli, A., et al. (2012). Clinicopathologic Study of 62 Acinar Cell Carcinomas of the Pancreas. *The American Journal of Surgical Pathology* **36**, 1782–1795.

La Rosa, S., Sessa, F. and Capella, C. (2015). Acinar Cell Carcinoma of the Pancreas: Overview of Clinicopathologic Features and Insights into the Molecular Pathology. *Front Med (Lausanne)* **2**, 41.

Laheru, D. and Jaffee, E. M. (2005). Immunotherapy for pancreatic cancer — science driving clinical progress. *Nat Rev Cancer* **5**, 459–467.

Lambert, A., Gavoille, C. and Conroy, T. (2017). Current status on the place of FOLFIRINOX in metastatic pancreatic cancer and future directions. *Therapeutic Advances in Gastroenterology* **10**, 631–645.

Lau, S. C. and Cheung, W. Y. (2017). Evolving treatment landscape for early and advanced pancreatic cancer. *World J Gastrointest Oncol* **9**, 281–292.

Law, J. K., Ahmed, A., Singh, V. K., Akshintala, V. S., Olson, M. T., Raman, S. P., Ali, S. Z., Fishman, E. K., Kamel, I., Canto, M. I., et al. (2014). A systematic review of solid-pseudopapillary neoplasms: are these rare lesions? *Pancreas* **43**, 331–337.

Lawrence, M. S., Stojanov, P., Polak, P., Kryukov, G. V., Cibulskis, K., Sivachenko, A., Carter, S. L., Stewart, C., Mermel, C. H., Roberts, S. A., et al. (2013). Mutational heterogeneity in cancer and the search for new cancer-associated genes. *Nature* **499**, 214–218.

Lee, A. T. K., Xu, Z., Pothula, S. P., Patel, M. B., Pirola, R. C., Wilson, J. S. and Apte, M. V. (2015). Alcohol and Cigarette Smoke Components Activate Human Pancreatic Stellate Cells: Implications for the Progression of Chronic Pancreatitis. *Alcohol. Clin. Exp. Res.* **39**, 2123–2133.

Lee, Y. M. and Chow, M. (1992). Myristate modification does not function as a

membrane association signal during poliovirus capsid assembly. *Virology* **187**, 814–820.

Lennette, E. H., Fox, V. L., Schmidt, N. J. and Culver, J. O. (1958). The Coe virus: an apparently new virus recovered from patients with mild respiratory disease. *Am J Hyg* **68**, 272–287.

Lennon, A. M., Wolfgang, C. L., Canto, M. I., Klein, A. P., Herman, J. M., Goggins, M., Fishman, E. K., Kamel, I., Weiss, M. J., Diaz, L. A., et al. (2014). The early detection of pancreatic cancer: what will it take to diagnose and treat curable pancreatic neoplasia? *Cancer Research* **74**, 3381–3389.

Lerner, B. H. (2004). Sins of omission--cancer research without informed consent. *N Engl J Med* **351**, 628–630.

Levey, J. M. and Banner, B. F. (1996). Adult Pancreatoblastoma: A Case Report and Review of the Literature. *American Journal of Gastroenterology* **91**, 1841–1844.

Lewis, R. B., Lattin, G. E. and Paal, E. (2010). Pancreatic endocrine tumors: radiologic-clinicopathologic correlation. *Radiographics* **30**, 1445–1464.

Li, J. P. and Baltimore, D. (1988). Isolation of poliovirus 2C mutants defective in viral RNA synthesis. *J. Virol.* **62**, 4016–4021.

Li, J. P. and Baltimore, D. (1990). An intragenic revertant of a poliovirus 2C mutant has an uncoating defect. *J. Virol.* **64**, 1102–1107.

Li, X., He, C., Liu, C., Ma, J., Ma, P., Cui, H., Tao, H. and Gao, B. (2015a). Expansion of NK cells from PBMCs using immobilized 4-1BBL and interleukin-21. *Int. J. Oncol.* **47**, 335–342.

Li, X., Hu, W., Zheng, X., Zhang, C., Du, P., Zheng, Z., Yang, Y., Wu, J., Ji, M., Jiang, J., et al. (2015b). Emerging immune checkpoints for cancer therapy. *Acta Oncol* **54**, 1706–1713.

Li, X., Wang, Z., Ma, Q., Xu, Q., Liu, H., Duan, W., Lei, J., Ma, J., Wang, X., Lv, S., et al. (2014). Sonic Hedgehog Paracrine Signaling Activates Stromal Cells to Promote Perineural Invasion in Pancreatic Cancer. *Clinical Cancer Research* **20**, 4326–4338.

Liang, S., Slattery, M. J., Wagner, D., Simon, S. I. and Dong, C. (2008). Hydrodynamic shear rate regulates melanoma-leukocyte aggregation, melanoma adhesion to the endothelium, and subsequent extravasation. *Ann Biomed Eng* **36**, 661–671.

Lieber, M. R., Lack, E. E., Roberts, J. R. J., Merino, M. J., Patterson, K., Restrepo, C., Solomon, D., Chandra, R. and Triche, T. J. (1987). Solid and Papillary Epithelial Neoplasm of the Pancreas An Ultrastructural and Immunocytochemical Study of Six Cases. *The American Journal of Surgical Pathology* **11**, 85.

Lieber, M., Mazzetta, J., Nelson-Rees, W., Kaplan, M. and Todaro, G. (1975). Establishment of a continuous tumor-cell line (panc-1) from a human carcinoma of the exocrine pancreas. *Int. J. Cancer* **15**, 741–747.

Ligneau, B., Lombard-Bohas, C., Partensky, C., Valette, P. J., Calender, A., Dumortier, J., Gouysse, G., Boulez, J., Napoleon, B., Berger, F., et al. (2001). Cystic endocrine tumors of the pancreas: clinical, radiologic, and histopathologic features in 13 cases. *The American Journal of Surgical Pathology* **25**, 752–760.

Liljenfeldt, L., Gkirtzimanaki, K., Vyrla, D., Svensson, E., Loskog, A. S. and Eliopoulos, A. G. (2013). Enhanced therapeutic anti-tumor immunity induced by co-administration of 5-fluorouracil and adenovirus expressing CD40 ligand. *Cancer Immunol. Immunother.* **63**, 273–282.

Lin, Y. C., Shun, C. T., Wu, M. S. and Chen, C. C. (2006). A Novel Anticancer Effect of Thalidomide: Inhibition of Intercellular Adhesion Molecule-1-Mediated Cell Invasion and Metastasis through Suppression of Nuclear Factor- B. *Clinical Cancer Research* **12**, 7165–7173.

Linehan, D. C. and Goedegebuure, P. S. (2005). CD25+ CD4+ regulatory T-cells in cancer. *Immunol. Res.* **32**, 155–168.

Liou, G.-Y., Döppler, H., Necela, B., Edenfield, B., Zhang, L., Dawson, D. W. and Storz, P. (2015). Mutant KRAS-induced expression of ICAM-1 in pancreatic acinar cells causes attraction of macrophages to expedite the formation of precancerous lesions. *Cancer Discov* **5**, 52–63.

Lipson, E. J. and Drake, C. G. (2011). Ipilimumab: an anti-CTLA-4 antibody for

metastatic melanoma. *Clin. Cancer Res.* **17**, 6958–6962.

Liu, B. L., Robinson, M., Han, Z.-Q., Branston, R. H., English, C., Reay, P., McGrath, Y., Thomas, S. K., Thornton, M., Bullock, P., et al. (2003). ICP34.5 deleted herpes simplex virus with enhanced oncolytic, immune stimulating, and anti-tumour properties. *Gene Therapy* **10**, 292–303.

Liu, J., Miwa, T., Hilliard, B., Chen, Y., Lambris, J. D., Wells, A. D. and Song, W.-C. (2005). The complement inhibitory protein DAF (CD55) suppresses T cell immunity in vivo. *J. Exp. Med.* **201**, 567–577.

Liu, Q., Liao, Q. and Zhao, Y. (2017). Chemotherapy and tumor microenvironment of pancreatic cancer. *Cancer Cell Int.* **17**, 68.

Liu, Y., Wang, C., Mueller, S., Paul, A. V., Wimmer, E. and Jiang, P. (2010). Direct Interaction between Two Viral Proteins, the Nonstructural Protein 2CATPase and the Capsid Protein VP3, Is Required for Enterovirus Morphogenesis. *PLOS Pathogens* **6**, e1001066.

Liu, Z., Guo, B. and Lopez, R. D. (2009). Expression of intercellular adhesion molecule (ICAM)-1 or ICAM-2 is critical in determining sensitivity of pancreatic cancer cells to cytolysis by human gammadelta-T cells: implications in the design of gammadelta-T-cell-based immunotherapies for pancreatic cancer. *J. Gastroenterol. Hepatol.* **24**, 900–911.

Liyanage, U. K., Goedegebuure, P. S., Moore, T. T., Viehl, C. T., Moo-Young, T. A., Larson, J. W., Frey, D. M., Ehlers, J. P., Eberlein, T. J. and Linehan, D. C. (2006). Increased prevalence of regulatory T cells (Treg) is induced by pancreas adenocarcinoma. *J. Immunother.* **29**, 416–424.

Longnecker, D. S., Adler, G., Hruban, R. H. and Klöppel, G. (2000). *Intraductal papillary-mucinous neoplasms of the pancreas*. (ed. IARC Lyon, France: WHO Classification of Tumours.

Loosen, S. H., Neumann, U. P., Trautwein, C., Roderburg, C. and Luedde, T. (2017). Current and future biomarkers for pancreatic adenocarcinoma. *Tumour Biol.* **39**, 1010428317692231.

Loskog, A. S. I. and Eliopoulos, A. G. (2009). The Janus faces of CD40 in cancer. *Semin. Immunol.* **21**, 301–307.

Loskog, A., Dzojic, H., Vikman, S., Ninalga, C., Essand, M., Korsgren, O. and Totterman, T. H. (2004). Adenovirus CD40 Ligand Gene Therapy Counteracts Immune Escape Mechanisms in the Tumor Microenvironment. *The Journal of Immunology* **172**, 7200–7205.

Lublin, D. M. and Atkinson, J. P. (1989). Decay-accelerating factor: biochemistry, molecular biology, and function. *Annu. Rev. Immunol.* **7**, 35–58.

Luchini, C., Capelli, P. and Scarpa, A. (2016). Pancreatic Ductal Adenocarcinoma and Its Variants. *Surgical Pathology* **9**, 547–560.

Lugea, A., Gerloff, A., Su, H.-Y., Xu, Z., Go, A., Hu, C., French, S. W., Wilson, J. S., Apte, M. V., Waldron, R. T., et al. (2017). Combination of Alcohol and Cigarette Smoke Induces Endoplasmic Reticulum Stress and Cell Death in Pancreatic Acinar Cells. *Gastroenterology*.

Luo, C., Goshima, F., Kamakura, M., Mutoh, Y., Iwata, S., Kimura, H. and Nishiyama, Y. (2012). Immunization with a highly attenuated replication-competent herpes simplex virus type 1 mutant, HF10, protects mice from genital disease caused by herpes simplex virus type 2. *Front Microbiol* **3**, 158.

Lynch, D. H. (2008). The promise of 4-1BB (CD137)-mediated immunomodulation and the immunotherapy of cancer. *Immunol Rev* **222**, 277–286.

Lynch, S. M., Vrieling, A., Lubin, J. H., Kraft, P., Mendelsohn, J. B., Hartge, P., Canzian, F., Steplowski, E., Arslan, A. A., Gross, M., et al. (2009). Cigarette smoking and pancreatic cancer: a pooled analysis from the pancreatic cancer cohort consortium. *Am. J. Epidemiol.* **170**, 403–413.

Ma, Y., Hwang, R. F., Logsdon, C. D. and Ullrich, S. E. (2013). Dynamic mast cell-stromal cell interactions promote growth of pancreatic cancer. *Cancer Research* **73**, 3927–3937.

Magee, W. E. and Miller, O. V. (1970). Individual Variability in Antibody Response of Human Volunteers to Infection of the Upper Respiratory Tract by Coxsackie A-21

Virus. *Journal of Infectious Diseases* **122**, 127–138.

Mahalingam, D., Patel, S., Nuovo, G., Gill, G., Selvaggi, G., Coffey, M. and Nawrocki, S. T. (2015). The combination of intravenous Reolysin and gemcitabine induces reovirus replication and endoplasmic reticular stress in a patient with KRAS-activated pancreatic cancer. *BMC Cancer* **15**, 513.

Man, Y. K. S., Davies, J. A., Coughlan, L., Pantelidou, C., Blázquez-Moreno, A., Marshall, J. F., Parker, A. L. and Halldén, G. (2018). The Novel Oncolytic Adenoviral Mutant Ad5-3Δ-A20T Retargeted to αvβ6 Integrins Efficiently Eliminates Pancreatic Cancer Cells. *Mol. Cancer Ther.* **17**, 575–587.

Mansh, M. (2011). Ipilimumab and cancer immunotherapy: a new hope for advanced stage melanoma. *Yale J Biol Med* **84**, 381–389.

Marlin, S. D. and Springer, T. A. (1987). Purified intercellular adhesion molecule-1 (ICAM-1) is a ligand for lymphocyte function-associated antigen 1 (LFA-1). *Cell* **51**, 813–819.

Marrelli, D., Caruso, S., Pedrazzani, C., Neri, A., Fernandes, E., Marini, M., Pinto, E. and Roviello, F. (2009). CA19-9 serum levels in obstructive jaundice: clinical value in benign and malignant conditions. *Am. J. Surg.* **198**, 333–339.

Marruchella, A. and Tondini, M. (1999). Gemcitabine toxicity. *Chest* **116**, 1491.

Martin, J. A., Bushnell, D. J., Duncan, I. B., Dunsdon, S. J., Hall, M. J., Machin, P. J., Merrett, J. H., Parkes, K. E. B. and Roberts, N. A. (1990). Synthesis and antiviral activity of monofluoro and difluoro analogs of pyrimidine deoxyribonucleosides against human immunodeficiency virus (HIV-1). *J. Med. Chem.* **33**, 2137–2145.

Martinez-Salas, E. and Fernandez-Miragall, O. (2004). Picornavirus IRES: Structure Function Relationship. *CPD* **10**, 3757–3767.

Martín-Belmonte, F., López-Guerrero, J. A., Carrasco, L. and Alonso, M. A. (2000). The amino-terminal nine amino acid sequence of poliovirus capsid VP4 protein is sufficient to confer N-myristoylation and targeting to detergent-insoluble membranes. *Biochemistry* **39**, 1083–1090.

Martínez-Vélez, N., Xipell, E., Vera, B., Acanda de la Rocha, A., Zalacain, M., Marrodán, L., Gonzalez-Huarriz, M., Toledo, G., Cascallo, M., Alemany, R., et al. (2016). The Oncolytic Adenovirus VCN-01 as Therapeutic Approach Against Pediatric Osteosarcoma. *Clin. Cancer Res.* **22**, 2217–2225.

Martuza, R. L., Malick, A., Markert, J. M., Ruffner, K. L. and Coen, D. M. (1991). Experimental therapy of human glioma by means of a genetically engineered virus mutant. *Science* **252**, 854–856.

Masamune, A. and Shimosegawa, T. (2009). Signal transduction in pancreatic stellate cells. *J. Gastroenterol.* **44**, 249–260.

Masamune, A. and Shimosegawa, T. (2013). Pancreatic stellate cells--multi-functional cells in the pancreas. *Pancreatology* **13**, 102–105.

Masamune, A. and Shimosegawa, T. (2015). Pancreatic stellate cells: A dynamic player of the intercellular communication in pancreatic cancer. *Clin Res Hepatol Gastroenterol* **39 Suppl 1**, S98–103.

Masamune, A., Sakai, Y., Kikuta, K., Satoh, M., Satoh, A. and Shimosegawa, T. (2002). Activated rat pancreatic stellate cells express intercellular adhesion molecule-1 (ICAM-1) in vitro. *Pancreas* **25**, 78–85.

Masamune, A., Watanabe, T., Kikuta, K. and Shimosegawa, T. (2009). Roles of pancreatic stellate cells in pancreatic inflammation and fibrosis. *Clin. Gastroenterol. Hepatol.* **7**, S48–54.

Mathison, A., Liebl, A., Bharucha, J., Mukhopadhyay, D., Lomberk, G., Shah, V. and Urrutia, R. (2010). Pancreatic Stellate Cell Models for Transcriptional Studies of Desmoplasia-Associated Genes. *Pancreatology* **10**, 505–516.

Matthaei, H., Schulick, R. D., Hruban, R. H. and Maitra, A. (2011). Cystic precursors to invasive pancreatic cancer. *Nat Rev Gastroenterol Hepatol* **8**, 141–150.

Mavroudis, D., Pappas, P., Kouroussis, C., Kakolyris, S., Agelaki, S., Kalbakis, K., Androulakis, N., Souglakos, J., Vardakis, N., Nikolaidou, M., et al. (2003). A dose-escalation and pharmacokinetic study of gemcitabine and oxaliplatin in patients with advanced solid tumors. *Ann. Oncol.* **14**, 304–312.

McCarroll, J. A., Naim, S., Sharbeen, G., Russia, N., Lee, J., Kavallaris, M., Goldstein, D. and Phillips, P. A. (2014). Role of pancreatic stellate cells in chemoresistance in pancreatic cancer. *Front Physiol* **5**, 141.

Medof, M. E., Kinoshita, T. and Nussenzweig, V. (1984). Inhibition of complement activation on the surface of cells after incorporation of decay-accelerating factor (DAF) into their membranes. *J. Exp. Med.* **160**, 1558–1578.

Meisel, S. R., Shapiro, H., Radnay, J., Neuman, Y., Khaskia, A. R., Gruener, N., Pauzner, H. and David, D. (1998). Increased expression of neutrophil and monocyte adhesion molecules LFA-1 and Mac-1 and their ligand ICAM-1 and VLA-4 throughout the acute phase of myocardial infarction: possible implications for leukocyte aggregation and microvascular plugging. *J. Am. Coll. Cardiol.* **31**, 120–125.

Metz, D. C. and Jensen, R. T. (2008). Gastrointestinal neuroendocrine tumors: pancreatic endocrine tumors. *Gastroenterology* **135**, 1469–1492.

Mews, P., Phillips, P., Fahmy, R., Korsten, M., Pirola, R., Wilson, J. and Apte, M. (2002). Pancreatic stellate cells respond to inflammatory cytokines: potential role in chronic pancreatitis. *Gut* **50**, 535–541.

Mian, O. Y., Ram, A. N., Tuli, R. and Herman, J. M. (2014). Management options in locally advanced pancreatic cancer. *Curr Oncol Rep* **16**, 388.

Mills, K., Birt, L., Emery, J. D., Hall, N., Banks, J., Johnson, M., Lancaster, J., Hamilton, W., Rubin, G. P. and Walter, F. M. (2017). Understanding symptom appraisal and help-seeking in people with symptoms suggestive of pancreatic cancer: a qualitative study. *BMJ Open* **7**, e015682.

Mitchell, W. L., Ravenscroft, P., Hill, M. L., Knutsen, L. J., Judkins, B. D., Newton, R. F. and Scopes, D. I. (1986). Synthesis and antiviral properties of 5-(2-substituted vinyl)-6-aza-2'-deoxyuridines. *J. Med. Chem.* **29**, 809–816.

Mizushima, S. and Nagata, S. (1990). pEF-BOS, a powerful mammalian expression vector. *Nucleic Acids Res.* **18**, 5322.

Mohamed, A., Saad, Y., Saleh, D., Elawady, R., Eletreby, R., Kharalla, A. S. and

Badr, E. (2016). Can Serum ICAM 1 distinguish pancreatic cancer from chronic pancreatitis? *Asian Pac. J. Cancer Prev.* **17**, 4671–4675.

Mohr, I. and Gluzman, Y. (1996). A herpesvirus genetic element which affects translation in the absence of the viral GADD34 function. *EMBO J* **15**, 4759–4766.

Mohr, I., Sternberg, D., Ward, S., Leib, D., Mulvey, M. and Gluzman, Y. (2001). A herpes simplex virus type 1 gamma34.5 second-site suppressor mutant that exhibits enhanced growth in cultured glioblastoma cells is severely attenuated in animals. *J. Virol.* **75**, 5189–5196.

Mohr, S. B., Garland, C. F., Gorham, E. D., Grant, W. B. and Garland, F. C. (2010). Ultraviolet B Irradiance and Vitamin D Status are Inversely Associated With Incidence Rates of Pancreatic Cancer Worldwide. *Pancreas* **39**, 669–674.

Moore, A. E. (1954). Effects of viruses on tumors. *Annu. Rev. Microbiol.* **8**, 393–410.

Moore, A. E., Rhoads, C. P. and Southam, C. M. (1957). Homotransplantation of human cell lines. *Science* **125**, 158–160.

Motzer, R. J., Escudier, B., McDermott, D. F., George, S., Hammers, H. J., Srinivas, S., Tykodi, S. S., Sosman, J. A., Procopio, G., Plimack, E. R., et al. (2015). Nivolumab versus Everolimus in Advanced Renal-Cell Carcinoma. *N Engl J Med* **373**, 1803–1813.

Moutinho-Ribeiro, P., Coelho, R., Giovannini, M. and Macedo, G. (2017). Pancreatology. *Pancreatology* 1–12.

Muniraj, T., Jamidar, P. A. and Aslanian, H. R. (2013). Pancreatic cancer: a comprehensive review and update. *Dis Mon* **59**, 368–402.

Murray, D. R., Cassel, W. A., Torbin, A. H., Olkowski, Z. L. and Moore, M. E. (1977). Viral oncolysate in the management of malignant melanoma. II. Clinical studies. *Cancer* **40**, 680–686.

Nakai, Y., Iwashita, T., Park, D. H., Samarasena, J. B., Lee, J. G. and Chang, K. J. (2015). Diagnosis of pancreatic cysts: EUS-guided, through-the-needle confocal laser-induced endomicroscopy and cystoscopy trial: DETECT study. *Gastrointest. Endosc.* **81**, 1204–1214.

Nakao, A., Kasuya, H., Sahin, T. T., Nomura, N., Kanzaki, A., Misawa, M., Shirota, T., Yamada, S., Fujii, T., Sugimoto, H., et al. (2011). A phase I dose-escalation clinical trial of intraoperative direct intratumoral injection of HF10 oncolytic virus in non-resectable patients with advanced pancreatic cancer. *Cancer Gene Ther* **18**, 167–175.

Napoléon, B., Lemaistre, A.-I., Pujol, B., Caillol, F., Lucidarme, D., Bourdariat, R., Morellon-Mialhe, B., Fumex, F., Lefort, C., Lepilliez, V., et al. (2015). A novel approach to the diagnosis of pancreatic serous cystadenoma: needle-based confocal laser endomicroscopy. *Endoscopy* **47**, 26–32.

National Cancer Institute (2017). SEER Stat Fact Sheets: Pancreas Cancer. *seer.cancer.gov/statfacts/html/pancreas.html*.

National Research Council (2010). *Guide for the Care and Use of Laboratory Animals: Eight Edition*. National Academies Press.

Neesse, A., Algül, H., Tuveson, D. A. and Gress, T. M. (2015). Stromal biology and therapy in pancreatic cancer: a changing paradigm. *Gut* **64**, 1476–1484.

Newcombe, N. G., Andersson, P., Johansson, E. S., Au, G. G., Lindberg, A. M., Barry, R. D. and Shafren, D. R. (2003). Cellular receptor interactions of C-cluster human group A coxsackieviruses. *J. Gen. Virol.* **84**, 3041–3050.

Newcombe, N. G., Beagley, L. G., Christiansen, D., Loveland, B. E., Johansson, E. S., Beagley, K. W., Barry, R. D. and Shafren, D. R. (2004a). Novel role for decay-accelerating factor in coxsackievirus A21-mediated cell infectivity. *J. Virol.* **78**, 12677–12682.

Newcombe, N. G., Johansson, E. S., Au, G., Lindberg, A. M., Barry, R. D. and Shafren, D. R. (2004b). Enterovirus capsid interactions with decay-accelerating factor mediate lytic cell infection. *J. Virol.* **78**, 1431–1439.

Newton, A. H., Danahy, D. B., Chan, M. A. and Benedict, S. H. (2015). Timely blockade of ICAM-1.LFA-1 interaction prevents disease onset in a mouse model of emphysema. *Immunotherapy* **7**, 621–629.

Nielsen, M. F. B., Mortensen, M. B. and Detlefsen, S. (2016a). Key players in

pancreatic cancer-stroma interaction: Cancer-associated fibroblasts, endothelial and inflammatory cells. *World Journal of Gastroenterology : WJG* **22**, 2678–2700.

Nielsen, S. R., Quaranta, V., Linford, A., Emeagi, P., Rainer, C., Santos, A., Ireland, L., Sakai, T., Sakai, K., Kim, Y.-S., et al. (2016b). Macrophage-secreted granulin supports pancreatic cancer metastasis by inducing liver fibrosis. *Nat Cell Biol* **18**, 549–560.

Nishimata, S., Kato, K., Tanaka, M., Ijiri, R., Toyoda, Y., Kigasawa, H., Ohama, Y., Nakatani, Y., Notohara, K., Kobayashi, Y., et al. (2005). Expression pattern of keratin subclasses in pancreatoblastoma with special emphasis on squamoid corpuscles. *Pathol Int* **55**, 297–302.

Noë, M. and Brosens, L. A. A. (2016). Pathology of Pancreatic Cancer Precursor Lesions. *Surgical Pathology* **9**, 561–580.

Nomoto, A., Kitamura, N., Golini, F. and Wimmer, E. (1977). The 5'-terminal structures of poliovirion RNA and poliovirus mRNA differ only in the genome-linked protein VPg. *Proc. Natl. Acad. Sci. U.S.A.* **74**, 5345–5349.

Noonan, A. M., Farren, M. R., Geyer, S. M., Huang, Y., Tahiri, S., Ahn, D., Mikhail, S., Ciombor, K. K., Pant, S., Aparo, S., et al. (2016). Randomized Phase 2 Trial of the Oncolytic Virus Pelareorep (Reolysin) in Upfront Treatment of Metastatic Pancreatic Adenocarcinoma. *Mol Ther* **24**, 1150–1158.

Noy, R. and Pollard, J. W. (2014). Tumor-associated macrophages: from mechanisms to therapy. *Immunity* **41**, 49–61.

Nugent, C. I. and Kirkegaard, K. (1995). RNA binding properties of poliovirus subviral particles. *J. Virol.* **69**, 13–22.

Nummer, D., Suri-Payer, E., Schmitz-Winnenthal, H., Bonertz, A., Galindo, L., Antolovich, D., Koch, M., Büchler, M., Weitz, J., Schirrmacher, V., et al. (2007). Role of tumor endothelium in CD4+ CD25+ regulatory T cell infiltration of human pancreatic carcinoma. *J Natl Cancer Inst* **99**, 1188–1199.

Okamoto, K., Koyama, I., Miyazawa, M., Toshimitsu, Y., Aikawa, M., Okada, K., Imabayashi, E. and Matsuda, H. (2011). Preoperative 18[F]-fluorodeoxyglucose

positron emission tomography/computed tomography predicts early recurrence after pancreatic cancer resection. *Int J Clin Oncol* **16**, 39–44.

Omary, M. B., Lugea, A., Lowe, A. W. and Pandol, S. J. (2007). The pancreatic stellate cell: a star on the rise in pancreatic diseases. *J. Clin. Invest.* **117**, 50–59.

Omiyale, A. O. (2015). Clinicopathological review of pancreatoblastoma in adults. *Gland Surg* **4**, 322–328.

Orimo, A. and Weinberg, R. A. (2014). Stromal Fibroblasts in Cancer: A Novel Tumor-Promoting Cell Type. *Cell Cycle* **5**, 1597–1601.

Owens, R. B., Smith, H. S., Nelson-Rees, W. A. and Springer, E. L. (1976). Epithelial cell cultures from normal and cancerous human tissues. *J Natl Cancer Inst* **56**, 843–849.

Pack, G. T. (1950). Note on the experimental use of rabies vaccine for melanomatosis. *AMA Arch Derm Syphilol* **62**, 694–695.

Pandol, S., Gukovskaya, A., Edderkaoui, M., Edderkoui, M., Dawson, D., Eibl, G. and Lugea, A. (2012). Epidemiology, risk factors, and the promotion of pancreatic cancer: role of the stellate cell. *J. Gastroenterol. Hepatol.* **27 Suppl 2**, 127–134.

Papi, A. and Johnston, S. L. (1999). Rhinovirus infection induces expression of its own receptor intercellular adhesion molecule 1 (ICAM-1) via increased NF-kappaB-mediated transcription. *J. Biol. Chem.* **274**, 9707–9720.

Pardoll, D. M. (2012). The blockade of immune checkpoints in cancer immunotherapy. *Nat Rev Cancer* **12**, 252–264.

Parrish, C. R. (1991). Mapping specific functions in the capsid structure of canine parvovirus and feline panleukopenia virus using infectious plasmid clones. *Virology* **183**, 195–205.

Parrish, C. R. and Kawaoka, Y. (2005). The origins of new pandemic viruses: the acquisition of new host ranges by canine parvovirus and influenza A viruses. *Annu. Rev. Microbiol.* **59**, 553–586.

Parrish, C. R., Have, P., Foreyt, W. J., Evermann, J. F., Senda, M. and Carmichael,

L. E. (1988). The Global Spread and Replacement of Canine Parvovirus Strains. *Journal of General Virology* **69**, 1111–1116.

Parsons, R., Bynoe, M. L., Pereira, M. S. and Tyrrell, D. A. (1960). Inoculation of human volunteers with strains of Coe virus isolated in Britain. *Br Med J* **1**, 1776–1778.

Pasquinucci, G. (1971). Possible effect of measles on leukaemia. *Lancet* **1**, 136.

Patel, N., Buthala, D. A. and Walker, J. S. (1964). Controlled Studies of Coxsackie A-21 (Coe) virus in Volunteers. *J. Infect. Dis.* **114**, 87–94.

Patra, K. C., Bardeesy, N. and Mizukami, Y. (2017). Diversity of Precursor Lesions For Pancreatic Cancer: The Genetics and Biology of Intraductal Papillary Mucinous Neoplasm. *Clin Transl Gastroenterol* **8**, e86.

Paul, A. V. and Wimmer, E. (2015). Initiation of protein-primed picornavirus RNA synthesis. *Virus Res.* **206**, 12–26.

Paul, A. V., Molla, A. and Wimmer, E. (1994). Studies of a putative amphipathic helix in the N-terminus of poliovirus protein 2C. *Virology* **199**, 188–199.

Paulo, J. A., Urrutia, R., Banks, P. A., Conwell, D. L. and Steen, H. (2011). Proteomic analysis of an immortalized mouse pancreatic stellate cell line identifies differentially-expressed proteins in activated vs nonproliferating cell states. *J. Proteome Res.* **10**, 4835–4844.

Peixoto, R. D., Ho, M., Renouf, D. J., Lim, H. J., Gill, S., Ruan, J. Y. and Cheung, W. Y. (2015). Eligibility of Metastatic Pancreatic Cancer Patients for First-Line Palliative Intent nab-Paclitaxel Plus Gemcitabine Versus FOLFIRINOX. *American Journal of Clinical Oncology*.

Peng, Y.-P., Xi, C.-H., Zhu, Y., Yin, L.-D., Wei, J.-S., Zhang, J.-J., Liu, X.-C., Guo, S., Fu, Y. and Miao, Y. (2016). Altered expression of CD226 and CD96 on natural killer cells in patients with pancreatic cancer. *Oncotarget* **7**, 66586–66594.

Peng, Y.-P., Zhang, J.-J., Liang, W.-B., Tu, M., Lu, Z.-P., Wei, J.-S., Jiang, K.-R., Gao, W.-T., Wu, J.-L., Xu, Z.-K., et al. (2014). Elevation of MMP-9 and IDO induced by pancreatic cancer cells mediates natural killer cell dysfunction. *BMC*

Cancer **14**, 738.

Pereira, M. S. and Pereira, H. G. (1959). Coe virus properties and prevalence in Great Britain. *The Lancet* **274**, 539–541.

Pereira, P. L. and Wiskirchen, J. (2003). Morphological and functional investigations of neuroendocrine tumors of the pancreas. *Eur Radiol* **13**, 2133–2146.

Pinho, D. F. and Subramaniam, R. M. (2017). PET-Computed Tomography and Precision Medicine in Pancreatic Adenocarcinoma and Pancreatic Neuroendocrine Tumors. *PET Clin* **12**, 407–421.

Poppers, J., Mulvey, M., Khoo, D. and Mohr, I. (2000). Inhibition of PKR activation by the proline-rich RNA binding domain of the herpes simplex virus type 1 Us11 protein. *J. Virol.* **74**, 11215–11221.

Poruk, K. E., Gay, D. Z., Brown, K., D Mulvihill, J., Boucher, K. M., Scaife, C. L., Firpo, M. A. and Mulvihill, S. J. (2013). The Clinical Utility of CA 19-9 in Pancreatic Adenocarcinoma: Diagnostic and Prognostic Updates. *Current Molecular Medicine* **13**, 340–351.

Pothula, S., Patel, M., Xu, Z., Lee, A., Goldstein, D., Pirola, R., Apte, M. and Wilson, J. (2014). The role of the hepatocyte growth factor/c-MET pathway in pancreatic stellate cell-endothelial cell interactions: Anti-angiogenic implications in Pancreatic Cancer. *Pancreatology* **14**, S9.

Powles, T., Eder, J. P., Fine, G. D., Braiteh, F. S., Loriot, Y., Cruz, C., Bellmunt, J., Burris, H. A., Petrylak, D. P., Teng, S.-L., et al. (2014). MPDL3280A (anti-PD-L1) treatment leads to clinical activity in metastatic bladder cancer. *Nature* **515**, 558–562.

Provenzano, P. P. and Hingorani, S. R. (2013). Hyaluronan, fluid pressure, and stromal resistance in pancreas cancer. *British Journal of Cancer* **108**, 1–8.

Provenzano, P. P., Cuevas, C., Chang, A. E., Goel, V. K., Hoff, Von, D. D. and Hingorani, S. R. (2012). Enzymatic targeting of the stroma ablates physical barriers to treatment of pancreatic ductal adenocarcinoma. *Cancer Cell* **21**, 418–429.

Putnak, J. R. and Phillips, B. A. (1981a). Picornaviral structure and assembly. *Microbiol. Rev.* **45**, 287–315.

Putnak, J. R. and Phillips, B. A. (1981b). Differences between poliovirus empty capsids formed in vivo and those formed in vitro: a role for the morphopoietic factor. *J. Virol.* **40**, 173–183.

Rahib, L., Smith, B. D., Aizenberg, R., Rosenzweig, A. B., Fleshman, J. M. and Matrisian, L. M. (2014). Projecting Cancer Incidence and Deaths to 2030: The Unexpected Burden of Thyroid, Liver, and Pancreas Cancers in the United States. *Cancer Research* **74**, 2913–2921.

Rasanen, K. and Vaheri, A. (2010). Activation of fibroblasts in cancer stroma. *Experimental Cell Research* **316**, 2713–2722.

Raza, A., Franklin, M. J. and Dudek, A. Z. (2010). Pericytes and vessel maturation during tumor angiogenesis and metastasis. *Am. J. Hematol.* **85**, 593–598.

Ren, B., Cui, M., Yang, G., Wang, H., Feng, M., You, L. and Zhao, Y. (2018). Tumor microenvironment participates in metastasis of pancreatic cancer. *Mol Cancer* **17**, 108.

Renehan, A. G., Zwahlen, M. and Egger, M. (2015). Adiposity and cancer risk: new mechanistic insights from epidemiology. *Nat Rev Cancer* **15**, 484–498.

Riall, T. S., Cameron, J. L., Lillemoe, K. D., Winter, J. M., Campbell, K. A., Hruban, R. H., Chang, D. and Yeo, C. J. (2006). Resected periampullary adenocarcinoma: 5-year survivors and their 6- to 10-year follow-up. *Surgery* **140**, 764–772.

Rice, J. C. and Bucy, R. P. (1995). Differences in the degree of depletion, rate of recovery, and the preferential elimination of naive CD4+ T cells by anti-CD4 monoclonal antibody (GK1.5) in young and aged mice. *J. Immunol.* **154**, 6644–6654.

Ridd, S. (2015). *Pancreas Cancer: Tips to Identifying the Signs and Symptoms to Diagnosis Pancreatic Cancer At Early Stages, Including Pancreas Cancer Treatment Options!* Lulu Press, Inc.

Rizvi, N. A., Hellmann, M. D., Snyder, A., Kvistborg, P., Makarov, V., Havel, J. J.,

Lee, W., Yuan, J., Wong, P., Ho, T. S., et al. (2015). Mutational landscape determines sensitivity to PD-1 blockade in non-small cell lung cancer. *Science* **348**, 124–128.

Rodriguez-Garcia, A., Gimenez-Alejandre, M., Rojas, J. J., Moreno, R., Bazan-Peregrino, M., Cascallo, M. and Alemany, R. (2015). Safety and Efficacy of VCN-01, an Oncolytic Adenovirus Combining Fiber HSG-Binding Domain Replacement with RGD and Hyaluronidase Expression. *Clinical Cancer Research* **21**, 1406–1418.

Rogulski, K. R., Freytag, S. O., Zhang, K., Gilbert, J. D., Paielli, D. L., Kim, J. H., Heise, C. C. and Kirn, D. H. (2000). In vivo antitumor activity of ONYX-015 is influenced by p53 status and is augmented by radiotherapy. *Cancer Research* **60**, 1193–1196.

Rohayem, J., Robel, I., Jäger, K., Scheffler, U. and Rudolph, W. (2006). Protein-primed and de novo initiation of RNA synthesis by norovirus 3Dpol. *J. Virol.* **80**, 7060–7069.

Rojas, J. J., Gimenez-Alejandre, M., Gil-Hoyos, R., Cascallo, M. and Alemany, R. (2012). Improved systemic antitumor therapy with oncolytic adenoviruses by replacing the fiber shaft HSG-binding domain with RGD. *Gene Therapy* **19**, 453–457.

Roland, C. L., Harken, A. H., Sarr, M. G. and Barnett, C. C. (2007). ICAM-1 expression determines malignant potential of cancer. *Surgery* **141**, 705–707.

Rombaut, B., Vrijsen, R. and Boeyé, A. (1990). New evidence for the precursor role of 14 S subunits in poliovirus morphogenesis. *Virology* **177**, 411–414.

Rooney, M. S., Shukla, S. A., Wu, C. J., Getz, G. and Hacohen, N. (2015). Molecular and genetic properties of tumors associated with local immune cytolytic activity. *Cell* **160**, 48–61.

Rosenbaum, J. N. and Lloyd, R. V. (2014). Pancreatic Neuroendocrine Neoplasms. *Surgical Pathology* **7**, 559–575.

Rosette, C., Roth, R. B., Oeth, P., Braun, A., Kammerer, S., Ekblom, J. and

Denissenko, M. F. (2005). Role of ICAM1 in invasion of human breast cancer cells. *Carcinogenesis* **26**, 943–950.

Rossmann, M. G. and Johnson, J. E. (1989). Icosahedral RNA virus structure. *Annu. Rev. Biochem.* **58**, 533–573.

Rossmann, M. G., He, Y. and Kuhn, R. J. (2002). Picornavirus-receptor interactions. *Trends Microbiol.* **10**, 324–331.

Roy, D. G. and Bell, J. C. (2013). Cell carriers for oncolytic viruses: current challenges and future directions. *Oncolytic Virotherapy* **2**, 47–56.

Russell, S. J., Peng, K.-W. and Bell, J. C. (2012). Oncolytic virotherapy. *Nature Biotechnology* **30**, 658–670.

Salman, B., Brat, G., Yoon, Y.-S., Hruban, R. H., Singhi, A. D., Fishman, E. K., Herman, J. M. and Wolfgang, C. L. (2013). The Diagnosis and Surgical Treatment of Pancreatoblastoma in Adults: A Case Series and Review of the Literature. *J Gastrointest Surg* **17**, 2153–2161.

Salmon, P. and Baix, A. (1922). Vaccine varioloque dans le cancer. *Compt. Rend. Soc. Biol.* **86**, 819–820.

Sarnecka, A. K., Zagozda, M. and Durlik, M. (2016). An Overview of Genetic Changes and Risk of Pancreatic Ductal Adenocarcinoma. *J Cancer* **7**, 2045–2051.

Sato, N., Cheng, X.-B., Kohi, S., Koga, A. and Hirata, K. (2016). Targeting hyaluronan for the treatment of pancreatic ductal adenocarcinoma. *Acta Pharm Sin B* **6**, 101–105.

Scarlett, C. J. (2013). Contribution of bone marrow derived cells to the pancreatic tumor microenvironment. *Front Physiol* **4**, 56.

Scarlett, C. J., Colvin, E. K., Pinese, M., Chang, D. K., Morey, A. L., Musgrove, E. A., Pajic, M., Apte, M., Henshall, S. M., Sutherland, R. L., et al. (2011a). Recruitment and activation of pancreatic stellate cells from the bone marrow in pancreatic cancer: a model of tumor-host interaction. *PLoS ONE* **6**, e26088.

Scarlett, C. J., Salisbury, E. L., Biankin, A. V. and Kench, J. (2011b). Precursor

lesions in pancreatic cancer: morphological and molecular pathology. *Pathology* **43**, 183–200.

Schmidt, C. M., Powell, E. S., Yiannoutsos, C. T., Howard, T. J., Wiebke, E. A., Wiesnauer, C. A., Baumgardner, J. A., Cummings, O. W., Jacobson, L. E., Broadie, T. A., et al. (2004). Pancreaticoduodenectomy. *Arch Surg* **139**, 718–727.

Schmidt, J., Mocevicius, P., Werner, J. and Ryschich, E. (2012). The role of the tumor endothelium in leukocyte recruitment in pancreatic cancer. *Surgery* **152**, S89–94.

Schmidt, N. J., Fox, V. L. and Lennette, E. H. (1961). Immunologic identification of Coxsackie A21 virus with Coe virus. *Proc. Soc. Exp. Biol. Med.* **107**, 63–65.

Schneemann, A. (2006). The Structural and Functional Role of RNA in Icosahedral Virus Assembly. *Annu. Rev. Microbiol.* **60**, 51–67.

Schneider, E., Schmid-Kotsas, A., Zhao, J., Weidenbach, H., Schmid, R. M., Menke, A., Adler, G., Waltenberger, J., Grünert, A. and Bachem, M. G. (2001). Identification of mediators stimulating proliferation and matrix synthesis of rat pancreatic stellate cells. *Am. J. Physiol., Cell Physiol.* **281**, C532–43.

Schnelldorfer, T., Ware, A. L., Sarr, M. G., Smyrk, T. C., Zhang, L., Qin, R., Gullerud, R. E., Donohue, J. H., Nagorney, D. M. and Farnell, M. B. (2008). Long-term survival after pancreatoduodenectomy for pancreatic adenocarcinoma: is cure possible? *Ann. Surg.* **247**, 456–462.

Schultz, R. M., Merriman, R. L., Toth, J. E., Zimmermann, J. E., Hertel, L. W., Andis, S. L., Dudley, D. E., Rutherford, P. G., Tanzer, L. R. and Grindey, G. B. (1993). Evaluation of new anticancer agents against the MIA PaCa-2 and PANC-1 human pancreatic carcinoma xenografts. *Oncol. Res.* **5**, 223–228.

Seo, Y. D. and Pillarisetty, V. G. (2016). T-cell programming in pancreatic adenocarcinoma: a review. *Cancer Gene Ther* **24**, 106–113.

Shackelton, L. A., Parrish, C. R., Truyen, U. and Holmes, E. C. (2005). High rate of viral evolution associated with the emergence of carnivore parvovirus. *Proc. Natl. Acad. Sci. U.S.A.* **102**, 379–384.

Shafren, D. R. (1998). Viral cell entry induced by cross-linked decay-accelerating factor. *J. Virol.* **72**, 9407–9412.

Shafren, D. R., Au, G. G., Nguyen, T., Newcombe, N. G., Haley, E. S., Beagley, L., Johansson, E. S., Hersey, P. and Barry, R. D. (2004). Systemic therapy of malignant human melanoma tumors by a common cold-producing enterovirus, coxsackievirus a21. *Clin. Cancer Res.* **10**, 53–60.

Shafren, D. R., Dorahy, D. J., Ingham, R. A., Burns, G. F. and Barry, R. D. (1997). Coxsackievirus A21 binds to decay-accelerating factor but requires intercellular adhesion molecule 1 for cell entry. *J. Virol.* **71**, 4736–4743.

Shafren, D. R., Dorahy, D. J., Thorne, R. F., Kinoshita, T., Barry, R. D. and Burns, G. F. (1998). Antibody binding to individual short consensus repeats of decay-accelerating factor enhances enterovirus cell attachment and infectivity. *J. Immunol.* **160**, 2318–2323.

Sharpe, A. H. (2009). Mechanisms of costimulation. *Immunol Rev* **229**, 5–11.

Shi, C., Washington, M. K., Chaturvedi, R., Drosos, Y., Revetta, F. L., Weaver, C. J., Buzhardt, E., Yull, F. E., Blackwell, T. S., Sosa-Pineda, B., et al. (2014). Fibrogenesis in pancreatic cancer is a dynamic process regulated by macrophage-stellate cell interaction. *Lab. Invest.* **94**, 409–421.

Sickles, G. M., Mutterer, M. and Plager, H. (1959). New types of Coxsackie virus, group A. Cytopathogenicity in tissue culture. *Proc. Soc. Exp. Biol. Med.* **102**, 742–743.

Sieben, M., Schäfer, P., Dinsart, C., Galle, P. R. and Moehler, M. (2013). Activation of the human immune system via toll-like receptors by the oncolytic parvovirus H-1. *Int. J. Cancer* **132**, 2548–2556.

Siegel, R. and Jemal, D. A. (2017). *Cancer Facts & Figures 2017*. Atlanta: American Cancer Society.

Siegel, R. L., Miller, K. D. and Jemal, A. (2017). Cancer statistics, 2017. *CA Cancer J Clin* **67**, 7–30.

Sinkovics, J. G. and Horvath, J. C. (2000). Newcastle disease virus (NDV): brief

history of its oncolytic strains. *J. Clin. Virol.* **16**, 1–15.

Skelding, K. A., Barry, R. D. and Shafren, D. R. (2009). Systemic targeting of metastatic human breast tumor xenografts by Coxsackievirus A21. *Breast Cancer Res. Treat.* **113**, 21–30.

Skelton, R. A., Javed, A., Zheng, L. and He, J. (2017). Overcoming the resistance of pancreatic cancer to immune checkpoint inhibitors. *J Surg Oncol* **116**, 55–62.

Smith, C. W., Marlin, S. D., Rothlein, R., Toman, C. and Anderson, D. C. (1989). Cooperative interactions of LFA-1 and Mac-1 with intercellular adhesion molecule-1 in facilitating adherence and transendothelial migration of human neutrophils in vitro. *J. Clin. Invest.* **83**, 2008–2017.

Song, J., Lee, J., Kim, J., Jo, S., Kim, Y. J., Baek, J. E., Kwon, E.-S., Lee, K.-P., Yang, S., Kwon, K.-S., et al. (2016). Pancreatic adenocarcinoma up-regulated factor (PAUF) enhances the accumulation and functional activity of myeloid-derived suppressor cells (MDSCs) in pancreatic cancer. *Oncotarget* **7**, 51840–51853.

Sousa, C. M., Biancur, D. E., Wang, X., Halbrook, C. J., Sherman, M. H., Zhang, L., Kremer, D., Hwang, R. F., Witkiewicz, A. K., Ying, H., et al. (2016). Pancreatic stellate cells support tumour metabolism through autophagic alanine secretion. *Nature* **536**, 479–483.

Southam, C. M. (1958). Homotransplantation of human cell lines. *Bull N Y Acad Med* **34**, 416–423.

Southam, C. M. and Moore, A. E. (1951). West Nile, Ilheus, and Bunyamwera virus infections in man. *Am. J. Trop. Med. Hyg.* **31**, 724–741.

Southam, C. M. and Moore, A. E. (1952). Clinical studies of viruses as antineoplastic agents with particular reference to Egypt 101 virus. *Cancer* **5**, 1025–1034.

Southam, C. M. and Moore, A. E. (1954). Induced virus infections in man by the Egypt isolates of West Nile virus. *Am. J. Trop. Med. Hyg.* **3**, 19–50.

Spickard, A., Evans, H., Knight, V. and Johnson, K. (1963). Acute respiratory disease in normal volunteers associated with Coxsackie A-21 viral infection. III.

Response to nasopharyngeal and enteric inoculation. *J. Clin. Invest.* **42**, 840–852.

Staunton, D. E., Marlin, S. D., Stratowa, C., Dustin, M. L. and Springer, T. A. (1988). Primary structure of ICAM-1 demonstrates interaction between members of the immunoglobulin and integrin supergene families. *Cell* **52**, 925–933.

Steil, B. P., Kempf, B. J. and Barton, D. J. (2010). Poly(A) at the 3“ end of positive-strand RNA and VPg-linked poly(U) at the 5” end of negative-strand RNA are reciprocal templates during replication of poliovirus RNA. *J. Virol.* **84**, 2843–2858.

Stromnes, I. M., Brockenbrough, J. S., Izeradjene, K., Carlson, M. A., Cuevas, C., Simmons, R. M., Greenberg, P. D. and Hingorani, S. R. (2014). Targeted depletion of an MDSC subset unmasks pancreatic ductal adenocarcinoma to adaptive immunity. *Gut* **63**, 1769–1781.

Strouch, M. J., Cheon, E. C., Salabat, M. R., Krantz, S. B., Gounaris, E., Melstrom, L. G., Dangi-Garimella, S., Wang, E., Munshi, H. G., Khazaie, K., et al. (2010). Crosstalk between mast cells and pancreatic cancer cells contributes to pancreatic tumor progression. *Clin. Cancer Res.* **16**, 2257–2265.

Sun, X.-J., Jiang, T.-H., Zhang, X.-P. and Mao, A.-W. (2016). Role of the tumor microenvironment in pancreatic adenocarcinoma. *Front Biosci (Landmark Ed)* **21**, 31–41.

Svitkin, Y. V., Imataka, H., Khaleghpour, K., Kahvejian, A., Liebig, H.-D. and Sonenberg, N. (2001). Poly(A)-binding protein interaction with eIF4G stimulates picornavirus IRES-dependent translation. *RNA* **7**, 1743–1752.

Sweeney, T. R., Abaeva, I. S., Pestova, T. V. and Hellen, C. U. T. (2013). The mechanism of translation initiation on Type 1 picornavirus IRESs. *EMBO J* **33**, 76–92.

Swords, D. S., Firpo, M. A., Scaife, C. L. and Mulvihill, S. J. (2016). Biomarkers in pancreatic adenocarcinoma: current perspectives. *Onco Targets Ther* **9**, 7459–7467.

Takakuwa, H., Goshima, F., Nozawa, N., Yoshikawa, T., Kimata, H., Nakao, A., Nawa, A., Kurata, T., Sata, T. and Nishiyama, Y. (2003). Oncolytic viral therapy

using a spontaneously generated herpes simplex virus type 1 variant for disseminated peritoneal tumor in immunocompetent mice. *Arch Virol* **148**, 813–825.

Tan, E. H. and Tan, C. H. (2011). Imaging of gastroenteropancreatic neuroendocrine tumors. *WJCO* **2**, 28–43.

Tan, G., Kasuya, H., Sahin, T. T., Yamamura, K., Wu, Z., Koide, Y., Hotta, Y., Shikano, T., Yamada, S., Kanzaki, A., et al. (2015). Combination therapy of oncolytic herpes simplex virus HF10 and bevacizumab against experimental model of human breast carcinoma xenograft. *Int. J. Cancer* **136**, 1718–1730.

Tan, M. H., Nowak, N. J., Loor, R., Ochi, H., Sandberg, A. A., Lopez, C., Pickren, J. W., Berjian, R., Douglass, H. O. and Chu, T. M. (1986). Characterization of a new primary human pancreatic tumor line. *Cancer Invest.* **4**, 15–23.

Taneja, S., MacGregor, J., Markus, S., Ha, S. and Mohr, I. (2001). Enhanced antitumor efficacy of a herpes simplex virus mutant isolated by genetic selection in cancer cells. *Proc. Natl. Acad. Sci. U.S.A.* **98**, 8804–8808.

Tang, Y., Xu, X., Guo, S., Zhang, C., Tang, Y., Tian, Y., Ni, B., Lu, B. and Wang, H. (2014). An increased abundance of tumor-infiltrating regulatory T cells is correlated with the progression and prognosis of pancreatic ductal adenocarcinoma. *PLoS ONE* **9**, e91551.

Taqi, A. M., Abdurrahman, M. B., Yakubu, A. M. and Fleming, A. F. (1981). Regression of Hodgkin's disease after measles. *Lancet* **1**, 1112.

Teijeira, A., Hunter, M. C., Russo, E., Proulx, S. T., Frei, T., Debes, G. F., Coles, M., Melero, I., Detmar, M., Rouzaut, A., et al. (2017). T Cell Migration from Inflamed Skin to Draining Lymph Nodes Requires Intralymphatic Crawling Supported by ICAM-1/LFA-1 Interactions. *Cell Rep* **18**, 857–865.

Tempia-Caliera, A. A., Horvath, L. Z., Zimmermann, A., Tihanyi, T. T., Korc, M., Friess, H. and Buchler, M. W. (2002). Adhesion molecules in human pancreatic cancer. *J Surg Oncol* **79**, 93–100.

Teterina, N. L., Gorbalenya, A. E., Egger, D., Bienz, K. and Ehrenfeld, E. (1997).

Poliovirus 2C protein determinants of membrane binding and rearrangements in mammalian cells. *J. Virol.* **71**, 8962–8972.

Teterina, N. L., Kean, K. M., Gorbalenya, A. E., Agol, V. I. and Girard, M. (1992). Analysis of the functional significance of amino acid residues in the putative NTP-binding pattern of the poliovirus 2C protein. *Journal of General Virology* **73**, 1977–1986.

Theoharides, T. C. (2008). Mast cells and pancreatic cancer. *N Engl J Med* **358**, 1860–1861.

Thind, K., Padrnos, L. J., Ramanathan, R. K. and Borad, M. J. (2017). Immunotherapy in pancreatic cancer treatment: a new frontier. *Therapeutic Advances in Gastroenterology* **10**, 168–194.

Thomas, N. J., Foreyt, W. J., Evermann, J. F., Windberg, L. A. and Knowlton, F. F. (1984). Seroprevalence of canine parvovirus in wild coyotes from Texas, Utah, and Idaho (1972 to 1983). *J Am Vet Med Assoc* **185**, 1283–1287.

Thosani, N., Dasari, C. S., Bhutani, M. S., Raimondo, M. and Guha, S. (2010). Molecular pathogenesis of intraductal papillary mucinous neoplasms of the pancreas. *Pancreas* **39**, 1129–1133.

Tien, Y.-W., Wu, Y.-M., Lin, W.-C., Lee, H.-S. and Lee, P.-H. (2009). Pancreatic carcinoma cells stimulate proliferation and matrix synthesis of hepatic stellate cells. *J. Hepatol.* **51**, 307–314.

Toda, M., Martuza, R. L. and Rabkin, S. D. (2000). Tumor growth inhibition by intratumoral inoculation of defective herpes simplex virus vectors expressing granulocyte-macrophage colony-stimulating factor. *Mol Ther* **2**, 324–329.

Toll, A. D., Mitchell, D., Yeo, C. J., Hruban, R. H. and Witkiewicz, A. K. (2011). Acinar Cell Carcinoma With Prominent Intraductal Growth Pattern. *International Journal of Surgical Pathology* **19**, 795–799.

Tomazin, R., van Schoot, N. E., Goldsmith, K., Jugovic, P., Sempé, P., Früh, K. and Johnson, D. C. (1998). Herpes simplex virus type 2 ICP47 inhibits human TAP but not mouse TAP. *J. Virol.* **72**, 2560–2563.

Topalian, S. L., Drake, C. G. and Pardoll, D. M. (2012). Targeting the PD-1/B7-H1(PD-L1) pathway to activate anti-tumor immunity. *Curr. Opin. Immunol.* **24**, 207–212.

Topalian, S. L., Sznol, M., McDermott, D. F., Kluger, H. M., Carvajal, R. D., Sharfman, W. H., Brahmer, J. R., Lawrence, D. P., Atkins, M. B., Powderly, J. D., et al. (2014). Survival, durable tumor remission, and long-term safety in patients with advanced melanoma receiving nivolumab. *J. Clin. Oncol.* **32**, 1020–1030.

Topkan, E., Parlak, C., Kotek, A., Yapar, A. F. and Pehlivan, B. (2011). Predictive value of metabolic 18FDG-PET response on outcomes in patients with locally advanced pancreatic carcinoma treated with definitive concurrent chemoradiotherapy. *BMC Gastroenterol* **11**, 123.

Torphy, R. J., Zhu, Y. and Schulick, R. D. (2018). Immunotherapy for pancreatic cancer: Barriers and breakthroughs. *Ann Gastroenterol Surg* **2**, 274–281.

Torres, M. P., Rachagani, S., Souchek, J. J., Mallya, K., Johansson, S. L. and Batra, S. K. (2013). Novel Pancreatic Cancer Cell Lines Derived from Genetically Engineered Mouse Models of Spontaneous Pancreatic Adenocarcinoma: Applications in Diagnosis and Therapy. *PLoS ONE* **8**, e80580.

Tortora, G. J. and Derrickson, B. H. (2008). *Principles of Anatomy and Physiology*. John Wiley & Sons.

Toshiyama, R., Noda, T., Eguchi, H., Iwagami, Y., Yamada, D., Asaoka, T., Wada, H., Kawamoto, K., Gotoh, K., Takeda, Y., et al. (2017). Two cases of resectable pancreatic cancer diagnosed by open surgical biopsy after endoscopic ultrasound fine-needle aspiration failed to yield diagnosis: case reports. *Surg Case Rep* **3**, 39.

Triebel, F. (2003). LAG-3: a regulator of T-cell and DC responses and its use in therapeutic vaccination. *Trends Immunol.* **24**, 619–622.

USFDA (1996). Gemcitabine Prescribing Information. *accessdata.fda.gov*.

van de Stolpe, A. and van der Saag, P. T. (1996). Intercellular adhesion molecule-1. *J Mol Med* **74**, 13–33.

Van den Broeck, A., Sergeant, G., Ectors, N., Van Steenbergen, W., Aerts, R. and Topal, B. (2009). Patterns of recurrence after curative resection of pancreatic ductal adenocarcinoma. *Eur J Surg Oncol* **35**, 600–604.

van Grevenstein, W. M. U., Hofland, L. J., Jeekel, J. and van Eijck, C. H. J. (2006). The expression of adhesion molecules and the influence of inflammatory cytokines on the adhesion of human pancreatic carcinoma cells to mesothelial monolayers. *Pancreas* **32**, 396–402.

Van Seventer, G. A., Shimizu, Y., Horgan, K. J. and Shaw, S. (1990). The LFA-1 ligand ICAM-1 provides an important costimulatory signal for T cell receptor-mediated activation of resting T cells. *The Journal of Immunology* **144**, 4579–4586.

Vance, L. M., Moscufo, N., Chow, M. and Heinz, B. A. (1997). Poliovirus 2C region functions during encapsidation of viral RNA. *J. Virol.* **71**, 8759–8765.

Vera, B., Martínez-Vélez, N., Xipell, E., Acanda de la Rocha, A., Patiño-García, A., Castresana, J. S., Gonzalez-Huarriz, M., Cascallo, M., Alemany, R. and Alonso, M. M. (2016). Correction: Characterization of the Antiglioma Effect of the Oncolytic Adenovirus VCN-01. *PLoS ONE* **11**, e0157619.

Verlinden, Y., Cuconati, A., Wimmer, E. and Rombaut, B. (2000). Cell-free synthesis of poliovirus: 14S subunits are the key intermediates in the encapsidation of poliovirus RNA. *J. Gen. Virol.* **81**, 2751–2754.

Vidhya, V. (2016). FDA Approved Drugs–October 2015. *Drug Discovery* **11**, 8–12.

Viterbo, D., Gausman, V. and Gonda, T. (2016). Diagnostic and therapeutic biomarkers in pancreaticobiliary malignancy. *World J Gastrointest Endosc* **8**, 128–142.

Vonlaufen, A., Joshi, S., Qu, C., Phillips, P. A., Xu, Z., Parker, N. R., Toi, C. S., Pirola, R. C., Wilson, J. S., Goldstein, D., et al. (2008). Pancreatic stellate cells: partners in crime with pancreatic cancer cells. *Cancer Research* **68**, 2085–2093.

Vrieling, A., Bueno-de-Mesquita, H. B., Boshuizen, H. C., Michaud, D. S., Severinsen, M. T., Overvad, K., Olsen, A., Tjønneland, A., Clavel-Chapelon, F.,

Boutron-Ruault, M.-C., et al. (2010). Cigarette smoking, environmental tobacco smoke exposure and pancreatic cancer risk in the European Prospective Investigation into Cancer and Nutrition. *Int. J. Cancer* **126**, 2394–2403.

Waddell, N., Pajic, M., Patch, A.-M., Chang, D. K., Kassahn, K. S., Bailey, P., Johns, A. L., Miller, D., Nones, K., Quek, K., et al. (2015). Whole genomes redefine the mutational landscape of pancreatic cancer. *Nature* **518**, 495–501.

Wagner, M., Redaelli, C., Lietz, M., Seiler, C. A., Friess, H. and Buchler, M. W. (2004). Curative resection is the single most important factor determining outcome in patients with pancreatic adenocarcinoma. *Br J Surg* **91**, 586–594.

Walter, F. M., Mills, K., Mendonça, S. C., Abel, G. A., Basu, B., Carroll, N., Ballard, S., Lancaster, J., Hamilton, W., Rubin, G. P., et al. (2016). Symptoms and patient factors associated with diagnostic intervals for pancreatic cancer (SYMPTOM pancreatic study): a prospective cohort study. *Lancet Gastroenterol Hepatol* **1**, 298–306.

Wang, C., Jiang, P., Sand, C., Paul, A. V. and Wimmer, E. (2012a). Alanine Scanning of Poliovirus 2CATPase Reveals New Genetic Evidence that Capsid Protein/2CATPase Interactions Are Essential for Morphogenesis. *J. Virol.* **86**, 9964–9975.

Wang, L., Tsutsumi, S., Kawaguchi, T., Nagasaki, K., Tatsuno, K., Yamamoto, S., Sang, F., Sonoda, K., Sugawara, M., Saiura, A., et al. (2012b). Whole-exome sequencing of human pancreatic cancers and characterization of genomic instability caused by MLH1 haploinsufficiency and complete deficiency. *Genome Res.* **22**, 208–219.

Wang, S., Coleman, E. J., Pop, L. M., Brooks, K. J., Vitetta, E. S. and Niederkorn, J. Y. (2005). Effect of an anti-CD54 (ICAM-1) monoclonal antibody (UV3) on the growth of human uveal melanoma cells transplanted heterotopically and orthotopically in SCID mice. *Int. J. Cancer* **118**, 932–941.

Wang, Y., Xiao, Y., Zhong, L., Ye, D., Zhang, J., Tu, Y., Bornstein, S. R., Zhou, Z., Lam, K. S. L. and Xu, A. (2014). Increased Neutrophil Elastase and Proteinase 3 and Augmented NETosis Are Closely Associated With β-Cell Autoimmunity in Patients With Type 1 Diabetes. *Diabetes* **63**, 4239–4248.

Wang-Gillam, A., Plambeck-Suess, S., Goedegebuure, P., Simon, P. O., Mitchem, J. B., Hornick, J. R., Sorscher, S., Picus, J., Suresh, R., Lockhart, A. C., et al. (2012). A phase I study of IMP321 and gemcitabine as the front-line therapy in patients with advanced pancreatic adenocarcinoma. *Invest New Drugs* **31**, 707–713.

Watanabe, D., Goshima, F., Mori, I., Tamada, Y., Matsumoto, Y. and Nishiyama, Y. (2008). Oncolytic virotherapy for malignant melanoma with herpes simplex virus type 1 mutant HF10. *J. Dermatol. Sci.* **50**, 185–196.

Watari, N., Hotta, Y. and Mabuchi, Y. (1982). Morphological studies on a vitamin A-storing cell and its complex with macrophage observed in mouse pancreatic tissues following excess vitamin A administration. *Okajimas Folia Anat Jpn* **58**, 837–858.

Wawryk, S. O., Novotny, J. R., Wicks, I. P., Wilkinson, D., Maher, D., Salvaris, E., Welch, K., Fecondo, J. and Boyd, A. W. (1989). The Role of the LFA-1/ICAM-1 Interaction in Human Leukocyte Homing and Adhesion. *Immunol Rev* **108**, 135–161.

Weiss, W. and Benarde, M. A. (1983). The temporal relation between cigarette smoking and pancreatic cancer. *Am J Public Health* **73**, 1403–1404.

Welte, T., Kim, I. S., Tian, L., Gao, X., Wang, H., Li, J., Holdman, X. B., Herschkowitz, J. I., Pond, A., Xie, G., et al. (2016). Oncogenic mTOR signalling recruits myeloid-derived suppressor cells to promote tumour initiation. *Nat Cell Biol* **18**, 632–644.

Wennier, S., Li, S. and McFadden, G. (2011). Oncolytic virotherapy for pancreatic cancer. *Expert Rev Mol Med* **13**, e18.

Whitton, J. L., Cornell, C. T. and Feuer, R. (2005). Host and virus determinants of picornavirus pathogenesis and tropism. *Nat. Rev. Microbiol.* **3**, 765–776.

Wilson, J. S., Pirola, R. C. and Apte, M. V. (2014). Stars and stripes in pancreatic cancer: role of stellate cells and stroma in cancer progression. *Front Physiol* **5**, 52.

Winter, J. M., Cameron, J. L., Campbell, K. A., Arnold, M. A., Chang, D. C.,

Coleman, J., Hodgin, M. B., Sauter, P. K., Hruban, R. H., Riall, T. S., et al. (2006). 1423 pancreaticoduodenectomies for pancreatic cancer: A single-institution experience. *J Gastrointest Surg* **10**, 1199–1211.

Wolpin, B. M., Chan, A. T., Hartge, P., Chanock, S. J., Kraft, P., Hunter, D. J., Giovannucci, E. L. and Fuchs, C. S. (2009). ABO Blood Group and the Risk of Pancreatic Cancer. *J Natl Cancer Inst* **101**, 424–431.

Wolpin, B. M., Kraft, P., Gross, M., Helzlsouer, K., Bueno-de-Mesquita, H. B., Steplowski, E., Stolzenberg-Solomon, R. Z., Arslan, A. A., Jacobs, E. J., LaCroix, A., et al. (2010). Pancreatic Cancer Risk and ABO Blood Group Alleles: Results from the Pancreatic Cancer Cohort Consortium. *Cancer Research* **70**, 1015–1023.

Workenhe, S. T. and Mossman, K. L. (2014). Oncolytic virotherapy and immunogenic cancer cell death: sharpening the sword for improved cancer treatment strategies. *Mol Ther* **22**, 251–256.

Wu, J., Matthaei, H., Maitra, A., Dal Molin, M., Wood, L. D., Eshleman, J. R., Goggins, M., Canto, M. I., Schulick, R. D., Edil, B. H., et al. (2011). Recurrent GNAS Mutations Define an Unexpected Pathway for Pancreatic Cyst Development. *Science Translational Medicine* **3**, 92ra66.

Xiang, Z., Gonzalez, R., Wang, Z., Ren, L., Xiao, Y., Li, J., Li, Y., Vernet, G., Paranhos-Baccalà, G., Jin, Q., et al. (2012). Coxsackievirus A21, Enterovirus 68, and Acute Respiratory Tract Infection, China. *Emerging Infectious Diseases* **18**, 821–824.

Xiao, C., Bator, C. M., Bowman, V. D., Rieder, E., He, Y., Hebert, B., Bella, J., Baker, T. S., Wimmer, E., Kuhn, R. J., et al. (2001). Interaction of Coxsackievirus A21 with Its Cellular Receptor, ICAM-1. *J. Virol.* **75**, 2444–2451.

Xiao, C., Bator-Kelly, C. M., Rieder, E., Chipman, P. R., Craig, A., Kuhn, R. J., Wimmer, E. and Rossmann, M. G. (2005). The crystal structure of coxsackievirus A21 and its interaction with ICAM-1. *Structure* **13**, 1019–1033.

Xu, J. X., Maher, V. E., Zhang, L., Tang, S., Sridhara, R., Ibrahim, A., Kim, G. and Pazdur, R. (2017). FDA Approval Summary: Nivolumab in Advanced Renal Cell

Carcinoma After Anti-Angiogenic Therapy and Exploratory Predictive Biomarker Analysis. *Oncologist* **22**, 311–317.

Xu, Z., Vonlaufen, A., Phillips, P. A., Fiala-Beer, E., Zhang, X., Yang, L., Biankin, A. V., Goldstein, D., Pirola, R. C., Wilson, J. S., et al. (2010). Role of Pancreatic Stellate Cells in Pancreatic Cancer Metastasis. *Am. J. Pathol.* **177**, 2585–2596.

Xue, R., Jia, K., Wang, J., Yang, L., Wang, Y., Gao, L. and Hao, J. (2018). A Rising Star in Pancreatic Diseases: Pancreatic Stellate Cells. *Front Physiol* **9**, 754.

Yamamura, K., Kasuya, H., Sahin, T. T., Tan, G., Hotta, Y., Tsurumaru, N., Fukuda, S., Kanda, M., Kobayashi, D., Tanaka, C., et al. (2014). Combination treatment of human pancreatic cancer xenograft models with the epidermal growth factor receptor tyrosine kinase inhibitor erlotinib and oncolytic herpes simplex virus HF10. *Ann Surg Oncol* **21**, 691–698.

Yang, F., Yu, X., Bao, Y., Du, Z., Jin, C. and Fu, D. (2016). Prognostic value of Ki-67 in solid pseudopapillary tumor of the pancreas: Huashan experience and systematic review of the literature. *Surgery* **159**, 1023–1031.

Yao, X., Ji, Y., Zeng, M., Rao, S. and Yang, B. (2010). Solid Pseudopapillary Tumor of the Pancreas. *Pancreas* **39**, 486–491.

Yin-Murphy, M. and Almond, J. W. (1996). Chapter 53 Picornaviruses. In *Medical Microbiology. 4th edition* (ed. Baron, S., University of Texas Medical Branch at Galveston.

Yonezawa, S., Higashi, M., Yamada, N. and Goto, M. (2008). Precursor lesions of pancreatic cancer. *Gut and Liver* **2**, 137–154.

Yoo, J., Kistler, C. A., Yan, L., Dargan, A. and Siddiqui, A. A. (2016). Endoscopic ultrasound in pancreatic cancer: innovative applications beyond the basics. *J Gastrointest Oncol* **7**, 1019.

Yu, Y., Sweeney, T. R., Kafasla, P., Jackson, R. J., Pestova, T. V. and Hellen, C. U. (2011). The mechanism of translation initiation on Aichivirus RNA mediated by a novel type of picornavirus IRES. *EMBO J* **30**, 4423–4436.

Yunis, A. A., Arimura, G. K. and Russin, D. J. (1977). Human pancreatic carcinoma

(MIA PaCa-2) in continuous culture: sensitivity to asparaginase. *J Cancer*.

Zee, S. Y., Hochwald, S. N., Conlon, K. C., Brennan, M. F. and Klimstra, D. S. (2005). Pleomorphic pancreatic endocrine neoplasms: a variant commonly confused with adenocarcinoma. *The American Journal of Surgical Pathology* **29**, 1194–1200.

Zeichhardt, H., Wetz, K., Willingmann, P. and Habermehl, K. O. (1985). Entry of poliovirus type 1 and Mouse Elberfeld (ME) virus into HEp-2 cells: receptor-mediated endocytosis and endosomal or lysosomal uncoating. *J. Gen. Virol.* **66 (Pt 3)**, 483–492.

Zhan, H.-X., Zhou, B., Cheng, Y.-G., Xu, J.-W., Wang, L., Zhang, G.-Y. and Hu, S.-Y. (2017). Crosstalk between stromal cells and cancer cells in pancreatic cancer: New insights into stromal biology. *Cancer Lett.* **392**, 83–93.

Zhang, J., Zhao, Z. and Berkel, H. J. (2005). Animal fat consumption and pancreatic cancer incidence: evidence of interaction with cigarette smoking. *Ann Epidemiol* **15**, 500–508.

Zhang, L., Daikoku, T., Ohtake, K., Ohtsuka, J., Nawa, A., Kudoh, A., Iwahori, S., Isomura, H., Nishiyama, Y. and Tsurumi, T. (2006). Establishment of a novel foreign gene delivery system combining an HSV amplicon with an attenuated replication-competent virus, HSV-1 HF10. *J. Virol. Methods* **137**, 177–183.

Zhang, P., Zou, M., Wen, X., Gu, F., Li, J., Liu, G., Dong, J., Deng, X., Gao, J., Li, X., et al. (2013). Development of serum parameters panels for the early detection of pancreatic cancer. *Int. J. Cancer* **134**, 2646–2655.

Zhang, Q., Chen, S., Zeng, L., Chen, Y., Lian, G., Qian, C., Li, J., Xie, R. and Huang, K.-H. (2017a). New developments in the early diagnosis of pancreatic cancer. *Expert Rev Gastroenterol Hepatol* **11**, 149–156.

Zhang, S., Wang, C., Huang, H., Jiang, Q., Zhao, D., Tian, Y., Ma, J., Yuan, W., Sun, Y., Che, X., et al. (2017b). Effects of alcohol drinking and smoking on pancreatic ductal adenocarcinoma mortality: A retrospective cohort study consisting of 1783 patients. *Scientific Reports* **7**, 9572.

Zhang, X.-W., Ma, Y.-X., Sun, Y., Cao, Y.-B., Li, Q. and Xu, C.-A. (2017c). Gemcitabine in Combination with a Second Cytotoxic Agent in the First-Line Treatment of Locally Advanced or Metastatic Pancreatic Cancer: a Systematic Review and Meta-Analysis. 1–13.

Zhao, X., Ouyang, W., Chester, C., Long, S., Wang, N. and He, Z. (2017). Cytokine-induced killer cell delivery enhances the antitumor activity of oncolytic reovirus. *PLoS ONE* **12**, e0184816.

Zhou, B., Xu, J.-W., Cheng, Y.-G., Gao, J.-Y., Hu, S.-Y., Wang, L. and Zhan, H.-X. (2017). Early detection of pancreatic cancer: Where are we now and where are we going? *Int. J. Cancer* **141**, 231–241.

Zou, L., Yi, L., Song, Y., Zhang, X., Liang, L., Ni, H., Ke, C., Wu, J. and Lu, J. (2017). A cluster of coxsackievirus A21 associated acute respiratory illness: the evidence of efficient transmission of CVA21. *Arch Virol* **162**, 1057–1059.

Zygiert, Z. (1971). Hodgkin's disease: remissions after measles. *Lancet* **1**, 593.

Chapter 9

Appendix

Table 9: PA1002a Tumour Microarray Specification Sheet. Source:

https://www.biomax.us/tissue-arrays/Pancreas/PA1002a

Position	Sex	Age	Organ	Pathology	Grade	Stage	TNM	Type
A1	F	41	Pancreas	Duct adenocarcinoma (metastatic duct adenocarcinoma of lymph node)	1	III	T3N1M0	Malignant
A2	M	65	Pancreas	Duct adenocarcinoma	1	II	T3N0M0	Malignant
A3	F	58	Pancreas	Duct adenocarcinoma	1	IB	T2N0M0	Malignant
A4	F	72	Pancreas	Duct adenocarcinoma	1	II	T3N0M0	Malignant
A5	M	60	Pancreas	Duct adenocarcinoma	1	II	T3N0M0	Malignant
A6	F	41	Pancreas	Duct adenocarcinoma	1	II	T3N0M0	Malignant
A7	M	65	Pancreas	Duct adenocarcinoma (duct tissue)	-	II	T3N0M0	Malignant
A8	F	58	Pancreas	Duct adenocarcinoma	1	IB	T2N0M0	Malignant
A9	F	72	Pancreas	Duct adenocarcinoma	1	II	T3N0M0	Malignant
A10	M	60	Pancreas	Duct adenocarcinoma	1	II	T3N0M0	Malignant
B1	M	52	Pancreas	Duct adenocarcinoma	1	III	T3N1M0	Malignant
B2	M	65	Pancreas	Duct adenocarcinoma	2	III	T3N1M0	Malignant
B3	M	41	Pancreas	Duct adenocarcinoma	2	I	T2N0M0	Malignant
B4	M	44	Pancreas	Duct adenocarcinoma	2	II	T3N0M0	Malignant
B5	F	55	Pancreas	Duct adenocarcinoma	1	IB	T2N0M0	Malignant
B6	M	52	Pancreas	Duct adenocarcinoma	1	III	T3N1M0	Malignant
B7	M	65	Pancreas	Duct adenocarcinoma	2	III	T3N1M0	Malignant
B8	M	41	Pancreas	Duct adenocarcinoma	2	I	T2N0M0	Malignant
B9	M	44	Pancreas	Duct adenocarcinoma	2	II	T3N0M0	Malignant
B10	F	55	Pancreas	Duct adenocarcinoma	1	IB	T2N0M0	Malignant
C1	M	55	Pancreas	Duct adenocarcinoma	1	II	T3N0M0	Malignant
C2	M	55	Pancreas	Duct adenocarcinoma	2	IB	T2N0M0	Malignant
C3	M	34	Pancreas	Duct adenocarcinoma	2	II	T3N0M0	Malignant
C4	M	42	Pancreas	Duct adenocarcinoma	2	II	T3N0M0	Malignant
C5	M	44	Pancreas	Duct adenocarcinoma (fibrous tissue and smooth muscle)	-	II	T3N0M0	Malignant
C6	M	55	Pancreas	Duct adenocarcinoma	1	II	T3N0M0	Malignant
C7	M	55	Pancreas	Duct adenocarcinoma	2	IB	T2N0M0	Malignant
C8	M	34	Pancreas	Duct adenocarcinoma	2	II	T3N0M0	Malignant
C9	M	42	Pancreas	Duct adenocarcinoma	2	II	T3N0M0	Malignant
C10	M	44	Pancreas	Duct adenocarcinoma	3	II	T3N0M0	Malignant
D1	M	59	Pancreas	Duct adenocarcinoma	2	II	T3N0M0	Malignant
D2	M	53	Pancreas	Duct adenocarcinoma	2	II	T3N0M0	Malignant
D3	M	52	Pancreas	Duct adenocarcinoma	2	II	T3N0M0	Malignant
D4	F	48	Pancreas	Duct adenocarcinoma	2	I	T3N0M0	Malignant
D5	F	68	Pancreas	Duct adenocarcinoma	3	II	T3N0M0	Malignant

D6	M	59	Pancreas	Duct adenocarcinoma	2	II	T3N0M0	Malignant
D7	M	53	Pancreas	Duct adenocarcinoma	2	II	T3N0M0	Malignant
D8	M	52	Pancreas	Duct adenocarcinoma	2	II	T3N0M0	Malignant
D9	F	48	Pancreas	Duct adenocarcinoma	2	I	T3N0M0	Malignant
D10	F	68	Pancreas	Duct adenocarcinoma	3	II	T3N0M0	Malignant
E1	M	41	Pancreas	Duct adenocarcinoma	3	III	T4N1M0	Malignant
E2	M	64	Pancreas	Duct adenocarcinoma	3	II	T3N0M0	Malignant
E3	F	58	Pancreas	Duct adenocarcinoma	3	II	T3N0M0	Malignant
E4	F	60	Pancreas	Duct adenocarcinoma	3	III	T4N0M0	Malignant
E5	F	72	Pancreas	Duct adenocarcinoma	3	II	T3N0M0	Malignant
E6	M	41	Pancreas	Duct adenocarcinoma	3	III	T4N1M0	Malignant
E7	M	64	Pancreas	Duct adenocarcinoma	3	II	T3N0M0	Malignant
E8	F	58	Pancreas	Duct adenocarcinoma	1	II	T3N0M0	Malignant
E9	F	60	Pancreas	Duct adenocarcinoma	3	III	T4N0M0	Malignant
E10	F	72	Pancreas	Duct adenocarcinoma	3	II	T3N0M0	Malignant
F1	M	56	Pancreas	Duct adenocarcinoma	3	III	T2N1M0	Malignant
F2	M	63	Pancreas	Duct adenocarcinoma	3	IB	T2N0M0	Malignant
F3	M	62	Pancreas	Duct adenocarcinoma	3	IB	T2N0M0	Malignant
F4	M	59	Pancreas	Duct adenocarcinoma	3	IB	T2N0M0	Malignant
F5	F	60	Pancreas	Duct adenocarcinoma (fibrous tissue with necrosis)	-	IV	T2N1M1	Malignant
F6	M	56	Pancreas	Duct adenocarcinoma	3	III	T2N1M0	Malignant
F7	M	63	Pancreas	Duct adenocarcinoma	3	IB	T2N0M0	Malignant
F8	M	62	Pancreas	Duct adenocarcinoma	3	IB	T2N0M0	Malignant
F9	M	59	Pancreas	Duct adenocarcinoma	3	IB	T2N0M0	Malignant
F10	F	60	Pancreas	Duct adenocarcinoma (tumor necrosis)	-	IV	T2N1M1	Malignant
G1	F	53	Pancreas	Duct adenocarcinoma	3	II	T3N0M0	Malignant
G2	M	50	Pancreas	Duct adenocarcinoma	3	III	T3N1M0	Malignant
G3	M	51	Pancreas	Duct adenocarcinoma	3	II	T3N0M0	Malignant
G4	F	62	Pancreas	Duct adenocarcinoma	3	II	T3N0M0	Malignant
G5	M	78	Pancreas	Duct adenocarcinoma	3	I	T2N0M0	Malignant
G6	F	53	Pancreas	Duct adenocarcinoma	3	II	T3N0M0	Malignant
G7	M	50	Pancreas	Duct adenocarcinoma	3	III	T3N1M0	Malignant
G8	M	51	Pancreas	Duct adenocarcinoma	3	II	T3N0M0	Malignant
G9	F	62	Pancreas	Duct adenocarcinoma	3	II	T3N0M0	Malignant
G10	M	78	Pancreas	Duct adenocarcinoma	3	I	T2N0M0	Malignant
H1	F	39	Pancreas	Duct adenocarcinoma	3	II	T3N0M0	Malignant
H2	M	55	Pancreas	Duct adenocarcinoma	3	IB	T2N0M0	Malignant
H3	F	76	Pancreas	Duct adenocarcinoma	3	III	T4N0M0	Malignant
H4	M	76	Pancreas	Duct adenocarcinoma	3	II	T3N0M0	Malignant
H5	F	57	Pancreas	Duct adenocarcinoma	3	IB	T2N0M0	Malignant
H6	F	39	Pancreas	Duct adenocarcinoma	3	II	T3N0M0	Malignant
H7	M	55	Pancreas	Duct adenocarcinoma	3	IB	T2N0M0	Malignant
H8	F	76	Pancreas	Duct adenocarcinoma	3	III	T4N0M0	Malignant
H9	M	76	Pancreas	Duct adenocarcinoma	3	II	T3N0M0	Malignant
H10	F	57	Pancreas	Duct adenocarcinoma	3	IB	T2N0M0	Malignant

I1	M	40	Pancreas	Normal pancreas tissue	-	-	-	Normal
I2	M	47	Pancreas	Normal pancreas tissue	-	-	-	Normal
I3	M	25	Pancreas	Normal pancreas tissue	-	-	-	Normal
I4	M	30	Pancreas	Normal pancreas tissue	-	-	-	Normal
I5	M	30	Pancreas	Normal pancreas tissue	-	-	-	Normal
I6	M	40	Pancreas	Normal pancreas tissue	-	-	-	Normal
I7	M	47	Pancreas	Normal pancreas tissue	-	-	-	Normal
I8	M	25	Pancreas	Normal pancreas tissue	-	-	-	Normal
I9	M	30	Pancreas	Normal pancreas tissue	-	-	-	Normal
I10	M	30	Pancreas	Normal pancreas tissue	-	-	-	Normal
J1	M	50	Pancreas	Normal pancreas tissue	-	-	-	Normal
J2	M	35	Pancreas	Normal pancreas tissue	-	-	-	Normal
J3	M	38	Pancreas	Normal pancreas tissue	-	-	-	Normal
J4	F	35	Pancreas	Normal pancreas tissue	-	-	-	Normal
J5	F	21	Pancreas	Normal pancreas tissue	-	-	-	Normal
J6	M	50	Pancreas	Normal pancreas tissue	-	-	-	Normal
J7	M	35	Pancreas	Normal pancreas tissue	-	-	-	Normal
J8	M	38	Pancreas	Normal pancreas tissue	-	-	-	Normal
J9	F	35	Pancreas	Normal pancreas tissue	-	-	-	Normal
J10	F	21	Pancreas	Normal pancreas tissue	-	-	-	Normal
-	M	42	Adrenal Gland	Pheochromocytoma (tissue marker)	-			Malignant

Table 10: HPan-A150CS-02 Tumour Microarray Specification Sheet. Source:

https://www.biomax.us/tissue-arrays/Pancreas/HPan-A150CS-02

Position	Sex	Age	Organ	Pathology	Grade	Stage	TNM	Type
A1	F	63	Pancreas	Ductal adenocarcinoma	II	1A	T1N0M0	Malignant
A2	F	63	Perilesional tissue	NAT				Nat
A3	M	51	Pancreas	Ductal adenocarcinoma	II	1A	T1N0M0	Malignant
A4	M	51	Perilesional tissue	NAT				Nat
A5	M	65	Pancreas	Ductal adenocarcinoma	II	1A	T1N0M0	Malignant
A6	M	65	Perilesional tissue	NAT				Nat
A7	M	84	Pancreas	Ductal adenocarcinoma	I-III	1A	T1N0M0	Malignant
A8	M	84	Perilesional tissue	NAT				Nat
A9	M	70	Pancreas	Ductal adenocarcinoma	II	1A	T1N0M0	Malignant
A10	M	70	Perilesional tissue	NAT				Nat
A11	M	49	Pancreas	Ductal adenocarcinoma	II-III	1B	T2N0M0	Malignant
A12	M	49	Perilesional tissue	NAT				Nat
A13	M	52	Pancreas	Ductal adenocarcinoma	II	1B	T2N0M0	Malignant
A14	M	52	Perilesional tissue	NAT				Nat
A15	F	70	Pancreas	Ductal adenocarcinoma	II	1B	T2N0M0	Malignant
A16	F	70	Perilesional tissue	NAT				Nat
B1	M	54	Pancreas	Ductal adenocarcinoma	II	1B	T2N0M0	Malignant

B2	M	54	Perilesional tissue	NAT				Nat
B3	M	63	Pancreas	Ductal adenocarcinoma	II	1B	T2N0M0	Malignant
B4	M	63	Perilesional tissue	NAT				Nat
B5	M	65	Pancreas	Ductal adenocarcinoma	II	1B	T2N0M0	Malignant
B6	M	65	Perilesional tissue	NAT				Nat
B7	M	58	Pancreas	Adenosquamous carcinoma	III	1B	T2N0M0	Malignant
B8	M	58	Perilesional tissue	NAT				Nat
B9	F	57	Pancreas	Adenosquamous carcinoma	II	1B	T2N0M0	Malignant
B10	F	57	Perilesional tissue	NAT				Nat
B11	M	71	Pancreas	Ductal adenocarcinoma	II	1B	T2N0M0	Malignant
B12	M	71	Perilesional tissue	NAT				Nat
B13	F	56	Pancreas	Ductal adenocarcinoma	II	1B	T2N0M0	Malignant
B14	F	56	Perilesional tissue	NAT				Nat
B15	M	52	Pancreas	Ductal adenocarcinoma	II	1B	T2N0M0	Malignant
B16	M	52	Perilesional tissue	NAT				Nat
C1	M	57	Pancreas	Ductal adenocarcinoma	II	1B	T2N0M0	Malignant
C2	M	57	Perilesional tissue	NAT				Nat
C3	M	51	Pancreas	Ductal adenocarcinoma	II	1B	T2N0M0	Malignant
C4	M	51	Perilesional tissue	NAT				Nat
C5	F	62	Pancreas	Ductal adenocarcinoma	II	1B	T2N0M0	Malignant
C6	F	62	Perilesional tissue	NAT				Nat
C7	F	55	Pancreas	Ductal adenocarcinoma	II	1B	T2N0M0	Malignant
C8	F	55	Perilesional tissue	NAT				Nat
C9	F	46	Pancreas	Ductal adenocarcinoma	II	1B	T2N0M0	Malignant
C10	F	46	Perilesional tissue	NAT				Nat
C11	M	69	Pancreas	Ductal adenocarcinoma	II-III	1B	T2N0M0	Malignant
C12	M	69	Perilesional tissue	NAT				Nat
C13	M	44	Pancreas	Ductal adenocarcinoma	I-II	1B	T2N0M0	Malignant
C14	M	44	Perilesional tissue	NAT				Nat
C15	M	64	Pancreas	Ductal adenocarcinoma	II	1B	T2N0M0	Malignant
C16	M	64	Perilesional tissue	NAT				Nat
D1	M	46	Pancreas	Ductal adenocarcinoma	I-II	1B	T2N0M0	Malignant
D2	M	46	Perilesional tissue	NAT				Nat
D3	F	52	Pancreas	Ductal adenocarcinoma	II	1B	T2N0M0	Malignant
D4	F	52	Perilesional tissue	NAT				Nat
D5	M	72	Pancreas	Ductal adenocarcinoma	II-III	1B	T2N0M0	Malignant
D6	M	72	Perilesional tissue	NAT				Nat
D7	M	71	Pancreas	Ductal adenocarcinoma	II	1B	T2N0M0	Malignant
D8	M	71	Perilesional tissue	NAT				Nat
D9	F	64	Pancreas	Ductal adenocarcinoma	I-II	1B	T2N0M0	Malignant
D10	F	64	Perilesional tissue	NAT				Nat

D11	M	62	Pancreas	Adenosquamous carcinoma	I-III	1B	T2N0M0	Malignant
D12	M	62	Perilesional tissue	NAT				Nat
D13	F	77	Pancreas	Ductal adenocarcinoma	II-III	1B	T2N0M0	Malignant
D14	F	77	Perilesional tissue	NAT				Nat
D15	M	61	Pancreas	Ductal adenocarcinoma	II-III	1B	T2N0M0	Malignant
D16	M	61	Perilesional tissue	NAT				Nat
E1	F	62	Pancreas	Ductal adenocarcinoma	II	1B	T2N0M0	Malignant
E2	F	62	Perilesional tissue	NAT				Nat
E3	M	80	Pancreas	Adenosquamous carcinoma	II-III	1B	T2N0M0	Malignant
E4	M	80	Perilesional tissue	NAT				Nat
E5	M	48	Pancreas	Ductal adenocarcinoma	II	1B	T2N0M0	Malignant
E6	M	48	Perilesional tissue	NAT				Nat
E7	M	64	Pancreas	Ductal adenocarcinoma	II	1B	T2N0M0	Malignant
E8	M	64	Perilesional tissue	NAT				Nat
E9	M	52	Pancreas	Ductal adenocarcinoma	II-III	1B	T2N0M0	Malignant
E10	M	52	Perilesional tissue	NAT				Nat
E11	M	64	Pancreas	Adenosquamous carcinoma	II	1B	T2N0M0	Malignant
E12	M	64	Perilesional tissue	NAT				Nat
E13	M	55	Pancreas	Adenosquamous carcinoma	II-III	1B	T2N0M0	Malignant
E14	M	55	Perilesional tissue	NAT				Nat
E15	F	63	Pancreas	Ductal adenocarcinoma	II	1B	T2N0M0	Malignant
E16	F	63	Perilesional tissue	NAT				Nat
F1	F	55	Pancreas	Ductal adenocarcinoma	II	1/2/16	T2M0	Malignant
F2	F	55	Perilesional tissue	NAT				Nat
F3	F	62	Pancreas	Ductal adenocarcinoma	II-III	1â€”2	T2M0	Malignant
F4	F	62	Perilesional tissue	NAT				Nat
F5	F	78	Pancreas	Ductal adenocarcinoma	II	2A	T3N0M0	Malignant
F6	F	78	Perilesional tissue	NAT				Nat
F7	M	63	Pancreas	Ductal adenocarcinoma	II	2A	T3N0M0	Malignant
F8	M	63	Perilesional tissue	NAT				Nat
F9	M	61	Pancreas	Adenosquamous carcinoma	II-III	2A	T3N0M0	Malignant
F10	M	61	Perilesional tissue	NAT				Nat
F11	M	55	Pancreas	Ductal adenocarcinoma	II	2A	T3N0M0	Malignant
F12	M	55	Perilesional tissue	NAT				Nat
F13	M	60	Pancreas	Ductal adenocarcinoma	II-III	2A	T3N0M0	Malignant
F14	M	60	Perilesional tissue	NAT				Nat
F15	M	64	Pancreas	Ductal adenocarcinoma	II	2B	T1N1M0	Malignant
F16	M	64	Perilesional tissue	NAT				Nat
G1	F	52	Pancreas	Ductal adenocarcinoma	II	2B	T1N1M0	Malignant
G2	F	52	Perilesional tissue	NAT				Nat
G3	M	69	Pancreas	Ductal adenocarcinoma	II	2B	T2N1M0	Malignant

G4	M	69	Perilesional tissue	NAT				Nat
G5	M	61	Pancreas	Ductal adenocarcinoma	III	2B	T2N1M0	Malignant
G6	M	61	Perilesional tissue	NAT				Nat
G7	M	52	Pancreas	Ductal adenocarcinoma	II	2B	T2N1M0	Malignant
G8	M	52	Perilesional tissue	NAT				Nat
G9	F	57	Pancreas	Ductal adenocarcinoma	II	2B	T2N1M0	Malignant
G10	F	57	Perilesional tissue	NAT				Nat
G11	F	60	Pancreas	Ductal adenocarcinoma	II-III	2B	T2N1M0	Malignant
G12	F	60	Perilesional tissue	NAT				Nat
G13	M	65	Pancreas	Ductal adenocarcinoma	III	2B	T2N1M0	Malignant
G14	M	65	Perilesional tissue	NAT				Nat
G15	M	65	Pancreas	Ductal adenocarcinoma	II	2B	T2N1M0	Malignant
G16	M	65	Perilesional tissue	NAT				Nat
H1	M	41	Pancreas	Ductal adenocarcinoma	II-III	2B	T2N1M0	Malignant
H2	M	41	Perilesional tissue	NAT				Nat
H3	M	64	Pancreas	Ductal adenocarcinoma	II	2B	T2N1M0	Malignant
H4	M	64	Perilesional tissue	NAT				Nat
H5	F	55	Pancreas	Ductal adenocarcinoma	II	2B	T2N1M0	Malignant
H6	F	55	Perilesional tissue	NAT				Nat
H7	M	71	Pancreas	Ductal adenocarcinoma	II	2B	T2N1M0	Malignant
H8	M	71	Perilesional tissue	NAT				Nat
H9	M	62	Pancreas	Ductal adenocarcinoma	I-II	2B	T2N1M0	Malignant
H10	M	62	Perilesional tissue	NAT				Nat
H11	M	73	Pancreas	Ductal adenocarcinoma	II	2B	T2N1M0	Malignant
H12	M	73	Perilesional tissue	NAT				Nat
H13	M	71	Pancreas	Ductal adenocarcinoma	II	2B	T2N1M0	Malignant
H14	M	71	Perilesional tissue	NAT				Nat
H15	M	65	Pancreas	Ductal adenocarcinoma	II	2B	T2N1M0	Malignant
H16	M	65	Perilesional tissue	NAT				Nat
I1	F	44	Pancreas	Ductal adenocarcinoma	III	1â€”2	T2â€”â€”M0	Malignant
I2	F	44	Perilesional tissue	NAT				Nat
I3	F	44	Pancreas	Ductal adenocarcinoma	I-II	2B	T2N1M0	Malignant
I4	F	44	Perilesional tissue	NAT				Nat
I5	M	62	Pancreas	Ductal adenocarcinoma	II	4	T2N0M1	Malignant
I6	M	62	Perilesional tissue	NAT				Nat
I7	F	60	Pancreas	Ductal adenocarcinoma	III	4	T2â€”â€”M1	Malignant
I8	F	60	Perilesional tissue	NAT				Nat
I9	M	53	Pancreas	Adenosquamous carcinoma	II-III	4	T2N1M1	Malignant
I10	M	53	Perilesional tissue	NAT				Nat
I11	M	72	Pancreas	Ductal adenocarcinoma	II-III	4	T2N1M1	Malignant
I12	M	72	Perilesional tissue	NAT				Nat

I13	F	56	Pancreas	Ductal adenocarcinoma	II-III	4	T3â€”â€”M1	Malignant
I14	F	56	Perilesional tissue	NAT				Nat
I15	F	60	Pancreas	Ductal adenocarcinoma	II	4	T3N1M1	Malignant
I16	F	60	Perilesional tissue	NAT				Nat
J1	F	61	Pancreas	Adenosquamous carcinoma	III	1A	T1N0M0	Malignant
J2	F	61	Pancreas	Ductal adenocarcinoma	II-III	1B	T2N0M0	Malignant
J3	F	77	Pancreas	Ductal adenocarcinoma	II-III	2A	T3N0M0	Malignant
J4	F	77	Pancreas	Ductal adenocarcinoma	II	2B	T2N1M0	Malignant
J5	F	73	Pancreas	Ductal adenocarcinoma	II	2B	T2N1M0	Malignant
J6	F	73	Pancreas	Ductal adenocarcinoma	II-III	4	T2N1M1	Malignant